AEOSR-TR- 91 0675

Copy No. 1

PHYSICS AND APPLICATIONS OF COHERENTLY COUPLED PHASE CONJUGATORS

FINAL REPORT FOR THE PERIOD
December 1, 1987 through March 31, 1991

CONTRACT NO. F49620-88-C-0023

Prepared for

Air Force Office of Scientific Research
Directorate of Physical and Geophysical Sciences
Building 410
Bolling, AFB, DC 20332-6448
Attn: Dr. Howard Schlossberg

Prepared by

R. Saxena, I. McMichael, M.J. Rosker, W.R. Christian and P. Yeh
Rockwell International
Science Center
1049 Camino Dos Rios
Thousand Oaks, CA 91360

JUNE 1991

Rockwell International
Science Center

UNCLASSIFIED

SECURITY CLASSIFICATION OF THIS PAGE

REPORT DOCUMENTATION PAGE

FORM APPROVED
OMB No. 0704-0188

1a. REPORT SECURITY CLASSIFICATION UNCLASSIFIED	1b. RESTRICTIVE MARKINGS
2a. SECURITY CLASSIFICATION AUTHORITY	3. DISTRIBUTION/AVAILABILITY OF REPORT Approved for public release; distribution is unlimited
2b. CLASSIFICATION/DOWNGRADING SCHEDULE	
4. PERFORMING ORGANIZATION REPORT NUMBER(S) SC5538.FR	5. MONITORING ORGANIZATION REPORT NUMBER(S)
6a. NAME OF PERFORMING ORGANIZATION ROCKWELL INTERNATIONAL Science Center 6b. OFFICE SYMBOL (If Applicable)	7a. NAME OF MONITORING ORGANIZATION AFOSR/NP/BLDG 410 Bolling AFB DC 20332-6448
6c. ADDRESS (City, State and ZIP Code) 1049 Camino Dos Rios Thousand Oaks , CA 91360	7b. ADDRESS (City, State and ZIP Code) AFOSR/NP/BLDG 410 Bolling AFB DC 20332-6448
8a. NAME OF FUNDING/SPONSORING ORGANIZATION Air Force Office of Scientific Research Directorate of Physical & Geophysical Sciences 8b. OFFICE SYMBOL (If Applicable) NP	9. PROCUREMENT INSTRUMENT IDENTIFICATION NUMBER CONTRACT NO. F49620-88-C-0023
8c. ADDRESS (City, State and ZIP Code) Building 410 Bolling AFB, DC 20332-6448	10. SOURCE OF FUNDING NOS. PROGRAM ELEMENT NO.: 61102F PROJECT NO.: 2301 TASK NO.: A1 WORK UNIT ACCESSION NO.

11. TITLE (Include Security Classification)

PHYSICS AND APPLICATIONS OF COHERENTLY COUPLED PHASE CONJUGATORS

12. PERSONAL AUTHOR(S)

Saxena, R., McMichael, I., Rosker, M., Christian, W., Yeh, P.

13a. TYPE OF REPORT	13b. TIME COVERED	14. DATE OF REPORT (Year, Month, Day)	15. PAGE COUNT
FINAL REPORT	FROM 87/12/1 TO 91/3/31	1991, JUNE	176

16. SUPPLEMENTARY NOTATION

17. COSATI CODES			18. SUBJECT TERMS (Continue on reverse if necessary and identify by block number)
FIELD	GROUP	SUB-GROUP	

19. ABSTRACT (Continue on reverse if necessary and identify by block number)

We investigated photorefractive double phase-conjugation oscillators. We demonstrated, both theoretically and experimentally, that the beat frequency between the counterpropagating waves in these oscillators is proportional to the nonreciprocal phase shift of the resonator. We examined the frequency locking behavior of such an oscillator when a weak seed beam is injected into the resonator along the same direction as the phase-conjugate output. Measurements were taken with both coherent and incoherent (with respect to the pump) seed light, and the beat frequency was measured as a function of the seed intensity and the nonreciprocal phase shift. Larger seed intensities are required for frequency locking the phase-conjugate ring oscillators when compared to conventional ring laser gyros, showing the superiority of the former device for inertial sensing. Incoherent seed light does not cause frequency locking even at high seed levels. The experimental results were shown to be in good agreement with theory.

20. DISTRIBUTION/AVAILABILITY OF ABSTRACT	21. ABSTRACT SECURITY CLASSIFICATION
UNCLASSIFIED/UNLIMITED ☒ SAME AS RPT. ☒ DTIC USERS ☐	UNCLASSIFIED

22a. NAME OF RESPONSIBLE INDIVIDUAL	22b. TELEPHONE NUMBER (INCLUDE AREA CODE)	22c. OFFICE SYMBOL
Dr Howard Schlossberg	202/767-4906	NP

DD FORM 1473 Previous editions are obsolete.

UNCLASSIFIED

SECURITY CLASSIFICATION OF THIS PAGE

TABLE OF CONTENTS

TABLE OF CONTENTS

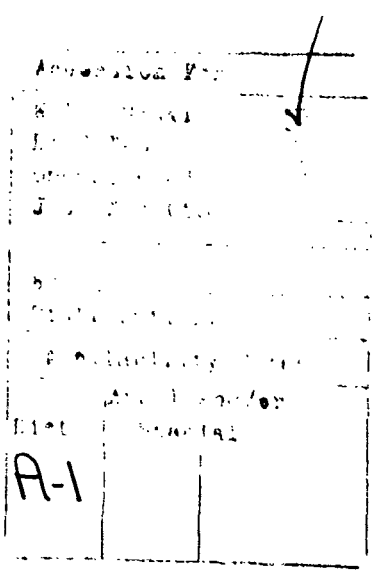

LIST OF FIGURES

1.0 SUMMARY

1.1 Contract Description

This contract focused on the physics of Coherently Coupled Phase Conjugators and the feasibility of these devices for inertial sensing. The effort began with a simple theoretical description of the nondegenerate oscillation in a linear double phase-conjugate oscillator (DPCO) due to nonreciprocal phase shift, and it could explain the operation of a linear position sensor and a phase-conjugate gyro. This was followed by the first experimental observations of oscillation and beat frequency in photorefractive double phase-conjugate ring oscillator (DPCRO) with nonreciprocal phase shift, using both the self-pumped and externally pumped phase-conjugate mirrors (PCM's). The effort culminated with the impressive demonstration and understanding of the frequency locking behavior of a photorefractive phase-conjugate ring oscillator (PCRO) due to contradirectional coupling of either a coherent or an incoherent seed beam. A theoretical study of the nondegenerate oscillations in an externally driven Fabry-Perot cavity with an intracavity phase-conjugate element was also carried out under this contract.

1.2 Scientific Problem

Two phase-conjugate mirrors with gain are coherently coupled by the oscillation that builds up between them.[1-3] This is called a double phase-conjugate oscillator (DPCO). DPCO's have many interesting properties that can be used to make sensors. For example, the frequencies of the counterpropagating oscillations are independent of the reciprocal optical path length of the resonator, and depend on the nonreciprocal optical path length. Since inertial effects produce nonreciprocal phase-shifts, the device can be used to sense motion with improvement in the frequency locking characteristics because the two counterpropagating waves support each other and do not compete for gain.[4,5] Under this contract, we studied in great detail the frequency locking behavior of a photorefractive DPCRO and PCRO both theoretically and experimentally. As a result of our work, we now have a clearer understanding as to why only coherent backscattered (or seed) light will cause frequency locking due to competition between the various gratings, whereas incoherent backscattered light will not affect the frequency locking behavior. The observation of higher harmonics of the beat frequency

in the photorefractive PCRO has been accounted for theoretically, and the experimental results are in good agreement with theory. In addition, we theoretically examined the nondegenerate oscillations in an externally driven Fabry-Perot cavity with an intracavity phase-conjugate element under this contract .

1.3 Progress Summary

Many areas of significant progress achieved under this contract are directly related to coherently coupled phase conjugators and their applications to inertial sensing. These include:

- Formulation of a simple theory for nondegenerate oscillation in DPCO that explains the operation of a linear position sensor and a phase-conjugate gyro.
- First experimental observation of oscillation in a self-pumped DPCRO.
- First experimental observation of oscillation in an externally pumped DPCRO.
- First experimental measurement of the beat frequency due to a nonreciprocal phase shift in an externally pumped DPCRO.
- First experimental study of the effects of incoherent contradirectional coupling on the beat frequency of an externally pumped DPCRO.
- First theoretical modeling of frequency locking due to a coherent seed beam in a photorefractive PCRO with nonreciprocal phase shift.
- First experimental measurements of frequency locking due to coherent seeding in a photorefractive PCRO with nonreciprocal phase shift.
- Theoretical formulation of the nondegenerate oscillations in an externally driven Fabry-Perot cavity with an intracavity phase-conjugate element.

Details of this progress are presented in Section 2.0, and in the publications included in this report as Appendices.

1.4 Publications and Presentations

1. M.J. Rosker, R. Saxena, and I. McMichael, "Measurement of Frequency Locking in Externally Seeded Phase-Conjugate Ring Gyroscopes," submitted to Opt. Lett.

2. R. Saxena, M.J. Rosker, and I. McMichael, "Theory of Frequency Locking in Externally Seeded Phase Conjugate Ring Oscillator," submitted to JOSA B.

3. W. S. Lee, S. Chi, P. Yeh and R. Saxena, "Theory of Phase-Conjugate Oscillators II," J. Opt. Soc. Am. B, in press.

4. W. S. Lee, S. Chi, P. Yeh and R. Saxena, "Theory of Phase-Conjugate Oscillators I," J. Opt. Soc. Am. B7, 1411 (1990).

5. M.J. Rosker, I. McMichael and R. Saxena, "Measurement of Frequency Locking in Phase-Conjugate Optical Gyroscopes," Technical Digest of OSA Annual Meeting, MW4 (1990).

6. W.S. Lee, S. Chi, R. Saxena and P. Yeh, "Theory of Phase-Conjugate Oscillator Applied to a Phase-Conjugate Resonator," Technical Digest of OSA Annual Meeting, ThY19 (1990).

7. R. Saxena, M.J. Rosker, W.R. Christian, I. McMichael and P. Yeh, "Frequency Locking in Ring Double Phase Conjugate Oscillators," Technical Digest of CLEO, CTUP4 (1990).

8. W.S. Lee, S. Chi, P. Yeh and R. Saxena,"Nondegenerate Oscillation in a Phase Conjugate Mirror with Linear Gain," Technical Digest of CLEO, CTHI27 (1990).

9. W.S. Lee, S. Chi, P. Yeh and R. Saxena, "Theory of Resonators with One Conventional Mirror and One PCM," ICO'15, Optics in Complex Systems, Garmisch-Partenkirchen, FDR (Aug. 5-10, 1990).

10. P. Yeh, "Optical Neural Computers", (Invited Paper) Bulletin of American Physical Society, Program of APS March Meeting 35, p.743 (1990).

11. P. Yeh, "Two-Wave Mixing in Nonlinear Media," IEEE J. of Quantum Electron. QE-25, 484 (1989).

12. P.H. Beckwith, W.R. Christian, I.C. McMichael, and P. Yeh, "Photorefractive Optics at Near-infrared Wavelengths," Proceedings SPIE 1060, 97 (1989).

13. W. S. Lee, S. Chi, P. Yeh and R. Saxena, "Phase-Conjugate Oscillators," OSA Technical Digest Series 18, TUX2-p.102 (1989).

14. P. Yeh, "Recent Advances in Photorefractive Nonlinear Optics." (Invited Paper) Conference in Lasers and Electro-optics, OSA Technical Digest Series 11, p.68 (1989).

15. P. Yeh, T. Chang and M. Khoshnevisan,"Photorefractive Nonlinear Optics," (Invited Paper), 19th Winter Colloquium on Quantum Electronics, Snowbird, UT (1989).

16. P. Yeh, "Photorefractive Conjugators and Applications," (Invited Paper) Australian Conference on Optics, Lasers, and Spectroscopy (Adelaide, 1989).

17. P. Yeh, "Recent Advances in Photorefractive Phenomena and Application," (Invited Paper) Proceed. Topical Meeting on Laser Materials and Laser Spectroscopy, 118-122 (World Scientific Publishing Company, 1988).

18. I. McMichael, P. Beckwith and P. Yeh, "Double Phase-Conjugate Oscillators," OSA Technical Digest Series 11, MR29-p. 54 (1988).

2.0 PROGRESS

2.1 Theory of Nondegenerate Oscillation in a DPCO

Consider the linear oscillator formed by two phase-conjugate mirrors PCM a and PCM b as shown in Fig. 1. The roundtrip phase condition is given by,

$$\phi_a - \phi_b + \Delta\omega\, L/c + \phi_{nr} = 2n\pi \tag{1}$$

where ϕ_a and ϕ_b are the phase shifts for reflection from the phase conjugate mirrors a and b respectively, $\Delta\omega = \omega_1 - \omega_2$ is the frequency splitting between the counterpropagating oscillations (note, if $\omega_1 = \omega_0 + \Delta\omega/2$, where ω_0 is the pump wave frequency for the phase-conjugate mirrors, then $\omega_2 = \omega_0 - \Delta\omega/2$), L is the length of the resonator, and ϕ_{nr} is the roundtrip nonreciprocal phase shift in the resonator. To gain some insight into how the phase condition determines the frequencies of oscillation, we make three simplifying assumptions. First we assume the case of weak coupling for which the phase of the phase conjugate reflection is given by[6,7]

$$\phi_3 = \phi_1 + \phi_2 - \phi_4 + \pi/2 + \phi_{\Delta n} + \phi_g \tag{2}$$

where ϕ_1 and ϕ_2 are the phases of the pumping waves, ϕ_4 is the phase of the incident wave, $\phi_{\Delta n}$ is the phase of the complex change in index, and ϕ_g is the phase shift of the grating with respect to the intensity pattern. Second, we assume that the frequency shift is small so that $\phi_g = \phi_{g0} + \Delta\omega\,\tau/2$, where ϕ_{g0} is the phase shift of the grating in the absence of any frequency shift, and τ is the response time of the phase-conjugate mirror. Third, we assume the phase-conjugate mirrors are identical, or the same, so that $\phi_a - \phi_b = \phi_{ga} - \phi_{gb} = \Delta\omega\,\tau$. Substituting into Eq. (1) we obtain the frequency splitting of the zeroth order counterpropagating modes,

$$\Delta\omega = \phi_{nr}/(\tau + L/C). \tag{3}$$

Equation (3) shows that the beat frequency is directly proportional to the nonreciprocal phase shift in the DPCO, the constant of proportionality being inversely proportional to the response time of the PCM and the cavity round trip time.

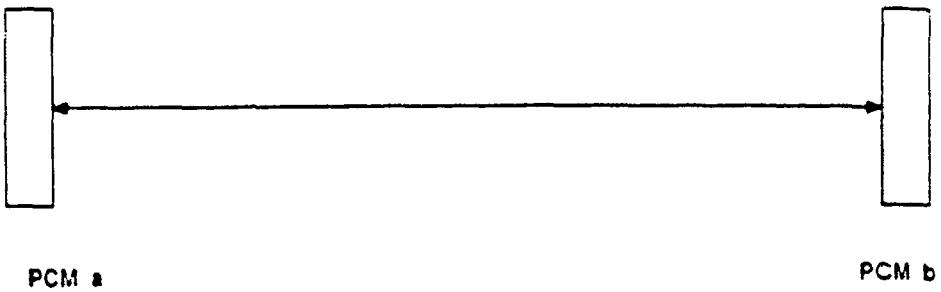

Fig. 1 Double phase-conjugate oscillator (DPCO) formed by two phase-conjugate mirrors PCM_a and PCM_b.

2.2 Observation of Beat Frequency in a Self-Pumped DPCRO

The experimental setup of our self-pumped DPCRO is shown in Fig. 2. Light from an argon laser is incident on a $BaTiO_3$ crystal to form a self-pumped "cat" conjugator.[8] The ring resonator is then formed by mirrors M1-M3 and the crystal. Greater than unity phase-conjugate reflectivity via four-wave mixing in the crystal (the incident light from the laser and its conjugate reflection provide the counterpropagating pump waves) is the gain source for the bidirectional oscillations. The outputs from M1 were combined and beat on detector D. As predicted by Eq. (3), in the absence of any nonreciprocal phase shift, the frequencies of the bidirectional oscillations are very nearly degenerate, and we measured a beat frequency - 10^{-3} Hz. When a Faraday cell was placed in the oscillator to produce a nonreciprocal phase shift, the bidirectional oscillations became nondegenerate, and we measured a beat frequency - 0.2 Hz. The qualitative dependence of the fringe motion at detector D on the magnitude and direction of the magnetic field applied to the Faraday cell agrees with the theory.

2.3 Observation of Beat Frequency in an Externally Pumped DPCRO

Using the experimental setup shown in Fig. 3, we demonstrated the ability of the double phase-conjugate ring oscillator to sense nonreciprocal intracavity phase shifts, and investigated the feasibility of using the oscillator as a rotation sensor. Light from an argon ion laser with the intracavity etalon removed is split by BS1 into two pump beams that are then directed into a $BaTiO_3$ crystal by mirrors M1-M3 as shown. Greater than unity phase-conjugate reflectivity via four-wave mixing in the crystal is the gain source for the bidirectional oscillations in the ring formed by the PCM and mirrors M4-M6. The

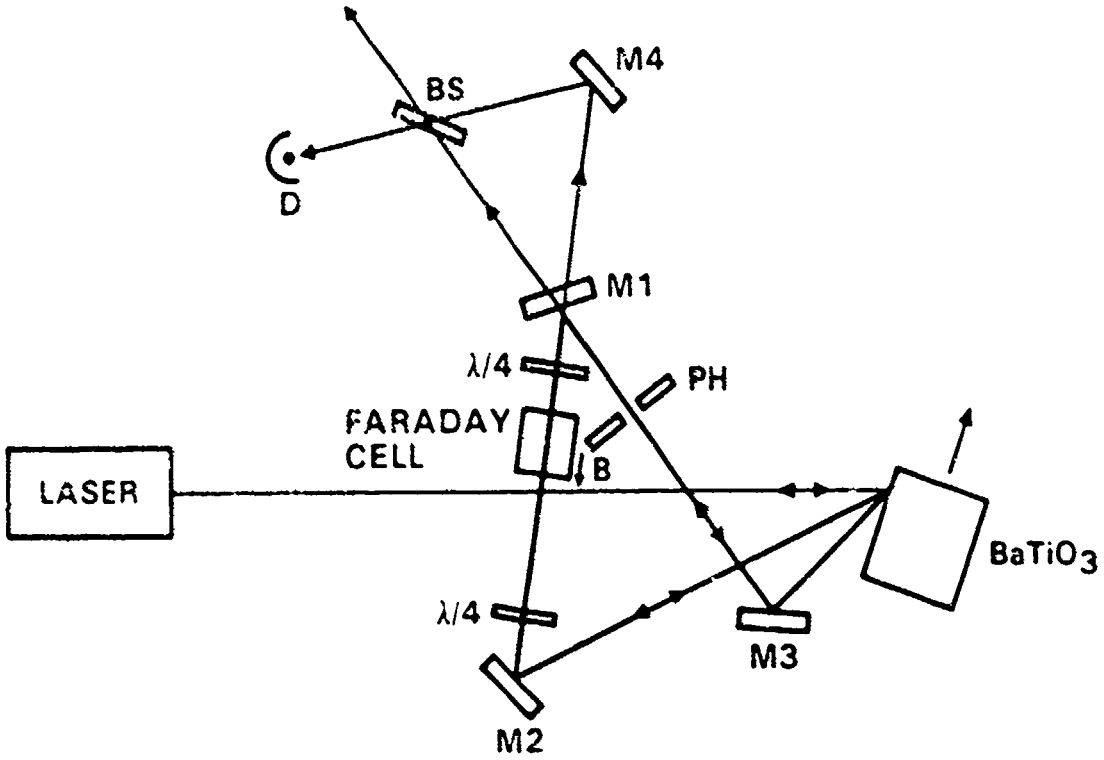

Fig. 2 Experimental setup of the self-pumped DPCRO.

Faraday cell in the oscillator is used to produce a nonreciprocal phase shift, as would be produced by the Sagnac effect if the cavity were rotated. When a nonreciprocal phase shift is inside the ring cavity, the counterpropagating beams no longer have the same frequency, and a beat frequency proportional to the nonreciprocal phase shift can be detected in the combined outputs at BS2. We measured a beat frequency $\sim 10^{-3}$ Hz in the absence of any nonreciprocal phase shift, and a beat frequency ~ 0.2 Hz was measured in its presence. Also, the beat frequency had the expected linear dependence on the nonreciprocal phase shift induced by the Faraday rotator inside the ring oscillator, as shown in Fig. 4. In this plot the nonreciprocal phase shift (ϕ_{nr}) has been expressed in terms of the bias frequency ($\Delta\nu$) that the Faraday rotator would introduce between the counterpropagating beams of a standard ring laser gyro. Due to the slow response of the $BaTiO_3$ crystal the sensitivity of the ring oscillator is scaled down by a factor of $L/(c\tau)$, where L is the perimeter and length of the ring resonator and τ is the response time of the photorefractive PCM.

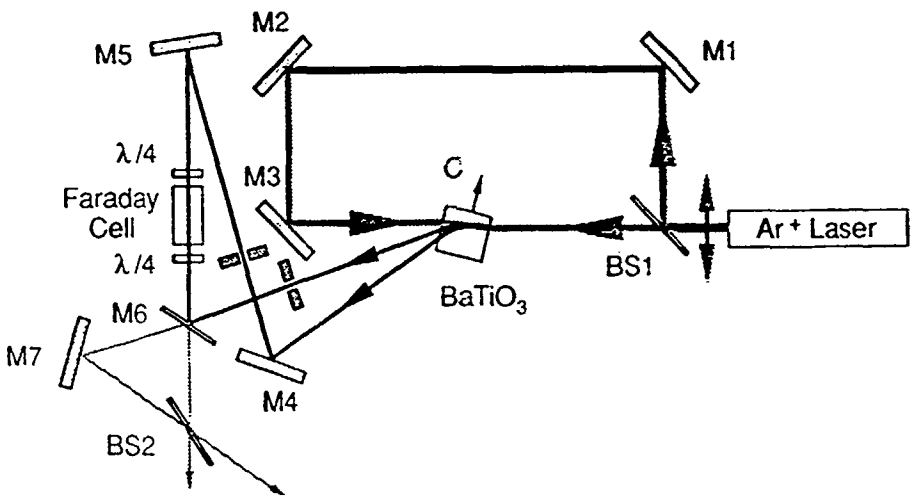

Fig. 3 Experimental arrangement used to examine the beat frequency in an externally pumped DPCRO.

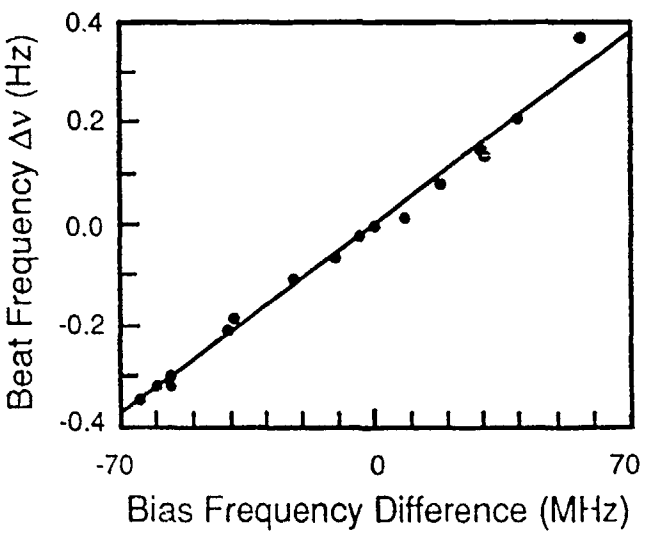

Fig. 4 Beat frequency between the counterpropagating oscillations as a function of bias frequency introduced by the Faraday rotator.

2.4 Frequency Locking in a Ring Phase-Conjugate Gyro

The rotation sensing ability of a conventional ring laser gyroscope is limited by the onset of frequency locking (zero beat frequency) at low rotation rates. This happens due to coupling of the otherwise independent counterpropagating laser oscillations by backscattering from, for example, the mirror surfaces and gain medium.[9] A ring

resonator containing a phase conjugate mirror with gain can also act as an optical gyroscope, with improved locking characteristics.[4,5] We have studied the frequency locking behavior of a ring phase conjugate optical gyroscope both theoretically and experimentally. The phase-conjugate mirror is a photorefractive crystal that phase conjugates an input beam via four-wave mixing.[10] The dynamics of beam coupling in the medium are described by the coupled-wave equations for the beam amplitudes, and an equation for the temporal buildup of the photorefractive grating. We use boundary conditions appropriate for a ring cavity with nonreciprocal phase shift, and use nonzero values for a weak seed beam at pump frequency, injected into the oscillator along the same direction as the phase conjugate output.

The frequency difference between the counterpropagating waves is studied as a function of the seed intensity and the nonreciprocal phase shift using the experimental geometry shown in Fig. 5. The experimentally observed behavior of the beat frequency with time at 20° nonreciprocal phase shift and for various seed powers is shown in Fig. 6. In each case, seed light was first introduced into the cavity at time t = 0. At the lowest injection levels, the beat behavior was sinusoidal and was almost indistinguishable from the no seed case. As the seed level was increased, significant deviation from simple sinusoidal behavior was seen. As the the seed level was further increased, complete frequency locking of the oscillator was observed at normalized seed level of 2×10^{-3}, as evidenced by the lack of fringe motion shown in Fig. 6.

In Fig. 7, we plot the beat signal $I(t_n)$ as a function of normalized time t_n at various seed levels ϵ, keeping the other parameters fixed at the following values: the coupling strength γl is equal to 2, the product of the mirror reflectivities in the ring ($= r_1^2\, r_2^2 \equiv R$) is 0.25 and the one-way nonreciprocal phase shift is 20°. For the case of no seed (we take $\epsilon = 10^{-12}$ for a self-starting process initiated by, say, quantum noise), the grating takes some time to establish itself, and in this time the beat signal is essentially due to the pump beam so that $I(t_n) = 1$. Once a moving grating is built up in the presence of the nonreciprocal phase shift in the ring, a sinusoidal oscillatory behavior is obtained in the beat signal with a well-defined beat frequency (equal to 0.044 Hz) at steady-state. We assume a photorefractive response time of 1 sec for the $BaTiO_3$ crystal, which is appropriate for the pump intensity used in the experiment. As we further increase the seed level, the instantaneous beat signal still exhibits a periodic behavior, with an average beat frequency slightly less than the negligible seed case. The

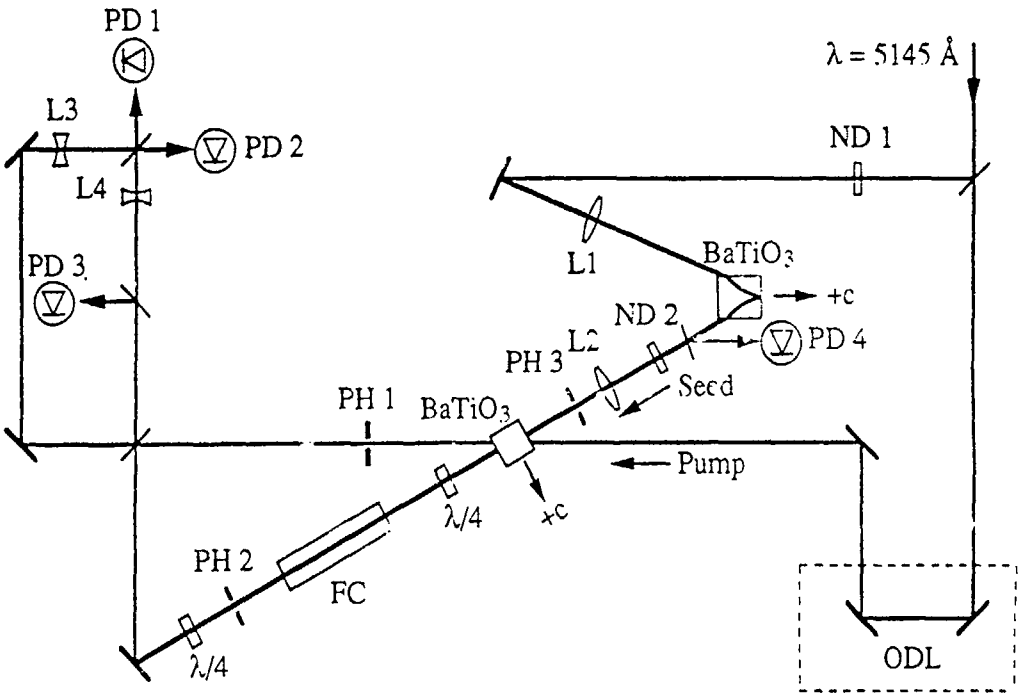

Fig. 5 The experimental schematic for ring phase-conjugate gyro.

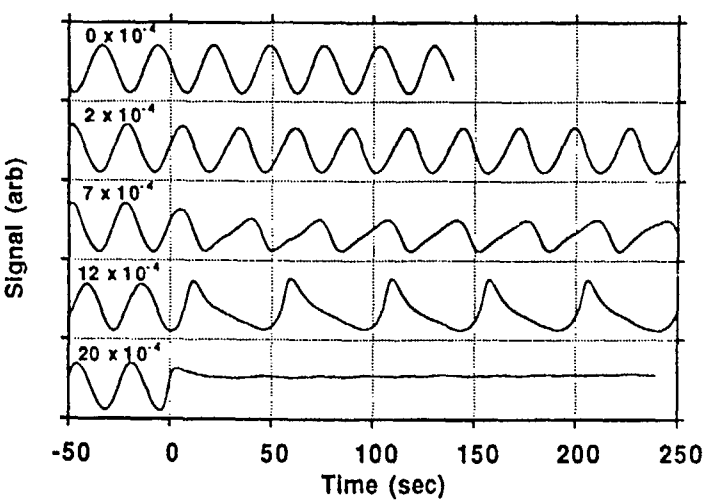

Fig. 6 Beat frequency as a function of time for the case of coherent seed injection and 20° nonreciprocal phase shift. The injected seed power normalized by the pump power was: (a) 0, (b) 2×10^{-4}, (c) 7×10^{-4}, (d) 1.2×10^{-3}, and (e) 2.0×10^{-3}. In each case, the seed light was first introduced into the cavity at time t = 0.

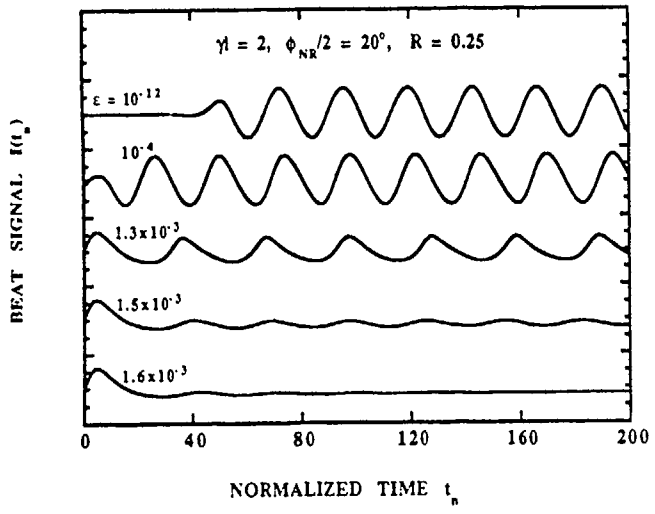

Fig. 7 Theoretical plot of beat signals as a function of time for various seed levels.

turn-on time of the oscillatory behavior in the beat signal is faster with larger seeds, with small departures from the perfectly sinusoidal shape. Both the period of oscillations and their shape depend on the seed level intensity. At still higher seed levels, the beat signal shows a sharp, asymmetric behavior, indicating that higher harmonics of beat frequency are now present in the signal. At seed levels of 2×10^{-3} of the input pump intensity, the zero beat frequency at steady-state shows that frequency locking has occurred. The experimental results are in qualitative agreement with theory.

2.5 Theory of Phase Conjugate Oscillators with Nondegenerate Operation

Optical resonators containing a phase-conjugate element have been of great interest during the last decade. For correction of intracavity aberration, the phase-conjugate element is used as an end mirror of the optical resonator. Oscillation is possible even without the conventional gain medium because of the parametric gain provided by the phase-conjugate mirror at the expense of its pumping beams. We have developed a theory for nondegenerate oscillations in a linear optical resonator with an intracavity phase conjugate element (Fig. 8). The phase-conjugate element consists of a nonlinear transparent medium that is pumped externally by a pair of counterpropagating laser beams of the same frequency w and intensity. A weak signal beam of slightly different frequency $\omega+\delta$ is injected into the resonator along its axis. We calculate the two reflection coefficients at the input mirror: one due to phase conjugation at

frequency $\omega-\delta$; and the other due to coherent reflections from the second mirror at frequency $\omega+\delta$. Similarly, we calculate the two transmission coefficients at the output mirror corresponding to the two waves at $\omega+\delta$ and $\omega-\delta$ in the resonator. For the special case of no conventional mirrors, the phase-conjugate oscillator reduces to a phase-conjugate mirror, and our general formulation yields the results of previous studies.[11,12] Nondegenerate oscillation is now possible in the presence of large linear gain or loss in the medium (Fig. 9).

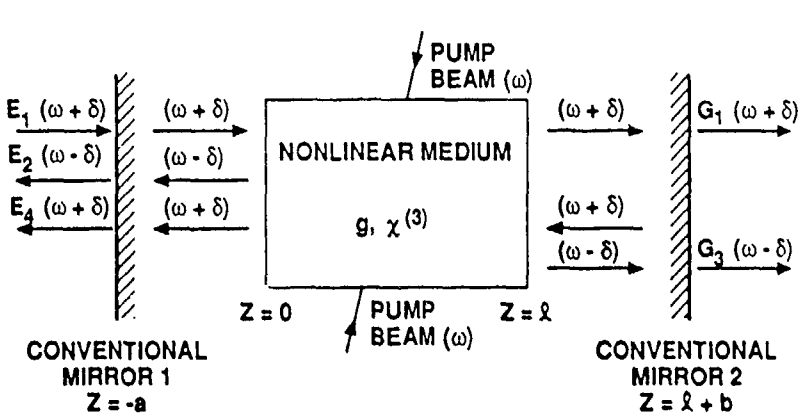

Fig. 8 Basic geometry of linear phase-conjugate oscillator using nearly degenerate four-wave mixing. In this case, the incident probe wave, whose frequency $\omega \pm \delta$ is slightly detuned from that of the pump waves (both at frequency ω), will result in a conjugate wave with an inverted frequency shift $\omega \mp \delta$. g is the linear gain coefficient.

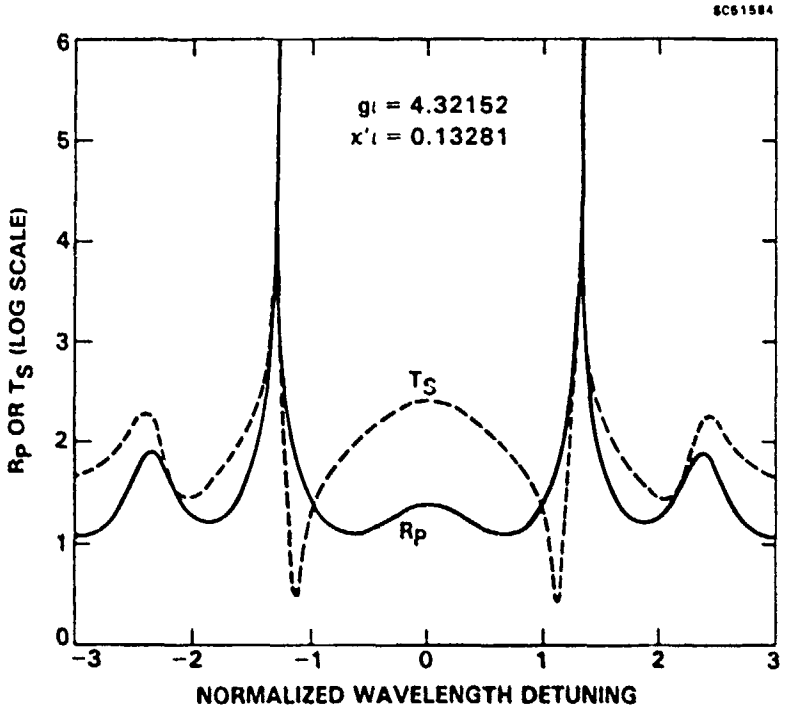

Fig. 9 Phase-conjugate power reflectivity R_p (solid curve) and coherent-power transmissivity T_s (dashed curve) versus normalized wavelength detuning ψ for $gl = 4.32152$, $\kappa'l = 0.13281$.

3.0 REFERENCES

1. J. Lam and W. Brown, Opt. Lett. 5, 61 (1980).
2. M. Ewbank, P. Yeh, M. Khoshnevisan, and J. Feinberg, Opt. Lett. 10, 282 (1985).
3. M. Cronin-Golomb, B. Fischer, S. Kwong, J. White, and A. Yariv, Opt. Lett. 7, 353 (1985).
4. J.C. Diels and I.C. McMichael, Opt. Lett. 6, 219 (1981).
5. P. Yeh, J. Tracy and M. Khoshnevisan, SPIE Proceedings 412, 240 (1983).
6. S. Kwong, A. Yariv, M. Cronin-Golomb, and B. Fischer, J. Opt. Soc. Am. A3, 157 (1986).
7. I. McMichael and P. Yeh, Opt. Lett. 12, 48 (1987).
8. J. Feinberg, Opt. Lett. 7, 486 (1982).
9. W. W. Chow et al, Rev. Mod. Phys. 57, 61 (1985).
10. M. Cronin-Golomb, B. Fischer, J. O. White, and A. Yariv, Appl. Phys. Lett. 42, 919 (1983); B. Fischer and S. Sternklar, Appl. Phys. Lett. 47, 1 (1985).
11. A. Yariv and D.M. Pepper, Opt. Lett. 1, 16 (1977).
12. D.M. Pepper and R.L. Abrams, Opt. Lett. 3, 212 (1978).

4.0 APPENDICES

Frequency Locking in Externally Seeded Phase-Conjugate Ring Gyroscopes

Frequency Locking in Externally Seeded Phase-Conjugate Ring Gyroscopes

M. J. Rosker, R. Saxena, and I. McMichael

Rockwell International Science Center

1049 Camino Dos Rios, Thousand Oaks, CA 91360

(805) 373 - 4463

ABSTRACT

Frequency locking in a photorefractive phase-conjugate ring oscillator (PCRO) was studied. For a seed beam coherent with the pump, frequency locking of the oscillator was observed, but only at feedback levels two orders of magnitude greater than that required for locking of a conventional ring laser gyroscope. At lower seed levels, higher harmonics of the beat frequency were observed. No evidence of locking was found for a seed incoherent with respect to the pump.

The first proposal for incorporating a four-wave mixing element into a rotational sensing device was made by Diels and McMichael,[1] who predicted that phase-conjugate coupling in a ring laser gyroscope would allow for the use of homogeneously broadened gain media and would lead to substantial reduction in the locking threshold. This theoretical result was confirmed by other workers.[2] In these studies, the four-wave mixing element was a transparent Kerr medium with instantaneous response, so that the dynamics of the fields in the ring was determined by the cavity round-trip time. For photorefractive phase-conjugate gyroscopes, however, the dynamics is affected by the slow speed of the material. In the first such study, the phase-conjugate ring oscillator (PCRO) was formed by a photorefractive crystal and two appropriately oriented, highly reflective mirrors.[3,4]. Later studies verified that the device acts as a phase-conjugate optical gyroscope,[5,6] i.e., the frequencies of the counterpropagating oscillations depend on the nonreciprocal, but not the reciprocal, optical path length of the resonator. The phase-conjugate nature of the counterpropagating waves in the ring eliminate the dependence on reciprocal phase shifts arising from thermal or mechanical effects.

Despite the interest in the photorefractive phase-conjugate ring oscillator, a number of issues remain unexplored. For example, frequency locking has not been considered, either theoretically or experimentally. The only previous study of the effects of injection of seed light into a photorefractive PCRO was performed by Królikowski et al.,[7] who applied a strong electric field to the photorefractive medium, a strontium barium niobate crystal, in order to shift the free-oscillation frequency from the pump frequency. A coherent seed beam at pump frequency was introduced in the oscillator in a direction counterpropagating to the pump beam. For seed/pump intensity ratios on the order of 10^{-3}, the time behavior on the output intensity from the oscillator was in some instances observed to exhibit strong, non-sinusoidal oscillations. However, in other cases the intensity varied erratically, suggesting chaotic behavior.

We have performed an investigation of the frequency locking characteristics of a photorefractive PCRO using the experimental arrangement shown in Fig. 1. The oscillator was pumped by 5 mW of p-polarized light from a CW Ar^+ laser at 514.5 nm. The Ar^+ laser, which had a coherence length of ~ 5 cm, was separated from the experiment by a Faraday isolator. The $BaTiO_3$ crystal was 6.5 mm in length and was oriented with its +c axis at approximately a 60° angle to the pump beam. The resonator was formed by the crystal and two high reflective mirrors and was determined by a pair of ~ 1 mm diameter apertures. The angle formed by the input and output pump beams was approximately 28°. One of the mirrors in the ring was 5% transmissive to provide for output coupling, which allowed for a simple way to inject the seed (through the photorefractive crystal). The cavity had an overall length of L = 90 cm and enclosed an area of A = 300 cm^2. A non-reciprocal phase shift simulating that induced by the Sagnac effect was generated with a pair of $\lambda/4$ retardation plates and a Faraday rotator. The rotation angle was continuously tunable by translation of the Faraday crystal in the magnetic field. Before each data set, this rotation angle was measured in situ.

The seed light was produced via mutually pumped phase conjugation (MPPC) in a bird-wing conjugator.[8] MPPC was utilized to insure that the seed was collinearly aligned with the oscillation beam. Because the ratio of the seed to the pump was so small, this alignment would have been extremely difficult to achieve had a simple mirror been used in place of the conjugator. A fraction of the pump beam was split off to provide one input for the bird-wing conjugator, while the other input was the pump output from the phase conjugate oscillator. The MPPC crystal was also $BaTiO_3$ and had a length of 5.8 mm. To optimize the phase conjugate reflectivity, the input beams were loosely focused into the MPPC crystal. A pair of matched, variable neutral density filters was used to controlled the seed injection power (i.e., the relevant phase conjugate return from the MPPC crystal) while keeping the ratio of the input intensities to the MPPC crystal nearly constant.

An optical delay line was used to control the mutual coherence of the pump and the seed light. For those experiments where the seed and pump were intended to be incoherent, the delay line was adjusted by roughly 30 cm, a distance longer than the coherence length of the pump source but shorter than the cavity length L.

The beat frequency between the pump and the phase conjugate wave which builds in the oscillator in the presence of a nonreciprocal phase shift was measured by overlapping the two counterpropagating directions (with appropriate relative delay) onto two photodiodes. The photodiodes were positioned 90° out of phase with one another so that the direction of the fringe motion could be inferred. A third photodiode monitored the intensity level in the phase conjugate direction, while a fourth was used to measure the injected seed power.

As an initial check, the seed arm was blocked and the beat frequency was measured as a function of the applied non-reciprocal phase shift. The expected linear dependence was observed over a wide range of range of non-reciprocal phase shifts. "Dancing modes" behavior[6] was not a limitation, although for large applied phase shifts we did (in a few instances) observe an abrupt change in the mode pattern, phase conjugate efficiency, and beat frequency. The null shift, which is the beat frequency measured for no applied non-reciprocal phase shift, was observed to be small and fairly repeatable. We attribute our differences from Ref. [6] to the fact that our resonator was physically larger and more well-defined (by the two apertures) and because we did not tightly focus into the photorefractive crystal.

Beat frequency measurements were made with a variable amount of seed light which was coherent with respect to the pump source. Data was collected by measuring the frequency shift between the counterpropagating directions at different seed injection levels at each of several non-reciprocal phase shifts. Typical raw results obtained at one particular non-reciprocal phase shift level are shown in Fig. 2. At the lower injection levels, the beat signal was sinusoidal and was almost indistinguishable from the no seed case. However,

as the seed level was increased, significant deviation from simple sinusoidal behavior was seen. This behavior resembles that reported in Ref. [7] for the phase-conjugate intensity; however, our data was apparently much more reproducible. The phase-conjugate reflectivity was observed to oscillate similarly. As the the seed level was further increased, complete frequency locking of the oscillator was observed. To verify that locking had occurred, data was collected for hours; the motion of the fringe patterns over these periods was slow and erratic and was attributed to thermal drift of the interferometer.

For no seed, the power spectrum of the data consisted of a single peak at the beat frequency. As the seed level was increased, a series of additional spikes was observed at frequencies which were integer multiples of that of the strongest peak, with amplitudes that displayed a power law dependence with harmonic number (Fig. 3). As the seed level was increased, the slope of this fit decreased. Locking occurred abruptly after this coefficient dropped below about 10 dB/harmonic.

We also measured the dependence of the beat frequency on seed level for several fixed non-reciprocal phase shifts. The beat frequency was essentially unaffected by a weak seed, but then dropped gradually to zero (locking) as the seed level was increased (Fig. 4). As expected, the locking threshold became greater as the non-reciprocal phase shift increased.

Direct comparison of these results with that of a conventional ring laser gyroscope (RLG) is complicated by the unfavorable scale factor of the PCRO, which results from the long time constant of the photorefractive crystal. From Fig. 4, a 5° applied non-reciprocal phase shift (in each direction) was shown to lock for seed levels of $R \sim 3 \times 10^{-4}$. Given the area subtended by this particular gyroscope, this phase shift is equivalent to that produced via the Sagnac effect with an $\Omega = 36$ rad/sec rate of rotation. A conventional gyroscope would be expected to lock according to the relation:

$$\Omega_l \approx \frac{c\,\lambda\,r}{8\,\pi\,A} \qquad (1)$$

where Ω_l is the locking frequency, r is the amplitude scatter coefficient, and A is the area enclosed by the cavity.[9] Taking $\Omega_l = 36$ rad/sec, a similar RLG would therefore lock for with a scatter reflectivity $R = |r|^2 \geq 3 \times 10^{-2}$. The PCRO was therefore measured to have a locking threshold two orders of magnitude smaller than that of the RLG.[10]

These experiment were repeated using a seed beam which was incoherent with respect to the pump light to test the sensitivity of the gyroscope to scattering from cavity elements more than one coherence length away from the phase-conjugate crystal, e.g., the cavity mirrors and the Faraday rotator apparatus. No difference in the fringe pattern whatsoever was observed compared to the no-seed case, even for relative seed powers as high as $\sim 3 \times 10^{-3}$, an order of magnitude greater power than that at which locking was observed for the coherent seed case. However, the phase-conjugate intensity displayed erratic transient behavior reminiscent of that observed in Ref. [7].

In conclusion, we have observed frequency locking behavior in a photorefractive phase-conjugate ring oscillator when a weak seed, coherent with respect to the pump, is injected into the oscillator. Locking thresholds were found to be significantly more favorable than those expected for a similar conventional RLG. For intermediate power levels, the beat signal displayed curious harmonic structure. This behavior provides insight into the locking mechanism for the PCRO, which we believe to be related to the development of competing gratings in the phase conjugate crystal.[11] The PCRO was determined to be relatively insensitive to incoherent optical feedback.

This work was sponsored by Air Force Office of Scientific Research, contract No. F49620-88-C-0023.

REFERENCES

1. J.-C. Diels, I. C. McMichael, "Influence of Wave-Front-Conjugated Coupling on the Operation of a Laser Gyroscope," Opt. Lett. **6**, 219-221 (1981).

2. P. Yeh, J. Tracy, M. Khoshnevisan, "Phase Conjugate Ring Gyroscopes," Proc. Soc. Photo-Opt. Instrum. Eng. **412**, 240-245 (1983).

3. M. Cronin-Golomb, B. Fischer, J. O. White, A. Yariv, "Passive Phase Conjugate Mirror Based on Self-Induced Oscillation in an Optical Ring Cavity," Appl. Phys. Lett. **42**, 919-921 (1983).

4. M. Cronin-Golomb, B. Fischer, J. O. White, A. Yariv, "Theory and Applications of Four-Wave Mixing in Photorefractive Media," IEEE Journal of Quantum Electronics **QE-20**, 12 (1984).

5. B. Fischer, S. Sternklar, "New Optical Gyroscope Based on the Ring Passive Phase Conjugator," Appl. Phys. Lett. **47**, 1-3 (1985).

6. J. P. Jiang, J. Feinberg, "Dancing Modes and Frequency Shifts in a Phase Conjugator," Opt. Lett. **12**, 266-268 (1987).

7. W. Królikowski, B. S. Chen, M. Cronin-Golomb, in *Photorefractive Materials, Effects, and Devices* (Aussois, France, 1990), pp. 212-215.

8. M. Ewbank, "Mechanism for Photorefractive Phase Conjugation Using Incoherent Beams," Opt. Lett. **13**, 47-49 (1988).

9. F. Aronowitz, "The Laser Gyro," in *Laser Applications*, M. Ross, Eds. (Academic Press, New York, 1971), pp. 133-200.

10. Note that seed level is only a lower bound upon the actual value of R for the PCRO. No attempt was made to estimate the scattering amplitude within the $BaTiO_3$ crystal, but such scattering is known to be significant.

11. R. Saxena, M.J. Rosker, and McMichael I., in preparation.

FIGURE CAPTIONS

Fig. 1: The experimental schematic. Key: ND = neutral density filter, L = lens, PH = pinhole, PD = photodiode, FC = Faraday crystal, $\lambda/4$ = quarter wave retardation plate, ODL = optical delay line. The ODL determines the relative coherence of the pump and seed beams.

Fig. 2: Beat signal as a function of time for the case of coherent seed injection. The injected seed power normalized by the pump power was: (a) 0, (b) 2×10^{-4}, (c) 7×10^{-4}, (d) 1.2×10^{-3}, and (e) 2.0×10^{-3}. In each case, the seed light was first introduced into the cavity at approximately time $t = 0$.

Fig. 3: A typical power spectrum for the coherent seed experiment. The dashed line represents a fit of the peak maxima to a straight line, with a slope of -18.5 dB/harmonic.

Fig. 4: Beat frequency vs. seed level for several values of non-reciprocal phase shift. The beat frequency was taken to be the value of the lowest frequency harmonic of the power spectrum. The solid lines are guides to the eye.

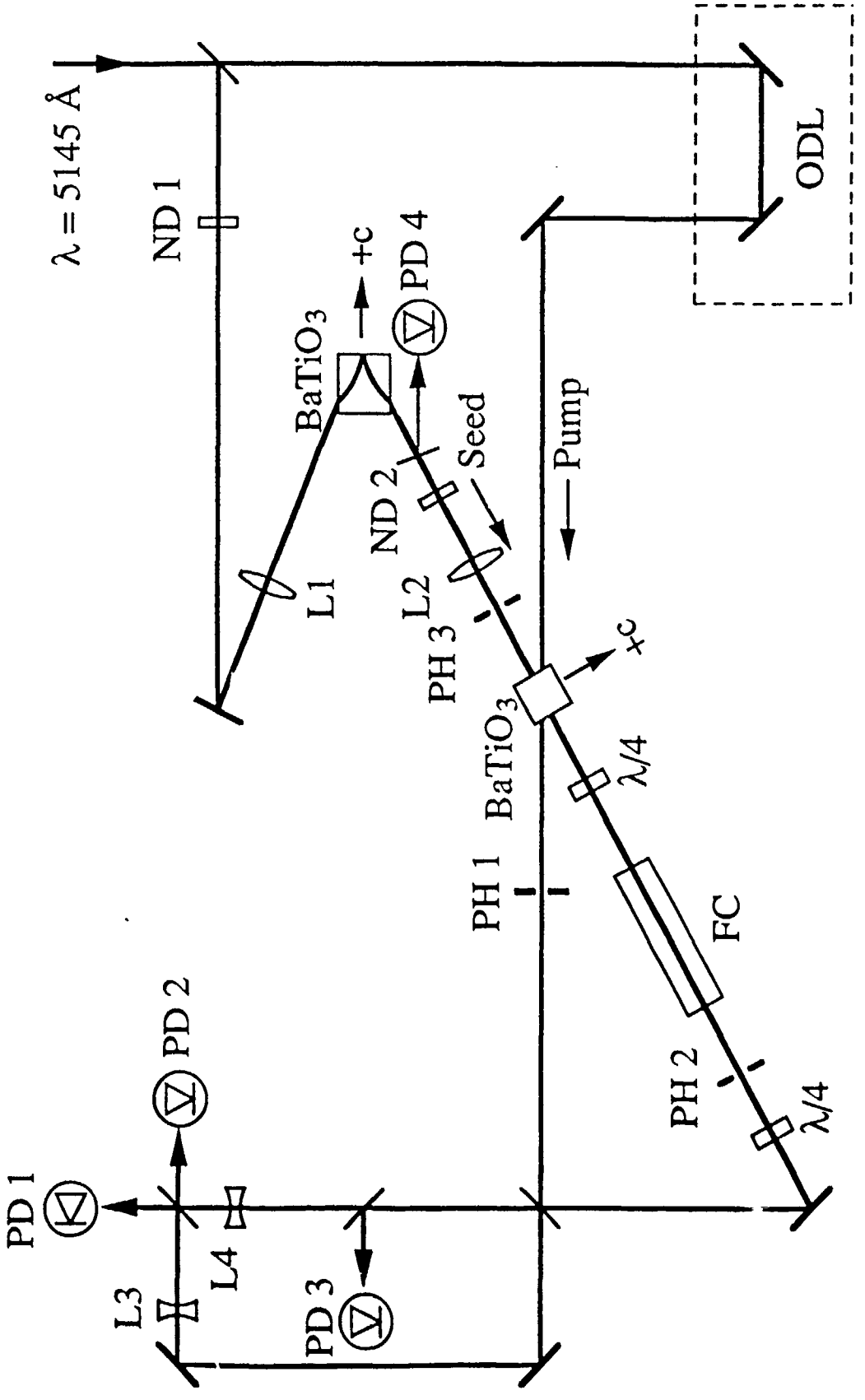
λ = 5145 Å
ND 1
ODL
+c
PD 4
BaTiO3
Seed
Pump
ND 2
L1
L2
PH 3
+c
BaTiO3
λ/4
PH 1
FC
PH 2
λ/4
PD 2
PD 1
L4
L3
PD 3

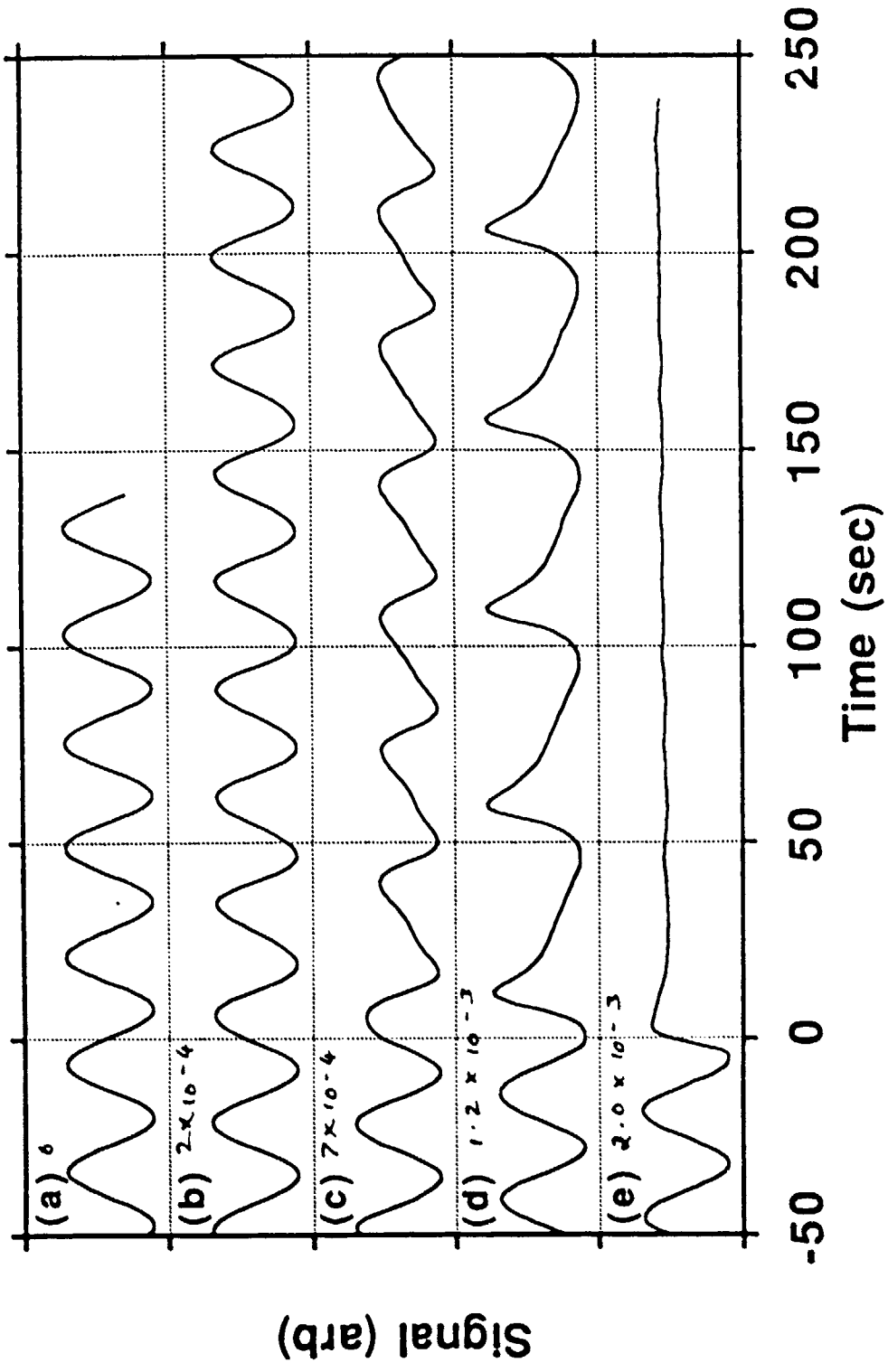
(a) 0
(b) 2×10⁻⁴
(c) 7×10⁻⁴
(d) 1.2 x 10⁻³
(e) 2.0 x 10⁻³
-50
0
50
100
150
200
250
Time (sec)
Signal (arb)

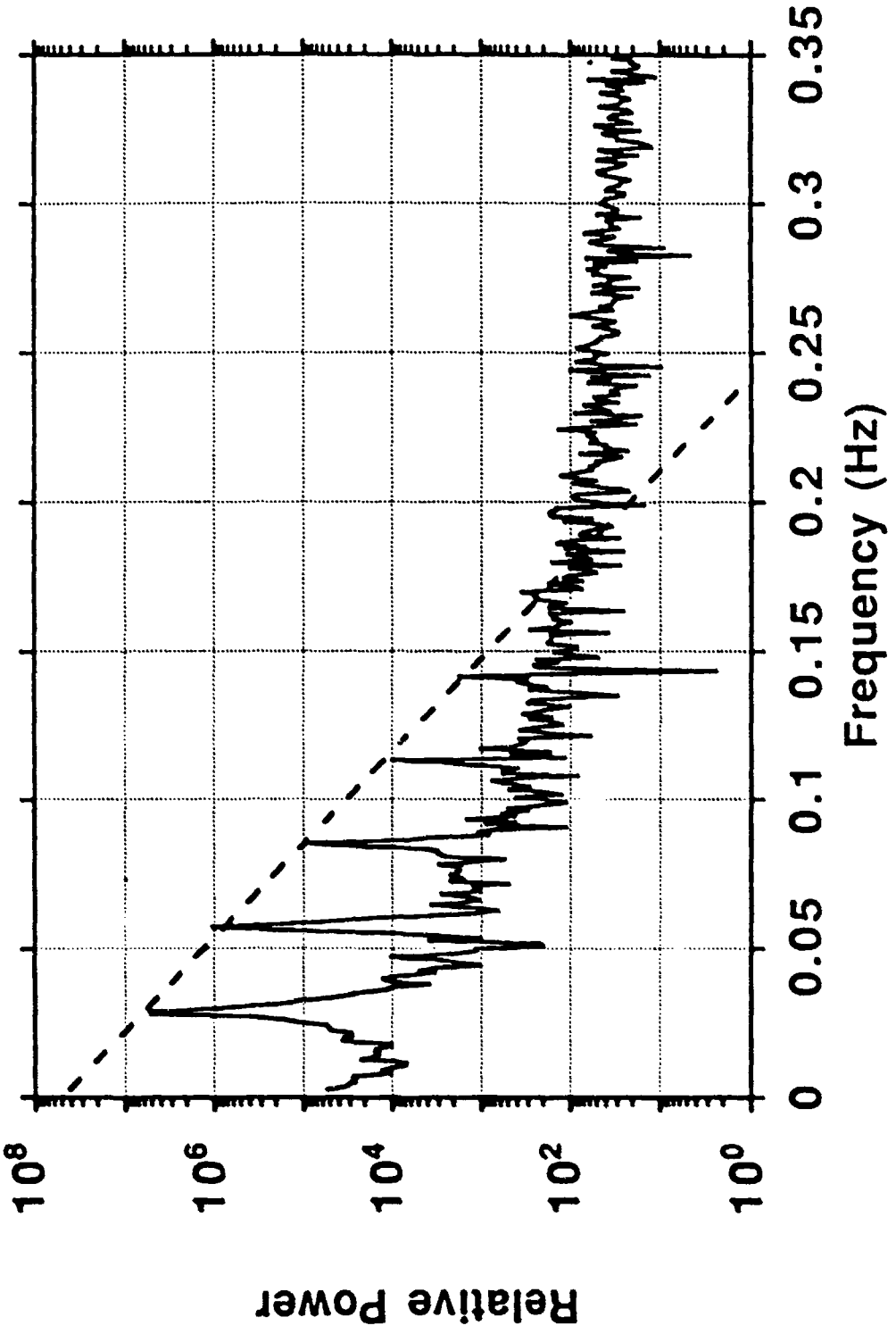
Relative Power
10^8
10^6
10^4
10^2
10^0
0
0.05
0.1
0.15
0.2
0.25
0.3
0.35
Frequency (Hz)

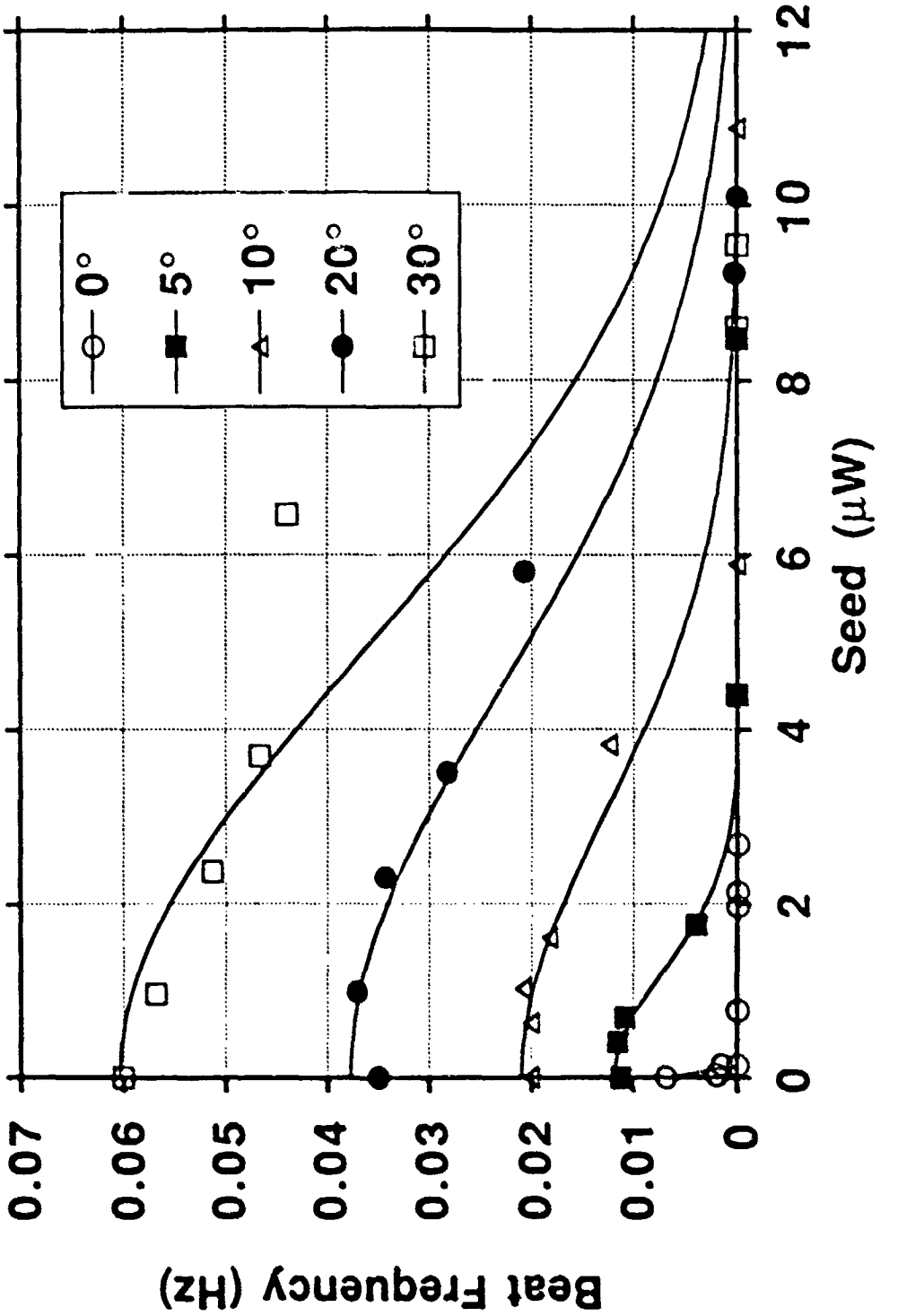
0°
5°
10°
20°
30°
Seed (μW)
0
2
4
6
8
10
12
Beat Frequency (Hz)
0.07
0.06
0.05
0.04
0.03
0.02
0.01
0

Theory of Frequency Locking in Externally Seeded Phase-Conjugate Ring Oscillators

Theory of Frequency Locking in Externally Seeded Phase-Conjugate Ring Oscillators

R. Saxena, M. J. Rosker and I. McMichael

Rockwell International Science Center

1049 Camino Dos Rios, Thousand Oaks, CA 91360

(805) 373 - 4463

ABSTRACT

The frequencies of the counterpropagating waves in a photorefractive phase-conjugate ring oscillator depend on the nonreciprocal optical path length. We examine the frequency locking behavior when a weak seed beam is injected into the oscillator. For a given coupling strength and mirror reflectivity, the nonreciprocal phase shift at which locking occurs is directly proportional to the field strength of the coherent seed beam. Higher harmonics of the beat frequency occur at seed levels close to locking and are accounted for qualitatively.

1. INTRODUCTION

The optical gyroscope is now established as a practical device for rotation sensing.[Chow, 1985 #463],[Anderson, 1986 #459] The two principal configurations are the ring laser gyroscope and the fiber optic gyroscope. Although these devices are compact and exhibit impressive performance, a number of practical problems remain. A primary limitation for conventional ring laser gyroscopes is frequency locking behavior, wherein weak backscattering couples together the counterpropagating laser oscillations. At low rotation rates, the beat frequency disappears and there is a strong imbalance between the amplitudes of the counterpropagating waves.[Kühlke, 1979 #535] For this reason, homogeneously broadened gain media cannot be used in the ring due to strong coupling of the counterpropagating waves in the gain media. At present, the primary limitation associated with fiber optic gyroscopes is caused by non-reciprocal phase shifts in the fiber.[Bergh, 1984 #464],[Kersey, 1989 #465] Mechanisms involved include Faraday rotation, the Kerr effect, and polarization mode coupling.

The first proposal for incorporating a four-wave mixing element into a rotational sensing device was made by Diels and McMichael in 1981.[Diels, 1981 #451] It was predicted that phase-conjugate coupling in a ring laser gyro would allow for the use of homogeneously broadened gain media and would lead to substantial reduction in the locking threshold. This theoretical result was confirmed by other workers [Yeh, 1983 #448]. In these studies, the four-wave mixing element was a transparent Kerr medium with instantaneous response, so that the dynamics of the fields in the ring was determined by the cavity round-trip time. For photorefractive phase-conjugate gyroscopes, we expect the dynamics to be affected by the slow speed of the material. In the first such study, the phase-conjugate ring oscillator (PCRO) was formed by a photorefractive crystal and two appropriately oriented, highly reflective mirrors.[Cronin-Golomb, 1983 #462], [Cronin-Golomb, 1984 #100]. Later studies verified that the device acts as a phase-conjugate

optical gyroscope [Fischer, 1985 #447], [Jiang, 1987 #467], i.e., the frequencies of the counterpropagating waves depend on the nonreciprocal, but not the reciprocal, optical path length of the resonator. The phase-conjugate nature of the counterpropagating waves in the ring eliminate the dependence on reciprocal phase shifts arising from thermal or mechanical effects.

Photorefractive phase-conjugate fiber-optic gyros using the interferometer configuration have also been demonstrated.[Yeh, 1986 #396] The sensing fibers can be longer than the coherence length of the laser for the self-pumped phase-conjugate fiber-optic gyro.[McMichael, 1986 #458] Multimode fibers can also be used in the gyro if the polarization is preserved during phase conjugation.[McMichael, 1987 #540]

Despite the interest in the photorefractive phase-conjugate ring oscillator, a number of issues remain unexplored. For example, frequency locking has not been considered theoretically or experimentally. Furthermore, the theoretical work done to date was in the steady-state, and no attempt has been made to force the phase of the oscillations via external seeding. The only previous study of the effects of injection of seed light into a photorefractive PCRO was performed by Królikowski et al.[Królikowski, 1990 #453] In their work, a strong electric field was applied to the photorefractive medium, a strontium barium niobate crystal, in order to shift the free-oscillation frequency from the pump frequency. A coherent seed beam at pump frequency was introduced in the oscillator in a direction counterpropagating to the pump beam. For seed/pump ratios on the order of 10^{-3}, the time behavior on the output intensity from the oscillator was in some instances observed to exhibit strong, non-sinusoidal oscillations. However, in other cases the intensity varied erratically, suggesting chaotic behavior.

We describe our investigation of the frequency locking characteristics for the photorefractive PCRO. A preliminary account of some of our experimental results was reported earlier.[M. J. Rosker et al., 1991] A weak seed beam is injected into the oscillator in the direction counterpropagating to the pump beam. The injected signal has the same

frequency as the pump beam, and may be coherent or incoherent with the pump field to simulate scatter attributed to the phase conjugate and conventional mirrors, respectively. The beat frequency between the counterpropagating waves is studied as a function of the the non-reciprocal phase shift for various values of seeding level, coupling strength or losses in the ring. The experimental results are shown to be in good agreement with theory.

2. THEORY

2.1 Formulation

The geometry for the nonlinear interaction responsible for PCRO is shown in Fig. 1, where we have used the notation introduced in Refs. [Cronin-Golomb, 1983 #462],[Cronin-Golomb, 1984 #100],[Fischer, 1985 #447],[Jiang, 1987 #467] for the various beams. A pump beam at frequency ω (labelled as beam 2 in figure 1) is incident on a photorefractive crystal. Light transmitted through the crystal is directed into a ring by mirrors r_1 and r_2 and returns to the crystal as beam 4. At large coupling strengths, an oscillation beam is self-generated in the photorefractive crystal (labelled as beam 3 in figure 1) in a direction counterpropagating to the pump beam, and the transmitted beam 3 is directed back to the crystal as beam 1 by the mirrors of the ring oscillator. Since the scattered light is coherent with the pump beam, a transmission index grating is induced by the interference of these two beams. The c-axis of the crystal is oriented so that beam 3 is amplified by two-beam coupling from the pump beam 2. Similarly, beams 1 and 4, which have the same optical path in the ring, create a transmission grating with the same wavevector, with amplification of beam 1 from beam 4 by two-beam coupling. Reflection gratings are eliminated by using a laser with short coherence length. The externally seeded case is described by nonzero amplitude of beam 3 at the $z = l$ plane of the photorefractive crystal. The dynamic coupling of the four waves in photorefractive media is described by

the four-wave mixing (FWM) equations for the complex beam amplitudes, accompanied by an equation describing the time evolution of the index grating:[Cronin-Golomb, 1984 #100]

$$\frac{\partial A_1}{\partial z_n} = \mathrm{Gl}\, A_4$$

$$\frac{\partial A_2^*}{\partial z_n} = \mathrm{Gl}\, A_3^*$$

$$\frac{\partial A_3}{\partial z_n} = -\mathrm{Gl}\, A_2$$

$$\frac{\partial A_4^*}{\partial z_n} = -\mathrm{Gl}\, A_1^*$$

$$\frac{\partial G}{\partial t_n} + G = \frac{\gamma}{I_0}\left(A_1 A_4^* + A_2^* A_3\right) \quad . \qquad (1)$$

In Eqs. (1), z_n is the distance normalized with respect to the interaction length l, the z-axis is taken normal to the surface of the medium, t_n is the time normalized by the photorefractive response time, τ, G is the complex amplitude of the photorefractive grating, and A_m is the complex electric field amplitude of the m th beam. I_0 is the total light intensity equal to $\sum_{m=1}^{4} |A_m|^2$ and γ is the complex amplitude coupling constant that is equal to $\frac{i\omega n_1 e^{-i\phi}}{2c\cos\theta}$. Here n_1 is the amplitude and ϕ is the phase of the photorefractive index change. θ is the angle made by the beams with the z axis. In this paper, we consider charge transport by diffusion only, so that $\phi = 90°$, and γ is a real, positive quantity. Note that if we put the time derivative equal to zero in the grating equation and substitute the steady-state grating amplitude in the couped wave equations, then we recover the familiar FWM equations for steady-state, [Cronin-Golomb, 1984 #100]with γ replaced by $-\gamma$.

The first four equations describe the diffraction of the beams off a photorefractive grating whose evolution with time is given by the last equation of (1). The time derivatives in the field equations have been ignored because the cavity round trip time is of the order of a few nanoseconds. This is much smaller than the response time of the photorefractive medium, which is ~ 1 sec in $BaTiO_3$ for moderate laser power. Hence a quasi-stationary grating diffracts the waves, and the optical waves follow the temporal evolution of the photorefractive grating adiabatically.[Królikowski, 1990 #460] The time dependence of two-wave mixing [Solymar, 1984 #412],[Cronin-Golomb, 1987 #354],[Vachss, 1990 #541] and four-wave mixing [Królikowski, 1990 #460], [Bledowski, 1989 #472] in photorefractive media has been studied before. Its application to optical resonators with external feedback and an injected signal [Weiss, 1989 #542][Lininger, 1990 #543] has been examined in ring resonators with two-wave mixing gain only.

We now consider the introduction of a nonreciprocal phase shift equal to $\phi_{NR}/2$ for single pass round the ring cavity. In the absence of the seed beam, the self-generated oscillation beam will have a frequency different from that of the pump beam. For large coupling strength γl and small nonreciprocal phase shift ϕ_{NR}, the frequency difference δ between the pump and the oscillation beam is linearly proportional to the nonreciprocal phase shift ϕ_{NR}.[Fischer, 1985 #447],[Jiang, 1987 #467] For a seeded PCRO, two index gratings grow initially: one is the usual moving grating at frequency δ induced by the pump and the self-oscillation beam and the additional grating is the stationary grating induced by the pump and the coherent seed beam, since both fields are at frequency ω. Readout of the stationary grating by the self-oscillation beam, and the moving grating by the seed beam, will generate new fields at frequencies $\omega + \delta$ and $\omega - \delta$ respectively in the direction of the pump beam. Further interference between the newly generated field at $\omega - \delta$ and the self-oscillation beam at $\omega + \delta$ will induce a grating at 2δ and so on. Since the higher harmonics are determined by higher orders of the diffraction efficiency of the grating, a quantity that is always less than unity, the power of the various harmonics is expected to decrease with

increasing harmonic number. Note that in the absence of the seed, or if the seed is incoherent with the pump beam, there is only a single moving grating induced by the interference of the pump beam with the self-oscillation beam. Each wave diffracts into the other direction with the right amount of Doppler shift, so that no new waves are generated by readout; hence in this case, there is only one fundamental beat frequency in the PCRO. The number of grating harmonics actually generated in the seeded PCRO will depend on the level of seeding and the nonreciprocal phase shift present in the ring.

In order to account for the optical waves at frequencies $\omega + n\delta$ in either direction, where $n = 0, \pm 1, \pm 2, \ldots$ and $\delta \sim 1$ Hz for photorefractive crystals, we recall that in deriving Eqs. (1), the fast time dependence of the complex wave amplitudes A_j at the optical frequency ω was already factored out. Due to buildup of the complex photorefractive index grating, the wave amplitudes are now slowly varying with time, thus allowing for the possibility of each wave in a given direction to be a superposition of plane waves at frequencies differing by multiples of δ:

$$E_m(r,t) = \frac{1}{2} A_m(z)\, e^{i(k_m \cdot r - \omega t)} [\, 1 + e^{-i\delta t} + e^{-2i\delta t} + \ldots] + \text{c.c.}$$

$$= \frac{1}{2} A_m(z, t)\, e^{i(k_m \cdot r - \omega t)} + \text{c.c.} \quad , \qquad m = 1 \text{ to } 4 \qquad (2)$$

where we have assumed that the wave vectors for the various harmonics are the same for a given wave. This approximation is valid since δ is of the order of a few Hz in photorefractive crystals, and the power of the various harmonics rapidly falls with increasing harmonic number.

We start with the boundary conditions of zero grating present initially, so that the pump field (normalized to unity) and the small seed value ϵ assumed for the seed intensity are uniform throughout the crystal:

$$G(z_n, t_n = 0) = 0$$

$$A_2(z_n = 1, t_n) = 1$$

$$A_3(z_n = 1, t_n) = \sqrt{\varepsilon}$$

$$A_1(z_n = 0, t_n = 0) = r_1 r_2 \, e^{i\phi_{NR}/2} \sqrt{\varepsilon}$$

$$A_4(z_n = 0, t_n = 0) = r_1 r_2 \, e^{-i\phi_{NR}/2} \quad . \qquad (3)$$

Here, r_i is the amplitude reflection coefficient of the i^{th} mirror in the ring and we have neglected the cavity-induced nonreciprocal phase shifts equal to $(n \delta L) / c$, where L is the optical path length in the ring cavity. With 90 cm as a typical value of L in the experiments, δ of the order of a few Hertz and only a few harmonics contributing to the process (no more than 8 harmonics were observed experimentally) , the corresponding phase shift is indeed small. When specifying the initial value of the time variable for fields 1 and 4, we have ignored the time taken by beams 3 and 2 to propagate round the ring cavity and return to the photorefractive crystal, so that on the photorefractive time-scale, the transmitted beams return instantaneously to the crystal.[Lininger, 1990 #543] As the grating builds up at subsequent times, the transmitted intensity of the pump and seed beams will change with time due to diffraction of one beam in the direction of the other. Hence the boundary conditions for fields 1 and 4 become time-varying:

$$A_1(z_n = 0, t_n) = r_1 r_2 \, e^{i\phi_{NR}/2} \, A_3(z_n = 0, t_n)$$

$$A_4(z_n = 0, t_n) = r_1 r_2 \, e^{-i\phi_{NR}/2} \, A_2(z_n = 0, t_n) \quad . \qquad (4)$$

We directly integrate the five nonlinear, coupled equations (1) numerically, following the procedure used in Refs. [Królikowski, 1990 #460]. Due to the form of these equations, the spatial and temporal integrations can be separated; the FWM equations can be regarded as diffraction of waves by a quasi-stationary grating, so that only spatial integration is

required of these equations, while the grating equation involves temporal integration at each point in space. Furthermore, the four coupled optical wave equations can be divided into two sets of coupled equations, one for beam pair A_1 and A_4, and the other for beams A_2 and A_3.[Królikowski, 1990 #460] The first set satisfies boundary conditions at $z_n = 0$, while the second set satisfies boundary conditions at $z_n = 1$. Hence for a known grating amplitude at an instant of time t_n, we may solve each set of coupled differential equations as an initial value problem. Thus, the problem of solving coupled differential equations with two-point boundary values is avoided. From the boundary conditions (3), there is no initial grating, so that the fields are uniform throughout the medium. Substituting the uniform fields in the grating equation, we calculate the new local grating at a small increment of time Δt_n. From the first four equations of (1), the new grating causes an energy exchange between the waves, which in turn modifies the interference pattern that drives the grating, and so on until a steady-state is reached in time. In the experiment described in Section 3, the beat signal is obtained by combining the counterpropagating fields A_2 and A_3 from the ring:

$$I(t_n) = |A_2(z_n = 0, t_n) + A_3(z_n = 0, t_n)|^2 \qquad (5)$$

We will now present some numerical plots of the beat signal and examine the conditions for frequency locking.

2.2 Numerical Simulations

In Fig. 2, we plot the beat signal $I(t_n)$ as a function of normalized time t_n at various seed levels ε, keeping the other parameters fixed at the following values: the coupling strength γl is equal to 2, the product of the mirror reflectivities in the ring ($= r_1^2 r_2^2 \equiv R$) is 0.25 and the one-way nonreciprocal phase shift ($= \phi_{NR} / 2$) is 20°. For the case of no seed (we take $\varepsilon = 10^{-12}$ for a self-starting process initiated by, say, quantum noise), the

grating takes some time to establish itself, and in this time the beat signal is essentially due to the pump beam so that $I(t_n) = 1$. Once a moving grating is built up in the presence of the nonreciprocal phase shift in the ring, a sinusoidal oscillatory behavior is obtained in the beat signal with a well defined beat frequency (equal to 0.044 Hz) at steady-state. We assume a photorefractive response time of 1 sec for the $BaTiO_3$ crystal, which is appropriate for the pump intensity used in the experiment. As we further increase the seed level, the instantaneous beat signal still exhibits a periodic behavior, with an average beat frequency slightly less than the zero seed case. The turn-on time of the oscillatory behavior in the beat signal is faster with larger seeds, with small departures from the perfectly sinusoidal shape. Both the period of oscillations and the shape of the beat signal depend on the seed level intensity. At still higher seed levels, the beat signal shows a sharp, asymmetric behavior, indicating that there are higher harmonics of beat frequency now present in the signal. At seed levels of 2×10^{-3} of the input pump intensity, the beat frequency at steady-state is zero, showing that frequency locking has occurred.

Fig. 3 shows power spectrum analysis of the nonsinusoidal beat signal at a seed level of $\epsilon = 1.3 \times 10^{-3}$, the other parameters remaining the same as in Fig. 2. The power spectrum consists of several peaks at frequencies that are integral multiples of δ. The number of harmonics of the beat frequency actually generated in the PCRO and their relative amplitudes will depend on the level of seeding and the nonreciprocal phase shift present in the ring. Fig. 4 shows the amplitude of the various harmonics as a function of the harmonic number. The amplitudes fall linearly with increasing harmonic number, and a fit to the points shows a slope of – 19.2 dB per harmonic.

Fig. 5 shows the average beat frequency as a function of the nonreciprocal phase shift in the ring for various coupling strengths. The seed intensity is kept fixed at $\epsilon = 10^{-4}$, the combined mirror reflectivity of the ring is taken to be 25 %, and photorefractive response time is taken to be 1 sec. Higher coupling yields a larger beat frequency, and the dependence of beat frequency on nonreciprocal phase shift is no longer linear at strong

coupling. A qualitatively similar behavior is obtained by varying losses in the ring for a fixed coupling strength (see Fig. 6). Smaller losses in the ring yield higher beat frequency accompanied with nonlinear dependence of the average beat frequency on the nonreciprocal phase shift.

Fig. 7 shows the average beat frequency as a function of the nonreciprocal phase shift in the ring at various seeding levels. As the seed level is increased, the range of nonreciprocal phase shift values for which beat frequency is zero increases. In fact, the nonreciprocal phase shift at which locking occurs is directly proportional to square-root of the seed level intensity: $\phi_{NR,Lock} \propto \sqrt{\epsilon}$, similar to the result for classical ring laser gyro.[Aronowitz, 1971 #534] Hence for the two curves showing locking in the figure, the ratio of nonreciprocal phase shifts at locking (10.46 and 7.4 degrees) is approximately equal to $\sqrt{2}$, the ratio of the seed amplitudes for the two curves.

3. EXPERIMENT

3.1 Technique

The experimental arrangement is shown in Fig. &A. The oscillator was pumped by 5 mW of light from a CW Ar^+ laser at 5145 Å with a coherence length of ≈ 5 cm. The pump was linearly polarized in the p-direction. The Ar^+ laser was separated from the experiment by a Faraday isolator. The $BaTiO_3$ crystal was 6.5 mm in length and was oriented with its +c axis at approximately a 60° angle to the pump beam.

The resonator was formed by the crystal and two high reflective mirrors and was determined by a pair of ~ 1 mm diameter apertures. The angle formed by the input and output pump beams was approximately 28°. One of the mirrors was 5% transmissive to provide for output coupling. This arrangement allowed for a simple way to inject the seed. The cavity had an overall length of approximately L ≈ 90 cm and enclosed an area of about A ≈ 300 cm^2.

The non-reciprocal phase shift was generated with a pair of $\lambda/4$ retardation plates and a Faraday rotator. The rotation angle was continuously tunable by translation of the Faraday crystal in the magnetic field. Before each data set, this rotation angle was measured in situ.

The seed light was produced via mutual pump phase conjugation (MPPC) in a bird-wing conjugator.[Ewbank, 1988 #466] MPPC was utilized to insure that the seed was collinearly aligned with the pump beam. Because the ratio of the seed to the pump was so small, this alignment would have been extremely difficult to achieve had a simple mirror been used in place of the conjugator. A fraction of the pump beam was split off to provide one input for the bird-wing conjugator, while the other input was the pump output from the phase conjugate oscillator. The MPPC crystal was also $BaTiO_3$ and had a length of 5.8 mm. To optimize the phase conjugate reflectivity, the input beams were loosely focussed into the crystal. A pair of matched, variable neutral density filters was used to controlled the seed injection power (i.e., the phase conjugate return from the MPPC crystal) while keeping the ratio of the input intensities to the MPPC crystal nearly constant.

A delay line arrangement was used to insure that the pump and the seed pumps were mutually coherent at the oscillator crystal. For those experiments where the seed and pump were intended to be incoherent, the delay line was adjusted by roughly 30 cm, which was much longer than the coherence length of the pump source but shorter than the cavity length L.

The beat frequency between the pump and the phase conjugate wave which builds in the oscillator was measured by overlapping the two counterpropagating directions (with appropriate relative delay) onto two photodiodes (Diodes 1 and 2 in Fig. &A). The photodiodes were positioned 90° out of phase with one another so that the direction of the fringe motion could be inferred. Another photodiode (Diode 3) monitored the intensity level in the phase conjugate direction, while a Diode 4 was used to measure the injected seed power.

3.1.1 Results obtained without seed

As an initial check, the seed arm was blocked and the beat frequency was measured as a function of the applied non-reciprocal phase shift. The expected linear dependence was observed over a wide range of range of phase shifts (Fig. &B). "Dancing modes" behavior[Jiang, 1987 #467] was not a limitation, although for large applied phase shifts we did in a few instances observe an abrupt change in the mode pattern, phase conjugate efficiency, and beat frequency. In further contrast to Ref. [Jiang, 1987 #467], the null shift we observed, which is the beat frequency measured for no applied non-reciprocal phase shift, was both small and reasonably repeatable. We attribute our differences from Ref. [Jiang, 1987 #467] to the fact that our resonator was physically larger and more well-defined (by the two apertures) and because we did not tightly focus into the photorefractive crystal.

3.1.2 Results with coherent seed

Beat frequency measurements were next made with a variable amount of seed light which was coherent with respect to the pump source. In analogy to the locking mechanism of conventional rotation sensors, this measurement tests the locking behavior of the device when the scattering level from the phase-conjugate crystal is varied. Data was collected by measuring the frequency shift between the counterpropagating directions at different seed injection levels at each of several non-reciprocal phase shifts.

Typical raw results obtained at one particular non-reciprocal phase shift level are shown in Fig. &C. At the lowest injection levels, the beat behavior was sinusoidal and was almost indistinguishable from the no seed case (c.f. Figs. &Ca and &Cb). As the seed level was increased (Figs. &Cc and &Cd), significant deviation from simple sinusoidal behavior was seen. As discussed below, this behavior resembles that reported in Ref. [Królikowski, 1990 #453] for the phase-conjugate intensity; however, our data was apparently much more reproducible. As the the seed level was further increased, complete

frequency locking of the oscillator was observed, as evidenced by the lack of fringe motion shown in Fig. &Ce. To verify that locking had occurred, data was collected for periods as long as hours; the motion of the fringe patterns over these periods was slight and erratic and was attributed to thermal drift of the interferometer.

As described earlier, we simultaneously monitored the phase-conjugate intensity (Photodiode 3) and the seed injection level (Photodiode 4). For the "intermediate regime," where the beat frequency was non-sinusoidal in shape, the phase-conjugate intensity showed similar anomalous behavior (Fig. &D). Occasionally, the seed injection level varied slowly with time after the seed was unblocked. We believe that this behavior was related to erasure mechanisms in the bird-wing conjugator and can be neglected here.

We performed power spectrum analysis of these fringe patterns. For no seed, the power spectrum consisted of a single peak. As the seed level is increased, a series of additional spikes was observed at frequencies which were integer multiples of that of the strongest peak (for example, Fig. &E). For each data set, we observed that the amplitude of these peaks displayed a power law dependence with harmonic number (e.g., the linear fit in Fig. &E). The relative amplitude of these harmonics increased with seed power. Fig. &F shows the power law coefficient obtained from the data fits as a function of the relative seed power. Locking generally occurred abruptly after this coefficient dropped below 10 dB/harmonic.

We also measured the dependence of the beat frequency on seed level for several fixed non-reciprocal phase shifts (Fig. &G). For those cases where more than one spectral peak was observed, the beat frequency was taken to be the value of the lowest frequency harmonic. For each non-reciprocal phase shift, the beat frequency was essentially unaffected for a weak seed, but then dropped gradually to zero (locking) as the seed level was increased.

These results are expressed in a more meaningful manner in Fig &H, in which the beat frequency is plotted as a function of non-reciprocal phase shift at various fixed seed

level. Note that Fig. &H was constructed by fitting the raw data of Fig. &G to an assumed curve (an exponential). Deviation from the ideal linear behavior is apparent.

3.1.3 Results with incoherent seed

These experiment were repeated using a seed beam which was incoherent with respect to the pump light. Such a situation can be thought of as measuring the sensitivity of the gyroscope to scattering from cavity elements more than one coherence length away from the phase-conjugate crystal, i.e. the cavity mirrors and the Faraday rotator apparatus.

Typical results are shown in Fig. &H. No apparent difference in the fringe pattern was observed whatsoever compared to the seed-free case, even for relative seed powers as high as $\sim 3 \times 10^{-3}$. This power, it should be noted, represents a value of at least an order of magnitude greater than that at which higher order harmonics were first resolved in the coherent seed case. However, the phase-conjugate intensity displayed erratic transient behavior (Fig. &I) reminiscent of that observed by [Królikowski, 1990 #453].

4. DISCUSSION

Comparison of experiment and theory

If we compare the theoretical plots of the beat signal shown in Fig. 2 with the experimentally observed behavior shown in Fig. 2 of Ref. [M. J. Rosker et al., 1991], we notice that though there is an asymmetric shape of the beat signals with increasing seed level, the modulation of the beat signal is not reproduced exactly in the theoretical curves. This is because of the simple expression for the beat signal (see Eq. (5)) that is assumed in calculating the theoretical curves; the reflectivity / transmissivity of the various beamsplitters used for monitoring the signal is not taken into account. For a nonreciprocal phase shift ($= \phi_{NR} / 2$) of 20°, the beat frequency was zero for a seed level of 2×10^{-3}, which is identical to the experimentally measured seed/pump ratio for frequency locking.

The amplitudes of the various harmonics fall linearly with increasing harmonic number (see Fig. 4), and a fit to the points shows a slope of – 19.2 dB per harmonic. This is in good agreement with the experimentally measured value of - 18.5 dB / harmonic reported in Ref. [M. J. Rosker et al., 1991] for the same set of parameters.

In trying to obtain theoretical curves that qualitatively agree with experimental data, the parameters that can be adjusted are the coupling strength in the photorefractive crystal and the losses in the ring. The experimentally observed behavior of beat frequency with nonreciprocal phase shift is linear even for large nonreciprocal phase shifts of 30°. This implies that the coupling strength must be small, otherwise Fig. 5 predicts a nonlinear behavior of beat frequency δ with nonreciprocal phase shift ϕ_{NR} for large coupling strength γl.

Comparison with Królikowski

Phase conjugate intensity oscillates because of two-wave mixing!

Chaos

Mechanism for locking

Higher order gratings

Implications to rotation sensing

Comparison with conventional gyroscopes

Scale factor

5. CONCLUSION

REFERENCES

FIGURE CAPTIONS

Fig. 1: Geometry for the photorefractive phase-conjugate ring oscillator.

Fig. 2: Beat signal from the ring as a function of normalized time for various seed intensities. The coupling strength γl is equal to 2, the product of the mirror reflectivities in the ring (= R) is 0.25 and the one-way nonreciprocal phase shift (= ϕ_{NR} / 2) is 20°.

Fig. 3: Power spectrum of the beat signal at seed level $\varepsilon = 1.3 \times 10^{-3}$. The other parameters are the same as in Fig. 2.

Fig. 4: Amplitude of the harmonics as a function of harmonic number. The parameter values are the same as in Fig. 3.

Fig. 5: Average beat frequency as a function of the nonreciprocal phase shift for various coupling strengths. $\varepsilon = 10^{-4}$, R = 0.25, and τ = 1 sec.

Fig. 6: Average beat frequency as a function of the nonreciprocal phase shift for various losses in the ring. $\varepsilon = 10^{-4}$, γl = 2, and τ = 1 sec.

Fig. 7: Average beat frequency as a function of the nonreciprocal phase shift at various seed levels. γl = 2, R = 0.25, and τ = 1 sec.

Fig. &A: The experimental schematic.

Fig. &B: Beat frequency as a function of non-reciprocal phase shift for the case of no injected seed.

Fig. &C: Beat frequency as a function of non-reciprocal phase shift for the case of coherent seed injection. The injected seed power normalized by the pump power was: (a) 0, (b) 2×10^{-4}, (c) 7×10^{-4}, (d) 1.2×10^{-3}, and (e) 2.0×10^{-3}. In each case, the seed light was first introduced into the cavity at time t = 0.

Fig. &D: A typical measured fringe pattern, phase-conjugate reflectivity, and seed injection level measured for the case of coherent seed injection. The normalized seed injection was ***.

Fig. &E: A typical power spectrum. The solid line represents a fit of the peak maxima to a line.

Fig. &F: Power law coefficient obtained from the data fits as a function of the relative seed power. For seed injection levels below *, only one peak was resolvable in the power spectrum. For seed injections above *, locking occurred.

Fig. &G: Beat frequency vs. seed level for several values of non-reciprocal phase shift.

Fig. &H: Beat frequency as a function of non-reciprocal phase shift for the case of incoherent seed injection. The injected seed power normalized by the pump power was: (a) 0 and (b) 7×10^{-4}. In the latter case, the seed light was first introduced into the cavity at time $t = 0$.

Fig. &I: Transient behavior reminiscent of that observed by [Królikowski, 1990 #453] was recorded in the phase-conjugate intensity measurements (Fig. &I).

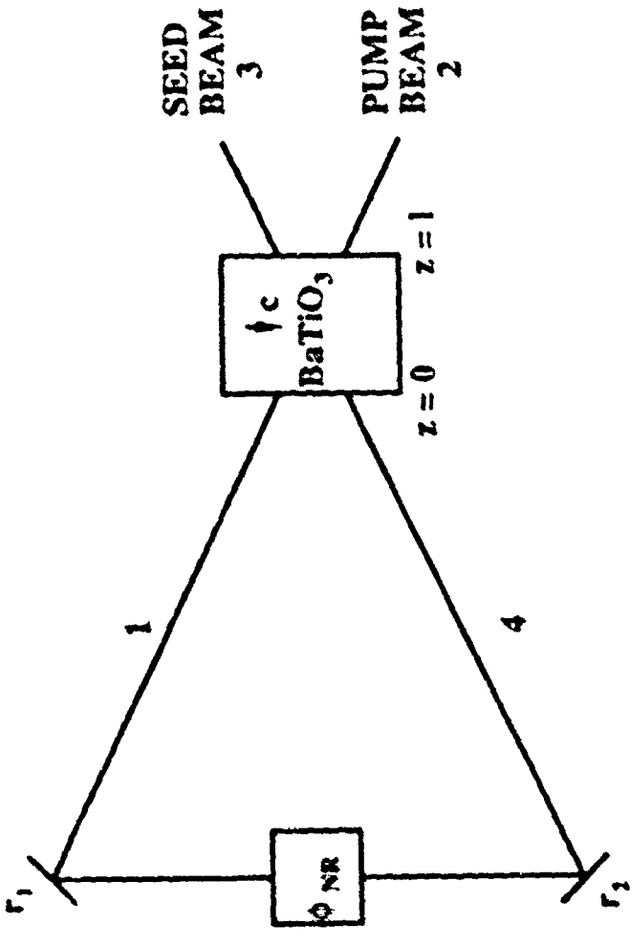
SEED BEAM 3
PUMP BEAM 2
z = l
z = 0
c
BaTiO3
1
4
r1
r2
NR

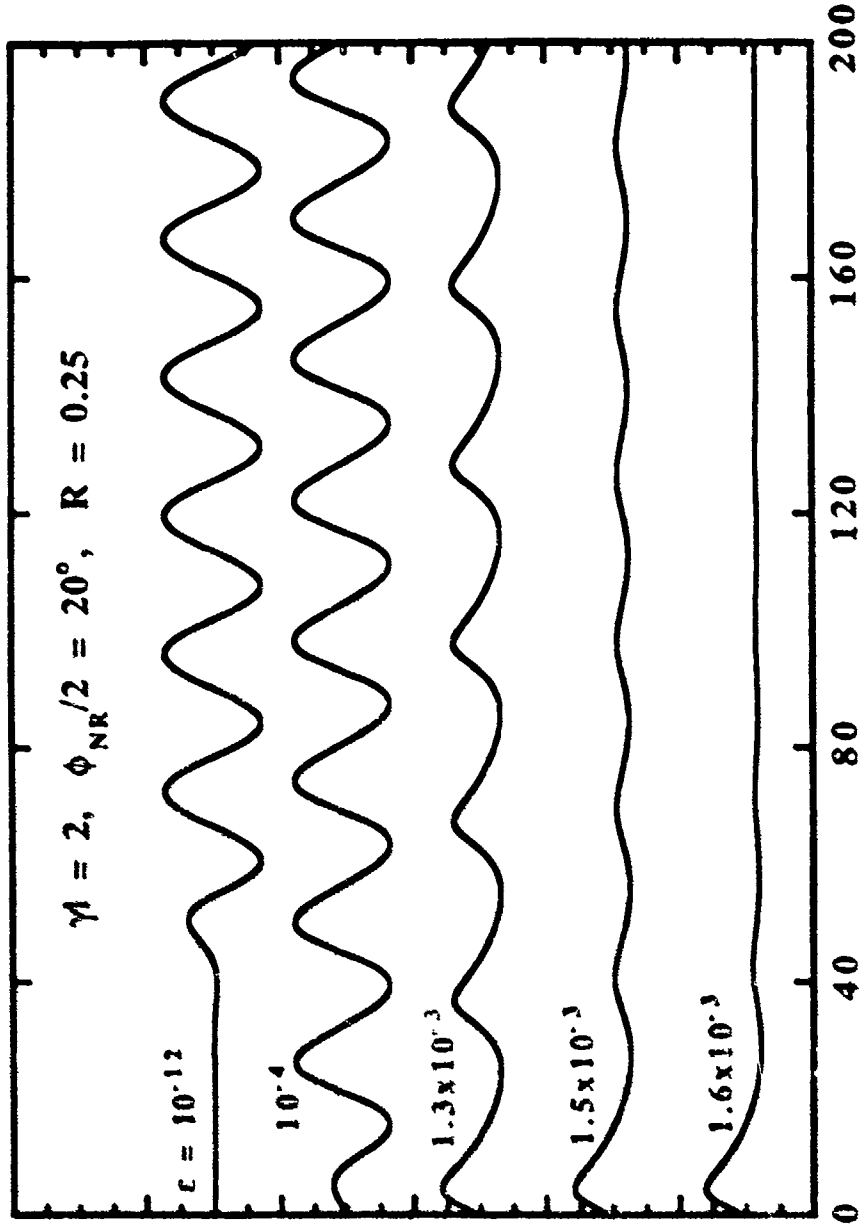
γ = 2, Φ_NR/2 = 20°, R = 0.25
ε = 10⁻¹²
10⁻⁴
1.3x10⁻³
1.5x10⁻³
1.6x10⁻³
0
40
80
120
160
200
NORMALIZED TIME t_n
BEAT SIGNAL I(t_n)

SC5538.FR

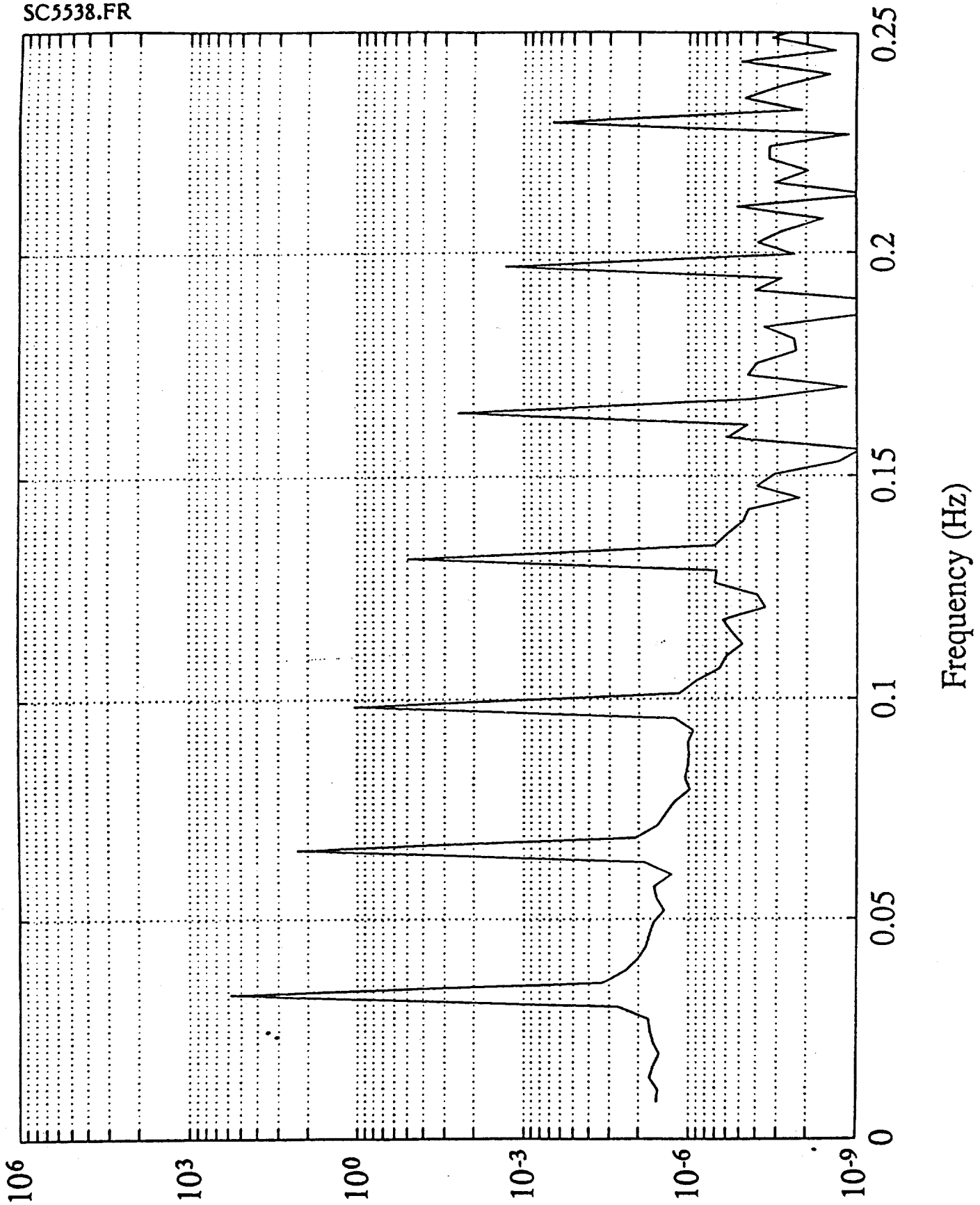
0.25
0.2
0.15
0.1
0.05
0
Frequency (Hz)
10^6
10^3
10^0
10^-3
10^-6
10^-9
Power (arb)

SC5538.FR

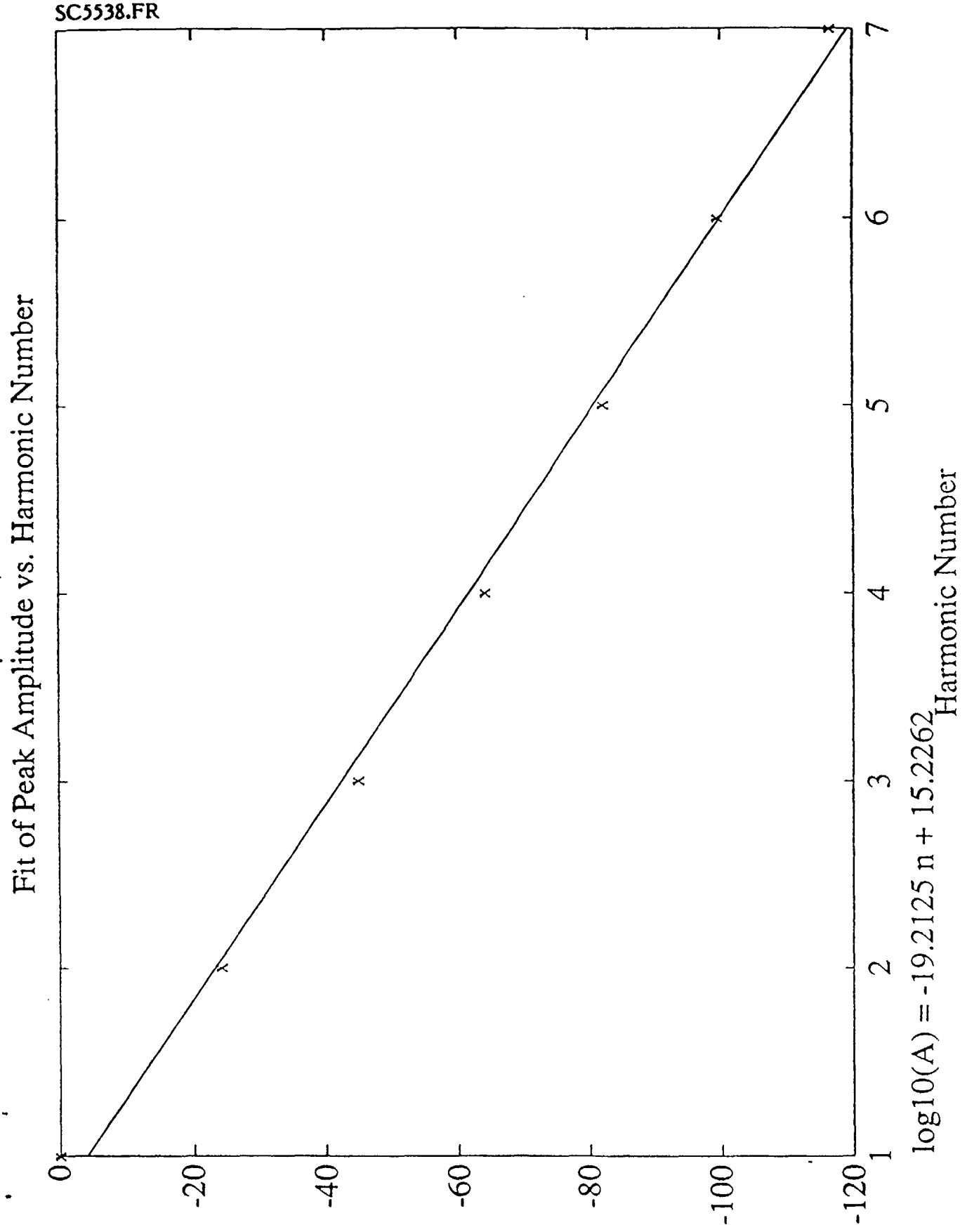
Fit of Peak Amplitude vs. Harmonic Number
log10(A) = -19.2125 n + 15.2262
Amplitude (dB)
Harmonic Number
0
-20
-40
-60
-80
-100
-120
1
2
3
4
5
6
7

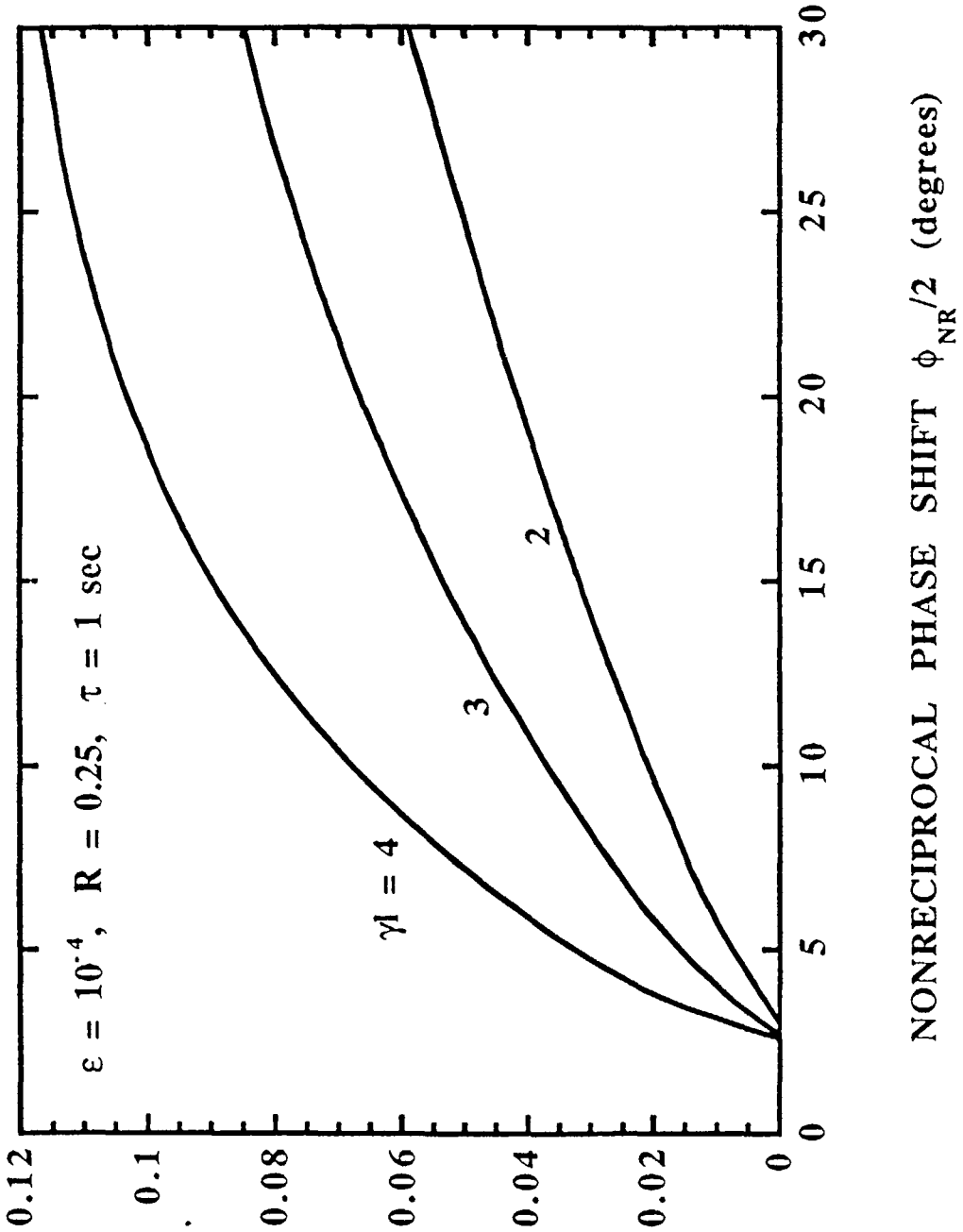
ε = 10⁻⁴, R = 0.25, τ = 1 sec
γl = 4
3
2
0.12
0.1
0.08
0.06
0.04
0.02
0
0
5
10
15
20
25
30
AVERAGE BEAT FREQUENCY δ (Hz)
NONRECIPROCAL PHASE SHIFT φNR/2 (degrees)

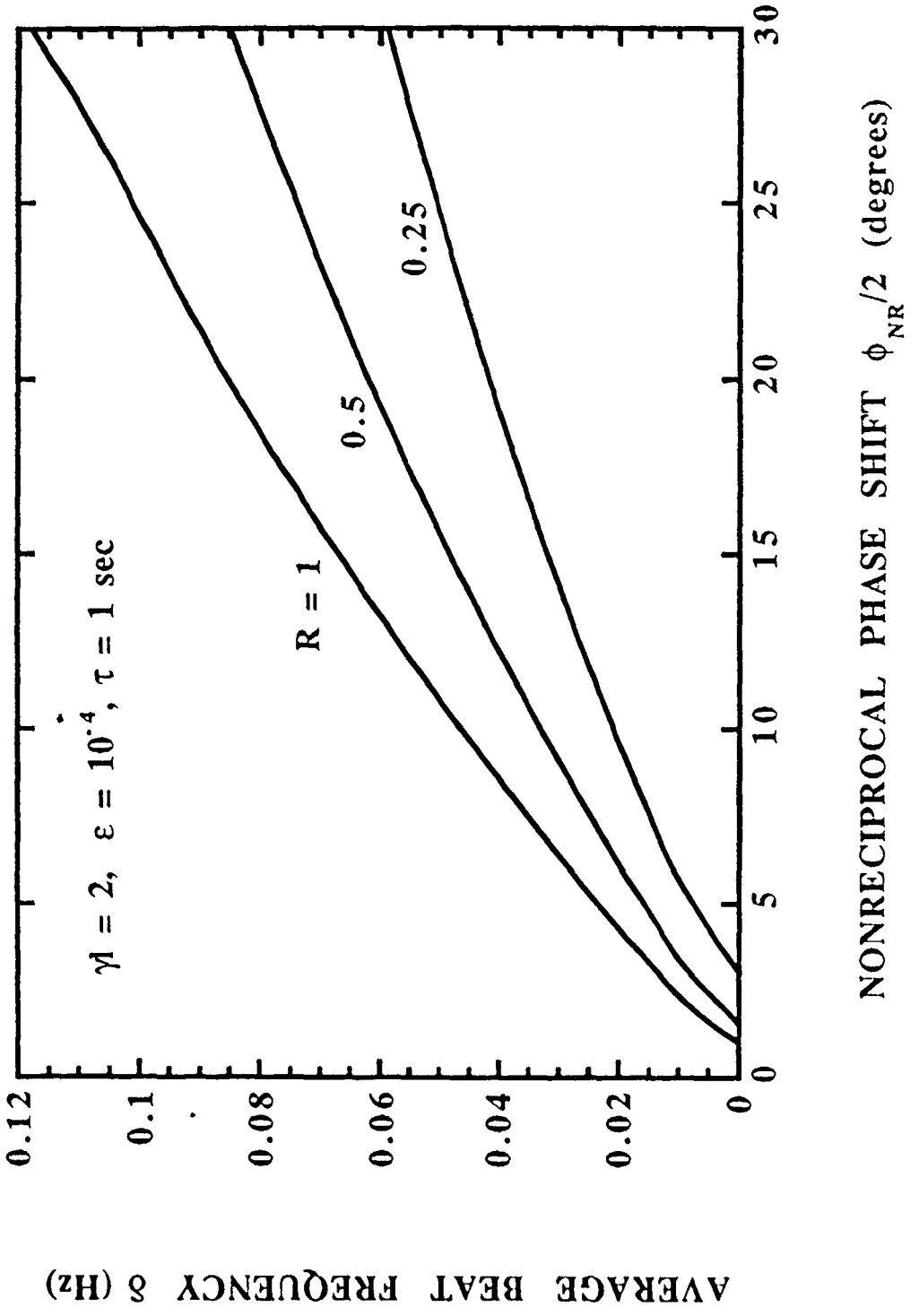
AVERAGE BEAT FREQUENCY δ (Hz)
0.12
0.1
0.08
0.06
0.04
0.02
0
0
5
10
15
20
25
30
NONRECIPROCAL PHASE SHIFT $\phi_{NR}/2$ (degrees)
$\gamma l = 2$, $\varepsilon = 10^{-4}$, $\tau = 1$ sec
R = 1
0.5
0.25

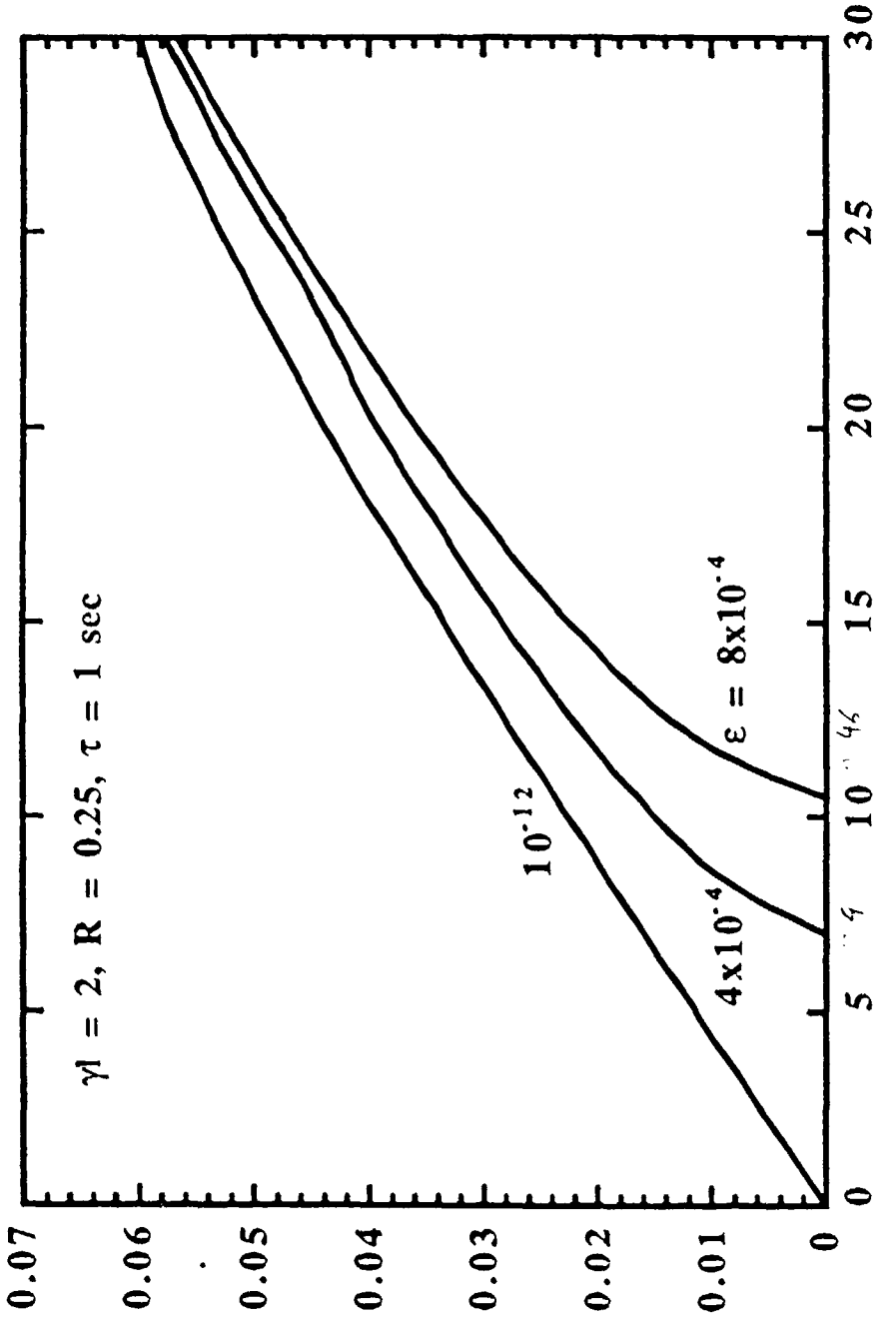
γ1 = 2, R = 0.25, τ = 1 sec
ε = 8x10⁻⁴
4x10⁻⁴
10⁻¹²
0.07
0.06
0.05
0.04
0.03
0.02
0.01
0
0
5
10
15
20
25
30

Theory of Phase-Conjugate Oscillators (I)

Rockwell International
Science Center

Reprinted from Journal of the Optical Society of America B

Theory of phase-conjugate oscillators. I

Wun-Shung Lee and Sien Chi

Institute of Electro-Optical Engineering, National Chiao Tung University, Hsinchu, Taiwan, China

Pochi Yeh and Ragini Saxena

Rockwell International Science Center, Thousand Oaks, California 91360

Received June 30, 1989; accepted March 8, 1990

We have developed a theory for nondegenerate oscillations in optical resonators containing an intracavity phase-conjugate element. The phase-conjugate element consists of a nonlinear transparent medium that is pumped externally by a pair of counterpropagating laser beams of the same frequency and intensity. Phase conjugation of an input beam of slightly different frequency occurs because of nondegenerate four-wave mixing. The theory takes into account linear absorption (or gain) in the medium and is applied to study the threshold behavior of phase-conjugate oscillators. For the special case of no conventional mirrors, the phase-conjugate oscillator reduces to an ordinary phase-conjugate mirror, and our general formulation yields the results of previous studies. Our analysis shows that the parametric gain required for oscillation increases (or decreases) as a result of linear absorption (or gain) in the medium, and oscillation can occur at a frequency different from that of the pump beams in the presence of large linear gain (or loss). The effects of linear absorption (or gain) on the filter operation are also examined.

INTRODUCTION

Optical resonators containing a phase-conjugate element have been a subject of great interest and importance. For correction of intracavity aberration, the phase-conjugate element can be employed as an end mirror of the optical resonator.[1-5] In these resonators, the phase-conjugate element acts as a unique kind of mirror (often called a phase-conjugate mirror) that combines reflection with phase reversal. Sufficiently high reflectivities are necessary for efficient operation.

In addition to their unique property of correcting wavefront aberrations, these phase-conjugate elements can also provide parametric gain and conjugate coupling between the oscillating beams. As a result of the parametric gain, oscillation is possible even without the conventional gain medium. Such oscillations are known as phase-conjugate oscillations.[6] Recent theoretical analysis indicates that the insertion of a phase-conjugate element inside a ring-laser cavity results in a reduction of the lock-in threshold and reduces the imbalance between the amplitudes of the oppositely directed traveling waves in some ring-laser systems.[7] In the extreme case of phase-conjugate oscillation without conventional gain media, it is shown that the lock-in can be completely eliminated.[8,9] The study of these resonators is also important in understanding the stability of laser oscillation in situations when backscattered laser radiation may enter the resonator and undergo parametric four-wave mixing with the oscillating beams.

Although a few special cases of phase-conjugate oscillators have been studied, a general theory that includes nondegenerate oscillations is not available. In this paper the authors develop a general theory of phase-conjugate oscillators by studying the problem of wave propagation along the axis of the resonator. The matrix method introduced in Ref. 6 is now extended to the case of nondegenerate four-wave mixing. The approach is general, so that many of the situations studied previously can be shown to be special cases in this formalism.

FORMULATION OF THE PROBLEM

Referring to Fig. 1, we consider a linear optical resonator that consists of two partially reflecting mirrors and a nonlinear medium that is pumped by a pair of external laser beams of equal intensity. These two laser beams are counterpropagating, and their frequency is ω. The nonlinear medium provides linear gain-absorption as well as parametric gain by means of optical four-wave mixing. We assume that the bandwidth of the linear gain is sufficiently broad. To investigate the general properties of such a resonator, we must treat the problem of wave propagation along the axis of the resonator.

Let the electric field of the waves be written as

$$\mathbf{E} = \begin{cases} \{\mathscr{E}_1 \exp[-\imath k_1(z+a)] + \mathscr{E}_4 \exp[\imath k_1(z+a)]\} \exp(\imath\omega_1 t) + \{\mathscr{E}_3 \exp[-\imath k_2(z+a)] + \mathscr{E}_2 \exp[\imath k_2(z+a)]\} \exp(\imath\omega_2 t) & \text{for } z < -a \\ \{\mathscr{A}_1(z)\exp(-\imath k_1 z) + \mathscr{A}_4(z)\exp(\imath k_1 z)\}\exp(\imath\omega_1 t) + \{\mathscr{A}_3(z)\exp(-\imath k_2 z) + \mathscr{A}_2(z)\exp(\imath k_2 z)\}\exp(\imath\omega_2 t) & \text{for } 0 < z < l, \\ \{\mathscr{E}_1 \exp[-\imath k_1(z-l-b)] + \mathscr{E}_4 \exp[\imath k_1(z-l-b)]\} \exp(\imath\omega_1 t) + \{\mathscr{E}_3 \exp[-\imath k_2(z-l-b)] & \\ + \mathscr{E}_2 \exp[\imath k_2(z-l-b)]\} \exp(\imath\omega_2 t) & \text{for } z > l+b \end{cases}$$

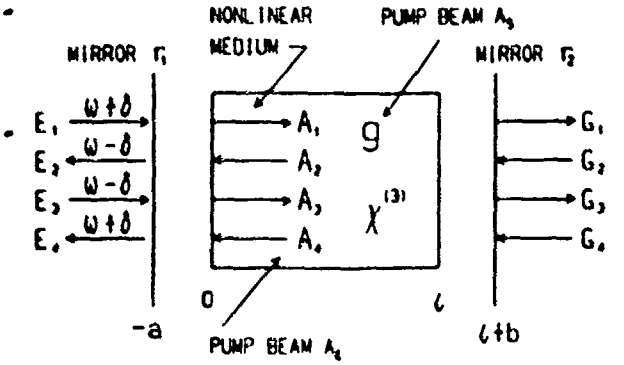

Fig. 1. Basic geometry of linear phase-conjugation oscillation by means of nearly degenerate four-wave mixing. In this case, the incident probe wave, whose frequency $\omega \pm \delta$ is slightly detuned from that of the pump waves (both at frequency ω), will result in a conjugate wave with an inverted frequency $\omega \mp \delta$. g is the linear nonsaturating background (intensity) net gain coefficient.

where $\mathcal{E}_1$, $\mathcal{E}_3$, $\mathcal{A}_1(z)$, $\mathcal{A}_3(z)$, $\mathcal{G}_1$, and $\mathcal{G}_3$ are the complex amplitudes of the plane waves traveling in the $+z$ direction and $\mathcal{E}_2$, $\mathcal{E}_4$, $\mathcal{A}_2(z)$, $\mathcal{G}_2$, and $\mathcal{G}_4$ are those of the plane waves traveling in the $-z$ direction. k_1, k_2, k_3, and k_4 are the wave numbers that correspond to the frequencies ω_1, ω_2, ω_3, and ω_4, respectively, where $\omega_1 = \omega + \delta$, $\omega_2 = \omega - \delta$, $\omega_3 = \omega_2$, and $\omega_4 = \omega_1$. E_i, A_i, and G_i are the plane waves corresponding to the complex amplitudes $\mathcal{E}_i$, $\mathcal{A}_i$, and $\mathcal{G}_i$ (where $i = 1, 2, 3$, and 4); A_3 and A_4 are pump laser beams; l is the length of the four-wave mixing interaction region; $-a$ and $l + b$ are the positions of the mirrors, and $\mathcal{A}_1$, $\mathcal{A}_2$, $\mathcal{A}_3$, and $\mathcal{A}_4$ are functions of z because of the linear absorption-gain and wave coupling owing to four-wave mixing in the nonlinear medium. The problem at hand is to derive expressions for all the wave amplitudes for a given set of boundary conditions.

If the regions between $z = -a$ and $z = 0$ and between $z = l$ and $z = l + b$ are linear dielectric media, then the following linear relationships between the wave amplitudes exist[10,11]:

$$\begin{bmatrix} A_1(0) \\ A_2(0) \\ A_3(0) \\ A_4(0) \end{bmatrix} = M_1 \begin{bmatrix} E_1 \\ E_2 \\ E_3 \\ E_4 \end{bmatrix}, \qquad \begin{bmatrix} G_1 \\ G_2 \\ G_3 \\ G_4 \end{bmatrix} = M_2 \begin{bmatrix} A_1(l) \\ A_2(l) \\ A_3(l) \\ A_4(l) \end{bmatrix}. \tag{2}$$

where M_1 and M_2 are 4×4 matrices. If we further assume that there is no Fresnel reflection at the surfaces ($z = 0$ and $z = l$) of the nonlinear medium and lump together all the reflections at $z = -a$ and $z = l + b$, then the matrices can be written as

$$M_1 = S(a)F_1, \tag{3}$$

$$M_2 = F_2 S(b), \tag{4}$$

with

$$F_i = \frac{1}{t_i} \begin{bmatrix} 1 & 0 & 0 & -r_i \\ 0 & 1 & -r_i & 0 \\ 0 & -r_i & 1 & 0 \\ -r_i & 0 & 0 & 1 \end{bmatrix}, \qquad i = 1, 2 \tag{5}$$

and

$$S(\phi) = \begin{bmatrix} \exp(-ik_1\phi) & 0 & 0 & 0 \\ 0 & \exp(ik_2\phi) & 0 & 0 \\ 0 & 0 & \exp(-ik_3\phi) & 0 \\ 0 & 0 & 0 & \exp(ik_4\phi) \end{bmatrix}, \tag{6}$$

where $\phi = a, b, l$; r_i and t_i are the amplitude reflection and transmission coefficients, respectively, of the end mirrors from the front surfaces (left sides). The matrices F_1 and F_2 account for the Fresnel reflection and transmission at the mirrors, whereas the matrices $S(a)$ and $S(b)$ account for the propagation through the bulk of the linear regions.

In the nonlinear medium between $z = 0$ and $z = l$, the waves A_1 and A_2 and the pump beams are coupled by optical four-wave mixing. The waves A_3 and A_4 and the pump beams are similarly coupled. If we assume no pump depletion of the waves A_3 and A_4 to describe oscillation near threshold, then the amplitudes $A_1(0)$, $A_2(0)$, $A_3(0)$, $A_4(0)$ and $A_1(l)$, $A_2(l)$, $A_3(l)$, $A_4(l)$ will be shown to be related by

$$\begin{bmatrix} A_1(l) \\ A_2(l) \\ A_3(l) \\ A_4(l) \end{bmatrix} = S(l)K \begin{bmatrix} A_1(0) \\ A_2(0) \\ A_3(0) \\ A_4(0) \end{bmatrix}, \tag{7}$$

where $S(l)$ and K are 4×4 matrices. Using an approach similar to that used in Ref. 6, we now determine the matrix K.

We derive this matrix by solving the coupled-mode equations for the four-wave mixing processes. As a result of four-wave mixing, the input wave $\mathcal{A}_1$ interacts with two external pumping laser beams $\mathcal{A}_3$ and $\mathcal{A}_4$, and a phase-conjugate wave $\mathcal{A}_2$ is generated. These two waves are related by the coupled-mode equation[12-15]

$$\frac{d\mathcal{A}_1^*}{dz} = \kappa_1 \mathcal{A}_2 \exp(-i\Delta k z) + \frac{g}{2}\mathcal{A}_1^*,$$

$$\frac{d\mathcal{A}_2}{dz} = \kappa_2^* \mathcal{A}_1^* \exp(i\Delta k z) - \frac{g}{2}\mathcal{A}_2, \tag{8}$$

where the amplitudes of waves 1 and 2 have been redefined in order to account for pump-induced phase modulation. $\kappa_1^* = (\omega_1/2)\sqrt{\mu/\epsilon}\,\chi^{(3)}\mathcal{A}_3\mathcal{A}_4 e^{i\phi_{34}}$ is the complex coupling coefficient, and in deriving Eqs. (8) we have assumed that the input wave and its conjugate beam are small compared with the pump beams. Then pump depletion is negligible, and $\mathcal{A}_3$ and $\mathcal{A}_4$ may be regarded as constants, so that our theory describes nondegenerate oscillation near threshold. Note that, if the two pumps have different intensities, then κ_1 becomes a function of z owing to the additional phase mismatch introduced by the unequal pumps.[12,13] In what follows we shall assume that the two pumps have equal intensities so that κ_1 is independent of z. $\Delta k = k_1 - k_2$ is the phase mismatch, and g is the linear, nonsaturable net gain (or loss) coefficient. In order to solve Eqs. (8) we introduce the new variables a_1 and a_2:

$$\mathcal{A}_1 = a_1 e^{gz/2},$$

$$\mathcal{A}_2 = a_2 e^{-gz/2}. \tag{9}$$

In terms of the new variables, the coupled equations (8) reduce to

$$\frac{d}{dz}a_1^* = i\kappa_1 a_2 \exp[-i(\Delta k - ig)z],$$

$$\frac{d}{dz}a_2 = i\kappa_2^* a_1^* \exp[i(\Delta k - ig)z]. \tag{10}$$

Solving the differential equations (10) in terms of $a_1^*(0)$ and $a_2(l)$, which are specified by boundary conditions, we obtain

$$a_1(l) = \frac{1}{D^*}\{a_1(0)s^* \exp[i(\Delta k + ig)l] - 2i\kappa_1^* a_2^*(l) \times \exp[i(\Delta k + ig)l]\} \sinh[s^*l/2],$$

$$a_2(0) = \frac{1}{D}\{-2i\kappa_2^* a_1^*(0) \sinh[sl/2] + a_2(l)s \times \exp[-i(\Delta k - ig)l]\},$$

where

$$s = [-(\Delta k - ig)^2 - 4\kappa_1\kappa_2^*]^{1/2},$$

$$D = (-g - i\Delta k)\sinh[sl/2] + s\cosh[sl/2]. \tag{12}$$

From Eqs. (9) and (11) we obtain the solutions in terms of the original variables:

$$\mathcal{A}_1(l) = \frac{1}{\alpha^*}\exp(i\Delta kl/2) \times \{[(\alpha^*)^2 - \kappa_1^*\kappa_2(\beta^*)^2]\mathcal{A}_1(0) - i\kappa_2^*\beta^*\mathcal{A}_2^*(0)\},$$

$$\mathcal{A}_2(l) = \frac{1}{\alpha}\exp(i\Delta kl/2)[i\kappa_2^*\beta\mathcal{A}_1^*(0) + \mathcal{A}_2(0)], \tag{13}$$

where

$$\alpha = \frac{1}{D}s,$$

$$\beta = \frac{2}{D}\sinh\left[\frac{sl}{2}\right]. \tag{14}$$

Equations (13) can be rewritten in matrix notation as

$$\begin{bmatrix}\mathcal{A}_1(l)\\ \mathcal{A}_2(l)\end{bmatrix} = \begin{bmatrix}M & PX\\ QX & N\end{bmatrix}\begin{bmatrix}\mathcal{A}_1(0)\\ \mathcal{A}_2(0)\end{bmatrix}, \tag{15}$$

where

$$M = \frac{1}{\alpha^*}\exp(i\Delta kl/2)[(\alpha^*)^2 - \kappa_1^*\kappa_2(\beta^*)^2],$$

$$N = \frac{1}{\alpha}\exp(i\Delta kl/2),$$

$$P = -\frac{i}{\alpha^*}\exp(i\Delta kl/2)\kappa_1^*\beta^*,$$

$$Q = \frac{i}{\alpha}\exp(i\Delta kl/2)\kappa_1^*\beta, \tag{16}$$

and X is the complex-conjugated operator, defined as $XH = H^*$, where H is an arbitrary number.

Similarly, we obtain the following matrix equation for the waves $\mathcal{A}_3$ and $\mathcal{A}_4$:

$$\begin{bmatrix}\mathcal{A}_3(l)\\ \mathcal{A}_4(l)\end{bmatrix} = \begin{bmatrix}M' & P'X\\ Q'X & N'\end{bmatrix}\begin{bmatrix}\mathcal{A}_3(0)\\ 0\end{bmatrix}, \tag{17}$$

where

$$M' = \frac{1}{\alpha}\exp(-i\Delta kl/2)[(\alpha)^2 - \kappa_1\kappa_2^*(\beta)^2],$$

$$N' = \frac{1}{\alpha^*}\exp(-i\Delta kl/2),$$

$$P' = -\frac{i}{\alpha}\exp(-i\Delta kl/2)\kappa_2^*\beta,$$

$$Q' = \frac{i}{\alpha^*}\exp(-i\Delta kl/2)\kappa_1^*\beta^*. \tag{18}$$

In arriving at Eqs. (17) and (18), we assumed exactly the same pumping, so that $\kappa_3 = \kappa_2$ and $\kappa_4 = \kappa_1$. By using Eqs. (15) and (17), we can now write the matrix K in Eq. (7):

$$K = \begin{bmatrix}M & PX & 0 & 0\\ QX & N & 0 & 0\\ 0 & 0 & M' & P'X\\ 0 & 0 & Q'X & N'\end{bmatrix}. \tag{19}$$

By using Eqs. (2)–(4) and (7), we can write the complex amplitudes G_1, G_2, G_3, G_4, E_1, E_2, E_3, and E_4:

$$\begin{bmatrix}G_1\\ G_2\\ G_3\\ G_4\end{bmatrix} = F_2S(l+b)KS(a)F_1\begin{bmatrix}E_1\\ E_2\\ E_3\\ E_4\end{bmatrix}. \tag{20}$$

Equation (20) may now be used to study the reflection and transmission properties of such a resonator. We consider the most general case, where $r_1r_2 \neq 0$, $g \neq 0$, $|\kappa_1\kappa_2^*| \neq 0$, and $\Delta k \neq 0$. Using Eqs. (5), (6), and (19) and carrying out the multiplication in Eq. (20), we obtain

$$\begin{bmatrix}G_1\\ G_2\\ G_3\\ G_4\end{bmatrix} = \frac{1}{t_2t_1t_1^*}\begin{bmatrix}F_{11} & F_{12}X & F_{13}X & F_{14}\\ F_{21}X & F_{22} & F_{23} & F_{24}X\\ F_{31}X & F_{32} & F_{33} & F_{34}X\\ F_{41} & F_{42}X & F_{43}X & F_{44}\end{bmatrix}\begin{bmatrix}E_1\\ E_2\\ E_3\\ E_4\end{bmatrix}, \tag{21}$$

where

$$F_{11} = t_1^*M\exp[-ik_1(l+b+a)] + t_1^*r_1r_2N\exp[ik_1(l+b+a)],$$

$$F_{12} = t_1P\exp[-ik_1(l+b) - ik_2a] + t_1r_1^*r_2^*Q\exp[ik_1(l+b) + ik_2a],$$

$$F_{13} = -t_1r_1^*P\exp[-ik_1(l+b) - ik_2a] - t_1r_2Q\exp[ik_1(l+b) + ik_2a],$$

$$F_{14} = -t_1^*r_1M\exp[-ik_1(l+b+a)] - t_1^*r_2N\exp[ik_1(l+b+a)].$$

$$F_{31} = t_1 Q \exp[ik_2(l + b) + ik_1 a] + t_1 r_2 r_1^* P' \exp[-ik_2(l + b) - ik_1 a],$$

$$F_{32} = t_1^* N \exp[ik_2(l + b + a)] + t_1^* r_1 r_2 M' \exp[-ik_2(l + b + a)],$$

$$F_{33} = -t_1^* r_1 N \exp[ik_2(l + b + a)] - t_1^* r_2 M' \exp[-ik_2(l + b + a)],$$

$$F_{34} = -t_1 r_1^* Q \exp[ik_2(l + b) + ik_1 a] - t_1 r_2 P' \exp[-ik_2(l + b) - ik_1 a],$$

$$F_{41} = -t_1 r_2 Q \exp[ik_2(l + b) + ik_1 a] - t_1 r_1^* P' \exp[-ik_2(l + b) - ik_1 a],$$

$$F_{42} = -t_1^* r_2 N \exp[ik_2(l + b + a)] - t_1^* r_1 M' \exp[-ik_2(l + b + a)],$$

$$F_{43} = t_1^* r_1 r_2 N \exp[ik_2(l + b + a)] + t_1^* M' \exp[-ik_2(l + b + a)],$$

$$F_{44} = t_1 r_1^* r_2 Q \exp[ik_2(l + b) + ik_1 a] + t_1 P' \exp[-ik_2(l + b) - ik_1 a],$$

$$F_{41} = -t_1^* r_2 M \exp[-ik_1(l + b + a)] - t_1^* r_1 N' \exp[ik_1(l + b + a)],$$

$$F_{42} = -t_1 r_2 P \exp[-ik_1(l + b) - ik_2 a] - t_1 r_1^* Q' \exp[ik_1(l + b) + ik_2 a],$$

$$F_{43} = t_1 r_2 r_1^* P \exp[-ik_1(l + b) - ik_2 a] + t_1 Q' \exp[ik_1(l + b) + ik_2 a],$$

$$F_{44} = t_1^* r_2 r_1 M \exp[-ik_1(l + b + a)] + t_1^* N' \exp[ik_1(l + b + a)]. \quad (22)$$

and we recall that X is the complex-conjugate operator.

If we view E_1, E_3, G_2, and G_4 as the input waves at the two mirrors, then the output waves E_2, E_4, G_1, and G_3 can be solved from Eqs. (21) in terms of E_1, E_3, G_2, and G_4.

At oscillation, a finite solution for output waves E_2, E_4, G_1, and G_3 at the two mirrors may exist even if there are no input waves. By setting $E_1 = E_3 = G_2 = G_4 = 0$ in Eqs. (21), we obtain

$$G_2 = 0 = \frac{1}{t_1 t_1^* t_2}[F_{22} E_2 + F_{24} E_4^*],$$

$$G_4 = 0 = \frac{1}{t_1 t_1^* t_2}[F_{42} E_2^* + F_{44} E_4] \quad (23)$$

For a nontrivial solution for the output waves E_2 and E_4, the determinant of the coefficients in Eq. (23) must vanish, i.e., $F_{24}^* F_{24} - F_{22}^* F_{44} = 0$. From Eqs. (22), this condition can be written as

$$\begin{aligned}&\{r_1 Q^* \exp[-ik_2(l + b) - ik_1 a] - r_2^* P'^* \exp[ik_2(l + b) + ik_1 a]\} \\ &\quad \times \{r_2 P \exp[-ik_1(l + b) - ik_2 a] + r_1^* Q' \exp[ik_1(l + b) + ik_2 a]\} \\ &= \{N'^* \exp[-ik_2(l + b + a)] + r_1^* r_2^* M'^* \exp[ik_2(l + b + a)]\} \\ &\quad \times \{r_2 r_1 M \exp[-ik_1(l + b + a)] + N' \exp[ik_1(l + b + a)]\}. \quad (24)\end{aligned}$$

where P, Q, P', Q', M, N, M', and N' are given by Eqs. (16) and (18).

The above oscillation condition depends on Δk, g, κ_1, κ_2, a, b, l, r_1, and r_2. In what follows, we investigate the oscillation condition by adjusting these parameters.

We now consider the case when there is only one input wave. For the case of incidence from the left on the mirror at $z = -a$, E_1 may be considered the incident wave, with a frequency of $\omega + \delta$. If this is the only incident wave, then $E_3 = 0$ at this mirror, while G_2 and G_4 are zero at the second mirror. The wave E_2 at $\omega - \delta$ is generated as a result of the optical four-wave mixing. The wave E_4 is produced by reflections off the second mirror at $z = l + b$. The problem at hand is to derive expressions for all the ouput waves E_2, E_4, G_1, and G_3, given an incident wave E_1 at $\omega + \delta$. Using Eqs. (21), we obtain

$$G_2 = 0 = F_{21} E_1^* + F_{22} E_2 + F_{24} E_4^*,$$

$$G_4 = 0 = F_{41} E_1 + F_{42} E_2^* + F_{44} E_4. \quad (25)$$

By eliminating E_4 we obtain the following expression for the phase-conjugate reflection coefficient:

$$r_p = \frac{E_2}{E_1^*} = -\frac{F_{21} F_{44}^* - F_{24} F_{41}^*}{F_{22} F_{44}^* - F_{24} F_{42}^*}, \quad (26)$$

while the phase-conjugate power reflectivity is given by $R_p = |r_p|^2$. Similarly, we may obtain the coherent reflection coefficient at $\omega + \delta$ as

$$r_s = \frac{E_4^*}{E_1^*} = -\frac{F_{21} F_{42}^* - F_{22} F_{41}^*}{F_{24} F_{42}^* - F_{22} F_{44}^*} \quad (27)$$

and the coherent power reflectivity is given by $R_s = |r_s|^2$.

In addition to the two reflected waves, there are also two transmitted waves, as illustrated in Fig. 1. These are the straight-through part of the incident beam G_1 at $\omega + \delta$. Reflection off the second mirror generates another incident beam at $\omega + \delta$. Phase conjugation with frequency flipping at the nonlinear medium generate the beam G_3 at $\omega - \delta$. Using Eq. (21), we obtain

$$G_1 = \frac{1}{t_2 t_1 t_1^*}[F_{11} E_1 + F_{12} E_2^* + F_{14} E_4],$$

$$G_3 = \frac{1}{t_2 t_1 t_1^*}[F_{31} E_1^* + F_{32} E_2 + F_{34} E_4^*] \quad (28)$$

Substituting Eqs. (26) and (27) for E_2 and E_4, respectively, into Eqs. (28), we obtain the expressions for the two transmission coefficients

$$t_s = \frac{G_1}{E_1} = \frac{1}{t_2 t_1 t_1^*}[F_{11} + F_{12} r_p^* + F_{14} r_s^*],$$

$$t_p = \frac{G_3}{E_1^*} = \frac{1}{t_2 t_1 t_1^*}[F_{31} + F_{32} r_p + F_{34} r_s], \quad (29)$$

while the power-transmission coefficients are given by $T_s = |t_s|^2$ and $T_p = |t_p|^2$.

The four reflection and transmission coefficients derived above for one input wave E_1 and $\omega + \delta$ are useful for studying the oscillation conditions for various types of phase-conjugate oscillator. The analysis for a single input

wave at $\omega - \delta$ is similar and may be obtained from our general formulation by taking E_3 as the input wave and $E_1 = G_2 = G_4 = 0$.

We are now ready to investigate three special cases of great interest. These are the following:

(i) No conventional mirrors ($r_1 = r_2 = 0$), so that the phase-conjugate oscillator reduces to a phase-conjugate mirror.

(ii) Only one conventional mirror ($r_1 = 0$), so that the phase-conjugate oscillator reduces to a phase-conjugate resonator, i.e., a resonator bounded by a conventional mirror and a phase-conjugate mirror.

(iii) Both conventional mirrors present ($r_1, r_2 \neq 0$), which is the phase-conjugate oscillator.

In each of the cases, we will consider four different operation conditions: (1) $\Delta k = 0$, $g = 0$, $|\kappa_1| = |\kappa_2| = |\kappa| \neq 0$, i.e., degenerate four-wave mixing without linear absorption/gain in the medium. (2) $\Delta k = 0$, $g \neq 0$, $|\kappa_1| = |\kappa_2| = |\kappa| \neq 0$, i.e., degenerate four-wave mixing with linear absorption/gain in the medium. (3) $\Delta k \neq 0$, $g = 0$, $|\kappa_1^* \kappa_2| > 0$, i.e., nondegenerate four-wave mixing in the absence of linear absorption/gain in the medium. (4) $\Delta k \neq 0$, $g \neq 0$, $|\kappa_1^* \kappa_2| > 0$, i.e., nondegenerate four-wave mixing with linear absorption/gain in the medium. In this paper we discuss only case (i). Cases (ii) and (iii) will be discussed in a subsequent paper.

PHASE-CONJUGATE OSCILLATORS WITHOUT CONVENTIONAL MIRRORS

In this section we set $r_1 = r_2 = 0$. The frequency of the input wave E_1 is $\omega + \delta$. In this case the problem then reduces to the standard nondegenerate four-wave mixing in a transparent medium,[12-14] which is characterized by a linear gain or absorption in addition to the parametric gain. We will show that the general theory developed in this paper yields the results of previous studies.[12-14]

From Eqs. (26), (22), (16), (18), and (12), the amplitudes of the reflected wave at the input plane ($z = 0$) can be written as

$$r_p = -\frac{2ik_2^* \sinh \frac{s}{2} l}{(-g - i\Delta k) \sinh \frac{s}{2} l + s \cosh \frac{s}{2} l},$$

$$r_s = 0. \tag{30}$$

Thus, in the absence of the conventional mirrors, there is no coherently reflected wave at $\omega + \delta$, only the phase-conjugated beam at $\omega - \delta$ is reflected by he nonlinear medium. The transmitted waves at output plane ($z = l$) are

$$t_p = 0,$$

$$t_s = \frac{s^*}{(-g + i\Delta k) \sinh \frac{s^*}{2} l + s^* \cosh \frac{s^*}{2} l} \times \exp[-i(k_1 + k_2)l/2]. \tag{31}$$

Thus, in the absence of the conventional mirrors, there is only one transmitted beam at $\omega + \delta$. We note that when $r_1 = r_2 = 0$ and $a = b = 0$, then $E_i = A_i(0)$ and $G_i = A_i(l)$, where $i = 1, 2, 3, 4$. If we define complex amplitude transmission as $t_s' = \mathcal{A}_3(l)/\mathcal{A}_1(0)$, then by Eq. (1) $A_1(l) = \mathcal{A}_1(l)\exp(-ik_1 l)$ and $A_1(0) = \mathcal{A}_1(0)$; hence by Eqs. (29) we obtain $t_s' = t_s \exp(ik_1 l)$, and when this equation is substituted into Eqs. (31) we get

$$t_s' = \frac{s^*}{(-g + i\Delta k) \sinh \frac{s^*}{2} l + s^* \cosh \frac{s^*}{2} l} \exp(i\Delta k l/2). \tag{32}$$

With $r_1 = r_2 = 0$, the oscillation condition [Eq. (24)] becomes $N'N^* = 0$. Substituting Eqs. (16), (18), and (12) into Eq. (24), we obtain the following oscillation condition:

$$D = (-g - i\Delta k)\sinh \frac{s}{2} l + s \cosh \frac{s}{2} l = 0. \tag{33}$$

Note that, at oscillation, r_p and t_s approach infinity according to Eqs. (30), (31), and (33). We now consider the four different operation situations and compare our results with previous studies.

$\Delta k = 0, g = 0, \kappa_1 = \kappa_2 = \kappa$ This is the case of degenerate four-wave mixing in a transparent medium without linear gain or absorption.[14]

Under these conditions the oscillation is provided by the parametric gain. From Eqs. (13), (30), and (31) we obtain the phase-conjugate complex reflection coefficient and coherent transmission coefficient. They are

$$r_p = -i\frac{\kappa^*}{|\kappa|} \tan|\kappa| l,$$

$$t_s = \frac{1}{\cos|\kappa| l} \exp(-ikl). \tag{34}$$

The oscillation condition will now be $|\kappa| l = \pi/2, 3\pi/2, \ldots$, etc. Similar results have been obtained by others.[14]

$\Delta k = 0, g \neq 0, \kappa_1 = \kappa_2 = \kappa$ This corresponds to degenerate four-wave mixing in a transparent medium that also exhibits linear gain or absorption.[12]

From Eqs. (13) and (32), the phase-conjugate complex reflection coefficient can be written as

$$r_p = -\frac{i\kappa^* \tan[|\kappa|^2 - (g/2)^2]^{1/2} l}{[|\kappa|^2 - (g/2)^2]^{1/2} - (g/2) \tan[|\kappa|^2 - (g/2)^2]^{1/2} l}. \tag{35}$$

According to Eq. (35), oscillation occurs when the following condition is satisfied:

$$\tan\{[|\kappa|^2 - (g/2)^2]^{1/2} l\} = \frac{2[|\kappa| - (g/2)^2]^{1/2}}{g}, \tag{36}$$

where $\kappa = (\omega/2)\sqrt{\mu/\epsilon}\ \chi^{(3)} A_5^* A_6^* e^{gl/2} = \kappa' e^{gl/2}$. Equations (35) and (40) agree formally with the results derived in Ref. 12, except that they have considered linear absorption only. Thus, if we replace g with $-\alpha$, we will obtain exactly the same result as in Ref. 12.

Using Eq. (36), in Fig. 2 we plot the parametric gain $|\kappa'|l$ versus linear gain gl at the oscillation conditions to show

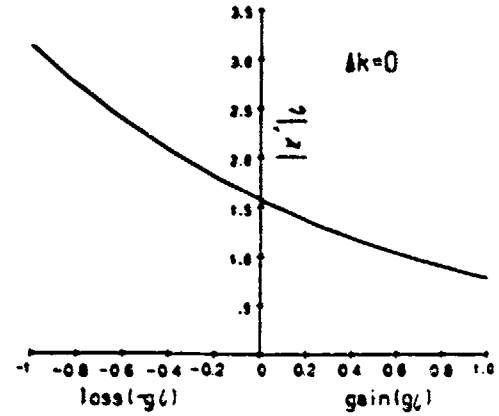

Fig. 2. Parametric gain $|\kappa'|l$ versus linear gain gl at the oscillation condition $\kappa = \kappa' e^{i\pi/2}$.

the effect of gain (or loss) on the coupling constant $|\kappa'|l$ for degenerate four-wave mixing. The figure shows that the parametric gain required for oscillation is considerably increased (decreased) owing to linear absorption (gain) in the medium.

$\Delta k \neq 0$, $g = 0$, $\kappa_1\kappa_2^* > 0$ This is the case of degenerate four-wave mixing in a transparent medium without linear absorption or gain.[13]

Substituting $g = 0$ into Eqs. (30), we obtain the phase-conjugate reflection coefficient:

$$r_p = \frac{-i\kappa_2^* \tan\{[\kappa_1\kappa_2^* + (\Delta k/2)^2]^{1/2} l\}}{[\kappa_1\kappa_2^* + (\Delta k/2)^2]^{1/2} - i(\Delta k/2)\tan\{[\kappa_1\kappa_2^* + (\Delta k/2)^2]^{1/2} l\}}. \quad (37)$$

which is identical to the result of Ref. 15. According to Eq. (37), oscillation occurs only when $\Delta k = 0$ and $\sqrt{\kappa_1\kappa_2^*}\, l = \pi/2, 3\pi/2, \ldots$, etc., so that nondegenerate oscillation due to four-wave mixing is not possible in a transparent Kerr medium. Oscillation with no input wave will occur only at the pump frequency.

$\Delta k \neq 0$, $g \neq 0$, $|\kappa_1\kappa_2^*| > 0$ This is the case of degenerate four-wave mixing in a transparent medium that exhibits linear absorption-gain and a parametric gain. This is the first time to our knowledge that the effects of nonsaturable background losses or gain in the transparent medium on phase conjugation by degenerate four-wave mixing have been studied.

By Eqs. (12), (30), and (31), the phase-conjugate complex reflection and coherent transmission coefficients are

$$r_p = \frac{-i\kappa_2^* \tan\{[\kappa_1\kappa_2^* + (\Delta k - ig)^2/4]^{1/2} l\}}{[\kappa_1\kappa_2^* + (\Delta k - ig)^2/4]^{1/2} - \frac{i(\Delta k - ig)}{2}\tan\{[\kappa_1\kappa_2^* + (\Delta k - ig)^2/4]^{1/2} l\}},$$

$$t_s = \frac{[\kappa_1^*\kappa_2 + (\Delta k + ig)^2/4]^{1/2}\sec\{[\kappa_1^*\kappa_2 + (\Delta k + ig)^2/4]^{1/2} l\}}{[\kappa_1^*\kappa_2 + (\Delta k + ig)^2/4]^{1/2} + \frac{i(\Delta k + ig)}{2}\tan\{[\kappa_1^*\kappa_2 + (\Delta k + ig)^2/4]^{1/2} l\}} \exp[-i(k_1 + k_2)l/2] \quad (38)$$

The oscillation condition can be obtained by either setting the denominators to zero in Eqs. (38) or simply using Eq. (33). With $s = u + iv$, Eq. (33) can be written as

$$D = \left[-\sinh\frac{u}{2}l\left(g\cos\frac{v}{2}l + v\sin\frac{v}{2}l\right) + \cosh\frac{u}{2}l\left(\Delta k\sin\frac{v}{2}l + u\cos\frac{v}{2}l\right)\right] + i\left[-\cosh\frac{u}{2}l\left(g\sin\frac{v}{2}l - v\cos\frac{v}{2}l\right) + \sinh\frac{u}{2}l\left(u\sin\frac{v}{2}l - \Delta k\cos\frac{v}{2}l\right)\right] = 0. \quad (39)$$

By setting the real and the imaginary parts of the denominator separately equal to zero, we obtain two simultaneous nonlinear equations involving three dimensionless variables: gl, $\kappa' l$, and $\Delta k l$, where $\kappa' = \sqrt{\kappa_1'\kappa_2^*}$. If we set $\Delta k l$ as the independent variable, then, by using Brown's method to solve the two nonlinear equations, we obtain multiple-valued solutions for gl and $\kappa' l$. Note that when $\Delta k l = 0$, the imaginary part of D is equal to zero, and the real part of D reduces to Eq. (36). Using Eq. (36), we find that for oscillation at the pump frequency the parametric gain required is $\kappa' l = 3.13824, 1.57050, 0.76250$ for a linear absorption-gain of $gl = -1, 0, 1$, respectively. Nondegenerate oscillation is not possible for these sets of parameter values. Figures 3 and 4 show the phase-conjugate power reflectivity R_p and the coherent power transmissivity T_s, respectively, versus normalized wavelength detuning Ψ for three values of $gl = 0, \pm 1$ at oscillation condition. By definition, $\Psi = (\Delta\lambda/2)(2\pi l/\lambda^2)$, which is also equal to the phase mismatch $\Delta k l$ divided by 2π. The wavelength-detuning parameter $\Delta\lambda/2$ corresponds to the difference in wavelengths of the probe field E_1 relative to the pump fields $A_{1,2}$. These two figures show that linear absorption losses in the medium substantially increase the threshold value of $\kappa' l$ for which oscillation will occur at the pump frequency. If the medium were somehow to exhibit linear gain instead of absorption, then the threshold value of the coupling strength would be correspondingly lowered owing to the additional gain then available from medium.

Using Eqs. (38), we plot in Fig. 5 the power-reflection coefficient R_p versus a normalized wavelength-detuning parameter Ψ for $|\kappa'|l = \pi/2$ and several values of the linear gain gl. For finite g, oscillation ceases to occur at $|\kappa'|l = \pi/2$, but it occurs at higher (lower) values for linear absorption (gain) in the medium.

Figures 6 and 7 are the normalized phase-conjugate power reflectivity and normalized coherent power transmissivity, respectively, versus normalized wavelength detuning Ψ. They show the effects of linear gain or absorption on the wavelength response for the filter application. Several prominent features should be noted. First,

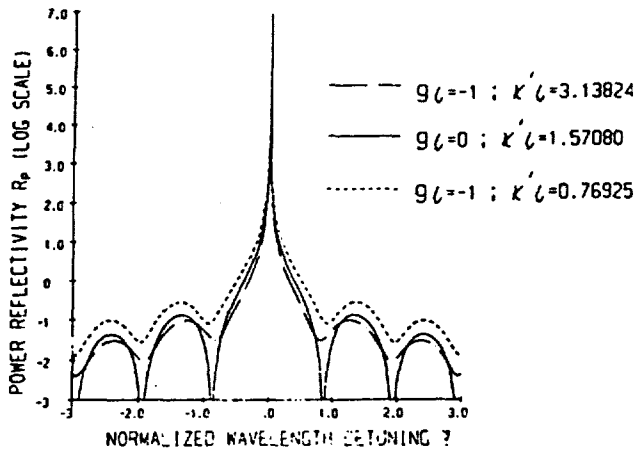

Fig. 3. Phase-conjugate power reflectivity R_p versus normalized wavelength detuning Ψ for several values of linear gain gl = 0, ±1 when $|\kappa' l|$ satisfies the oscillation condition. For the example given in the text, unity along the abscissa corresponds to $\Delta\lambda/2$ = 0.0772 Å, or $\Delta\nu$ = 9.29 GHz.

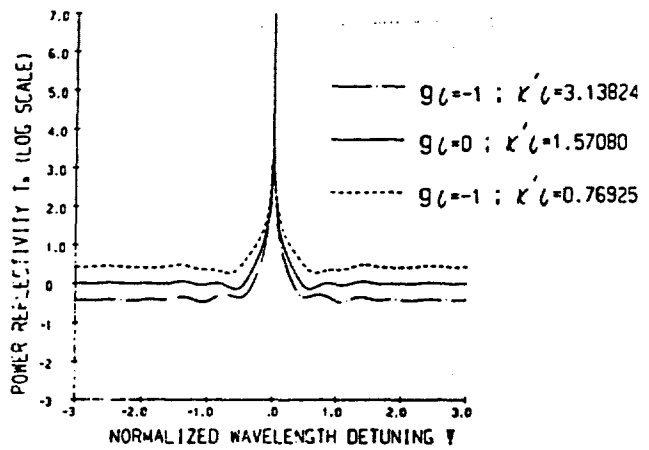

Fig. 4. Coherent power transmissivity R_s versus normalized wavelength detuning Ψ for several values of linear gain gl = 0, ±1 when $|\kappa' l|$ satisfies the oscillation condition. For the example given in the text, unity along the abscissa corresponds to $\Delta\lambda/2$ = 0.0772 Å, or $\Delta\nu$ = 9.26 GHz.

when $|gl|$ is less than 0.1, the effect on the filter of gain ($gl > 0$) or loss ($gl < 0$) on the filter characteristic is negligible. Second, larger linear gain (or loss) degrades the filter characteristics. Third, the filter characteristics of the phase-conjugate reflection are better than those of transmission for finite gain (or loss).

In practice, linear gain of the nonlinear medium depends on the pumping source. Using Eqs. (38), we plot in Figs. 8 and 9 the linear gain (or loss) gl versus normalized wavelength detuning Ψ for constant reflectances and transmittances, respectively, when $|\kappa' l| = \pi/2$. We recall that $\kappa = (\omega/2)\sqrt{\mu/\epsilon}\,\chi^{(3)} A_5^* A_6^* e^{gl/2} = \kappa' e^{lh/2}$. In these figures, we plot only the minimum absolute linear gain $|g|l$ versus normalized wavelength detuning Ψ, because gl is a multiple-valued function of Δk for constant reflectances or transmittances in Eqs. (38).

If we increase the absolute value of $|gl|$ above 2, then nondegenerate oscillation at a frequency different from that of the pumps becomes possible. Figure 10 shows the solution of $D = 0$ for gl and $\kappa' l$ versus normalized wavelength detuning Ψ. Because the solution is multiple valued, it is possible to have many pairs of gl and $\kappa' l$ values for a particular value of Ψ. In this figure, the curve pair 3 (shown as a dashed curve) for $\kappa' l$ is not shown because it is greater than 1.8. The curve pair 1 (shown the solid curve) shows that, for example, if linear gain gl is increased to 4.32152, then one can decrease the parametric gain $\kappa' l$ to 0.13281 in order to observe nondegenerate

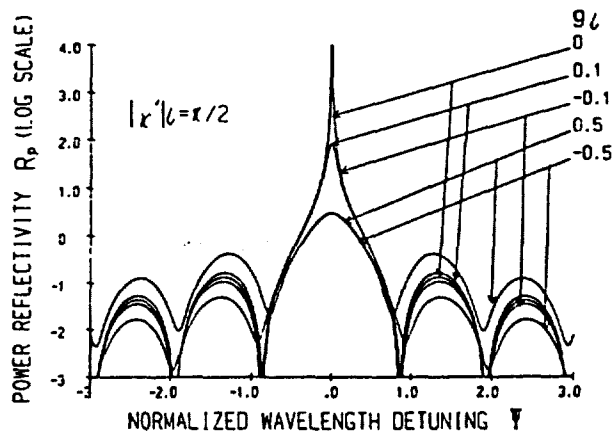

Fig. 5. Power-reflection coefficient R_p versus a normalized wavelength-detuning parameter Ψ for $|\kappa' l| = \pi/2$ and several values of the linear gain gl. For the example given in the text, unity along the abscissa corresponds to $\Delta\lambda/2$ = 0.0772 Å, or $\Delta\nu$ = 9.26 GHz.

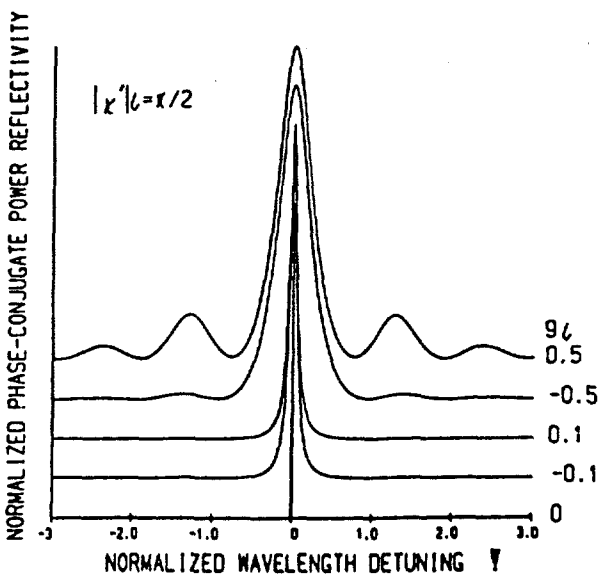

Fig. 6. Normalized phase-conjugate power reflectivity versus normalized wavelength detuning Ψ for parametric gain $|\kappa| l = \pi/2$ and several values of linear gain gl. All curves are normalized to unity power reflectivity to emphasize the frequency bandpass of the interaction.

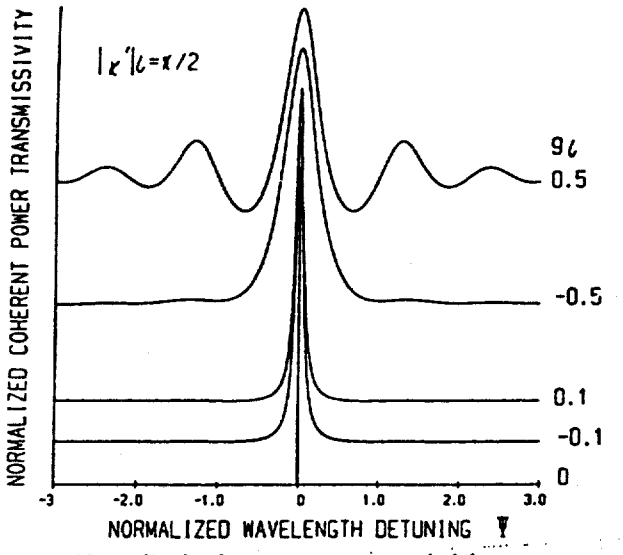

ig. 7. Normalized coherent power transmissivity versus nor-alized wavelength detuning Ψ for parametric gain $|\kappa|l = \pi/2$ nd several values of linear gain gl. All curves are normalized to nity power transmission to emphasize the frequency bandpass f the interaction.

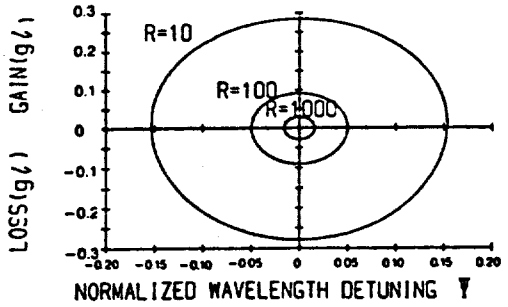

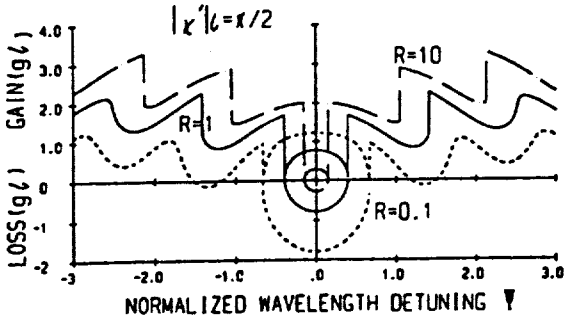

'ig. 8. Contours of equal reflectance for $|\kappa'|l = \pi/2$ on the linear ain (or loss) versus normalized wavelength-detuning plane. For he example given in the text, unity along the abscissa correponds to $\Delta\lambda/2 = 0.0772$ Å, or $\Delta\nu = 9.26$ GHz.

oscillation at $|\Psi| = 1.31$. Figure 11 is a plot of R_p and T_c versus the normalized wavelength detuning for $gl = 1.32152$; $\kappa'l = 0.13281$, showing the possibility of observing oscillation at a frequency different from that of the pump beam for this set of parameter values.

CONCLUSION

In conclusion, we have treated the generalized theory of the propagation of electromagnetic radiation in phase-conjugate oscillators. Wavelength detuning and linear and parametric gain are all taken into account. Phase-conjugate power reflectivity and transmissivity, coherent power reflectivity and transmissivity, and the oscillation condition are derived. We have studied the special case of no conventional mirrors by using this general theory and compared our results with those of previous studies. Our

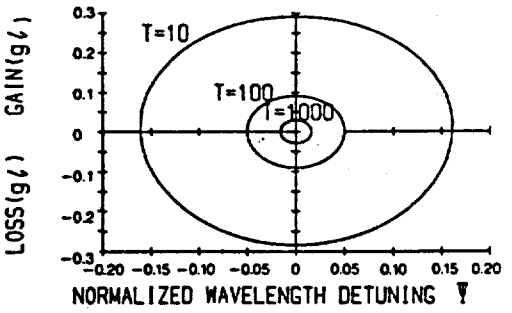

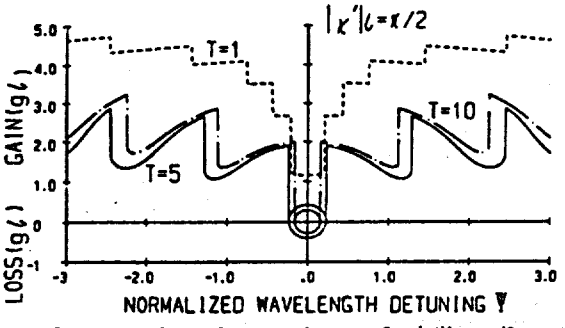

Fig. 9. Contours of equal transmittance for $|\kappa'|l = \pi/2$ on the linear gain (or loss) versus normalized wavelength-detuning plane. For the example given in the text, unity along the abscissa corresponds to $\Delta\lambda/2 = 0.0772$ Å, or $\Delta\nu = 9.26$ GHz.

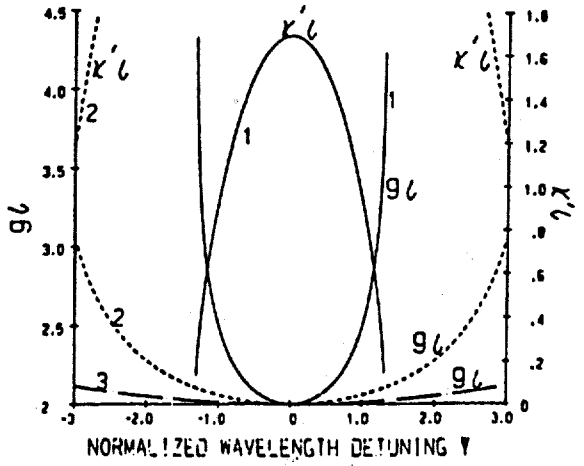

Fig. 10. Parametric gain $\kappa'l$ and linear gain gl versus normalized wavelength detuning at the oscillation condition.

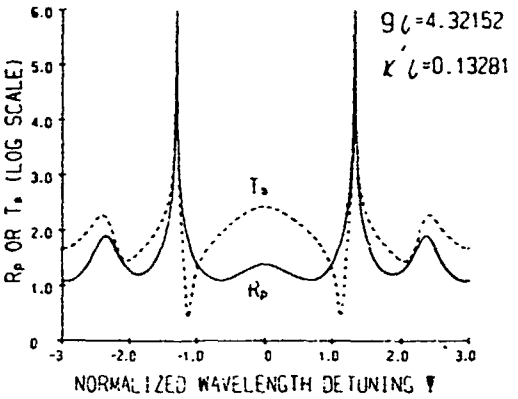

Fig. 11. Phase-conjugate power reflectivity R_p (solid curve) and coherent-power transmissivity T_s (dashed curve) versus normalized wavelength detuning Ψ for gl = 4.32152, $\kappa'l$ = 0.13281.

results indicate that in the presence of large linear gain (or loss), oscillation can occur at a frequency different from that of the pump beams.

ACKNOWLEDGMENTS

Wun-Shung Lee and Sien Chi acknowledge helpful discussions with Senfer Wen. Pochi Yeh and Ragini Saxena gratefully acknowledge the support of the U.S. Air Force Office of Scientific Research under contract F49620-88-C-0023.

REFERENCES

1. J. Au Yeung, D. Fekete, D. M. Pepper, and A. Yariv, IEEE J. Quantum Electron. **QE-15**, 1180 (1979).
2. P. A. Belanger, A. Hardy, and A. E. Seigman, Appl. Opt. **19**, 602 (1980).
3. J. M. Bel'dyugin, M. G. Galushkin, and E. M. Zemskov, Sov. J. Quantum Electron. **9**, 20 (1979).
4. J. F. Lam and W. P. Brown, Opt. Lett. **5**, 51 (1980).
5. P. A. Belanger, Opt. Eng. **21**, 266 (1982).
6. P. Yeh, J. Opt. Am. **A 2**, 727 (1985).
7. J.-C. Diels and I. C. McMichael, Opt. Lett., **6**, 219 (1981).
8. P. Yeh, J. Tracy, and M. Khoshnevisan, Proc. Soc. Photo-Opt. Instrum. Eng. **412**, 240 (1983).
9. P. Yeh and M. Khoshnevisan, Proc. Soc. Photo-Opt. Instrum. Eng. **487**, 102 (1984).
10. See, for example, A. Yariv and P. Yeh, *Optical Waves in Crystals* (Wiley, New York, 1984), p. 165.
11. P. Yeh, A. Yariv, and C. Hong, J. Opt. Soc. Am. **67**, 423 (1977).
12. R. A. Fisher, ed., *Optical Phase Conjugation* (Academic, New York, 1983), Chap. 2.
13. G. Grynberg, B. Kleinmann, M. Pinard, and P. Verkerk, Opt. Lett. **8**, 614 (1983).
14. A. Yariv and D. M. Pepper, Opt. Lett. **1**, 16 (1977).
15. D. M. Pepper and R. L. Abrams, Opt. Lett. **3**, 212 (1978).

Theory of Phase-Conjugate Oscillators (II)

THEORY OF PHASE-CONJUGATE OSCILLATORS (II)

Wun-Shung Lee and Sien Chi
Institute of Electro-Optical Engineering
National Chiao Tung University,
Hsinchu, Taiwan, R.O.C.

Pochi Yeh and Ragini Saxena
Rockwell International Science Center
Thousand Oaks,California 91360

Abstract

This paper is the second of a series describing propagation of electromagnetic radiation in phase–conjugate oscillators. We apply the formulation developed in the first paper to study the phase–conjugate resonator (PCR) and the Fabry–Perot cavity with an intracavity phase–conjugate mirror (PCM). Our results show that nondegenerate oscillation occur in the PCR for large parametric gains and fixed separation between the conventional reflector and PCM. The bandwidth is considerably reduced from that of a PCM alone. In the phase–conjugate oscillator, oscillation will occur at the pump frequency only if there is no separation between the conventional mirrors and the phase–conjugate element, and the nonlinear medium fills the entire Fabry–Perot cavity.

INTRODUCTION

In part I of this series,[1] we formulated the power reflectivity/transmissivity and oscillation condition in phase–conjugate oscillators. Thase oscillators consist of conventional Fabry–perot cavities with an intracavity, transparent Kerr medium that is pumped externally by a pair of off–axis, counterpropagating pump beams. An external signal with a frequency different from that of the pump beams is injected into the cavity along its axis. Nearly Degenerate Four–Wave Mixing (NDFWM) generates a wave that is phase–conjugate of the signal beam. Additional waves arise due to the presence of the conventional end mirrors of the cavity. Extermally driven, intracavity four–wave mixing in Fabry–perot resonators has been considered before by Agrawal[2] and Yaholam and Yariv[3] in saturable absorbers and photorefractive media respectively, and for equal frequency of the interacting waves. In contrast to our study, Refs. 2 and 3 consider the external driving field bouncing back and forth between the two mirrors of the cavity as the counterpropagating pumps for the nonlinear medium, while another external, weak signal that is not part of the cavity probes such a device, thereby combing DFWM with cavity operation.

We apply our general formulation of nondegenerate operation of phase–conjugate oscillators to the special case of a Fabry–Perot cavity with one conventional mirror and a PCM, i.e., a PCR. This device has been studied extensively.[4-8] Refs. 4–6 examined the transverse modes in a PCR. Refs 7 and 8 looked at the fields within and outside a PCR without taking into account the nature of the nonlinear process responsible for phase–conjugate reflection. Ref. 9 examines the effects of a noisy probe field incident on a phase–conjugate Fabry–Perot resonator. Our theory describes nondegenerate oscillation in a PCR by taking into account the four–wave mixing process responsible for generate of the phase–conjugate wave. Analytic expressions are obtained for power reflectivity and transmissivity, as well as the oscillation condition, showing their dependence on linear and

parametric gain of the PCM, mirror reflectivities and separation between mirrors and PCM. Numerical plots are presented to illustrate this parameter dependence.

PHASE CONJUGATE OSCILLATORS BOUNDED BY ONE CONVENTIONAL REFLECTOR AND ONE PHASE CONJUGATE MIRROR

Referring to Fig.1, we consider a linear optical resonator bounded by a PCM and one conventional mirror r_2. The PCM is a transparent Kerr medium with linear gain (or loss), and it is pumped externally by a pair of counterpropagating, off–axis laser beams of frequency ω. A weak probe field at frequency $\omega+\delta$, where $\delta<<\omega$, is incident on the PCM from the left. The field E_2 at frequency $\omega-\delta$ and propagating backwards to the left of the PCM, is generated by NDFWM at the PCM. The field E_4 at frequency $\omega+\delta$ and propagating backwards to the left of the PCM is generated by reflections off the conventional mirror of the beam transmitted by the PCM. Waves G_1 and G_3, at frequencies $\omega+\delta$ and $\omega-\delta$ respectively, propagate in the forward direction to the right of the conventional mirror, and can be similarly interpreted. Using the formulation developed in Ref.1, the complex phase–conjugate reflectivity and transmissivity, r_p and t_p and the coherent reflectivity and transmissivity, r_s and t_s, respectively are given by:

$$r_p=\frac{E_2}{E_1^*}=-i\kappa_2^*\beta\left[1+\frac{|r_2|^2\alpha^2}{e^{-2i\Delta kb}-\kappa_1\kappa_2^*\beta^2|r_2|^2}\right]$$

$$t_p=\frac{G_3}{E_1^*}=\frac{-i\kappa_2^*\beta\alpha r_2^*(1-r_2^2)\,e^{-i\Delta kl/2}\,e^{-i\Delta kb+ik_1(l+b)}}{t_2[e^{-2i\Delta kb}-\kappa_1\kappa_2^*\beta^2|r_2|^2]} \qquad (1)$$

$$r_e=\frac{E_4^*}{E_1^*}=\frac{\alpha^2 e^{i(k_1+k_2)(l+b)}\ r_2^*}{e^{-i\Delta kb}-\kappa_1\kappa_2^*\beta^2|r_2|^2e^{i\Delta kb}} \tag{1}$$

$$t_e=\frac{G_1}{E_1}=\frac{(1-r_2^2)\ \alpha^* e^{-ik_1(l+b)}e^{i\Delta kl/2}e^{2i\Delta kb}}{t_2[e^{2i\Delta kb}-\kappa_1^*\kappa_2\ \beta^{*2}|r_2|^2]}$$

where

$$\kappa_i^*=\frac{\omega_i}{2}\sqrt{\frac{\mu}{\epsilon}}\chi^{(3)}\mathcal{A}_5\mathcal{A}_6e^{gl/2}\ ;\ \Delta k=k_1-k_2$$

$$\alpha=\frac{1}{D}s$$

$$\beta=\frac{2}{D}\sinh[\frac{s}{2}l] \tag{2}$$

$$s=\sqrt{-(\Delta k-ig)^2-4\kappa_1\kappa_2^*}$$

$$D=(-g-i\Delta k)\sinh[s\ l/2]+s\cosh[s\ l/2]$$

The oscillation condition is

$$\kappa_1\kappa_2^*\beta^2|r_2|^2=e^{-2i\Delta kb} \tag{3}$$

Note that the power reflectivities R_p, R_s, power transmissivities T_p, T_s, and oscillation condition are independent of the phase introduced by reflection or transmission at mirror 2, where $R_p=|r_p|^2$, $R_s=|r_s|^2$, $T_p=|t_p|^2$ and $T_s=|t_s|^2$. Note that in the absence of mirror 2 ($r_2=0$) $r_s= t_p=0$, while r_p and t_s reduce to the results of Ref.(1) for a PCM, except that the wave G_1 now measured at $l+b$ instead of l.

We shall now discuss four different operation conditions: (1) $\Delta k=0$, $g=0$, $\kappa_1=\kappa_2=\kappa$; (2) $\Delta k=0$, $g\neq 0$, $\kappa_1=\kappa_2=\kappa$; (3)$\Delta k\neq 0$, $g=0$, $\kappa_1^*\kappa_2>0$; (4)$\Delta k\neq 0$, $g\neq 0$, $\kappa_1^*\kappa_2>0$. For each case, we shall discuss the phase–conjugate power reflectivity and transmissivity, coherent power reflectivity and transmissivity and the oscillation condition.

(1) $\Delta k=0$, $g=0$, $\kappa_1=\kappa_2=\kappa$

This is the case of Degenerate Four Wave Mixing (DFWM) in the phase–conjugate element of the PCR.

By Eqs. (1) and (2) the complex phase–conjugate reflectivity r_p and transmissivity t_p, coherent reflectivity r_s and transmissivity t_s are given by

$$r_p=-i\frac{\kappa^*}{|\kappa|}\tan|\kappa|l\frac{1+|r_2|^2}{1-|r_2|^2\tan^2|\kappa|l}$$

$$t_p=-\frac{i\kappa^*}{|\kappa|}\tan|\kappa|l\sec|\kappa|le^{ik(l+b)}\frac{t_2r_2^*}{1-|r_2|^2\tan^2|\kappa|l}$$

$$r_s=\sec^2|\kappa|le^{2ik(l+b)}\frac{r_2^*}{1-|r_2|^2\tan^2|\kappa|l} \qquad (4)$$

$$t_s=\sec|\kappa|le^{-ik(l+b)}\frac{t_2}{1-|r_2|^2\tan|\kappa|l}$$

where $k=k_1=k_2$. Note that if $r_2=0$, then we recover the results of Refs.(1) and (9) for DFWM in a PCM. Identifying $\tan^2|\kappa|l$ and $\sec^2|\kappa|l$ as the phase–conjugate power reflectivity and coherent transmissivity of a PCM,[1,9] we note that equations (5) are similar to the results obtained in Ref.8 for the fields in a PCR. The differences arise because Vesperinas[8] considers the external probe field to be incident on the mirror instead of the PCM, and does not account for the nonlinear process responsible for phase conjugation at the PCM.

By Eqs.(2) and (3) the oscillation condition is

$$|r_2|^2\tan^2|\kappa|l=1 \qquad (5)$$

Equation (5) is identical to the result obtained in Ref.(9), and shows that if mirror 2 is perfectly reflecting, then oscillation occurs at $|\kappa|l=\pi/4$, which is lower than that for a PCM alone by a factor of 2.

Note that for the PCR, the oscillation condition (5) and the four power coefficients in Eq.(4) are independent of the separation b between the PCM and the conventional mirror.

(2) $\Delta k=0$, $g\neq 0$, $\kappa_1=\kappa_2=\kappa$

This is the case of DFWM in the nonlinear medium with linear gain or loss besides the parametric gain.

Substituting Eqs.(2) in Eq.(3) and simplifying, the oscillation condition becomes

$$\tan\left[l\sqrt{|\kappa|^2-(g/2)^2}\right]=\frac{2\sqrt{|\kappa|^2-(g/2)^2}}{g+2|\kappa_2|} \qquad (6)$$

The above equation shows how the presence of linear gain (or loss) will affect the values of parametric gain required for oscillation in a PCR.

The resonator oscillation frequency ω is also independent of the separation between the two reflectors for DFWM in the PCM.

In Fig.2, we plot the parametric gain $\kappa' l$ required for oscillation versus the linear gain or loss gl for several values of conventional mirror reflectivity: $|r_2|^2$=1, 0.8, 0.5, and 0.1. When there is no linear gain/loss (g=0) and $|r_2|^2$=1, the coupling strength required for oscillation is $\pi/4$, as expected from Ref.(9) for a PCM in the presence of a perfectly reflecting mirror. Linear absorption losses in the medium substantially increase the threshold value of $|\kappa'|l$ for which oscillation will occur. If the medium were somehow to exhibit linear gain instead of absorption, then the threshold value of the coupling strength is correspondingly lowered due to the additional gain now available from the medium. Also, for a given linear gain/loss in the nonlinear medium, the threshold value of $|\kappa'|l$ for oscillation increases as losses at the conventional mirror of the phase–conjugate resonator are increased.

(3) $\Delta k \neq 0$, $g=0$, $\kappa_1\kappa_2^*>0$

This is the case of NFWM in the PCM of the phase–conjugate resonator.

The oscillation condition can be separated into an amplitude and a phase part. The equality of amplitude part yields

$$4|r_2|^2\kappa_1\kappa_2^* \sin^2\left(\frac{\sqrt{\Delta k^2+4\kappa_1\kappa_2^*}}{2}l\right)=\Delta k^2+4\kappa_1\kappa_2^* \cos^2\left(\frac{\sqrt{\Delta k^2+4\kappa_1\kappa_2^*}}{2}l\right) \qquad (7)$$

and the equality phase part yields

$$\tan(b\Delta k)=-\frac{\Delta k}{\sqrt{\Delta k^2+4\kappa_1\kappa_2^*}}\tan\left(\frac{\sqrt{\Delta k^2+4\kappa_1\kappa_2^*}}{2}l\right) \qquad (8)$$

Due to NDFWM in the PCM of the phase–conjugate resonator, the oscillation condition is now a function of the separation 'b' between the PCM and the conventional mirror. For practical applications, if we choose b=0, i.e. the conventional mirror is placed exactly at the back of the PCM, and if we consider nondegenerate oscillation ($\Delta k\neq 0$), then Eq.(8) requires $\sqrt{\Delta k^2+4\kappa_1\kappa_2^*}\,l=2p\pi$, where p is an integer. This however can not satisfy Eq.(7) because $\kappa_1\kappa_2^*$ is a real and positive number. Hence if b=0, oscillation will only occur at the pump frequency with $\Delta k=0$. From Fig.(2), the minimum parametric gain required for oscillation will occur for a perfectly reflecting conventional mirror with $|r_2|^2=1$. Hence for this special case, the oscillation condition of Eq.(7) can be simplified to

$$\cos\sqrt{\Delta k^2+4\kappa_1\kappa_2^*}\,l=-\frac{\Delta k^2}{4\kappa_1\kappa_2^*} \qquad (9)$$

Since the magnitude of cosine function cannot exceed unity, by Eq.(9), oscillation can be achieved only when the absolute value of the the maximum wave number detuning $|\Delta k|$ is equal or less than $2(\kappa_1\kappa_2^*)^{1/2}$. Let $\kappa_1\kappa_2^*\equiv\kappa^2$; then Eq.(9) can be solved for κl as a function of $\Delta k l/2\pi$ by numerical methods and we can obtain b/l from Eq.(8).

We plot the phase conjugate power reflectivity R_p versus normalized wavelength detuning $\Psi=\Delta k l/2\pi = (-\Delta\lambda/2)(2\,n\,l/\lambda^2)$ in Fig.(3). The dot–dashed curve represents the case of no conventional mirror ,i.e., an ordinary PCM based on NFWM, with a parametric gain of $\pi/2$. The solid curve corresponds to a linear resonator with a PCM and a perfectly reflecting conventional mirror placed exactly at the back of the PCM. The parametric gain for this curve is $\pi/4$. Notice that the introduction of the mirror not only reduced the parametric gain required for oscillation, but it also dramatically decreased the bandwidth of the filter. This is because feedback from the mirror in the form of reflected light along the axis of the resonator increases the internal gain available from the PCM, thus increasing the finesse of the resonator.[10] Oscillation occurs at pump frequency in both cases. A larger value of the parametric gain above this threshold value ($\kappa l=1.11065$, as in the dashed curve of the same figure) shows that nondegenerate oscillation is now possible at $\Delta k l/2\pi=\pm 0.353$, but for the fixed separation of $b/l=0.70722$. The bandwidth of the dashed curve is less than that of the solid curve.

(4) $\Delta k\neq 0$, $g\neq 0$, $\kappa_1\kappa_2^*>0$

This is the case of NFWM in the externally pumped nonlinear medium with linear gain or loss besides the usual parametric gain.

Numerical plots of the phase–conjugate reflectivity of the PCR is shown in Fig.4 as a function of normalized wavelength detuning Ψ, respectively for $r_2=-1$, $\kappa' l=1$ and two linear gain $gl=\pm 0.2$. For filter applications, linear gain ($g>0$) is better than linear loss ($gl<0$) because the central peak (at $\Delta k l/2\pi=0$) is smaller for linear gain than for linear loss, and the side–lobe structure is reduced.

We may rewrite Eq.(3) as

$$\kappa_1 \kappa_2^* \beta^2 |r_2|^2 = e^{-i(2\Delta k b + 2\pi p)} \qquad (10)$$

where p is an integer. Then b/l has multiple–valued solution for the phase part of Eq.(10) when $\kappa' l$, gl and Ψ are fixed. We plot the phase–conjugate power reflectivity versus normalized wavelength detuning in Fig.5 to show the effects of different values of b/l corresponding to p=0,1 on the mode spacing at the oscillation condition. This figure shows that when we increase p ,i.e. increase separation b/l, then it will have the detrimental effect of decreasing the mode spacing and increasing the power reflectivity in side–lobes other than that at the oscillation frequency.

PHASE–CONJUGATE OSCILLATOR[1]

Referring to Fig.6, we consider an optical resonator that consists of two partially reflecting mirrors r_1 and r_2 and an intracavity PCM that provides linear gain (or loss) besides parametric gain via FWM.

(1) $g=0$, $\kappa_1=\kappa_2=0$, $\Delta k=0$, $R_1R_2\neq 0$

This is the case of a Fabry–Perot cavity, with no intracavity PCM.

The coherent reflection and transmission is

$$r_e = \frac{r_2^* e^{ikd} + r_1^* e^{-ikd}}{r_1^* r_2^* e^{ikd} + e^{-ikd}}$$

$$t_e = \frac{1}{t_1 t_2}\left[\frac{1 + r_1^2 r_2^2 - r_1^2 - r_2^2}{r_1 r_2 e^{-ikd} + e^{ikd}}\right] \qquad (11)$$

where $d = l + a + b$, $k = k_1 = k_2$. These two equations can reduce to Airy's formula. Note that $t_e = 0$ if $r_2^2 = 1$, since there is no transmitted wave G_1 if mirror 2 is perfectly reflecting. Also note that $r_p = t_p = 0$, as expected in the absence of the intracavity PCM.

(2) $g \neq 0$, $\kappa_1 = \kappa_2 = 0$, $\Delta k = 0$, $R_1 R_2 \neq 0$.

This is the case of a Fabry Perot cavity with an intracavity linear gain medium.

Using $r_1 = \sqrt{R_1}$, $r_2 = -\sqrt{R_2}$, the oscillation condition can be written as

$$1 + R_1 R_2 e^{2gl} - 2\sqrt{R_1 R_2}\, e^{gl} \cos(2kd) = 0 \qquad (12)$$

where R_1 and R_2 are real numbers. Solving this equation, we obtain

$$\sqrt{R_1 R_2}\, e^{gl} = 1 \qquad (13a)$$

which means that laser round trip gain must be equal to unity, and

$$2n\frac{\omega}{c}(l+a+b)=2p\pi \qquad (13b)$$

where p is an integer. Hence in a Fabry–Perot cavity with an intracavity gain medium, the net phase change acquired in one round trip must be an integral multiple of 2π.

(3) $g=0$, $\kappa_1=\kappa_2=\kappa$, $\Delta k=0$, $R_1R_2\neq 0$.[7]

This is the case of DFWM in the PCM bounded by two conventional mirrors.

Using the formulation developed in Ref.1, we get the phase conjugate reflection coefficient

$$r_p=\frac{-t_1(1-r_1^{*2})(1+R_2)\,i\,\frac{\kappa^*}{|\kappa|}\tan|\kappa|l}{t_1^*\{1+R_1R_2-\tan^2|\kappa|l[R_1+R_2]+(1+\tan^2|\kappa l|)[r_1r_2e^{-2ikd}+r_1^*r_2^*e^{2ikd}]\}} \qquad (14)$$

Eq.(14) shows that when $\kappa=0$, then $r_p=0$, which means that when there is no four wave mixing, phase conjugate wave cannot be generated. Note also that if $R_1=0$, then we recover the results for r_p (Eqs.(4)) for the PCR. If $R_1=1$, then $r_p=0$ because then phase–conjugated light cannot be transmitted to the left by mirror 1.

Similarly, we can obtain the coherent reflection coefficient

$$r_c=\frac{(1-\tan^2|\kappa|l)(r_2^*e^{2ikd}+R_1r_2e^{-2ikd})+r_1\tan^2|\kappa|l+r_1^*+R_2(r_1^*\tan^2|\kappa|l+r_1)}{1+R_1R_2-\tan^2|\kappa|l(R_1+R_2)+(1+\tan^2|\kappa l|)(r_1r_2e^{-2ikd}+r_1^*r_2^*e^{2ikd})} \qquad (15)$$

where $R_i=|r_i|^2$; i=1,2. Note that this equation reduces to Airy's formula given by Eqs.(11) when $|\kappa|l=0$. For oscillation to occur the denominator of Eq.(15) must be zero. The resulting equation can reduce to the result of Yeh.[12]

(4) $g\neq 0$, $\kappa_1=\kappa_2=\kappa$, $\Delta k=0$, $R_1R_2\neq 0$.

This is the case of DFWM in a transparent medium with linear gain (or loss) and parametric gain bounded by two conventional mirrors.

In Fig.7, we plot the threshold parametric gain $|\kappa'|l$ as a function of the normalized cavity length $\phi=k(l+a+b)=kd$ with $r_2=-1$, $r_1=\sqrt{0.9}$, and linear gain (or loss) $gl=\pm 0.05268$. Note that for cavity lengths with $\phi=\gamma\pi$, oscillation can still occur for γ not an integer and the minimum threshold occurs when γ is an integer. We plot the parametric gain $\kappa'l$ versus linear gain gl at threshold oscillation condition for various γ in Fig.8 when $|r_2|=-1$, $|r_1|=\sqrt{0.9}$. It shows the effects of gain (or loss) on oscillation. When γ is an integer (minimum threshold) and linear gain of medium reaches its threshold value, $gl=\frac{1}{2}\ln(\frac{1}{R_1R_2})$, then $\kappa'l=0$ for oscillation, as given by Eq. (13a).

(5) $g=0$, $\Delta k\neq 0$, $|\kappa_1\kappa_2|\neq 0$, $R_1R_2\neq 0$.

This is the case of NDFWM in the transparent nonlinear medium bounded by two conventional mirror.

Consider example 1, with a=b=0, $\kappa_1\kappa_2^*=\kappa^2$ and adjust the phase of r_1 and r_2 such that

$$r_1r_2e^{-i(k_1+k_2)l}+r_1^*r_2e^{i(k_1+k_2)l}=2|r_1r_2|\cos[(k_1+k_2)l+\xi] \tag{16}$$

where ξ is the total phase of reflection from mirrors r_1 and r_2. The oscillation condition reduces to

$$2(\alpha^*)^2|r_1r_2|\cos[(k_1+k_2)l+\xi]+R_1R_2[(\alpha^*)^2-\kappa^2(\beta^*)^2]^2+1-\kappa^2(\beta^*)^2[R_1+R_2]=0 \qquad (17)$$

By separating the above equation into real and imaginary parts, Eq.(17) reduces to

$$(1-R_1R_2)\Delta k\sqrt{\Delta k^2+4\kappa^2}\sin\sqrt{\Delta k^2+4\kappa^2}\,l=0 \qquad (18a)$$

$$2\sqrt{R_1R_2}(\Delta k^2+4\kappa^2)\cos[(k_1+k_2)l+\xi]+(R_1R_2+1)\left(\Delta k^2\cos\sqrt{\Delta k^2+4\kappa^2}\,l+4\kappa^2\cos^2\frac{\sqrt{\Delta k^2+4\kappa^2}}{2}l\right)$$

$$-4\kappa^2(R_1+R_2)\sin^2\frac{\sqrt{\Delta k^2+4\kappa^2}}{2}l=0 \qquad (18b)$$

Note that when $\Delta k=0$ Eq.(18a) is alway satisfied and Eq.(18b) reduces to the result of Ref.(12).

For $R_1R_2<1$ and $\Delta k\neq 0$, $\sin\sqrt{\Delta k^2+4\kappa^2}\,l=0$, and Eq.(18b)reduces to

$$\cos[(k_1+k_2)l+\xi]=-\frac{1+R_1R_2}{2\sqrt{R_1R_2}} \qquad \text{neither} \qquad (19)$$

$$\Delta k^2\{2\sqrt{R_1R_2}\cos[(k_1+k_2)l+\xi]+R_1R_2+1\}+4\kappa^2\{2\sqrt{R_1R_2}\cos[(k_1+k_2)l+\xi]-R_1-R_2\}=0 \qquad (19)$$

These are not possible for $R_1R_2<1$. Hence when a=b=0, oscillation can only occur for $\Delta k=0$. Hence nondegenerate oscillation is not possible if the nonlinear medium fills the

entire Fabry–Perot cavity.

For example 2, let $r_1=\sqrt{R_1}$, $r_2=-1$ and $\kappa^2=\kappa_1\kappa_2^*$, $ab\neq 0$, where R_1 is real number and $\kappa_i^*=\frac{\omega_i}{2}\sqrt{\frac{\mu}{\epsilon}}\chi^{(3)}\mathcal{A}_3\mathcal{A}_6$. Then oscillation condition simplifies to

$$\kappa^2(\beta^*)^2[R_1e^{i\Delta k(b-a)}+e^{-i\Delta k(b-a)}]-e^{i\Delta k(a+b)}-R_1[(\alpha^*)^2-\kappa^2(\beta^*)^2]^2e^{-i\Delta k(a+b)}$$

$$=-2\sqrt{R_1}(\alpha^*)^2\cos[(k_1+k_2)(l+a+b)] \tag{20}$$

Comparing the imaginary parts of Eq.(20), we obtain

$$4\kappa^2\sin^2\frac{\sqrt{\Delta k^2+4\kappa^2}}{2}l\sin\Delta k(b-a)+[\Delta k^2\cos\sqrt{\Delta k^2+4\kappa^2}\,l+4\kappa^2\cos^2\frac{\sqrt{\Delta k^2+4\kappa^2}}{2}l]\sin\Delta k(a+b)$$

$$+\Delta k\sqrt{\Delta k^2+4\kappa^2}\sin\sqrt{\Delta k^2+4\kappa^2}\,l\cos\Delta k(a+b)=0 \tag{21}$$

and comparing the real parts, we obtain

$$\frac{2r_1}{1+R_1}(\Delta k^2+4\kappa^2)\cos[(k_1+k_2)(l+a+b)]$$

$$=-4\kappa^2\sin^2\frac{\sqrt{\Delta k^2+4\kappa^2}}{2}l\cos\Delta k(b-a)+[\Delta k^2\cos\sqrt{\Delta k^2+4\kappa^2}\,l+4\kappa^2\cos^2\frac{\sqrt{\Delta k^2+4\kappa^2}}{2}l]\cos\Delta k(a+b)$$

$$-\Delta k\sqrt{\Delta k^2+4\kappa^2}\sin\sqrt{\Delta k^2+4\kappa^2}\,l\sin\Delta k(a+b) \tag{22}$$

Cancelling $\Delta k(b-a)$ and from Eqs.(21) and (22) we can obtain a single formula that is a function of κl, $\Delta k l$, $(k_1+k_2)l$, and $(a+b)/l$ only. Then we can use Mueller's iteration scheme of successive bisection and interpolation method to find κl for a given $\Delta k l$, $(a+b)/l$ and $(k_1+k_2)l$. Actually, because $(k_1+k_2)l$ is much greater than $\Delta k l$, hence when we change $(a+b)/l$ the term $\cos(k_1+k_2)(l+a+b)$ on the left hand side of Eq.(22) will oscillate much faster than $\cos\Delta k(b+a)$ and $\sin\Delta k(b+a)$ of Eq.(21) and right hand side of Eq.(22). So, when pumping frequency is chosen (i.e., $(k_1+k_2)l$=constant) then we can choose X and Y as independent variables such that

$$X=\sin[\Delta k(a+b)]$$
$$Y=\cos[(k_1+k_2)(l+a+b)] \tag{23}$$

and introduce integers (p,q) such that

$$1+\frac{a+b}{l}=\frac{1}{(k_1+k_2)l}[\cos^{-1}Y+2\pi q]$$
$$\Delta k l=\frac{\sin^{-1}X+2\pi p}{(a+b)/l} \tag{24}$$

Then we can solve κl by using Eq.(21) and (22). Fig.9 shows X–Y plane versus nonlinear parametric gain κl for $(k_1+k_2)l$=10000 ,(p,q)=(1,10000) ,$r_1=\sqrt{0.9}$,$r_2=-1$ and reflection

index n=1.62 at oscillation condition. Note that q must be greater then $(k_1+k_2)l$ such that $(a+b)/l$ is positive and using Eq.(21) we can obtain $(b-a)/l$, and Δkl is dependent on (p,q) so that the solution of Eqs.(21) (22) for κl is also dependent on (p,q).

(6) $g\neq 0$, $\Delta k\neq 0$, $\kappa_1\kappa_2^*=\kappa^2$, $R_1R_2\neq 0$.

This is the case of NDFWM on the transparent nonlinear medium which exhibits linear and a parametric gain and is bounded by two conventional mirrors.

For example , let a=b=0, $\kappa_1\kappa_2^*=\kappa^2$ and r_1,r_2 are real. The oscillation condition reduces to

$$R_1R_2[\alpha^2-\kappa_1\kappa_2^*\beta^2]^2+1-\kappa_1\kappa_2^*\beta^2[R_1+R_2]+2\alpha^2r_1r_2\cos[(k_1+k_2)l]=0 \qquad (25)$$

This equation can also be separated into two equations for real and imaginary parts and function of $\cos[(k_1+k_2)l]$, $\kappa' l$, gl, and Δkl. Then we can use Brown's method for determination of $\kappa' l$ and gl from these two equations for constant $\cos[(k_1+k_2)l]$. For example, Fig.(10) shows the normalized wavelength detuning Ψ versus parametric gain $\kappa' l$ and linear gain gl for the oscillation condition at $\cos[(k_1+k_2)l]=1$ and $R_1=0.4$,$R_2=0.4$. Because it is a multiple valued solution, hence it is possible to have many pairs of gl and $\kappa' l$ for a particular value of Ψ (not shown in this figure).

CONCLUSION

In summary, we have developed a general theory of electromagnetic propagation in phase conjugate oscillators. Specifically, the authors have treated the propagation of electromagnetic radiation in a resonator bounded by one conventional reflector and one phase–conjugate mirror and resonators containing an intracavity phase–conjugate element. Wavelength detuning, linear and parametric gains are considered. Phase-conjugate power reflectivity, coherent power reflectivity and threshold oscillation condition are derived. The results indicate that: (1) nondegenerate oscillation are possible ($\Delta k \neq 0$) for the cases of $gl=0$ as Fig.1 for $b \neq 0$, Fig.6 for $ab \neq 0$ and all cases of $gl \neq 0$,and oscillation will only occur at pump frequency ($\Delta k=0$) for the cases of $gl=0$ as Figs.1 for $b=0$ and Fig.6 for $ab=0$. (2) we can use small $\kappa' l$ to generate self oscillation and simultaneous produce the coherent and phase–conjugate waves.

ACKNOWLEDGMENT

Wun–Shung Lee and Sien Chi wish to acknowledge helpful discussions with Senfer Wen. Pochi Yeh and Ragini Saxena gratefully acknowledge the support of the Air Force Office of Scientific Research under Contract No. F49620–88–C–0023.

REFERENCES

1. W. S. Lee, S. Chi, P. Yeh and R. Saxena, J. Opt. Soc. Am. B7, 1411 (1990)
2. G. P. Agrawal, J. Opt. Soc. Am. 73, 654 (1983).
3. R. Yaholam, and A. Yariv, J. Opt. Soc. Am. B5, 1783 (1988)
4. J.Au Yeung, D. Fekete, D. M. Pepper, and A. Yariv, Ieee J. Quantum Electron.QE–15, 1180 (1979)
5. I. M. Bel'dyugin, M. C. Galushkin, and E. M. Zemskov, Sov. J. Quantum Electron. 9, 20 (1979).
6. P. A. Belanger, A. Hardy and A. E. Siegman, Appl. Opt. 19, 602 (1980).
7. A. T. Friberg, and P. D. Drummond, J. Opt, Soc. Am. 73, 1216 (1983).
8. M. Nieto–Vesperinas, J. Opt. Soc. Am. b2, 427 (1985).
9. A. M. Lazaruk, A. T. Fnberg and R. Rainer E. Salomaa, IEEE J. Quantum Electron. QE–26,378 (1990).
10. A. Yariv and D. M. Pepper, Opt. Lett. 1, 16 (1977).
11. D. M. Pepper and R. L. Abrams, Opt. Lett. 3, 212 (1978)
12. R.C.Lind and D.G.Steel, Opt. Lett. 6, 554(1981).
13. P.Yeh, J. Opt. Soc. Am. A, Vol.2, p.727, May (1985)

FIGURE CAPTIONS

Fig. 1 The basic geometry of a linear phase–conjugate resonator via nearly degenerate four–wave mixing. In this case, the incident probe wave, whose frequency $\omega+\delta$ is slightly detuned from that of the pump waves (both at frequency ω),will result in a conjugate wave with an "inverted" frequency $\omega-\delta$. g is the linear nonsaturating background (intensity) net gain coefficient.

Fig. 2 Parametric gain $|\kappa'|l$ versus linear gain gl at oscillation condition for $\Delta k=0$ and several values of conventional mirror's reflectivity: $|r_2|^2=1$, 0.8, 0.5 and 0.1.

Fig. 3 The phase conjugate power reflectivity R_p versus normalized wavelength detuning Ψ for linear gain g=0. The dot–dashed curve represents the case of no conventional mirrors and $\kappa l=\pi/2$. The solid and dashed curves correspond to a linear resonator with a PCM and a perfectly reflecting conventional mirror at its two ends with nonlinear gain $\kappa l=\pi/4$ and $\kappa l=1.11065$ respectively. Note that when nonlinear gain is above $\pi/4$, then nondegenerate oscillation is possible, and the bandwidth of dashed line is narrower than the other two lines.

Fig. 4 The phase–conjugate and coherent power reflectivities R_p, versus normalized wavelength detuning Ψ with $r_2=-1$, $\kappa' l=1$ for $gl=-0.2$, $b/l=2.37018$ and $gl=0.2$, $b/l=0.57008$. These graphs show that for constant nonlinear gain $\kappa' l$, it is possible to detune the frequency of oscillation if we vary linear gain gl and choose a suitable b/l.

Fig. 5 The phase–conjugate power reflectivity versus normalized wavelength detuning at oscillation to show the effect of different b/l.

SC5538.FR

Fig. 6 The basic geometry of linear phase–conjugate oscillator via nearly degenerate four–wave mixing. In this case, the incident probe wave, whose frequency $\omega\pm\delta$ is slightly detuned from that of the pump waves (both at frequency ω), will result in a conjugate wave with an "inverted" frequency $\omega\mp\delta$. g is the linear nonsaturating background (intensity) net gain coefficient.

Fig.7 The threshold parametric gain $\kappa' l$ required for oscillation as a function of normalized cavity length $\phi\equiv k(l+a+b)$ with $r_2=-1$, $r_1=\sqrt{0.9}$ for linear gain ($gl=0.05268$) and linear loss ($gl=0.05268$).

Fig.8 The parametric gain $\kappa' l$ versus linear gain gl at threshold oscillation condition for various γ, whewe $k\phi=\gamma\pi$, $r_2=-1$, $r_1=\sqrt{0.9}$.

Fig.9 The X–Y plane versus nonlinear parametric gain κl for $(k_1+k_2)l=10000$,$(p,q)=(1,10000)$, $n=1.62$ and $r_1=\sqrt{0.9}$,$r_2=-1$ at the oscillation condition, where $X=\sin[\Delta k(a+b)]$, $Y=\cos[(k_1+k_2)(l+a+b)]$ and p,q are defined in equation (24).

Fig. 10 The normalized wavelength detuning Ψ versus parametric gain $\kappa' l$ and linear gain gl for the oscillation condition at $\cos[(k_1+k_2)l]=1$,$R_1=0.4$,$R_2=0.4$. and $a=b=0$

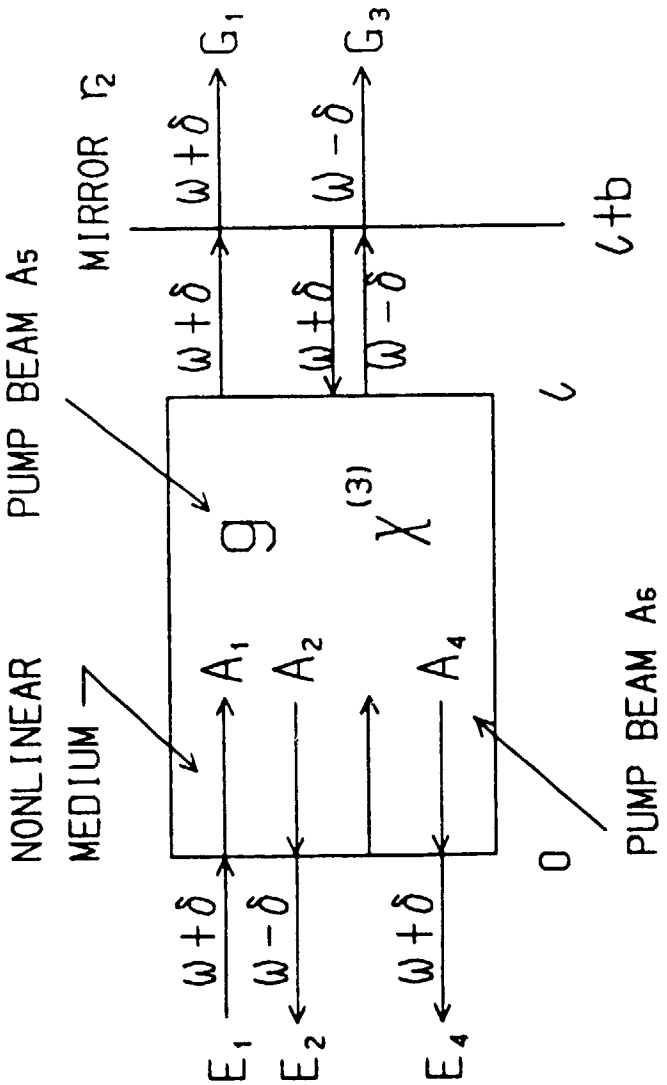
MIRROR r_2
G_1
G_3
$\omega+\delta$
$\omega-\delta$
$\ell+b$
ℓ
PUMP BEAM A_5
g
$\chi^{(3)}$
NONLINEAR MEDIUM
A_1
A_2
A_4
0
PUMP BEAM A_6
E_1
E_2
E_4

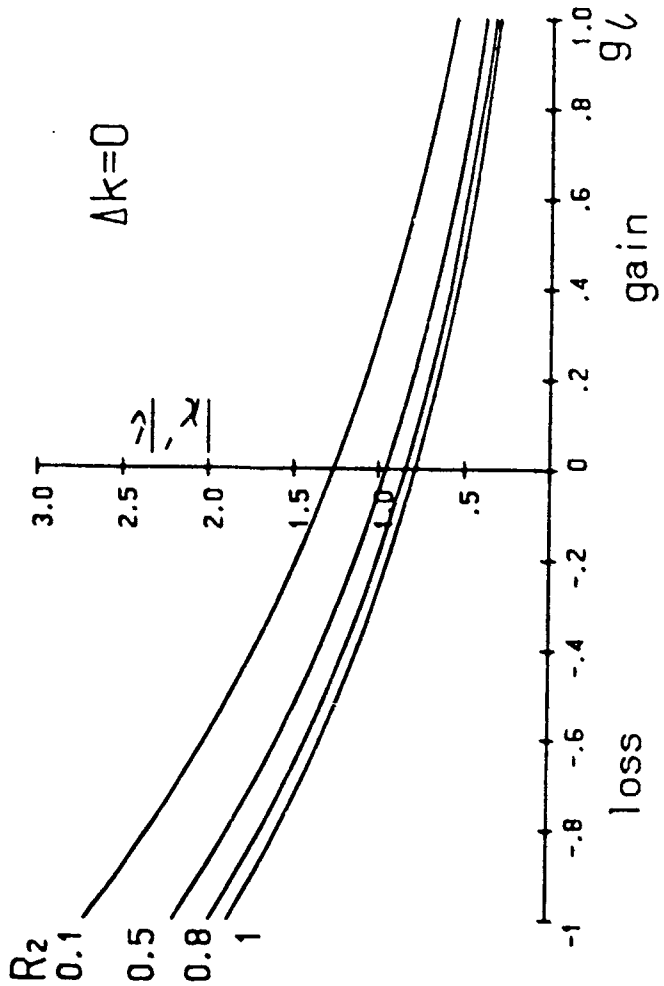
Δk=0
gain
loss
g
1.0
.8
.6
.4
.2
0
-.2
-.4
-.6
-.8
-1
.5
1.0
1.5
2.0
2.5
3.0
R2
0.1
0.5
0.8
1

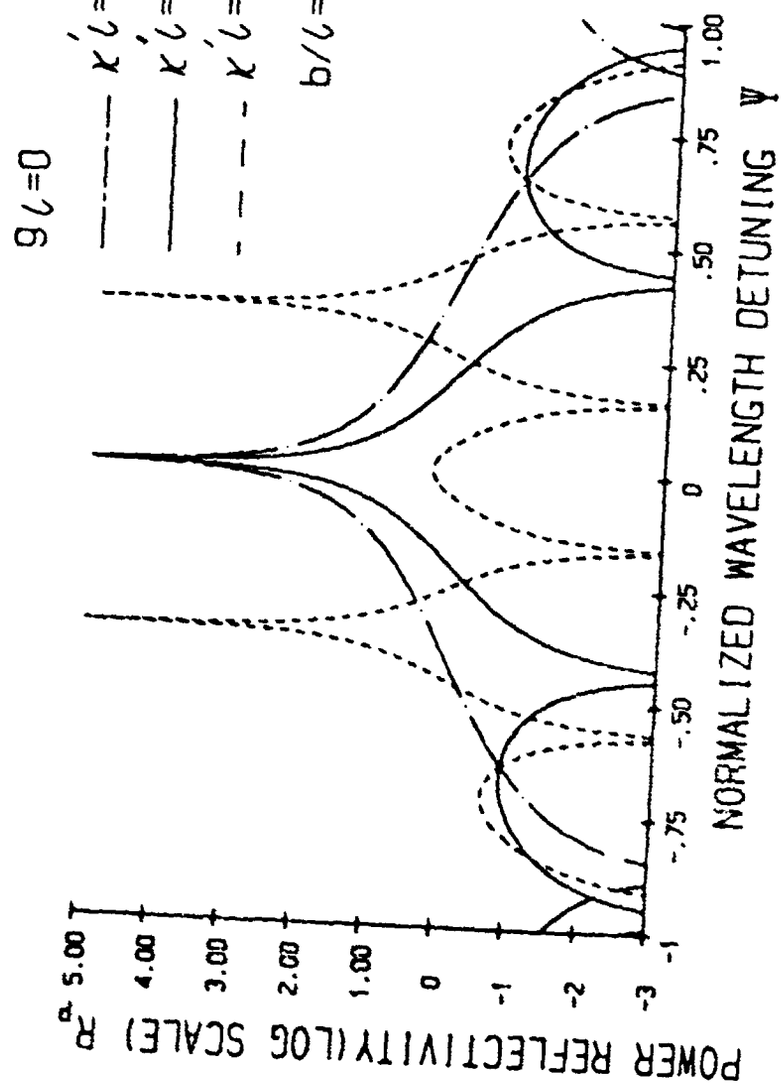
9ζ=0
κ'ζ=π/2 ; r2=0
κ'ζ=π/4 ; b/ζ=0 ; r2=-1
κ'ζ=1.11065 ;
b/ζ=0.70722 ; r2=-1
POWER REFLECTIVITY(LOG SCALE) Rd
5.00
4.00
3.00
2.00
1.00
0
-1
-2
-3
1.00
.75
.50
.25
0
-.25
-.50
-.75
-1
NORMALIZED WAVELENGTH DETUNING Ψ

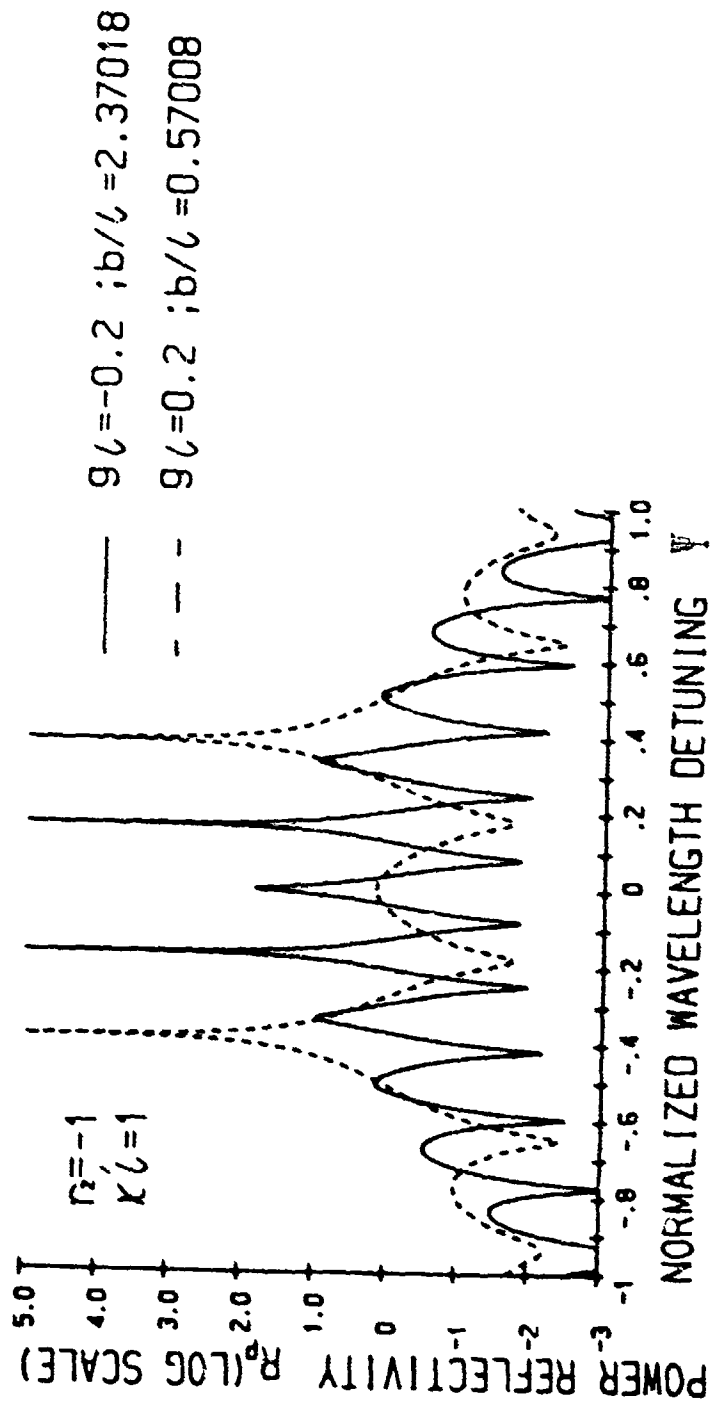
$g\zeta$=-0.2 ;b/ζ=2.37018
$g\zeta$=0.2 ;b/ζ=0.57008
r_2=-1
$\kappa\zeta$=1
POWER REFLECTIVITY R_p(LOG SCALE)
NORMALIZED WAVELENGTH DETUNING Ψ

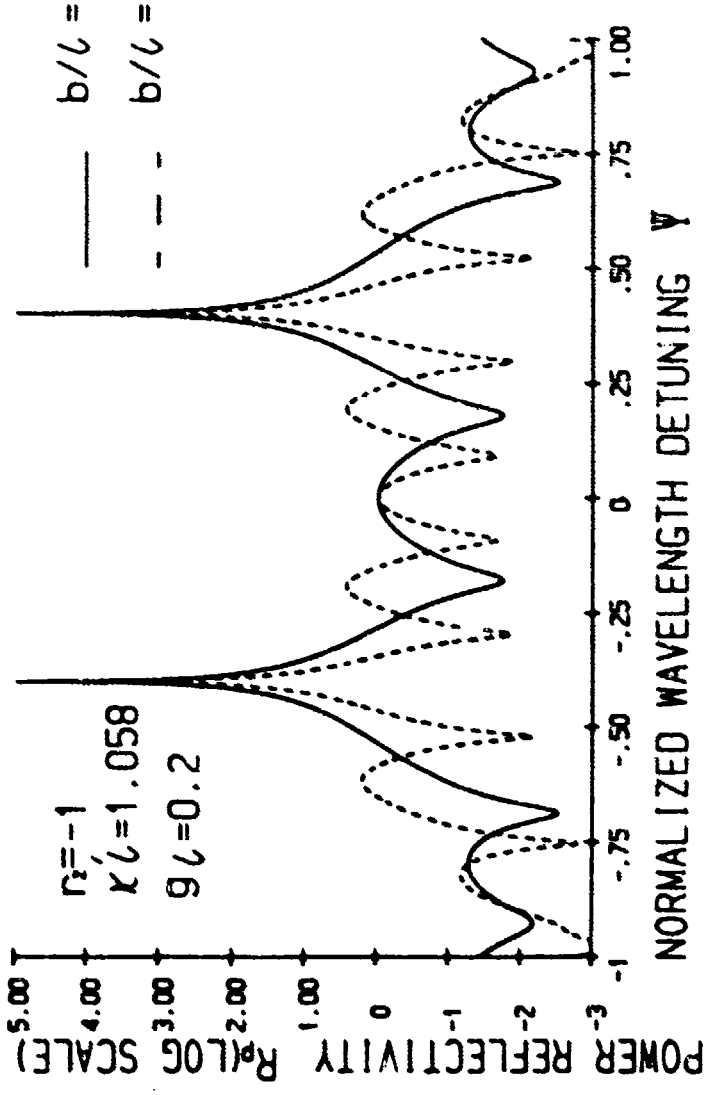
b/ℓ =0.50674
b/ℓ =1.75674
r₂=-1
κ'ℓ=1.058
gℓ=0.2
POWER REFLECTIVITY Rp(LOG SCALE)
NORMALIZED WAVELENGTH DETUNING Ψ
5.00
4.00
3.00
2.00
1.00
0
-1
-2
-3
-1
-.75
-.50
-.25
0
.25
.50
.75
1.00

Fig. 5

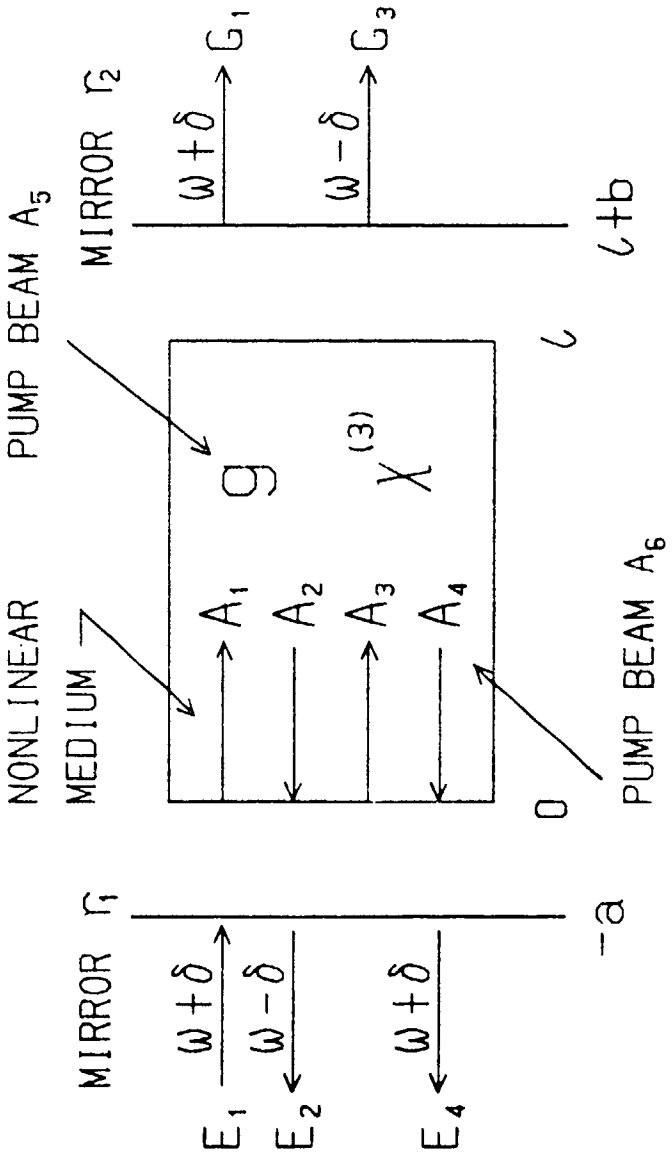
MIRROR r_2
G_1
G_3
$\omega+\delta$
$\omega-\delta$
$\ell+b$
PUMP BEAM A_5
NONLINEAR MEDIUM
g
$\chi^{(3)}$
A_1
A_2
A_3
A_4
ℓ
0
PUMP BEAM A_6
MIRROR r_1
E_1
E_2
E_4
$-a$

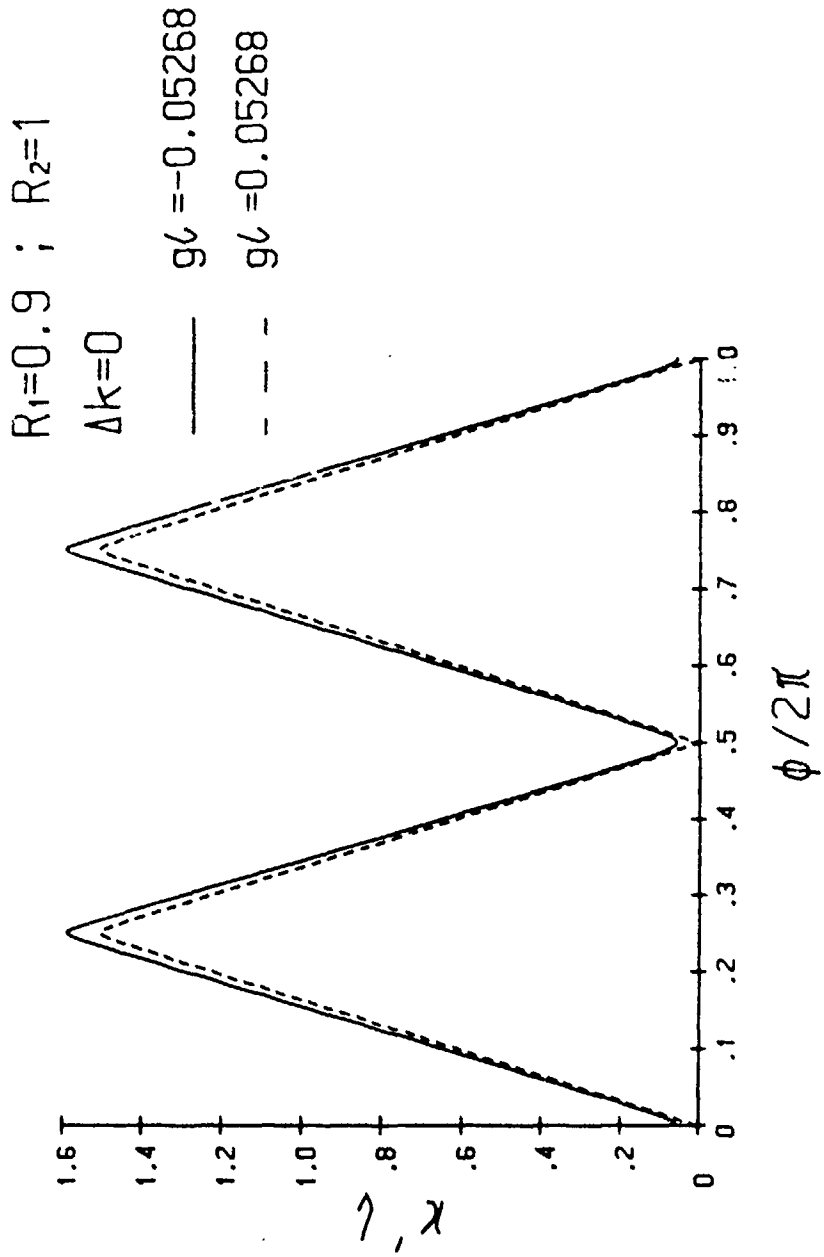
R1=0.9 ; R2=1
Δk=0
gζ =-0.05268
gζ =0.05268
η, χ
φ/2π
1.6
1.4
1.2
1.0
.8
.6
.4
.2
0
.1
.2
.3
.4
.5
.6
.7
.8
.9
1.0

Fig. 7

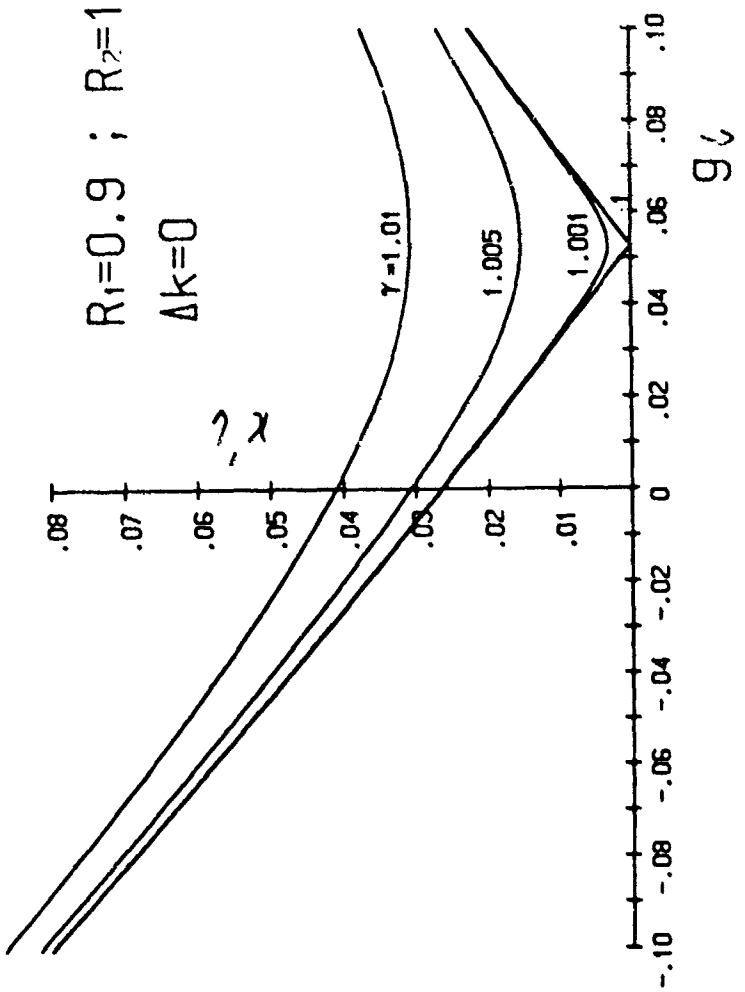
R1=0.9 ; R2=1
Δk=0
γ=1.01
1.005
1.001
1
γ, χ
gγ
.08
.07
.06
.05
.04
.03
.02
.01
0
-.02
-.04
-.06
-.08
-.10
.10
.08
.06
.04
.02

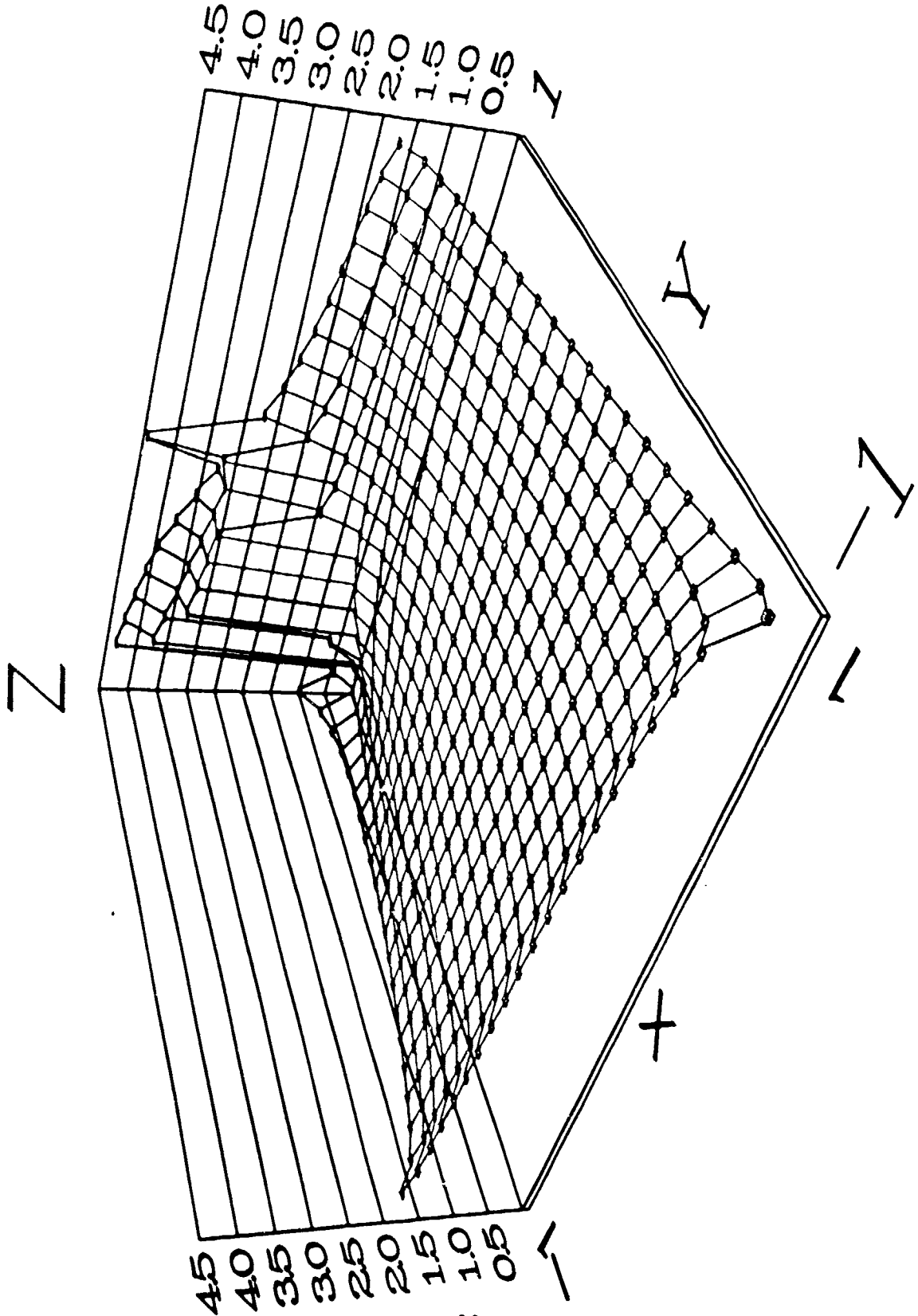

C11264DD/ejw

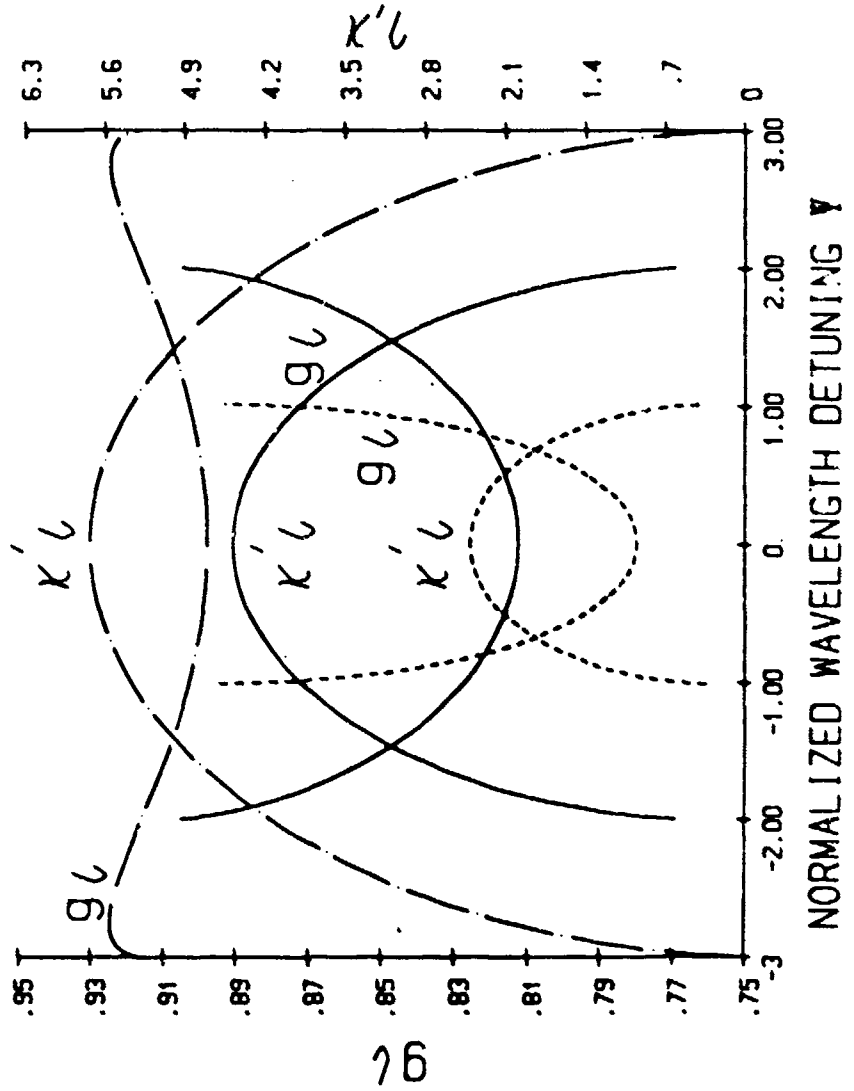
κ'ℓ
6.3
5.6
4.9
4.2
3.5
2.8
2.1
1.4
.7
0
3.00
2.00
1.00
0.
-1.00
-2.00
-3
NORMALIZED WAVELENGTH DETUNING
gℓ
gℓ
gℓ
κ'ℓ
κ'ℓ
κ'ℓ
.95
.93
.91
.89
.87
.85
.83
.81
.79
.77
.75
gℓ

Measurement of Frequency Locking in Phase-conjugate Optical Gyroscopes

spatial mode of the cw beam onto the pulsed beam. In my experiments, I have observed MPPC in a photorefractive $BaTiO_3$ crystal between the beams from a Q-switched flashlamp-pumped Nd:YAG laser and a diode-pumped cw Nd:YAG laser, both operating at 532 nm. The experimental results showed convincing spatial-mode cleanup of the pulsed beam. This method can also modify the incident pulsed beam to any desirable spatial pattern by using a spatial light modulator in the cw reference. To my knowledge, this is the first reported MPPC between pulsed and cw laser beams.

Reference

1. M. D. Ewbank, Opt. Lett. 13, 47 (1988).

11:00am

MW3 Incoherent light four-wave mixing for the measurement of reorientational relaxation of dye molecules

Yi-Zhong Yu

Laser Section, Department of Precision Instruments, Tianjin University, Tianjin 300072, China

I present a new convenient optical phase-conjugation technique for measurement of ultrafast reorientational relaxation time (T) in the study of dye solutions. This new method uses temporally incoherent light instead of short pulses. This method is different from those appropriate to optical Kerr media.

A frequency-doubled YAG laser with a pulse width of 8 ns was used in the experiment. Time resolution is governed by the coherence time (t_c) of laser light; it is short enough to measure T for the Rhodamine 6G, which is in the subnanosecond time region. The phase-conjugated signal (ϵ) was measured by changing delay time (τ) between two writing beams. The readout beam had a fixed time delay that was uncorrelated with the other two beams. Orthogonal and parallel polarization configurations were used. The theoretical calculation for orthogonally polarized beams shows a single exponential decay with exponent $-2\tau/T$ ($1/T = 1/T_1 + 1/T_r$, where T_1 is the first excited state lifetime). There is a coherent spike $|I(t)^2|$, and background terms

$$\epsilon(\tau) = 1 + T/t_c\,|I(t)|^2 + (\tfrac{1}{2})(t_c/T)\exp(-2\tau/T)$$

However, in the parallel polarization configuration the conjugated signal shows a complicated dependence on T owing to formation of thermal grating. The experimental results coincide with data measured by means of the other method.

11:15am

MW4 Measurement of frequency locking in phase-conjugate optical gyroscopes

M. J. Rosker, I. McMichael, and K. Saxena

Rockwell International Science Center, 1049 Camino Dos Rios, Thousand Oaks, California 91360

A ring resonator containing a phase-conjugate mirror can act as a phase-conjugate optical gyroscope (PCOG).[1] The frequencies of the counterpropagating oscillations depend on the nonreciprocal, but not on the reciprocal, optical path length of the resonator; thus, the device is potentially useful for inertial sensing of rotational motion. A primary limitation of conventional ring-laser gyroscopes is frequency-locking behavior, wherein backscattering couples the counterpropagating laser oscillations. Our previous theoretical results[2] indicated that, for nonreciprocal phase shifts of $-\pi/10$ rad, frequency locking occurs when the ratio of backscattered light to pump light exceeds -10^{-3}. We describe our experimental investigation of the frequency-locking characteristics for the ring PCOG. A weak seed beam was injected into the oscillator along the same direction as the phase-conjugate output. The frequency difference between the counterpropagating waves was measured as a function of the seed intensity and the nonreciprocal phase shift. Measurements were made with both coherent and incoherent (with respect to the pump) seed light to simulate scatter contributed by the phase-conjugate and conventional mirrors, respectively. The experimental results are in good agreement with theory.

References

1. B. Fischer and S. Sternklar, Appl. Phys. Lett. 47, 1 (1985).
2. R. Saxena, M. J. Rosker, W. R. Christian, I. McMichael, and P. Yeh, in *International Quantum Electronics Conference* (Optical Society of America, Washington, D.C., 1990), paper CTuP4.

11:30am

MW5 Optical novelty filtering using a phase-grating carrier

Francis T. S. Yu, Shudong Wu, Sumati Rajan, and Andy Mayers

Department of Electrical Engineering, 121 Electrical Engineering East, University Park, Pennsylvania 16802

Techniques using photorefractive effects for novelty filtering have recently been suggested by several investigators. Examples include the four-wave-mixing interferometric method,[1] the two-wave-mixing beam depleting method, and the beam fanning method.[2]

In this paper we use a phase grating carrier in a four-wave mixing configuration to realize a novelty filter. In the experimental setup the output phase modulated object encoded beam with a phase grating is imaged into a BSO crystal. The reconstructed phase conjugated beam, with all the phase information of the object and the grating, is produced by a real-time beam. After emerging from the input object, the phase conjugated beam is phase compensated. Thus, only a dc spot can be observed at the output focal plane without higher order diffraction. However, if the phase grating object is suddenly moved in the setup because of the finite response time of the photorefractive material, the higher diffraction orders of the grating appear. Each of the diffraction orders carries the input object information. Thus, by selecting the strongest diffraction order, the object function can be observed at the output image plane within the response time of the crystal. This proposed technique offers the simplicity of optical setup, it avoids the critical zero-phase problem of the interferometric method, and it has high sensitivity and image contrast. Detailed analysis and experimental demonstrations of the proposed technique are presented.

References

1. D. Z. Anderson, D. M. Lininger, and J. Feinberg, Opt. Lett. 12, 123–125 (1987).
2. J. E. Ford, Y. Fainman, and S. H. Lee, Opt. Lett. 13, 856–858 (1988).

NOTES

Theory of Phase-conjugate Oscillator Applied to a Phase-conjugate Resonator

beam splitter in conjunction with a wave plate, the reflected light can be coupled out without loss in amplitude. We report on the angular sensitivity, wavelength dependence, and amplitude threshold needed for SSPC to occur in these fibers.

References

1. R. A. Mullen, G. C. Valley, and D. M. Pepper, Conference on Lasers and Electro-Optics Technical Digest (Optical Society of America, Washington, D.C., 1989), paper TUS4.
2. A. V. Mamaevand V. V. Shkunov, Sov. J. Quantum Electron. 19, 1199 (Sept. 1989).
3. L. Hesselink, "Photorefractive fibers for optical data storage and processing," IEEE Intl. J. Opto-electronics, Special issue on optical computing, 1990.

ThY18 Response of a self-pumped phase-conjugate mirror for two mutually coherent inputs

T. Honda and H. Matsumoto

National Research Laboratory of Metrology, 1-1-4, Umezono, Tsukuba, Ibaraki, 305, Japan

Photorefractive self-pumped phase conjugation is attractive for its simplicity and high reflectivity with low-power light sources. In order to realize its potential applications, it is important to study its response. So far the response of a phase-conjugate wave has been described with its rise time. It has not studied how the phase-conjugate wave responds when the spatial structure of an input probe wave is changed dynamically. We investigated the response of the phase conjugate wave by using two mutually coherent input beams, which can be regarded as components of a probe wave, and by introducing sinusoidal phase changes into one of them with varied frequencies. Each input beam has a power of 6 mW at the wavelength of 515 nm. A $BaTiO_3$ crystal was employed as a self-pumped phase-conjugate mirror.[1] By measuring relative phase between the two output beams, which can be regarded as components of a phase-conjugate wave, we found the response characteristic represented by a time-lag of first order, which is similar to RC circuit. The response time thus determined was 0.32 s, which was much shorter than the rise time of 30 s obtained with the same condition.

References

1. J. Feinberg, Opt. Lett. 7, 486-488 (1982).

ThY19 Theory of phase-conjugate oscillator applied to a phase-conjugate resonator

Wun Shung Lee, Sien Chi, Ragou Saxena,* and Pochi Yeh*

Institute of Electro-Optical Engineering, National Chiao Tung University, Hsinchu, Taiwan, China

Optical resonators containing a phase conjugate mirror (PCM) have been a subject of great interest, especially for cases in which the PCM is employed as an end mirror of a resonator cavity for intracavity aberration correction.[1] Recent theoretical analysis indicates that the insertion of a PCM inside a ring-laser cavity results in a reduction of the lock-in threshold and reduces the imbalance between the amplitudes of the oppositely directed travelling waves.[2] We have developed a general theory for nondegenerate oscillations in a phase-conjugate oscillator (PCO) that consists of a Fabry–Perot cavity with a PCM as an intracavity element. The PCM is a nonlinear transparent medium pumped by a pair of counterpropagating laser beams of the same frequency and intensity. Phase conjugation with gain is possible for an injected signal of a slightly different frequency by nearly degenerate four-wave mixing (NDFWM). The linear absorption/gain in the medium is also taken into account. In this presentation, we apply the results of the general theory to a phase-conjugate resonator by equating the reflectivity of one of the conventional mirrors to zero. Analytic expressions are obtained for the two reflection coefficients and the two transmission coefficients of the injected signal, and the condition for oscillation is derived. A novel approach yields the mode spacing of such a phase-conjugate resonator.

*Rockwell International Science Center, 1049 Camino Dos Rios, Thousand Oaks, California 91360.

References

1. A. E. Siegman, P. A. Belanger, and A. Hardy, *Optical Phase Conjugation*, R. A. Fisher, ed. (Academic Press, New York, New York, 1983), Ch. 13.
2. J. C. Diels and I. C. McMichael, Opt. Lett. 6, 219 (1981).

ThY20 Variational model of soliton interaction in two-mode fibers

C. Paré, M. Florjanczyk, and P. A. Bélanger

Département de physique, Université Laval, Québec, Québec, G1K 7P4, Canada

All-optical switching in a nonlinear directional coupler and the evolution of the state of polarization in a nonlinear birefringent fiber represent two important practical problems of propagation in a two-mode, nonlinear dispersive system. Both cases are described by a nonintegrable system of coupled nonlinear Schrödinger equations. On the basis of numerical simulations,[1] it has already been shown that solitons present important advantages over differently shaped pulses. To improve our physical insight into the dynamics resulting from the complex interplay between nonlinearity (self- and cross phase modulation), dispersion, and linear coupling, we have developed an approximate *all analytical* model of soliton interaction. An extension of a variational method[2] has been used, and the results can be recast in a suggestive potential well picture. Besides improved estimates of optical switching powers, a symmetry breaking instability can easily be anticipated. A detailed comparison with numerical simulations, showing a good overall agreement between exact and approximate results, will be presented.

References

1. S. Trillo *et al.*, Opt. Lett. 13, 672 (1988).
2. D. Anderson, M. Lisak, and T. Reichel, Phys. Rev. 38A, 1618 (1988).

ThY21 Nonlinear-optical response in suspensions of organic and inorganic colloidal systems

P. R. Schuster, C. A. Vianda, and R. S. Potember

JHU Applied Physics Laboratory, Johns Hopkins Road, Laurel, Maryland 20723-6099

The third-order nonlinear optical response of various colloidal suspensions has been investigated. The transmissive properties of these systems are of particular interest in terms of the speed of the switching response, the switching threshold, the recovery time, and the dynamic range over which optical density is generated. We have seen resonant and non-resonant behavior in the nonlinear response of these materials. These suspensions are composed of both inorganic and organic materials homogeneously distributed within a dielectric matrix. In certain studies, these materials have been synthesized as charge-transfer complexes by using an inorganic electron donor combined with an organic electron acceptor. Our results concerning the third-order nonlinear optical properties of these materials, our development of methods for the enhancement of their nonlinear optical response will also be reported.

This work supported by the Department of the Navy contract N00039-89-C-5301.

ThY22 Efficient coupling of multiple diode laser arrays to an optical fiber

T. T. Fan

MIT Lincoln Laboratory, P.O. Box 73, Lexington, Massachusetts 02173

Diode lasers are efficient sources of laser radiation, but their coupling to an optical fiber has been limited to applications that require low power. Here we demonstrate that these high power diode lasers can be coupled with high efficiency into a single multimode optical fiber by geometric multiplexing. In principle, many more diodes could be used and tens of watts of power could be obtained from a single fiber with incoherent multiple diode input. We have coupled three high power diode arrays to a 200 μm core, 0.2 N.A. optical fiber with 59% efficiency and have obtained 700 mW at the output of the fiber for 1.19 W at the input. Based on the properties of the beams from these high power diode laser sources, it should be possible to efficiently couple over 100 of these lasers to this optical fiber and obtain tens of watts of deliverable power. Calculations show that the number of identical sources that can be efficiently coupled to an optical fiber is proportional to the square of the product of the core diameter and numerical aperture.

Frequency Locking in Ring Double Phase Conjugate Oscillators

$$D(t) = \frac{I_{sc}(t) - I_{sc}(t)}{I_{sc}(o) - I_{sc}(o)}. \qquad (6)$$

The noise fanout phenomenon was also recently used in time-integrating interferometry by Ford *et al.*[8]

A $BaTiO_3$ crystal was used for the experimental demonstration. First, the effect of the dynamic range compression is simulated by applying different intensities of the input laser beam to the crystal. It can be seen that for the higher input power, the decay of the output power is faster than that for the lower input power. This result follows our assumption. Physically the noise based scattering diffraction gratings are established more swiftly when the input intensity is stronger. These diffraction gratings scatter light away from the input beam. Next, for a few different levels of input intensities, it can be seen that the dynamic range of the output decreased while the dynamic range of the input remains constant. In the above, reduction of the DR with respect to time is clearly demonstrated.

We might point out that the predetection DRC is a unique optical problem.[9] Since by definition the 2-D signal has not yet been detected before compression, there is no counterpart solution that can be provided by digital electronics.

1. H. K. Liu and L. J. Cheng, Appl. Opt. 27, 1006 (1988).
2. A. Ashkin *et al.*, Appl. Phys. Lett. 9, 72 (1966).
3. R. Magnusson and T. K. Gaylord, Appl. Opt. 13, 1545 (1974).
4. W. Phillips, J. J. Amodei, and D. L. Staebler, RCA Rev. 33, 105 (1972).
5. S. M. Avakyan, S. A. Alaverdyan, K. G. Belyaev, V. Kh. Sarkisov, and R. M. Tumanyan, Sov. Phys. Solid State 20, 1401 (1978).
6. N. V. Kukhtarev, V. P. Markov, S. G. Odulov, M. S. Soskin, and V. L. Vinetskii, Ferroelectrics 22, 949 (1979).
7. R. A. Rupp and F. W. Drees, Appl. Phys. B 39, 223 (1986).
8. J. E. Ford, Y. Fainman, and S. H. Lee, Opt. Lett. 13, 856 (1988).
9. For other uses, see a recent review paper: P. Yeh, A. E. Chiou, J. Hong, P. Beckwith, T. Chang, and M. Khoshnevisan, Opt. Eng. 26, 328 (1987).

5:15 PM
CTUP4 Frequency locking in ring double phase conjugate oscillators

RACHEL SARENA, M. J. RUDERER, WILLIAM K. CHRISTIAN, J. McMICHAEL, P. YEH, Rockwell International Science Center, 1049 Camino Dos Rios, Thousand Oaks, CA 91360

When two phase conjugate mirrors (PCMs) with gain are placed next each other, an oscillation builds between them.[1] This is called a double phase conjugate oscillator (DPCO). The beat frequency between the counterpropagating oscillations is independent of the reciprocal optical path length of the resonator but does depend on the nonreciprocal optical path length—a property that can be used for inertial sensing of rotational motion in a ring DPCO.

A primary limitation for conventional ring laser gyroscopes is frequency-locking, wherein backscattering may couple together counterpropagating laser oscillations. It is, therefore, of particular interest to determine the frequency-locking characteristics of the ring DPCO.

We have developed a theory that determines the intensities and frequencies of the counterpropagating modes in DPCOs using the self-consistent formalism of Lamb.[2] Our analysis shows that the frequency splitting $\Delta\omega$ between the zeroth-order counterpropagating modes is linearly proportional to ϕ_{nr}, the round-trip nonreciprocal phase shift in the resonator:

$$\Delta\omega = \phi_{nr}/(\tau + L/c), \qquad (1)$$

where L is the length of the resonator and τ is the response time of the phase conjugate mirror. In deriving Eq. (1), we have made the simplifying assumptions of weak coupling, small frequency shifts, and identical phase conjugate mirrors. For oscillators using slow phase conjugate mirrors, the constant of proportionality is the reciprocal of the response time of the phase conjugate mirror, while for DPCOs using fast PCMs the constant of proportionality is the reciprocal of the transit time in the resonator. We have experimentally verified the above relationship in the first regime, using externally pumped phase conjugate mirrors in photorefractive crystals of barium titanate and potassium niobate.

We have theoretically examined the intensities and frequencies of the counterpropagating modes in the presence of contradirectional coupling to determine in what conditions frequency-locking occurs (if at all). Our preliminary experimental results show that frequency-locking does not occur despite intracavity incoherent backscatter coupling as great as 30%. We describe the results of experiments to measure frequency-locking as a function of the level of back scattering coupling and coherence.

1. J. Lam and W. Brown, Opt. Lett. 5, 61 (1980); M. Cronin-Golomb, B. Fischer, J. K. Kwong, J. O. White, and A. Yariv, Opt. Lett. 7, 353 (1982); P. Yeh, M. Khoshnevisan, M. Ewbank, and J. Tracy, Opt. Commun. 57, 387 (1986).
2. M. Sargent III, M. O. Scully, and W. E. Lamb, Jr., Laser Physics (Addison Wesley, Reading, MA, 1974), Chaps. 8, 10, and references therein.

5:30 PM
CTUP5 Second-order polarizability holograms in few-mode fibers: phase conjugation and angular selectivity

YU. E. KAPITZKY, B. YA. ZELDOVICH, Polytechnic Institute, Nonlinear Optics Laboratory, 7a Pramp Lenina, Chelyabinsk 454080, USSR

It was discovered in Ref. 1 that a second-order polarizability grating can be formed by simultaneous irradiation of an optical fiber by neodymium laser picosecond pulses and its second harmonic (SH); see also Refs. 2 and 3. In the present work some features of a second-order polarizability grating $\beta_3^{(2)}$ were studied for fibers possessing few modes for both the fundamental frequency and its SH. Information about the interference of IR and SH waves is written as a hologram of the cube of the light field:

$$\beta_3^{(2)}(r,z) = \text{const} \cdot E_1^2(r,z)E_2^* \times \exp(i\Delta kz) + \text{c.c.},$$

where $\Delta k = 2k_1 - k_2$. Fields $E_1(r,z)$ and $E_2(r,z)$ are the superimpositions of several transverse modes and, therefore, produce a speckle structure inside the fiber. If the reading IR field $R_1(r,z)$ exactly coincides with the writing IR field, $R_1(r,z) = E_1(r,z)$, the SH polarization $|E_1|^2E_2(r,z)$ effectively generates an SH wave which has the structure of the writing SH wave. For different $R_1(r,z)$ and $E_1(r,z)$ of the projection of $R_1(r,z)$ to $E_1(r,z)$ only reads the hologram effectively. There must be a reconstruction of the phase conjugated SH $E_2(r,z)$ via the reading hologram by an IR wave in the direction opposite to the writing IR wave.

In the experiment we used a cw active mode-locked active Q-switched Nd:YAG laser with f = 4000 Hz, with about thirty pulses in a bunch with a 100-ps duration for each pulse. About 0.2 W of IR power and 0.01 W of SH were transmitted through the quartz fiber with the 8-μm core diameter and 1-m length using a 20× microobjective. A 40 mm thick glass plate was installed in front of the objective; a turn of the plate allows one to change the angle of incidence of light into the fiber. Figure 1 shows the efficiency of reading η vs input angle α of the IR for the fixed transmitted reading power. It is interesting that the selectivity curve width was 2 times smaller than the angular width of the main IR fiber mode. By turning the 6-mm thick glass plate during writing we could change the phase difference $\Delta\varphi = \varphi_2 - 2\varphi_1$ of the fields introduced to the fiber. A second exposure by E_1 and E_2 fields with a π-shifted $\Delta\varphi$ with respect to the first one coherently erased the previous hologram.

For a demonstration of phase conjugation by a $\chi^{(2)}$ hologram the SH was introduced at an angle relative to the IR while writing. The reading IR wave was introduced from the other end of the fiber. During the first 2-10 min the reconstructed SH was in the direction opposite that of the writing SH, which was interpreted as phase conjugation. Turning the angle of the reading IR wave resulted in a change of intensity of SH only but not the angular distribution. Later, the SH pattern changed to an axially symmetric one, probably due to rewriting during the reading stage.

1. U. Osterberg and W. Margulis, Opt. Lett. 11, 516 (1986); 12, 57 (1987).
2. R. H. Stolen and H. Tom, Opt. Lett. 12, 585 (1987).
3. N. B. Baranova and B. Ya. Zeldovich, Sov. Phys. JETP Lett. 45, 717 (1987).

5:45 PM
CTUP6 Spectral features including polarizational of two- and four-wave interactions for nonlinearity accumulated during a pulse

O. F. KASHAEV, I. G. KUZNETSOV, P. N. Lebedev Physics Institute, 53 Leninsky Pramp., Moscow 117924, USSR

We report the original results of theoretical and experimental investigations[1-3] of a

Nondegenerate Oscillation in a Phase Conjugate Mirror with Linear Gain

Experiments were performed using a low pressure CO_2 laser in both standing-wave and ring resonator configurations for two resonator magnifications. A variable frequency shift in the return beam was produced with two acoustooptic modulators (as shown in Fig. 1). Laser output power and beam quality were measured as a function of fed-back power and frequency shift. The frequency shift varied from 0 MHZ to the longitudinal mode spacing. Although the amplification factor was relatively constant if the return frequency was far from that of any of the lowest loss modes, there was a strong dependence on frequency if the return frequency was near a lowest loss mode.

The amount of beam quality degradation or power loss was also dependent on the magnification of the resonator: higher magnification resonators were more sensitive to return power. Returns of $\sim 7 \times 10^{-4}$ ($M = 1.5$) and 1.4×10^{-4} ($M = 2.0$) were sufficient to cause a 5% degradation in beam quality for the standing-wave resonators. This was consistent with analysis predictions of 10^{-3} ($M = 1.5$) and 10^{-4} ($M = 2$). The beam quality degradation vs return fraction for the standing-wave resonator with magnification of 1.5 is shown in Fig. 2. For low levels of return, the beam quality of the forward wave in the ring resonator was insensitive to the return power; however, the ring resonator did exhibit an intensity drop as return power increases (see Fig. 3).

(Poster paper)

CTHI25 Investigation into quantum statistics of light using high-sensitivity phase conjugation

O. V. KULAGIN, G. A. PASMANIK, A. A. SHILOV, Institute of Applied Physics, Academy of Sciences of the U.S.S.R., 46 Uljanov St., 603600 Gorky, U.S.S.R.

A semiclassical theory is developed describing transformation of the quantum statistics of radiation on its passage through various optical systems (OSs) including semitransparent mirrors and amplifying and absorbing media (Fig. 1). The signal intensity is defined in terms of this theory as the intensity of the total field of this signal and zero noises which have passed through an OS minus intensity of the input noise in the reception band:

$$I = \frac{c}{2\pi}\left|\langle(\hat{\epsilon} + \epsilon)^2\rangle - |\epsilon|^2\right|, \qquad (1)$$

where $\hat{\epsilon}$ is the operator to describe OS taking into account its internal noises.

Let us introduce the photon numbers n to characterize the total radiation energy per one resolution element. Their mean values and the quantum dispersion $(\overline{\Delta n})^2$ at the input and output of OS including an amplifier or attenuator (the transmissivity k) are related as

$$\bar{n} = (k-1)\Delta f_s[1 + \tilde{N} + \tilde{N}(-T_s)] + \eta k \bar{n}_0,$$

$$(\overline{\Delta n})^2 = (k-1)^2\Delta f_s[1 + \tilde{N} + \tilde{N}(-T_s)]^2 + \eta k^2 \bar{n}_0(1 + 2\tilde{N}).$$

Here $\tilde{N} = [\exp(\hbar w/kT) - 1]$, T is the ambient temperature, $T_s = \hbar w/\ln(N_1/N_2)$ is the amplifier/attenuator temperature, Δf_s is the product of the amplifier/attenuator frequency band Δf by the registration time τ, η is the quantum efficiency depending on the difference δf between the signal frequency and the amplifier eigenfrequency ($\eta = 1$ at $k = 1$ or $\delta f \ll \Delta f$). This theory has been verified experimentally using a double pass amplifier optical system comprising a phase conjugate mirror with $\lambda = 1.05\ \mu m$ and the sensitivity of about two photons per resolution element, the number of elements being 380 × 380. The transverse distribution of a light beam was processed by means of a matrix photodetector and numerical averaging of the results over a large number of elements. This OS was used to analyze the statistics of thermal radiation in the laser breakdown region ($T \gtrsim 3,\ldots,5$ eV), statistics of spontaneous and stimulated scattering, as well as of linear scattering at small particles. It was also shown that the phase shift by π in one beam (attenuated to $\bar{n}_0 \simeq 1$) of a two-beam interferometer with a phase conjugate mirror leads to a change in the SNR value from 1 to 2. The possibility of splitting a light beam into several (two, four,...) channels with $\bar{n}_0 < 1$ followed by a phase-locked PC of radiation from each of these channels in their respective PC mirrors pumped by the same laser beam was demonstrated. (Poster paper)

CTHI26 Paper withdrawn

CTHI27 Nondegenerate oscillation in a phase conjugate mirror with linear gain

WUN-SHUNG LEE, SIEN CHI, National Chao Tung U., Institute of Electrooptical Engineering, Hsinchu, Taiwan, China; RAGINI SAXENA, POCHI YEH, Rockwell International Science Center, Thousand Oaks, CA 91360.

Optical resonators containing a phase conjugate mirror (PCM) have been a subject of great interest, where the PCM is employed as an end mirror of the resonator cavity for intracavity aberration correction.[1] Recent theoretical analysis indicates that the insertion of a PCM inside a ring laser cavity results in a reduction of the lock-in threshold and reduces the imbalance between the amplitudes of the oppositely directed traveling waves.[2] In the extreme case of phase conjugate oscillation without conventional gain, lock-in can be completely eliminated.[3]

We have developed a general theory for nondegenerate oscillations in a phase conjugate oscillator (PCO), i.e., an optical resonator with a PCM as an intracavity element.[4] The theory is formulated by studying the problem of wave propagation along the axis of the resonator and by extending the matrix method introduced by Yeh[5] to describe the case of nondegenerate four-wave mixing (NFWM). The PCM is taken to be a nonlinear transparent medium pumped by a pair of counterpropagating laser beams of the same frequency and intensity. Phase conjugation of an input probe beam of slightly different frequency is achieved by NFWM. Linear absorption or gain in the medium is also taken into account.

For negligible linear absorption (gain) in the medium and with no conventional mirrors, the PCO behaves like an ordinary PCM, and the results of our general theory are identical with those of Pepper and Abrams[6]—a phase conjugate wave can be generated without a probe beam and the corresponding phase conjugate reflection coefficient and probe transmission coefficient will be infinitely large. This self-oscillation can occur only at the pump frequency and when the parametric gain is an integral multiple of $\pi/2$. In the presence of linear absorption (gain) in the medium, our study shows that the parametric gain required for self-oscillation at the pump frequency is considerably increased (decreased), while the bandwidth and sidelobe structure of the bandpass filter are also affected. Also, nondegenerate self-oscillation can now occur if the medium has large linear gain. Figure 1 is a plot of the phase conjugate reflectivity R_p and the probe transmission coefficient T_s vs the normalized wavelength detuning between the probe and pump beams for a linear gain of 4.32 and a parametric gain of 0.13. Note that R_p and T_s become infinitely large at a nonzero wavelength detuning, i.e., in the absence of a probe beam, self-oscillation at a frequency different from that of the pump beams is possible in a medium with linear gain.

(Poster paper)

1. A. E. Siegman, P. A. Belanger, and A. Hardy, *Optical Phase Conjugation*, R. A. Fisher, Ed. (Academic, New York, 1983), Chap. 13 and references therein.
2. J. C. Diels and I. C. McMichael, Opt. Lett. 6, 219 (1981).
3. P. Yeh, J. Tracy, and M. Khoshnevisan, Proc. Soc. Photo-Opt. Instrum. Eng. 412, 240 (1983); P. Yeh and M. Khoshnevisan, Proc. Soc. Photo-Opt. Instrum. Eng. 487, 102 (1984).
4. W. S. Lee, S. Chi, P. Yeh, and R. Saxena, *OSA Annual Meeting*, 1989 Technical Digest Series, Vol. 18 (Optical Society of America, Washington, DC, 1989), p. 102.
5. P. Yeh, J. Opt. Soc. Am. A 2, 727 (1985).
6. D. M. Pepper and R. L. Abrams, Opt. Lett. 3, 212 (1978).

CTHI28 Laser beam noise cleanup using Brillouin mirrors, and the problem of associative memory

N. F. ANDREEV, V. A. DAVYDOV, E. V. KATIN, A. Z. MATVEEV, O. V. PALASHOV, G. A. PASMANIK, P. S. RAZENSHTEIN, Institute of Applied Physics, Academy of Sciences of the U.S.S.R., 46 Uljanov St., 603600 Gorky, U.S.S.R.

Possible ways of laser beam cleanup from speckle noise imposed on this beam are considered. Such a cleanup is required: (1) when a self-focusing instability causes buildup of a parasitic field with a speckle inhomogeneous transverse structure against a high power beam with a diffraction-limited divergence. Speckles can also be generated by the defects of optical elements; (2) when a weak signal with the diffraction-limited divergence is amplified in a narrowband amplifier. It is necessary

Poster Thursday

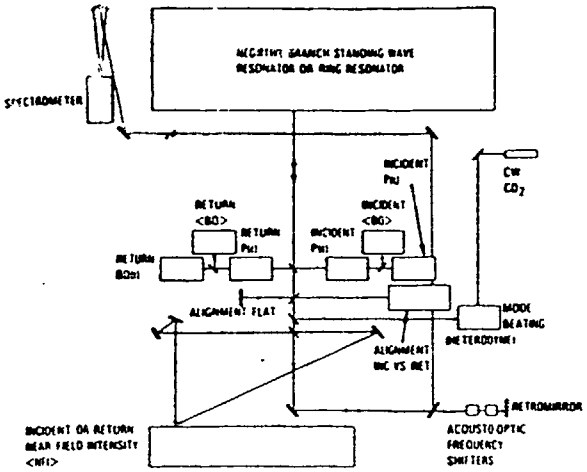

CTHI24 Fig. 1. Optical layout for oscillator isolation experiments.

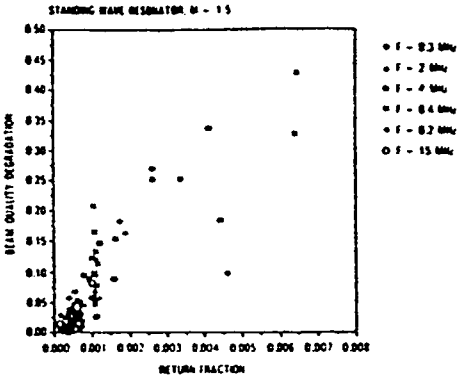

CTHI24 Fig. 2. BQ degradation vs return fraction.

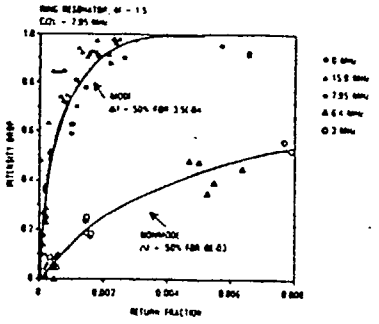

CTHI24 Fig. 3. Intensity drop vs return fraction.

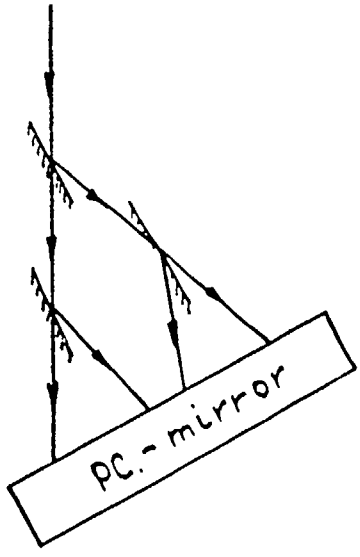

CTHI25 Fig. 1. Optical system of semi-transparent mirrors with amplifying and absorbing media.

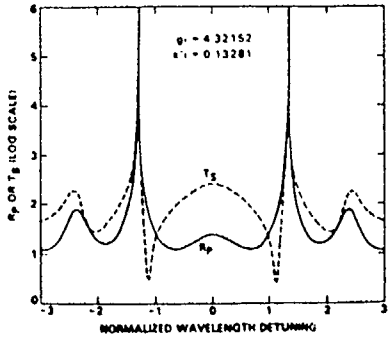

CTHI27 Fig. 1. Plot of phase conjugate reflectivity R_p and probe transmission coefficient T_s vs the normalized wavelength detuning between the probe and pump beams for a linear gain of 4.32 and a parametric gain of 0.13.

Poster Thursday

Two-Wave Mixing in Nonlinear Media

484 IEEE JOURNAL OF QUANTUM ELECTRONICS, VOL. 25, NO. 3, MARCH 1989

Two-Wave Mixing in Nonlinear Media

POCHI YEH, SENIOR MEMBER, IEEE

(Invited Paper)

Abstract—**The coupling of two electromagnetic waves in various nonlinear media is treated. The nonlinear media considered include photorefractive crystals, Kerr media, etc. The theory, some of the experiments, and several applications are described.**

I. Introduction

TWO-WAVE mixing (sometimes referred to as two-beam coupling) is an exciting area of research in nonlinear optics. This area involves the use of nonlinear optical media for the coupling of two electromagnetic waves, especially the energy exchange between them.

Two-wave mixing is a physical process which takes advantage of the nonlinear response of some materials to the illumination of electromagnetic radiation. For example, let us consider the interference pattern formed by two laser beams in a nonlinear medium. Such a pattern is characterized by a spatial variation (usually periodic) of the intensity. If the medium responds nonlinearly, then an index variation is induced in the medium. The process of forming an index variation pattern inside a nonlinear medium using two-beam interference is similar to that of hologram formation. Such an index variation pattern is often periodic and is called a volume grating. When the two waves propagate through the grating induced by them, they undergo Bragg scattering [1]. One beam scatters into the other and vice versa. Such scatterings are reminiscent of the read-out process in holography [2].

Energy exchange between two electromagnetic waves in nonlinear media has been known for some time. Stimulated Brillouin scattering (SBS) and stimulated Raman scattering (SRS) are the best examples [3]. Both of these processes require relatively high intensities for efficient coupling. Recent interest in two-wave mixing arises from the strong nonreciprocal energy exchange at relatively lower intensities between two coherent laser beams in a new class of materials called photorefractive crystals. In addition, these materials are very efficient for the generation of phase-conjugated waves [4]–[6]. Materials such as barium titanate ($BaTiO_3$) and strontium barium niobate ($Sr_xBa_{1-x}Nb_2O_6$, SBN) are by far the most efficient nonlinear media for the generation of phase-conjugate waves, as well as the coupling of two laser beams using relatively low light intensities (e.g., 1 W/cm^2). Optical phase conjugation via four-wave mixing in nonlinear media also involves the formation of a volume index grating. The main difference between two-wave mixing and phase conjugation via four-wave mixing is that in four-wave mixing, a third beam is used to read out the volume hologram, whereas in two-wave mixing, the same beams read the mutually-induced volume hologram. To satisfy the Bragg condition, this third beam must be counterpropagating relative to one of the two beams that are involved in the formation of the volume hologram. In two-wave mixing, the Bragg condition is automatically satisfied.

In this paper, we first describe briefly the physics of the photorefractive effect. A coupled-mode theory is then developed to analyze the coupling of two coherent electromagnetic waves inside a photorefractive medium. Both codirectional and contradirectional coupling are considered. The coupled-mode theory is then extended to consider the case of nondegenerate two-wave mixing. This is followed by a discussion of the fundamental limit of the speed of photorefractive effect. The concept of an artificial photorefractive effect is then introduced. In the section that follows, we consider the coupling of two polarized beams inside photorefractive cubic crystals. The formulation is focused on the cross-polarization two-beam coupling in semiconductors such as GaAs. In Section IV, we treat the coupling of two electromagnetic waves inside a Kerr medium and discuss the electrostrictive Kerr effect. A new concept of nonlinear Bragg scattering is introduced. We also point out the similarity among various kinds of two-wave mixing, including SBS and SRS. In the last section, we discuss several applications of two-wave mixing. These include photorefractive resonators, optical nonreciprocity, resonator model of self-pumped phase conjugators, real-time holography, and nonlinear optical information processing.

II. Photorefractive Materials

The photorefractive effect is a phenomenon in which the local index of refraction is changed by the spatial variation of the light intensity. Such an effect was first discovered in 1966 [7]. The spatial index variation leads to a distortion of the wavefront, and such an effect was referred to as "optical damage." The photorefractive effect has since been observed in many electrooptic crystals, including $LiNbO_3$, $BaTiO_3$, SBN, BSO, BGO, GaAs, InP,

Manuscript received May 20, 1988; revised July 24, 1988. This work was supported in part by the Office of Naval Research under Contracts N00014-85-C-0219, N00014-85-C-0557, N00014-88-C-0230, and N00014-88-C-0231.

The author is with the Rockwell International Science Center, Thousand Oaks, CA 91360.

IEEE Log Number 8825875.

0018-9197/89/0300-0484$01.00 © 1989 IEEE

etc. It is generally believed that the photorefractive effect arises from optically-generated charge carriers which migrate when the crystal is exposed to a spatially-varying pattern of illumination with photons having sufficient energy. Migration of the charge carriers due to drift or diffusion produces a space-charge separation, which then gives rise to a strong space-charge field. Such a field induces refractive index change via the Pockels' effect. This simple picture of the photorefractive effect explains several interesting steady-state optical phenomena in these media.

A. Kukhtarev-Vinetskii's Model

Although there are several models for the photorefractive effect [8]-[11], the Kukhtarev-Vinetskii model is the most widely accepted one [8], [9]. In this model, the photorefractive materials are assumed to contain donor and acceptor traps. These traps which arise from the imperfections in the crystal, create intermediate electronic energy states in the bandgap of the insulators. When photons with sufficient energy are present, electronic transitions due to photoexcitations take place. As a result of the transitions, charge carriers are excited into the conduction band and the ionized donors become empty trap sites. The rate of carrier generation is $(sI + \beta)(N_D - N_D^+)$, whereas the rate of trap capture is $\gamma_R N N_D^+$. Here, s is the cross section of photoionization, β is the rate of thermal generation, γ_R is the carrier-ionized trap recombination rate, and N and N_D^+ stand for the concentration of the carriers and ionized traps. N_D is the density of the donor traps.

The space-charge field produced by the migration of the charge carriers is determined by the following set of equations:

$$\frac{\partial}{\partial t} N = \frac{\partial}{\partial t} N_D^+ - \frac{1}{e} \nabla \cdot \vec{J} \tag{1}$$

$$\frac{\partial}{\partial t} N_D^+ = (sI + \beta)(N_D - N_D^+) - \gamma_R N N_D^+ \tag{2}$$

$$\vec{J} = e\mu N\left(\vec{E} - \frac{kT}{e} \nabla \log N\right) + pI\vec{c} \tag{3}$$

$$\nabla \cdot (\epsilon \vec{E}^{sc}) = e(N_A + N - N_D^+) \tag{4}$$

where $\vec{c}$ is the unit vector along the c axis of the crystal, I is the light intensity, N_A is the acceptor concentration, μ is the mobility, T is temperature, k is the Boltzmann constant, n is the index of refraction, ϵ is the dielectric tensor, pI is the photovoltaic current, and p is the photovoltaic constant. $\vec{E}^{sc}$ stands for the space-charge field. $\vec{E}$ is the total field which includes $\vec{E}^{sc}$ and any external or internal fields (such as chemical or internal ferroelectric fields).

As a result of the presence of the space-charge field, a change in the index of refraction is induced via the linear electrooptic effect [1] (Pockels effect):

$$\Delta\left(\frac{1}{n^2}\right)_{ij} = r_{ijk} \vec{E}_k^{sc} \tag{5}$$

where r_{ijk} is the electrooptic coefficient (with $i, j, k = x, y, z$).

B. Degenerate Two-Wave Mixing

We now consider the interaction of two laser beams inside a photorefractive medium (see Fig. 1). If the two beams are of the same frequency, a stationary interference pattern is formed. Let the electric field of the two waves be written

$$E_j = A_j e^{i(\omega t - \vec{k}_j \cdot \vec{r})} \qquad j = 1, 2 \tag{6}$$

where A_1, A_2 are the wave amplitudes, ω is the angular frequency, and $\vec{k}_1$, $\vec{k}_2$ are the wave vectors. For simplicity, we also assume that both beams are polarized perpendicular to the plane of incidence (i.e., s-polarized).

Within a factor of proportionality, the intensity of the electromagnetic radiation can be written

$$I = |E|^2 = |E_1 + E_2|^2. \tag{7}$$

Using (6) for the electric field, the intensity can be written

$$I = |A_1|^2 + |A_2|^2 + A_1^* A_2 e^{-i\vec{K} \cdot \vec{r}} + A_1 A_2^* e^{i\vec{K} \cdot \vec{r}} \tag{8}$$

where

$$\vec{K} = \vec{k}_2 - \vec{k}_1. \tag{9}$$

The magnitude of the vector $\vec{K}$ is $(2\pi/\Lambda)$, where Λ is the period of the fringe pattern. The intensity [(8)] represents a spatial variation of optical energy inside the photorefractive medium. According to Kukhtarev's model, such an intensity pattern will generate and redistribute photocarriers. As a result, a space-charge field is created in the medium. This field induces a volume index grating via the Pockels effect. In general, the index grating will have a spatial phase shift relative to the interference pattern [8]. The index of refraction including the fundamental component of the intensity-induced gratings can be written

$$n = n_o + \frac{n_1}{2} e^{i\phi} \frac{A_1^* A_2}{I_o} \exp(-i\vec{K} \cdot \vec{r}) + \text{c.c.} \tag{10}$$

where

$$I_o = I_1 + I_2 \equiv |A_1|^2 + |A_2|^2. \tag{11}$$

n_o is the index of refraction when no light is present, ϕ is real, and n_1 is a real and positive number. Here again, for the sake of simplicity, we assume a scalar grating. The phase ϕ indicates the degree to which the index grating is shifted spatially with respect to the light interference pattern. In photorefractive media that operate by diffusion only (i.e., no external static field), e.g., $BaTiO_3$, the magnitude of ϕ is $\pi/2$ with its sign depending on the direction of the c axis. $\vec{K}$ is the grating wave vector and I_o is the sum of the intensities. The parameter n_1 depends on the grating spacing and its direction, as well as on the material properties of the crystal, e.g., the electrooptic coefficient. Expressions for $n_1 e^{i\phi}$ can be found in [9] and [10].

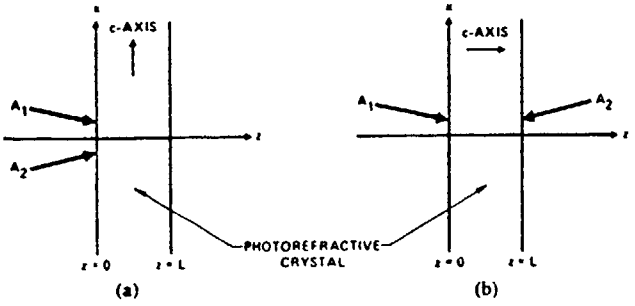

Fig. 1. (a) Schematic drawing of codirectional two-wave mixing. (b) Schematic drawing of contradirectional two-wave mixing.

The finite spatial phase shift between the interference pattern and the induced volume index grating has been known for some time [8], [12]. The presence of such a phase shift allows for the possibility of nonreciprocal steady-state transfer of energy between the beams [9], [13]–[15]. To investigate the coupling, we substitute (10) for the index of refraction and $E = E_1 + E_2$ for the electric field into the following wave equation:

$$\nabla^2 E + \frac{\omega^2}{c^2} n^2 E = 0 \tag{12}$$

where c is the velocity of light.

We assume that both waves propagate in the xz plane. Generally speaking, if the beams are of finite extent (i.e., comparable to the intersection of the beams), the amplitudes may depend on both x and z. Here we assume, for the sake of simplicity, that the transverse dimension of the beams is of infinite extent so that the boundary condition requires that the wave amplitudes A_1 and A_2 be functions of z only (see Fig. 1). We will solve for the steady states so that A_1 and A_2 are also taken to be time-independent.

Using the slowly-varying approximation, i.e.,

$$\left|\frac{d^2}{dz^2} A_j\right| \ll \left|\beta_j \frac{d}{dz} A_j\right| \qquad j = 1, 2$$

we obtain

$$2i\beta_1 \frac{d}{dz} A_1 = \frac{\omega^2 n_o n_1}{c^2 I_o} e^{-i\phi} A_2^* A_2 A_1$$

$$2i\beta_2 \frac{d}{dz} A_2 = \frac{\omega^2 n_o n_1}{c^2 I_o} e^{i\phi} A_1^* A_1 A_2 \tag{13}$$

where β_1 and β_2 are the z components of the wave vectors $\vec{k}_1$ and $\vec{k}_2$ inside the medium, respectively. The energy coupling depends on the relative sign of β_1 and β_2. Thus, two-wave mixing is divided into the following two categories.

1) Codirectional Two-Wave Mixing ($\beta_1\beta_2 > 0$): Referring to Fig. 1(a), we consider the case when the two laser beams enter the medium from the same side at $z = 0$. Without loss of generality, we assume that

$$\beta_1 = \beta_2 = k \cos(\theta/2) = \frac{2\pi}{\lambda} n_o \cos(\theta/2) \tag{14}$$

where θ is the angle between the beam inside the medium, and n_o is the index of refraction of the medium.

Substituting (14) for β_1 and β_2 in (13), and using $(\omega/c) = 2\pi/\lambda$, we obtain

$$\frac{d}{dz} A_1 = -i \frac{\pi n_1}{\lambda I_o \cos(\theta/2)} e^{-i\phi} |A_2|^2 A_1 - \frac{\alpha}{2} A_1$$

$$\frac{d}{dz} A_2 = -i \frac{\pi n_1}{\lambda I_o \cos(\theta/2)} e^{i\phi} |A_1|^2 A_2 - \frac{\alpha}{2} A_2 \tag{15}$$

where we have added terms that account for the attenuation and α is the bulk absorption coefficient.

We now write

$$A_1 = \sqrt{I_1} \exp(-i\psi_1)$$

$$A_2 = \sqrt{I_2} \exp(-i\psi_2) \tag{16}$$

where ψ_1 and ψ_2 are pnases of the complex amplitudes A_1 and A_2, respectively. Using (16) and (11), the coupled equation (15) can be written as

$$\frac{d}{dz} I_1 = -\gamma \frac{I_1 I_2}{I_1 + I_2} - \alpha I_1$$

$$\frac{d}{dz} I_2 = \gamma \frac{I_1 I_2}{I_1 + I_2} - \alpha I_2 \tag{17}$$

and

$$\frac{d}{dz} \psi_1 = \beta \frac{I_2}{I_1 + I_2}$$

$$\frac{d}{dz} \psi_2 = \beta \frac{I_1}{I_1 + I_2} \tag{18}$$

where

$$\gamma = \frac{2\pi n_1}{\lambda \cos(\theta/2)} \sin\phi \tag{19}$$

$$\beta = \frac{\pi n_1}{\lambda \cos(\theta/2)} \cos\phi. \tag{20}$$

The solutions for the intensities $I_1(z)$ and $I_2(z)$ are [16]

$$I_1(z) = I_1(0) \frac{1 + m^{-1}}{1 + m^{-1} e^{\gamma z}} e^{-\alpha z} \tag{21}$$

$$I_2(z) = I_2(0) \frac{1 + m}{1 + m e^{-\gamma z}} e^{-\alpha z} \tag{22}$$

where m is the input intensity ratio

$$m = \frac{I_1(0)}{I_2(0)}. \tag{23}$$

Note that in the absence of absorption ($\alpha = 0$), $I_2(z)$ is an increasing function of z and $I_1(z)$ is a decreasing function of z, provided γ is positive. The sign of γ depends on the direction of the c axis. As the result of the coupling for $\gamma > 0$ in Fig. 1, beam 2 gains energy from beam 1. If this two-wave mixing gain is large enough to overcome

the absorption loss, then beam 2 is amplified. Such an amplification is responsible for the fanning and stimulated scatterings of laser beams in photorefractive crystals [17].

With $I_1(z)$, $I_2(z)$ known, the phases ψ_1 and ψ_2 can be obtained by a direct integration of (18). Substituting (21) and (22) into (18) for I_1 and I_2, respectively, we obtain

$$\psi_2(z) - \psi_2(0) = \int_0^z \frac{\beta\, dz'}{1 + m^{-1}e^{\gamma z'}}. \tag{24}$$

Note that this photorefractive phase shift is independent of the absorption coefficient α. Carrying out the integration in (24), we obtain

$$\psi_2(z) - \psi_2(0) = \frac{\beta}{\gamma} \ln\left(\frac{1 + m}{1 + me^{-\gamma z}}\right). \tag{25}$$

From (18), we note that

$$\frac{d}{dz}(\psi_1 + \psi_2) = \beta. \tag{26}$$

Thus, $\psi_1(z)$ can be written

$$\psi_1(z) - \psi_1(0) = \beta z - [\psi_2(z) - \psi_2(0)]$$
$$= -\frac{\beta}{\gamma} \ln\left(\frac{m + 1}{m + e^{\gamma z}}\right). \tag{27}$$

If we refer to A_2 as the signal beam, then a useful parameter is the gain

$$g = \frac{I_2(L)}{I_2(0)} = \frac{1 + m}{1 + me^{-\gamma L}} e^{-\alpha L} \tag{28}$$

where we recall that m is the intensity ratio at input face ($z = 0$). Fig. 2 plots the gain as a function of the length of interaction L for various values of m.

2) Contradirectional Two-Wave Mixing: We now consider the case when the two beams enter the medium from opposite faces, as shown in Fig. 1(b). In codirectional two-wave mixing, the sum of the beam power is a constant of integration provided the medium is lossless, whereas in contradirectional two-wave mixing, the difference of the beam power (i.e., net Poynting power flow) is a constant. In addition, the coupled-mode equation which governs the wave amplitudes is also different from that of codirectional coupling. This leads to qualitative differences in the energy exchange between the two waves in two cases.

Let

$$\beta_1 = -\beta_2 = k \cos(\theta/2) = \frac{2\pi}{\lambda} n_o \cos(\theta/2) \tag{29}$$

where $\theta/2$ is the angle between each of the beams and the z axis. Substitution of (29) for β_1 and β_2 in (13) yields a similar set of coupled equations. Using (16), such a set of coupled equations becomes

$$\frac{d}{dz} I_1 = -\gamma \frac{I_1 I_2}{I_1 + I_2} - \alpha I_1$$
$$\frac{d}{dz} I_2 = -\gamma \frac{I_1 I_2}{I_1 + I_2} + \alpha I_2 \tag{30}$$

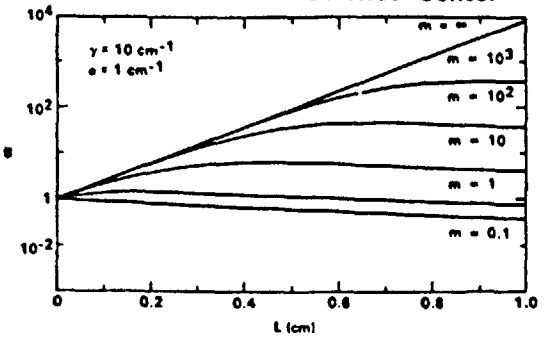

Fig. 2. Gain versus L for various values of m.

and

$$\frac{d}{dz}\psi_1 = \beta \frac{I_2}{I_1 + I_2}$$
$$\frac{d}{dz}\psi_2 = -\beta \frac{I_1}{I_1 + I_2} \tag{31}$$

where β and γ are phase and intensity coupling constants and are given by

$$\gamma = \frac{2\pi n_1}{\lambda \cos(\theta/2)} \sin\phi$$
$$\beta = \frac{\pi n_1}{\lambda \cos(\theta/2)} \cos\phi.$$

Comparing with (17) and (18), we notice the sign difference in these equations for beam 2.

The solutions for (30) and (31) can be obtained in closed form for the case when $\alpha = 0$ (i.e., lossless). In the lossless case, we note that the Poynting power flow along $+z$ is conserved, i.e.,

$$\frac{d}{dz}(I_1 - I_2) = 0 \tag{32}$$

and the solution of (30) with $\alpha = 0$ is [18]

$$I_1(z) = -C + \sqrt{C^2 + B \exp(-\gamma z)}$$
$$I_2(z) = C + \sqrt{C^2 + B \exp(-\gamma z)} \tag{33}$$

where B and C are constants and are related to the boundary condition. B and C can be expressed in terms of any two of the four boundary values $I_1(0)$, $I_2(0)$, $I_1(L)$ and $I_2(L)$, where L is the length of interaction. In terms of $I_1(0)$ and $I_2(0)$, B and C are given by

$$B = I_1(0)\, I_2(0)$$
$$C = [I_2(0) - I_1(0)]/2. \tag{34}$$

In practice, it is convenient to express B and C in terms of the incident intensities $I_1(0)$ and $I_2(L)$. In this case, B and C become

$$B = I_1(0)\, I_2(L) \frac{I_1(0) + I_2(L)}{I_2(L) + I_1(0)\exp(-\gamma L)}$$
$$C = \frac{1}{2} \frac{I_2^2(L) - I_1^2(0)\exp(-\gamma L)}{I_2(L) + I_1(0)\exp(-\gamma L)}. \tag{35}$$

According to (30), both $I_1(z)$ and $I_2(z)$ are increasing functions of z, provided γ is negative. The transmittance for both waves, according to (34) and (35), are

$$t_1 = \frac{I_1(L)}{I_1(0)} = \frac{1 + m^{-1}}{1 + m^{-1}\exp(\gamma L)}$$

$$t_2 \equiv \frac{I_2(0)}{I_2(L)} = \frac{1 + m}{1 + m\exp(-\gamma L)} \qquad (36)$$

where m is the incident intensity ratio $m \equiv I_1(0)/I_2(L)$. Note that $t_1 < 1$ and $t_2 > 1$ for positive γ. The sign of γ depends on the direction of the c axis. It is interesting to note that these expressions for transmittance are formally identical to those of the codirectional coupling, even though the spatial variations of $I_1(z)$ and $I_2(z)$ with respect to z are very different. Note that t_1 and t_2 are related by $t_2 = t_1 \exp(\gamma L)$.

The relative phase of the two waves is obtained by solving (30) in cooperation with (33), and is given by

$$\psi_2 - \psi_1 = -\tfrac{1}{2}\beta z + \text{constant} \qquad (37)$$

where β is the phase coupling constant. The relative phase varies linearly with z, and thus leads to a change in the grating wave vector by $\beta/2$ along the z direction (i.e., the grating wave vector becomes $\vec{K} - \frac{1}{2}\beta\hat{z}$).

The nonreciprocal transmittance of photorefractive media may have important applications in many optical systems. It is known that in linear optical media, the transmittance of a layered structure (including absorbing material) is independent of the side of incidence (the so-called left and right incidence theorem). Right now, with the photorefractive material available, it is possible to make a "one-way" window which favors transmission from one side only. These applications will be addressed later in Section V-C.

The solutions of (33) did not take into account the effect of the bulk absorption of light. The attenuation due to finite absorption coefficient is reflected by the $-\alpha I_1$ term on the right-hand side of the first equation in (30), and the $+\alpha I_2$ term on the RHS of the other equation. With these two additional terms accounting for bulk absorption, closed-form solutions are not available [19]. However, (30) can still be integrated numerically. It is found that a very good approximate solution is

$$I_1^{\alpha}(z) = I_1^{\alpha=0}(z)\exp(-\alpha z)$$

$$I_2^{\alpha}(z) = I_2^{\alpha=0}(z)\exp[\alpha(z - L)]. \qquad (38)$$

The approximation is legitimate provided $\alpha \ll |\gamma|$.

Fig. 3 illustrates the intensity variation with respect to z for the case when $\gamma = -10^{-1}$ cm, $\alpha = 1.6\ \text{cm}^{-1}$, and $L = 2.5$ mm. If the loss were neglected (i.e., $\alpha = 0$), the transmittance would be $t_1 = 1.81$ and $t_2 = 0.15$. With $\alpha = 1.6\ \text{cm}^{-1}$, the transmittances become $t_1 = 1.27$ and $t_2 = 0.11$ according to a numerical integration. The approximate solution [(38)] would lead to $t_1 = 1.21$ and $t_2 = 0.10$. Note that even with the presence of absorption, the transmittance can still be greater than unity.

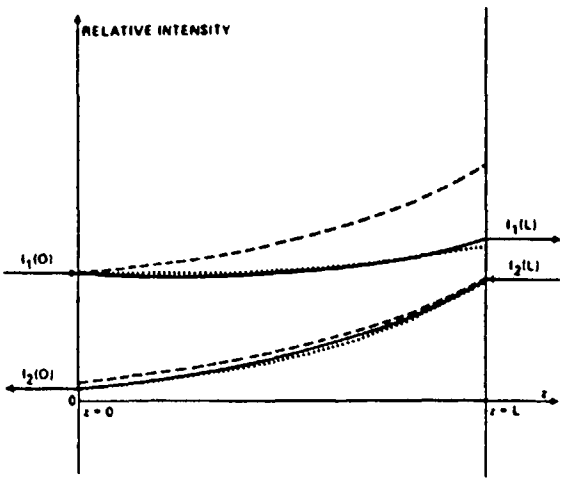

Fig. 3. Intensity variation with respect to z in photorefractive crystals. The coupling constant is taken as $\gamma = -10\ \text{cm}^{-1}$ and interaction length L is 2.5 mm. The dashed curves are for the lossless case (i.e., $\alpha = 0$). The solid curves are obtained by numerical integration including the loss ($\alpha = 1.6\ \text{cm}^{-1}$). The dotted curves are the approximate solution (38).

By using the approximation solution [(38)], the transmittances become

$$t_1 = \frac{1 + m^{-1}}{1 + m^{-1}\exp(\gamma L)}\exp(-\alpha L)$$

$$t_2 = \frac{1 + m}{1 + m\exp(-\gamma L)}\exp(-\alpha L). \qquad (39)$$

There are two extreme cases worth mentioning. In the case when $I_2(L) \gg I_1(0)$, $m \ll 1$, the transmittances become $t_1 \simeq \exp[(-\gamma - \alpha)L]$ and $t_2 \simeq \exp(-\alpha L)$, whereas in the case when $I_1(0) \gg I_2(L)$, $m \gg 1$, the transmittances are $t_1 \simeq \exp(-\alpha L)$ and $t_2 \simeq \exp[(\gamma - \alpha)L]$.

C. Nondegenerate Two-Wave Mixing

When the frequencies of the two laser beams are different, the interference fringe pattern is no longer stationary. A volume index grating can still be induced provided the fringe pattern does not move too fast. The amplitude of the index modulation decreases as the speed of the fringe pattern increases. This is related to the finite time needed for the formation of index grating in the photorefractive medium. In the next section, we will consider the fundamental limit of the speed of photorefractive effect.

Let ω_1 and ω_2 be the frequency of the two beams. The electric field of these two beams can be written

$$E_j = A_j e^{i(\omega_j t - \vec{k}_j \cdot \vec{r})} \qquad j = 1, 2 \qquad (40)$$

where $\vec{k}_1$ and $\vec{k}_2$ are the wave vectors and A_1, A_2 are the wave amplitudes. The intensity of the electromagnetic radiation, similar to that given by (8), can be written

$$I = |A_1|^2 + |A_2|^2 + A_1^* A_2 e^{i(\Omega t - \vec{K} \cdot \vec{r})} + A_1 A_2^* e^{-i(\Omega t - \vec{K} \cdot \vec{r})} \qquad (41)$$

where

$$\Omega = \omega_2 - \omega_1$$

$$\vec{K} = \vec{k}_2 - \vec{k}_1. \tag{42}$$

Such an intensity distribution represents a traveling fringe pattern at a speed of

$$v = \frac{\Omega}{K} = \frac{\Omega\Lambda}{2\pi} \tag{43}$$

where Λ is the period of the fringe pattern.

The index of refraction including the fundamental component of the intensity-induced grating can be written

$$n = n_o + \frac{n_1}{2}\left\{e^{i\phi}\frac{A_1^* A_2}{I_o}\exp\left[i(\Omega t - \vec{K}\cdot\vec{r})\right] + \text{c.c.}\right\} \tag{44}$$

where

$$I_o = I_1 + I_2 \equiv |A_1|^2 + |A_2|^2. \tag{45}$$

ϕ is real and n_1 is a real and positive number. Here again, for the sake of simplicity, we assume a scalar grating. The phase ϕ indicates the degree to which the index grating is shifted spatially with respect to the light interference pattern. According to [20], ϕ and n_1 can be written, respectively, as

$$\phi = \phi_o - \tan^{-1}(\Omega\tau) \tag{46}$$

and

$$n_1 = \frac{2}{(1 + \Omega^2\tau^2)^{1/2}}\Delta n_s \tag{47}$$

where τ is the decay time constant of the holograph grating, Δn_s is the saturation value of the photoinduced index change, and ϕ_o is a constant phase shift related to the nonlocal response of the crystal under fringe illumination. Both parameters Δn_s and ϕ_o depend on the grating spacing ($2\pi/K$) and its direction, as well as on the material properties of the crystal, e.g., the electrooptic coefficients. Expressions for Δn_s and ϕ_o can be found in [9] and [10]. In photorefractive media, e.g., $BaTiO_3$, that operate by diffusion only (i.e., no external static field), the magnitude of ϕ_o is $\pi/2$ with its sign depending on the orientation of the c axis (note that these crystals are acentric).

Following the procedure similar to the one used in the previous section, coupled equations for the intensities $I_1(z)$, $I_2(z)$ and the phases $\psi_1(z)$, $\psi_2(a)$ are obtained. They are formally identical to those of the degenerate case, i.e., (17) and (18) for codirectional coupling and (30) and (31) for contradirectional coupling. The intensity coupling constant γ, however, is now a function of the frequency detuning Ω.

For crystals such as $BaTiO_3$ that operate by diffusion only, the coupling constant can be written, according to (19), (46), and (47), as

$$\gamma = \gamma_o/\left[1 + (\Omega\tau)^2\right] \tag{48}$$

where γ_o is the coupling constant for the case of degenerate two-wave mixing (i.e., $\Omega = \omega_1 - \omega_2 = 0$) and is given by

$$\gamma_o = \frac{4\pi\Delta n_s}{\lambda\cos\theta}. \tag{49}$$

In deriving (48), we have used $\pi/2$ for ϕ_o in (46).

The two-wave mixing gain can be written

$$g \equiv \frac{I_2(L)}{I_2(0)} = \frac{1 + m}{1 + me^{-\gamma L}}e^{-\alpha L} \tag{50}$$

where we recall that m is the input beam ratio $m = I_1(0)/I_2(0)$ and L is the length of interaction.

Fig. 4 shows the signal gain [(50)] as a function of the frequency detuning $\Omega\tau$ for various values of m. We note that for the case of pure diffusion, signal gain decreases as $\Omega\tau$ increases. This is true for both codirectional and contradirectional coupling. When $\Omega\tau >> 1$, the intensity coupling constant γ decreases significantly. The time constant τ depends on materials as well as on the intensity of the laser beams. The fundamental limit of such a time constant τ is discussed next.

D. Speed of Photorefractive Effect—Grating Formation Time

As mentioned earlier, photorefractive crystals such as $BaTiO_3$, $Sr_xBa_{1-x}Nb_2O_6$ (SBN), $Bi_{12}SiO_{20}$ (BSO), etc., are by far the most efficient media for the generation of phase-conjugated optical waves using relatively low light intensities (1–10 W/cm^2). In addition, these materials also exhibit several interesting and important phenomena such as self-pumped phase conjugation, two-beam energy coupling, and real-time holography. All of these phenomena depend on the formation of volume index gratings inside the crystals [8], [9].

One of the most important issues involved in device applications is the speed of the grating formation (or the time constant τ). Such a speed of the light-induced index gratings has been investigated theoretically using Kukhtarev's model and others, as well as experimentally in various crystals [8]–[10], [21]. The issue of fundamental limit of the speed of photorefractive effect has been a subject of great interest recently. Using Kukhtarev's model, let us examine the four fundamental processes involved in the photorefractive effect in sequence: 1) photoexcitation of carriers, 2) transport, 3) trap, and 4) Pockels effect. The photorefractive effect is a macroscopic phenomenon and requires the generation and transport of a large number of charge carriers. We note that without the presence of charge carriers, photorefractive gratings can never be formed, and no matter how fast the carriers can move (even at the speed of light, 3×10^8 m/s), the formation of index grating is still limited by the rate of carrier generation. Therefore, although each of the four processes involved imposes a theoretical limit on the response time of photorefractive effect, the fundamental limit of the speed of photorefractive effect is determined by the pho-

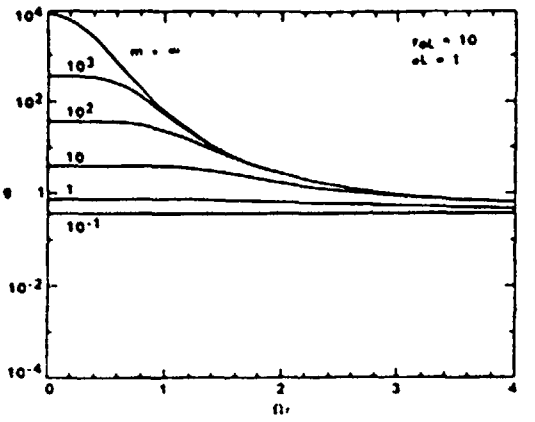

Fig. 4. Signal gain g as a function of $\Omega\tau$ for various values of m.

toexcitation of carriers and not by the carrier transport. In other words, the charge carriers must be generated before they can be transported. Any finite time involved in the transport process can only lengthen the formation time of the grating. From this point of view, the fundamental limit may also be called the photon-flux limit, or simply the photoexcitation limit. Although the fundamental limit can be derived from (1)–(4) of Kukhtarev's model, it has been recently derived using a relatively simple method [22]. Such a fundamental limit has been confirmed experimentally [23]. In the limit when the crystal is illuminated with infinite intensity, the speed of the photorefractive effect will be limited by the charge transport process [24].

Assuming that the separation of a pair of charge particles requires the absorption of at least one photon, we can calculate the energy required to form a given volume index grating. To illustrate this, let us consider the photorefractive effect in $BaTiO_3$. Generally speaking [10], an efficient beam coupling would require a charge carrier density of approximately 10^{16} cm^{-3}. Such a charge separation would require the absorption of at least 10^{16} photons in a volume of 1 cm^3. Using a light intensity of 1 W in the visible spectrum, the photon flux would be approximately 10^{19}/s. Thus, assuming a quantum efficiency of 100 percent, it takes at least 1 ms just to deposit enough photons to create the charge separation. The actual grating formation time can be much longer because not all of the charge carriers are trapped at the appropriate sites.

According to the model described in [22], the minimum time needed for the formation of an index grating, which provides a coupling constant of γ, is given by

$$t = \left(\frac{h\nu}{e}\right)\left(\frac{\lambda}{\Lambda}\right)\left(\frac{\gamma}{\alpha_p}\right)\frac{2}{\pi\eta} \cdot \frac{\epsilon}{In^3 r} \qquad (51)$$

where $h\nu$ is the photon energy, e is electronic charge, λ is wavelength of light, Λ is the grating period, α_p is photorefractive absorption coefficient, η is the quantum efficiency, ϵ is dielectric constant, r is the relevent electrooptic coefficient, and I is the intensity of light. Note that the time constant is directly proportional to the coupling constant γ and is inversely proportional to the light intensity. Equation (51) is the expression for the minimum time required for the formation of an index grating which provides a coupling constant γ.

A figure-of-merit for photorefractive material is often defined as

$$Q = \frac{n^3 r}{\epsilon}. \qquad (52)$$

Table I lists such parameters for some photorefractive materials. Using such a parameter, the photon-limited time for the index grating formation becomes

$$t = \left(\frac{h\nu}{e}\right)\left(\frac{\lambda}{\Lambda}\right)\left(\frac{\gamma}{\alpha_p}\right)\frac{2}{\pi\eta IQ}. \qquad (53)$$

Here, we note that this photon-limited time is inversely proportional to the material's figure-of-merit and is proportional to the coupling constant γ.

We now discuss this photon-limited time for the formation of an index grating which yields a coupling constant of 1 cm^{-1}. For materials such as $BaTiO_3$, SBN, BSO, and GaAs, the figure-of-merit Q is of the order of 1 (see Table I) in MKS units (M^2/FV). In many of the experiments reported recently, $h\nu$ is approximately 2 eV, (λ/Λ) is of the order of 0.1. We further assume that the photoexcitation absorption coefficient is 0.1 cm^{-1} and that the quantum efficiency η is 100 percent. Using these parameters and a light intensity of 1 W/cm^2, (53) yields a photon-limited time constant of 0.15 ms. This is the minimum time required for the formation of an index grating which can provide a two-wave mixing coupling constant of 1 cm^{-1}. By virtue of its photoexcitation nature, the photorefractive effect is relatively slow at low intensities because of the finite time required to absorb the photons. Table II shows the comparison between the measured time constants with the calculated minimum time from (53). The only way to speed up the photorefractive process is by using higher intensities. Fig. 5 plots this minimum time constant for $BaTiO_3$ (or GaAs) as a function of intensity.

The photoexcitation process imposes a fundamental limit on the speed of photorefractive effect at a given power level. The time constant given by (51) here is the absolute minimum time required to generate a volume grating of given index modulation. We assume that the transport is instantaneous and the quantum efficiency is unity. Thus the derived time constant is the absolute minimum time. Any finite time involved in the transport process can only slow down the photorefractive process.

The fundamental limit discussed here can also provide important guidelines for many workers in the area of material research. For example, if we compare it with the experimental results, we find that the time constant of some materials (e.g., $BaTiO_3$, SBN) is two orders of magnitude larger than the fundamental limit. Thus, the calculation of such a fundamental limit and a simple comparison point out the room for improvement by either increasing the photorefractive absorption or the quantum ef-

TABLE I
FIGURE-OF-MERIT FOR SOME PHOTOREFRACTIVE MATERIALS [22]

Materials	λ μm	r pm/V	n	ϵ/ϵ_0	Q^* pm/Vϵ_0	Q(MKS)
$BaTiO_3$	0.5	$r_{42} = 1640$	$n_e = 2.4$	$\epsilon_1 = 3600$	6.3	0.71
SBN	0.5	$r_{33} = 1340$	$n_e = 2.3$	$\epsilon_3 = 3400$	4.8	0.54
GaAs	1.1	$r_{12} = 1.43$	$n_e = 3.4$	$\epsilon = 12.3$	4.7	0.53
BSO	0.6	$r_{41} = 5$	$n = 2.54$	$\epsilon = 56$	1.5	0.17
$LiNbO_3$	0.6	$r_{33} = 31$	$n_e = 2.2$	$\epsilon_3 = 32$	10.3	1.16
$LiTaO_3$	0.6	$r_{33} = 31$	$n_e = 2.2$	$\epsilon_3 = 45$	7.3	0.83
$KNbO_3$	0.6	$r_{42} = 380$	$n = 2.3$	$\epsilon_3 = 240$	19.3	2.2

*The figure-of-merit Q depends on the configuration of interaction.

TABLE II
COMPARISON OF MEASURED TIME CONSTANTS τ AND THE FUNDAMENTAL LIMIT t

Materials	λ μm	Λ μm	α_p cm^{-1}	γ cm^{-1}	τ^a s	t^b s	Remarks
GaAs	1.06	1.0	1.2	0.4	80×10^{-6}	45×10^{-6}	(25)
GaAs:Cr	1.06	1.1	4.0	0.6	53×10^{-6}	31×10^{-6}	(26)
$BaTiO_3$	0.515	1.3	1.0	20.0	1.3	2×10^{-3}	(27)
BSO	0.568	23.0	0.13	10.0	15×10^{-3}	2×10^{-3}	(28)
SBN	0.515	1.5	0.1	0.6	2.5	6×10^{-3}	(29)
SBN:Ce	0.515	1.5	0.7	14.0	0.8	2×10^{-3}	(29)

[a] τ and t are time constants at incident intensity of 1 W/cm^2.
[b] t is the calculated time constant by using (53) and assuming a quantum efficiency of 1.

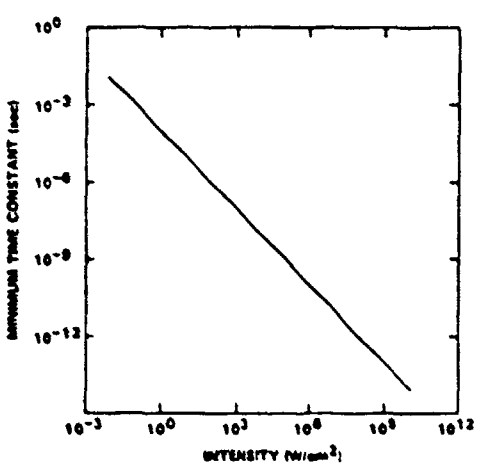

Fig. 5. Fundamental limit of the speed of photorefractive effect of $BaTiO_3$ (or GaAs) with coupling constant of 1 cm^{-1}.

ficiency. There are some materials (e.g., GaAs) whose photorefractive response is close to the fundamental limit, leaving no more room for further improvement by any means (e.g., heat treatment, doping, or reduction.) Recently, highly-reduced crystals of $KNbO_3$ were prepared which exhibit a photorefractive response time very close to the fundamental limit [23].

In summary, the photorefractive effect is a macroscopic phenomenon. It involves the transport of a large number of charge carriers for the formation of any finite grating. The fundamental limit is the minimum time needed for the generation of these carriers. The speed is fundamentally limited by the finite time needed to absorb a large number of photons at a given power level. By counting the total number of photons needed for the formation of an index grating, the photon-limited time constant is derived. This time constant is inversely proportional to the light intensity. We further estimated this minimum time constant for some typical photorefractive crystals. Such a fundamental limit provides important guidelines for researchers in the areas of device application and material research.

III. Photorefractive Two-Wave Mixing in Cubic Crystals

Photorefractive two-beam coupling in electrooptic crystals has been studied extensively for its potential in many applications. Much attention has been focused on materials such as $BaTiO_3$, BSO, SBN, etc., because of their large coupling constants (see, for example, Table II). Although these oxide materials are very efficient for two-beam coupling, they are very slow in response at low operating powers [22]. Recently, several experimental investigations have been carried out to study two-wave mixing in cubic crystals such as GaAs, which responds much faster than any of the previously mentioned oxides at the same operating power [25], [26].

In addition to the faster temporal response, the optical isotropy and the tensor nature of the electrooptic coefficients of cubic crystals allow for the possibility of cross-polarization coupling. Such cross-polarization two-wave mixing is not possible in $BaTiO_3$ and SBN because of the optical anisotropy, which leads to velocity mismatch. The velocity mismatch also exists in BSO crystals because of

the circular birefringence. A number of special cases of two-wave mixing have been analyzed. Recently, a general theory of photorefractive two-wave mixing in cubic crystals was developed [30]. Such a theory predicts the existence of cross-polarization signal beam amplification. These cross-polarization couplings have been observed in GaAs crystals [31]–[33]. In what follows, we describe the coupled-mode theory of photorefractive two-wave mixing in cubic crystals, especially those with point group symmetry of $\bar{4}3m$. The theory shows that cross-polarization two-wave mixing is possible in cubic crystals such as GaAs. Exact solutions of coupled mode equations are obtained for the case of codirectional coupling.

A. Coupled-Mode Theory

Referring to Fig. 6, we consider the intersection of two polarized beams inside a cubic photorefractive crystal. Since the crystal is optically isotropic, the electric field of the two beams can be written as

$$\vec{E} = (\vec{s}A_s + \vec{p}_1 A_p)\exp(-i\vec{k}_1 \cdot \vec{r}) + (\vec{s}B_s + \vec{p}_2 B_p)\exp(-i\vec{k}_2 \cdot \vec{r}) \quad (54)$$

where $\vec{k}_1$ and $\vec{k}_2$ are wave vectors of the beams, $\vec{s}$ is a unit vector perpendicular to the plane of incidence, and $\vec{p}_1$, $\vec{p}_2$ are unit vectors parallel to the plane of incidence and perpendicular to the beam wave vectors, respectively. Since each beam has two polarization components, there are four waves involved and A_s, A_p, B_s, and B_p are amplitudes of the waves. All of the waves are assumed to have the same frequency. In addition, we assume that the crystal does not exhibit optical rotation.

In the photorefractive crystal (from $z = 0$ to $z = L$), these two beams generate an interference pattern,

$$\vec{E}^* \cdot \vec{E} = A_s^* A_s + A_p^* A_p + B_s^* B_s + B_p^* B_p + [(A_s B_s^* + A_p B_p^* \vec{p}_1 \cdot \vec{p}_2) \cdot \exp(i\vec{K} \cdot \vec{r}) + \text{c.c.}] \quad (55)$$

where $\vec{K} = \vec{k}_2 - \vec{k}_1$ is the grating wave vector, and c.c. represents the complex conjugate. We note that there are two contributions to the sinusoidal variation of the intensity pattern. As a result of the photorefractive effect, a space-charge field E^{sc} is formed which induces a volume index grating via the Pockels effect,

$$(\Delta\epsilon)_{ij} = -\epsilon_0 n^4 r_{ijk} E_k \quad (56)$$

where ϵ_0 is the dielectric permittivity of vacuum, n is the index of refraction of the crystal, r_{ijk} is the electrooptic coefficient, and E_k is the k component ($k = x, y, z$) of the space-charge field. The fundamental component of the induced grating can be written

$$\Delta\epsilon = -\epsilon_0 \epsilon_1 [(A_s B_s^* + A_p B_p^* \cos\theta) \cdot \exp(i\vec{K} \cdot \vec{r} + \phi) + \text{c.c.}]/I_o \quad (57)$$

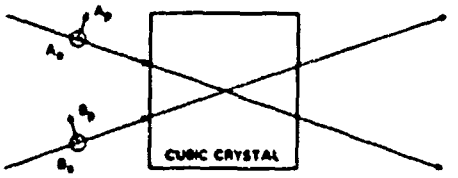

Fig. 6. Schematic drawing of photorefractive two-beam coupling in cubic crystals.

where ϵ_1 is a 3×3 tensor, ϕ is the spatial phase shift between the index grating and the intensity pattern, θ is the angle between the beams inside the crystal, and I_o is given by

$$I_o = A_s^* A_s + A_p^* A_p + B_s^* B_s + B_p^* B_p. \quad (58)$$

For cubic crystals with point group symmetry of $\bar{4}3m$, ϵ_1 is given by

$$\epsilon_1 = n^4 r_{41} \begin{pmatrix} 0 & E_z & E_y \\ E_z & 0 & E_x \\ E_y & E_x & 0 \end{pmatrix} \quad (59)$$

where $r_{41} = r_{231} = r_{312} = r_{123}$, and E_x, E_y, and E_z are the three components of the amplitude of the space-charge field.

Substitution of the index grating equation (56) into Maxwell's wave equation leads to the following set of coupled equations:

$$\begin{aligned}
\frac{d}{dz}A_s &= \frac{i}{2\beta_1} e^{i\phi}[\Gamma_{ss}B_s + \Gamma_{sp}B_p] \cdot (A_s B_s^* + A_p B_p^* \cos\theta)/I_o \\
\frac{d}{dz}B_s &= \frac{i}{2\beta_2} e^{-i\phi}[\Gamma_{ss}A_s + \Gamma_{sp}A_p] \cdot (A_s^* B_s + A_p^* B_p \cos\theta)/I_o \\
\frac{d}{dz}A_p &= \frac{i}{2\beta_1} e^{i\phi}[\Gamma_{ps}B_s + \Gamma_{pp}B_p] \cdot (A_s B_s^* + A_p B_p^* \cos\theta)/I_o \\
\frac{d}{dz}B_p &= \frac{i}{2\beta_2} e^{-i\phi}[\Gamma_{ps}A_s + \Gamma_{pp}A_p] \cdot (A_s^* B_s + A_p^* B_p \cos\theta)/I_o
\end{aligned} \quad (60)$$

where

$$\Gamma = \omega^2 \mu \epsilon_0 \epsilon_1 \quad (61)$$

and

$$\Gamma_{ij} = \langle i|\Gamma|j\rangle \qquad i, j = \vec{s}, \vec{p}_1, \vec{p}_2 \quad (62)$$

and β_1, β_2 are the z components of the wave vectors.

As indicated by the subscripts, Γ_{ij}'s are the coupling constants between the ith and jth polarized waves. Thus, Γ_{ss} and Γ_{pp} are the parallel coupling constants, and Γ_{sp}, Γ_{ps} are the cross-coupling constants.

A similar set of equations had been derived by previous workers and exact solutions were obtained for the case of codirectional parallel coupling [34]. Here we focus our attention on the case of cross-polarization coupling. In cross-polarization coupling, the s component of beam 1 is coupled with the p component of beam 2, and the p component of beam 1 is coupled with the s component of beam 2.

B. Codirectional Cross Coupli. g

To illustrate the use of the coupled equation (60), in the case of codirectional cross coupling, we consider a special case in which the crystal orientation does not allow the parallel coupling to occur. Such a two-beam coupling configuration is shown in Fig. 7(a). The two beams enter the crystal in such a way that the grating wave vector is along the [110] direction of the crystal. In this configuration, the unit vector $\vec{s}$ is parallel to [001] and the unit vectors p_1, p_2 are perpendicular to [001]. The amplitude of the induced index grating ϵ_1 can thus be written, according to (59),

$$\epsilon_1 = \frac{1}{\sqrt{2}} n^4 r_{41} \begin{pmatrix} 0 & 0 & 1 \\ 0 & 0 & 1 \\ 1 & 1 & 0 \end{pmatrix} E^{sc} \tag{63}$$

where E^{sc} is the amplitude of the space-charge field.

According to (63) and (62), and after a few steps of algebra, the coupling constants can be written

$$\Gamma_{ss} = \Gamma_{p\bar{p}} = 0 \tag{64}$$

$$\Gamma_{s\bar{p}} = \Gamma_{ps} = \Gamma_{s\bar{p}} = \Gamma_{\bar{p}s} = (2\pi/\lambda)^2 n^4 r_{41} E^{sc} \cos(\theta/2) \tag{65}$$

where we assume that the beams enter the crystal symmetrically such that

$$\beta_1 = \beta_2 = (2\pi/\lambda) n \cos(\theta/2). \tag{66}$$

We now substitute (65) and (66) into the coupled equation (60). This leads to

$$\begin{aligned} \frac{d}{dz} A_s &= -\gamma B_p (A_s B_s^* + A_p B_p^* \cos\theta)/I_o \\ \frac{d}{dz} B_s &= \gamma A_p (A_s^* B_s + A_p^* B_p \cos\theta)/I_o \\ \frac{d}{dz} A_p &= -\gamma B_s (A_s B_s^* + A_p B_p^* \cos\theta)/I_o \\ \frac{d}{dz} B_p &= \gamma A_s (A_s^* B_s + A_p^* B_p \cos\theta)/I_o \end{aligned} \tag{67}$$

where we have taken $\phi = \pi/2$, and γ is real and is given by

$$\gamma = \tfrac{1}{2}(2\pi/\lambda) n^3 r_{41} E^{sc} \tag{68}$$

We notice from the coupled equation (67) that there are two contributions to the holographic index grating. The relative phase of these two contributions is very important because it determines whether these two parts enhance or destroy the index grating. Such a relative phase is determined by the relative phases of the four amplitudes. Thus, the energy exchange among the four waves depends on the input polarization states.

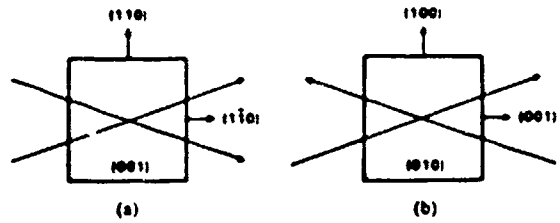

Fig. 7. (a) A configuration for codirectional cross polarization coupling in a cubic crystal of point group symmetry $\bar{4}3m$. (b) a configuration for contradirectional cross polarization coupling in the same class of crystals

We now derive the solutions of these coupled equations. According to (67), the total intensity I_o is a constant (i.e., independent of z). Thus, it is convenient to normalize the beam amplitudes such that $I_o = 1$. Here, remember that we neglect the material absorption in the coupled equation. We will obtain the closed form solutions of these coupled equations for the case of no absorption. In the case when the material absorption cannot be neglected, the solutions are obtained by simply multiplying an exponential factor accounting for the absorption. This is legitimate provided that all four waves have the same attenuation coefficient.

To obtain the solutions of the coupled equation (67), it is useful to employ some of the constants of integration which are given by

$$A_s A_s^* + B_p B_p^* = c_1 \tag{69}$$

$$A_p A_p^* + B_s B_s^* = c_2 \tag{70}$$

$$A_s A_p^* + B_s^* E_p = c_3 \tag{71}$$

$$A_s B_s - A_p B_p = c_4. \tag{72}$$

Using a change of variable similar to that used in [34] and [35], the coupled equations can be written

$$\frac{d}{dz} g = -\gamma (g^2 c_2 \cos\theta + g\sigma^* - c_3) \tag{73}$$

$$\frac{d}{dz} f = \gamma (f^2 c_1 \cos\theta + f\sigma - c_3) \tag{74}$$

where

$$f = A_p/A_s, \qquad g = B_p/B_s \tag{75}$$

$$\sigma = c_3 - c_3^* \cos\theta \tag{76}$$

Equations (73) and (74) c A be integrated, and the results are

$$f = A_p/A_s = \left[-\sigma + \gamma \tanh(-\varphi\gamma z/2 + C) \right] / (2c_1 \cos\theta)$$

$$g = B_p/B_s = [-\sigma^* + q^* \tanh (q^*\gamma z/2 + C')]/(2c_2 \cos\theta) \quad (77)$$

with

$$q^2 = 4c_1c_2 + \sigma^2 \quad (78)$$

where C and C' are constants of integration which are determined by the boundary condition at $z = 0$.

Once f and g are known, the intensity of all four waves is given by

$$|A_p|^2 = \frac{|f|^2c_1 - |fg|^2c_2}{1 - |fg|^2}$$

$$|B_p|^2 = \frac{|g|^2c_2 - |fg|^2c_1}{1 - |fg|^2}$$

$$|A_s|^2 = \frac{|A_p|^2}{|f|^2} = \frac{c_1 - |g|^2c_2}{1 - |fg|^2}$$

$$|B_s|^2 = \frac{|B_p|^2}{|g|^2} = \frac{c_2 - |f|^2c_1}{1 - |fg|^2}. \quad (79)$$

We now consider a special case of particular interest in which the cubic crystal is sandwiched between a pair of cross polarizers. Such a configuration is useful to eliminate unwanted background radiation which often causes noises in the detection of signals. The boundary conditions in this case may be taken as

$$A_p(0) = B_p(0) = 0. \quad (80)$$

Using (71) and (75)-(78), we have $f(0) = g(0) = 0$, $\sigma = 0$, and $\sigma = 0$, and the solutions become

$$f = -\frac{q \tanh (q\gamma z/2)}{2c_2 \cos\theta}$$

$$g = \frac{q \tanh (q\gamma z/2)}{2c_2 \cos\theta} \quad (81)$$

where $q = 2\sqrt{c_1c_2}$.

Taking $\theta = 0$, and using (79), the intensity of the four waves becomes

$$|A_s|^2 = c_1 \frac{1}{1 + \tanh^2 (q\gamma z/2)}$$

$$|A_p|^2 = c_2 \frac{\tanh^2 (q\gamma z/2)}{1 + \tanh^2 (q\gamma z/2)}$$

$$|B_s|^2 = c_2 \frac{1}{1 + \tanh^2 (q\gamma z/2)}$$

$$|B_p|^2 = c_1 \frac{\tanh^2 (q\gamma z/2)}{1 + \tanh^2 (q\gamma z/2)} \quad (82)$$

where $c_1 = |A_s(0)|^2$, $c_2 = |B_s(0)|^2$. Fig. 8(a) shows the variation of these intensities as functions of position for the case of $c_2/c_1 = 0.1$. We note that for strong coupling ($\gamma L >> 1$), one-half of the incident pump energy $A_s(0)$ is coupled to the p component of the signal beam B_p, and one-half of the incident signal energy $B_s(0)$ is coupled to the p component of the pump beam. As a result of the opposite signs in the wave amplitudes ($f < 0$), the two contributions to the index grating tend to cancel each other. Thus, when the energy of the p components reaches one half of the incident energies, the coupling ceases.

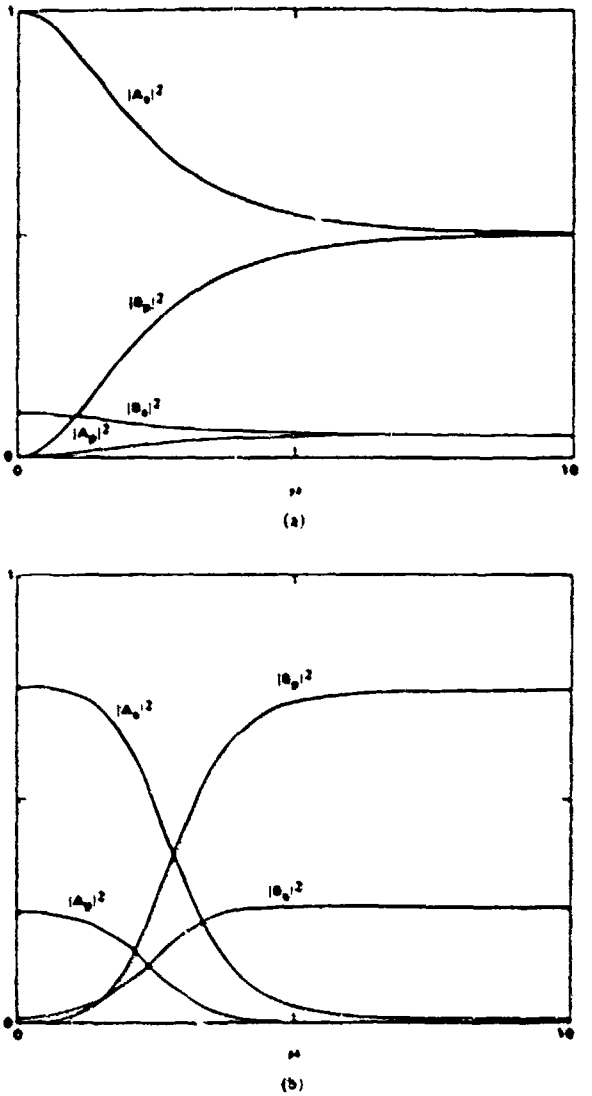

Fig. 8. Intensity of the four waves are plotted as functions of distance for various interaction situations. (a) Both incident beams are s polarized (i.e., $(A_p(0) = B_p(0) = 0, c_2/c_1 = 0.1)$. (b) The pump beam is linearly polarized at an azimuth angle of 30° relative to the s direction, and the signal beam is s-polarized, $c_2/c_1 = 0.01$.

It is possible that the p component of the signal beam B_p receives most of the incident pump energy A_s. Fig. 8(b) illustrates a case in which the pump beam has both s and p components, whereas the signal beam is s-polarized. We note that for strong coupling ($\gamma L >> 1$), most of the energy of the s component of the pump beam is coupled to the p component of the signal beam. The nonreciprocal transfer of energy is very similar to that of conventional two-wave mixing.

The exact solutions of (77) and (79) are useful when the coupling is strong ($\gamma L >> 1$) and the energy exchange is significant. For the case of weak coupling ($\gamma L << 1$), or very little pump depletion, we may assume that the pump beam amplitudes (A_s, A_p) remain virtually unchanged throughout the interaction. Under these conditions, the coupled equations become

$$\frac{d}{dz} B_s = \gamma a B_p + \gamma b B_s$$

$$\frac{d}{dz} B_p = \gamma c B_p + \gamma d B_s \tag{83}$$

where a, b, c, and d are dimensionless constants and are given by

$$a = |A_p|^2 \cos\theta / I_o$$

$$b = A_p A_s^* / I_o$$

$$c = A_s A_p^* \cos\theta / I_o$$

$$d = |A_s|^2 / I_o. \tag{84}$$

We note that the magnitude of all four of these constants is less than unity.

The coupled equation (83) can be easily integrated and the results are

$$B_s(z) = \left\{[bB_s(0) + aB_p(0)] \exp[(b + c)\gamma z] + [cB_s(0) - aB_p(0)]\right\}/(b + c)$$

$$B_p(z) = \left\{c[bB_s(0) + aB_p(0)] \exp[(b + c)\gamma z] - b[cB_s(0) - aB_p(0)]\right\}/[a(b + c)] \tag{85}$$

where $B_s(0)$ and $B_p(0)$ are the amplitudes of the signal beams at $z = 0$.

If we set $B_p(0) = 0$ in (85), we obtain

$$B_s(z) = B_s(0)[be^{(b+c)\gamma z} + c]/(b + c)$$

$$B_p(z) = B_s(0)bc[e^{(b+c)\gamma z} - 1]/[a(b + c)]. \tag{86}$$

If we assume further that $\gamma z << 1$, (86) can be written approximately as

$$B_s(z) = B_s(0) + B_s(0) \frac{A_p A_s^*}{I_o} \gamma z$$

$$B_p(z) = B_s(0) \frac{|A_s|^2}{I_o} \gamma z. \tag{87}$$

We note that the amplitude of B_s may increase or decrease depending on the polarization state of the pump beam A, whereas the amplitude B_p is an increasing function of γz.

In the above derivation, a spatial phase shift between the index grating and the intensity pattern was assumed to be exactly $\pi/2$, which corresponds to the case of pure diffusion (i.e., no externally-applied static electric field). In the event when the spatial phase shift is not $\pi/2$, (69)–(72) are still valid and exact solutions are still available. They are given by

$$f = A_p/A_s = [-\sigma + q \tanh(ieq\gamma z/2 + C)]/(2c_1 \cos\theta) \tag{88}$$

$$g = B_p/B_s = [-\sigma^* + q^* \tanh(ie^* q^* \gamma z/2 + C')]/(2c_2 \cos\theta) \tag{89}$$

where e is an exponential factor given by

$$e = \exp(i\phi). \tag{90}$$

We note that the solutions are formally identical to the previous case, except the complex phase factors ie^* and $-ie$ in the argument of the transcendental function. Deviation from $\sigma = \pi/2$ is known to occur in nondegenerate two-wave mixing [see (46)]. Such a deviation for the case of degenerate two-wave mixing has been observed in oxide crystals such as $BaTiO_3$ and $Sr_{0.6}Ba_{0.4}Nb_2O_6$ [36].

For the special case of particular interest in which the cubic crystal is sandwiched between a pair of cross polarizers, the boundary conditions are given by (8). Using (71) and (75)–(78), we have $f(0) = g(0) = 0$, $c_3 = 0$, and $\sigma = 0$, and the solutions become

$$f = \frac{q \tanh(ieq\gamma z/2)}{2c_1 \cos\theta}$$

$$g = \frac{q \tanh(ie^* q\gamma z/2)}{2c_2 \cos\theta} \tag{91}$$

where $q = 2\sqrt{c_1 c_2}$.

Consider the special case of $\phi = 0$. The solutions (91) become

$$f = \frac{iq \tan(q\gamma z/2)}{2c_1 \cos\theta}$$

$$g = \frac{iq \tan(q\gamma z/2)}{2c_2 \cos\theta} \tag{92}$$

Taking $\theta = 0$, and using (79), the intensity of the four waves becomes

$$|A_s|^2 = c_1 \cos^2(q\gamma z/2)$$

$$|A_p|^2 = c_2 \sin^2(q\gamma z/2)$$

$$|B_s|^2 = c_2 \cos^2(q\gamma z/2)$$

$$|B_p|^2 = c_1 \sin^2(q\gamma z/2) \tag{93}$$

where $c_1 = |A_s(0)|^2$, $c_2 = |B_s(0)|^2$. Note that the intensities of these waves are periodic functions of z. This is distinctly different from the case when $\phi = \pi/2$. The case of $\phi = 0$ corresponds to a pure local response of the material. Although the energy is exchanged back and forth between A_s and B_p as well as between A_p and B_s, there is no nonreciprocal energy transfer. In other words, there is no unique direction of energy flow as compared with the case when $\phi \neq 0$. For cases with $0 < |\phi| < \pi$, nonreciprocal energy transfer is possible according to our so-

lutions (88) and (89) with maximum energy transfer at $\phi = \pm\pi/2$.

C. Contradirectional Cross Coupling

Referring to Fig. 7(b), we consider a case of contradirectional coupling which does not permit the parallel coupling to occur. The two beams enter the crystal in such a way that the grating wave vector is along the [001] direction of the crystal. In this configuration, the unit vector $\vec{s}$ is parallel to [010] and the unit vectors $\vec{p}_1$, $\vec{p}_2$ are perpendicular to [010]. The amplitude of the induced index grating ϵ_1 can thus be written, according to (59),

$$\epsilon_1 = n^4 r_{41} \begin{pmatrix} 0 & 1 & 0 \\ 1 & 0 & 0 \\ 0 & 0 & 0 \end{pmatrix} E^{sc} \tag{94}$$

where E^{sc} is the amplitude of the space-charge field.

According to (62) and (94), and after few steps of algebra, the coupling constants can be written

$$\Gamma_{ss} = \Gamma_{p_1p_2} = 0$$

$$\Gamma_{sp_1} = \Gamma_{p_1s} = \Gamma_{sp_2} = \Gamma_{p_2s} = n^4 r_{41} E^{sc} \cos(\theta/2) \tag{95}$$

where we assume that the beams enter the crystal symmetrically [see Fig. 7(b)] such that

$$\beta_1 = -\beta_2 = -(2\pi/\lambda) n \cos(\theta/2). \tag{96}$$

We now substitute (95) and (96) into the coupled equation (60). This leads to

$$\frac{d}{dz} A_s = \gamma B_p (A_s B_s^* + A_p B_p^* \cos\theta)/I_o$$

$$\frac{d}{dz} B_s = \gamma A_p (A_s^* B_s + A_p^* B_p \cos\theta)/I_o$$

$$\frac{d}{dz} A_p = \gamma B_s (A_s B_s^* + A_p B_p^* \cos\theta)/I_o$$

$$\frac{d}{dz} B_p = \gamma A_s (A_s^* B_s + A_p^* B_p \cos\theta)/I_o \tag{97}$$

where we have taken $\phi = \pi/2$, and γ is real and is given by

$$\gamma = \tfrac{1}{2}(2\pi/\lambda) n^3 r_{41} E^{sc}. \tag{98}$$

Notice that the coupled mode equation (97) is similar to that of (67), except for the signs. The difference in signs is due to the direction of propagation of the pump beam (A_s, A_p). As a result of this difference, the total intensity I_o is no longer a constant. According to (97), $(A_s^* A_s + A_p^* A_p - B_s^* B_s - B_p^* B_p)$, which is proportional to the net Poynting power flow along the $+z$ direction, is a constant [37]. There are other constants of integration. These include

$$A_s^* A_s - B_p^* B_p = c_1$$

$$A_p^* A_p - B_s^* B_s = c_2$$

$$A_s A_p^* - B_s B_p^* = c_3$$

$$A_s B_s - A_p B_p = c_4. \tag{99}$$

Because I_o is not a constant, the integration of the coupled equation (97) is not as simple as that of (67). As of now, there is no closed form solution available. However, numerical techniques can be used to integrate the coupled equations.

For the case of no pump depletion, we may treat A_s and A_p as constants. In this case, the coupling equations for B_s and B_p are identical to those of the codirectional coupling, and the solutions are given by (85) and (86).

In summary, we have derived a general theory of the coupling of polarized beams in cubic photorefractive crystals. As a result of the optical isotropy of the crystal and the tensor nature of the holographic photorefractive grating, cross-polarization energy coupling occurs. Exact solutions for the case of codirectional coupling are obtained. Such cross-polarization coupling may be useful for the suppression of background noises.

D. Cross-Polarization Two-Beam Coupling in GaAs Crystals

Cross-polarization two-beam coupling has been observed in GaAs crystals recently. The experimental results are in good agreement with the coupled-mode theory presented earlier [31]–[33].

In a contradirectional two-beam coupling experiments as described in [33], a 1.15 μm beam from a He-Ne laser is split into two by a beam splitter. The two beams intersect inside a liquid-encapsulated Czochralski (LEC) grown, undoped, semiinsulating GaAs crystal from opposite sides of the (001) faces [see Fig. 7(b)]. The intersecting angle of two beams is approximately 168°. The wave vector of the induced index grating is along the [001] crystalline direction.

One beam, B, is polarized along the [010] direction (s-polarization) using a polarizer, which fits the condition of $B_p(0) = 0$. The other beam, A, is transmitted through another polarizer (along the [100] direction), followed by a half-wave plate, which is used to vary the polarization of the pump beam. The power of beams A and B is 80 mW/cm^2 and 1 mW/cm^2, respectively. The GaAs crystal is 5 mm thick. The gain coefficient of the crystal measured with the regular beam-coupling configuration is about 0.1/cm. These values fit well with the conditions of no beam A depletion and $\gamma L \ll 1$, which are used to derive (87). A mechanical chopper, which operates at 100 Hz, is used to modulate beam A. An analyzer is placed in front of a Ge photodetector. The analyzer is used so that the intensity of both the s and p components of transmitted beam B can be measured. The signal from the photodetector was amplified by a current amplifier, whose output can be used as the dc component of $|B_s(L)|^2$. A lock-in amplifier is used to measure the ac component of $|B_s(L)|^2$ and $|B_p(L)|^2$.

According to (87), the beam intensities can be written

$$|B_s(L)|^2 = |B_s(0)|^2[1 + (\sin 2\psi)\gamma L] \quad (100)$$

$$|B_p(L)|^2 = |B_s(0)|^2[(\cos\psi)^4(\gamma L)^2] \quad (101)$$

where $|B_s(0)|^2$ is the intensity of beam B at $z = 0$ and ψ is the angle between the $\vec{s}$ vector and the polarization direction of beam A. In addition, we have used the intensity of beam A to be approximately equal to I_o and neglected the $(\gamma L)^2$ term in the first equation of (87). There are several interesting features in (87) which should be pointed out. $|B_s(L)|^2$ may increase or decrease depending on the polarization state of the pump beam A, whereas $|B_p(L)|^2$ is an increasing function of γL. Both $|B_s(L)|^2$ and $|B_p(L)|^2$ are independent of θ. The ac component of $|B_s(L)|^2$ has a function of $\sin 2\psi$ which has a maximum at $\psi = 45°$ and a minimum of $\psi = 135°$, whereas $|B_p(L)|^2$ is a function of $(\cos\psi)^4$ and has maxima at $\psi = 0$ and 180°. These features have been validated with experimental data [33].

In addition, it is observed that the maximum value of $|B_p(L)|^2$ is smaller than the maximum ac component of $|B_s(L)|^2$ by a factor of 0.052. From (100) and (101), it is clear that the factor of 0.52 is γL. This leads to $\gamma = 0.104$/cm, which is practically the same as the γ of the sample measured by a regular beam-coupling technique.

In codirectional interaction configurations, the output of a CW Nd:YAG laser beam was used [31]. A laser beam operating at 1.06 μm was split into two by a beam splitter and then recombined inside a semiinsulating (undoped) GaAs crystal. The beam diameter of both beams was about 1 mm just before entering the crystal. The intensities of the pump and the probe were about 1 W/cm^2 and 10 mW/cm^2, respectively, and the angle between the beams was 90° outside the crystal. A neutral density filter was used in the probe beam to achieve the desired intensity ratio between the pump and the probe. The half-wave plate $\lambda/2$ was used in the pump beam to control the initial mixture of the s and p components. Also, a chopper was used to modulate the pump beam at about 100 Hz. Finally, the probe beam transmitted through the crystal was analyzed by a polarizing beam splitter, and the p and s components were simultaneously monitored independently by two photodetectors. Various polarization states of the pump beam were achieved by rotating the half-wave plate, while both $|B_s(L)|^2$ and $|B_p(L)|^2$ were monitored simultaneously. There is good agreement between the experimental data and the theoretical calculations.

The coupling coefficient can be calculated from (100) and (101). One can solve for the coupling γL by taking the ratio of the measured value of $|B_s(L)|^2$ and $|B_p(L)|^2$ at $\psi = 0$. Using the measured interaction length L of 0.5 cm, we have calculated the cross-polarization coupling coefficient γ to be about 0.4 cm^{-1}. This value is consistent with the gain coefficient measured for parallel-polarization coupling in the same sample. According to the theory, the gain coefficients for both parallel- and cross-polarization coupling should be the same. The coupling coefficient of $\gamma = 2.6$ cm^{-1} has been observed recently in a sample of GaAs crystal [38]. Using moving fringes in the GaAs/Cr crystal, an even higher coupling coefficient of $\gamma = 6 \sim 7$ cm^{-1} has also been reported [39]. Such coupling coefficients allow the possibility of net gain (amplification) in two-wave mixing.

IV. Kerr Media

In the above discussion, we notice that the nonlocal response (i.e., $\phi \neq 0$) in photorefractive media plays a key role in the nonreciprocal energy transfer. The existing materials such as $BaTiO_3$, $LiNbO_3$, SBN, BSO, BGO, etc. are very slow and are also effective only for visible light. Photorefractive crystals such as GaAs, CdTe, GaP, InP, and other semiconductors are faster and are also effective in the near-IR spectral region [25], [26]. However, for high-power laser application, these solids are no longer useful. Gases or fluids, because of their optical isotropy and local response, have never been considered as candidate materials for degenerate two-wave mixing. In what follows, we show that nonlocal response in gases or fluids can be artificially induced by applying an external field or simply by moving the media. Using such a concept, gases or fluids become the best candidate materials for high power laser beam coupling. Energy coupling also occurs in stationary media when the frequencies of the two beams are properly detuned, as in SBS and SRS.

A. Two-Wave Mixing in Kerr Media

The concept of using moving gratings in local media for energy coupling was first proposed in 1973 by a group of Soviet scientists [41]–[44]. It was recognized that a spatial phase shift between the index grating and the light intensity pattern can be induced by moving the grating relative to the medium. Such a spatial phase shift is a result of the inertia (temporal) of the hologram formation process and leads to a nonreciprocal energy transfer. If the formation time of the hologram is finite, a spatial phase shift occurs when the intensity pattern is moving relative to the medium. In addition to the phase shift, such a motion also leads to a decrease in the depth of modulation of the induced index grating. Several possibilities of achieving such a spatial phase shift have been proposed. These include moving the medium itself relative to a thermally induced grating [41], using the Lorentz force to move free-carrier grating in a semiconducting medium [45], and nondegenerate two-wave mixing in which a frequency shift between the beams results in a moving grating [46]–[49]. It is important to note that a temporal phase shift itself is not enough for energy coupling. The induced index grating must be physically shifted in space relative to the intensity pattern in order to achieve energy coupling.

It is known that the Kerr effect in gases or fluids is a local effect. In media with local response ($\phi = 0$), there is no steady-state transfer of energy between two lasers of the same frequency. In what follows, we will show that nonlocal response can be induced by moving the Kerr medium relative to the beams. Such an induced nonlocal re-

sponse is only possible when the material response time τ is finite.

The propagation of electromagnetic waves in media possessing a strong Kerr effect is one subject of long and sustained interest. A number of interesting phenomena manifest themselves at high incident beam powers. This includes self-phase modulation, mode-locking and self-focusing. The effect is described by a dependence of the index of refraction on the electric field according to

$$n = n_o + n_2 \langle E^2 \rangle \tag{102}$$

where n_o is the index of refraction, n_2 is the Kerr coefficient (see Appendix A), and $\langle E^2 \rangle$ is the time average of the varying electric field.

Consider the case of degenerate two-wave mixing. The time average of the electric field, is given by

$$\langle E^2 \rangle = E_o^2 [1 + \cos(\vec{K} \cdot \vec{r})] \tag{103}$$

where we assume $E_o = A_1 = A_2$. The index of refraction, according to (102) and (103), is given by

$$n = n_o + n_2 E_o^2 [1 + \cos(\vec{K} \cdot \vec{r})]. \tag{104}$$

Comparing (104) with (103), we note that the response is local and there can be no energy coupling, even if n_2 is complex.

Using the interference of two beams with different frequencies, a moving fringe pattern can be obtained inside the medium. As a result of the finite temporal response of the material, a spatial phase shift exists between the induced index grating and the intensity pattern. Such a finite phase shift leads to energy transfer between the beams. Coupled-mode analysis has been used to study the beam coupling in these media [40]. In what follows, we describe the coupling of two beams with different frequencies in the codirectional configuration.

Inside the Kerr medium, the two waves form an interference pattern which corresponds to a spatially periodic variation of the time-averaged field $\langle E^2 \rangle$. In a Kerr medium, such a periodic intensity produces a volume grating. Thus, the problem we address is most closely related to the phenomenon of self-diffraction from an induced grating. The formulation of such a problem is very similar to that of the holographic two-wave coupling in photorefractive crystals [8], [9], [12]. However, there exists a fundamental difference between these two types of two-wave mixing. In photorefractive media, the index modulation is proportional to the contrast of the interference fringes, whereas in Kerr media the index modulation is directly proportional to the field strength. Thus, in Kerr media the coupling strength is proportional to the beam intensities, whereas in photorefractive media the coupling strength is determined by the ratio of beam intensities.

Let the electric field of the two waves be written

$$E_j = A_j \exp[i(\omega_j t - \vec{k}_j \cdot \vec{r})] \qquad j = 1, 2 \tag{105}$$

where ω_j's are the frequencies and $\vec{k}_j$'s are the wave vectors. In (105), we assume for simplicity that both waves are s-polarized and the medium is isotropic. We further assume that no optical rotation is present in the material. A_1 and A_2 are the amplitudes and are taken as functions of z only for a steady-state situation. The z axis is taken normal to the surface of the medium (see Fig. 9).

In the Kerr medium (from $z = 0$ to $z = L$), these two waves generate an interference pattern. Such a pattern is traveling if $\omega_1 \neq \omega_2$. This interference pattern is described by $\langle E^2 \rangle$, where E is the total electric field

$$E = E_1 + E_2 \tag{106}$$

and the averaging is taken over a time interval T such that

$$\omega_1 T \gg 1, \quad \omega_2 T \gg 1 \tag{107}$$

and

$$|\omega_2 - \omega_1| T \ll 1. \tag{108}$$

Using $\langle E^2 \rangle = \frac{1}{2} \operatorname{Re}[E^* E]$ and (105) and (106), we obtain

$$\langle E^2 \rangle = \tfrac{1}{2}\{|A_1|^2 + |A_2|^2 + A_1^* A_2 e^{i(\Omega t - \vec{K} \cdot \vec{r})} + A_1 A_2^* e^{-i(\Omega t - \vec{K} \cdot \vec{r})}\} \tag{109}$$

where

$$\Omega = \omega_2 - \omega_1 \tag{110}$$

$$\vec{K} = \vec{k}_2 - \vec{k}_1. \tag{111}$$

This interference pattern [(109)] induces a volume index grating via the Kerr effect. In general, the index grating will have a finite phase shift relative to the interference pattern because of the time-varying nature of the pattern. Thus, we can generalize (102) and write the index of refraction including the fundamental components of the Kerr-induced grating as

$$n = n_o + \Delta n_o + \tfrac{1}{2}\{n_2 e^{i\phi} A_1^* A_2 e^{i(\Omega t - \vec{K} \cdot \vec{r})} + \text{c.c.}\} \tag{112}$$

where both ϕ and n_2 are real and Δn_o is a uniform change in index. Here again for the sake of simplicity we assume a scalar grating. The phase ϕ indicates the degree to which the index grating is temporally delayed (or spatially shifted) with respect to the interference pattern. Generally speaking, both n_2 and ϕ are functions of Ω.

Here, $n_2 \exp(i\phi)$ can be regarded as a complex Kerr coefficient. The finite phase shift is a result of the finite response of the material. A complex Kerr coefficient corresponds to a complex third-order nonlinear optical polarizability. It is known that the imaginary part of the third-order nonlinear optical polarizability is responsible for phenomena such as stimulated Brillouin scattering and stimulated Raman scattering [3]. Thus, we expect that the complex Kerr coefficient induced by moving gratings will also lead to energy coupling between the two waves.

To illustrate the physical origin of such a finite phase shift, we will now examine a classical model. In this

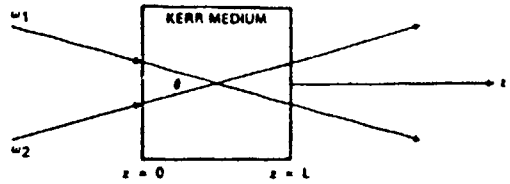

Fig. 9. Schematic drawing of two-wave mixing in Kerr media.

model, we assume that the formation of the holographic grating is instantaneous and the decay constant τ is finite. When the two waves are degenerate in frequency, a steady-state nonlinear response is described by (102) without phase shift. In the case of nondegenerate two-wave mixing, the intensity fringe, as described by (109), is moving in the nonlinear medium at a constant speed. The steady-state value of the self-induced index change must be derived from a treatment which considers the finite response time of the medium with respect to the displacement speed. Let the decay of index change be exponential, then the steady-state index change can be written

$$\Delta n = \frac{1}{\tau} n_{20} \int_{-\infty}^{t} \langle E^2(t') \rangle e^{(t'-t)/\tau} dt' \qquad (113)$$

where n_{20} is the value of index change for the degenerate case.

Integration of (113) yields the following expression for $n_2 \exp(i\phi)$:

$$n_2 \exp(i\phi) = \frac{n_{20}}{1 + i\Omega\tau}. \qquad (114)$$

Note that the finite phase shift is related to the motion of the intensity pattern relative to the nonlinear medium. In addition to the finite phase shift, the motion of the fringe pattern relative to the medium also causes the index modulation to increase. According to (112) and (114), the index grating is spatially shifted relative to the intensity pattern by

$$\phi = -\tan^{-1}(\Omega\tau) \qquad (115)$$

where we recall that τ is the response time of the medium.

1) Codirectional Two-Wave Mixing: Now, by using (112) for n and the scalar wave equation and by using the parabolic approximation (i.e., slowly-varying amplitudes), we can derive the following coupled equations:

$$\frac{d}{dz} A_1 = -i \frac{\omega^2 n_o n_2}{2k_z c^2} e^{-i\phi} |A_2|^2 A_1$$

$$\frac{d}{dz} A_2 = -i \frac{\omega^2 n_o n_2}{2k_z c^2} e^{i\phi} |A_1|^2 A_2 \qquad (116)$$

where we assume that $\omega_2 = \omega_1 = \omega$, and k_z is the z component of the wave vectors (i.e., $k_z = k_1 \cos \frac{1}{2}\theta = k_2 \cos \frac{1}{2}\theta$). The parameter θ is the angle between the two beams. In (116), we have neglected the term Δn_o.

We now write

$$A_1 = \sqrt{I_1} e^{-i\psi_1}, \quad A_2 = \sqrt{I_2} e^{-i\psi_2} \qquad (117)$$

where ψ_1 and ψ_2 are the phases of the amplitudes A_1 and A_2, respectively. Using (116) and (117), the coupled equations (116) can be written as

$$\frac{d}{dz} I_1 = -g I_1 I_2 - \alpha I_1$$

$$\frac{d}{dz} I_2 = g I_1 I_2 - \alpha I_2 \qquad (118)$$

and

$$\frac{d}{dz} \psi_1 = \beta I_2$$

$$\frac{d}{dz} \psi_2 = \beta I_1 \qquad (119)$$

where

$$g = \frac{2\pi}{\lambda \cos(\theta/2)} n_2 \sin\phi, \quad 0 \le \theta < \pi/2 \qquad (120)$$

$$\beta = \frac{\pi}{\lambda \cos(\theta/2)} n_2 \cos\phi. \qquad (121)$$

In (118), we have added the attenuation term due to bulk absorption. The parameter α is the absorption coefficient. Note that beam 2 will be amplified, provided $gI_1 > \alpha$, according to (118). Also notice that the coupled equations (118) are exactly identical to those of the stimulated Brillouin scattering and stimulated Raman scattering. Solutions for the lossless case had been derived by previous workers [2]. We now derive the solution for the case of lossy nonlinear medium. Using the classical model mentioned above, beam 2 will gain energy from beam 1, provided that the phase shift ϕ is positive. Thus, according to (115), the low-frequency beam will always see gain.

The coupled equations (118) can be integrated exactly, and the solution is (see Appendix B)

$$I_1(z) = I_1(0) \cdot \frac{1 + m^{-1}}{1 + m^{-1} \exp\left[\frac{\gamma}{\alpha}(1 - e^{-\alpha z})\right]} \cdot e^{-\alpha z} \qquad (122)$$

$$I_2(z) = I_2(0) \cdot \frac{1 + m}{1 + m \exp\left[\frac{\gamma}{\alpha}(1 - e^{-\alpha z})\right]} \cdot e \qquad (123)$$

where m is the input beam ratio

$$m = \frac{I_1(0)}{I_2(0)} \qquad (124)$$

and γ is given by

$$\gamma = g[I_1(0) + I_2(0)]. \qquad (125)$$

Substituting (122) and (123) for I_1 and I_2, respectively, into (119) and carrying out the integrations, we obtain

$$\psi_1(z) - \psi_1(0) = \frac{\beta}{g} \log \left\{ \frac{1 + m^{-1}}{1 + m^{-1} \exp\left[\frac{\gamma}{\alpha}(1 - e^{-\alpha z})\right]} \right\} \tag{126}$$

and

$$\psi_2(z) - \psi_2(0) = -\frac{\beta}{g} \log \left\{ \frac{1 + m}{1 + m \exp\left[\frac{\gamma}{\alpha}(1 - e^{-\alpha z})\right]} \right\}. \tag{127}$$

Note that according to (126) and (127), the phases of the two waves are not coupled. In other words, these two waves can exchange energy without any phase crosstalk. Such a phenomenon has been known in stimulated Raman scattering for some time, and can be employed to pump a clean signal beam with an aberrated beam. Here, the result can be applied to more cases, including forward stimulated Brillouin scattering.

If we neglect absorption (i.e., $\alpha = 0$), then $I_2(z)$ is an increasing function of z and $I_1(z)$ is a decreasing function of z, according to (122) and (123), provided γ is positive. Transmittance for both waves for the lossless case, according to (122) and (123), is

$$T_1 \equiv \frac{I_1(L)}{I_1(0)} = \frac{1 + m^{-1}}{1 + m^{-1} \exp(\gamma L)}$$

$$T_2 = \frac{I_2(L)}{I_2(0)} = \frac{1 + m}{1 + m \exp(\gamma L)} \tag{128}$$

where m is the incident intensity ratio $m = I_1(0)/I_2(0)$. Note that $T_2 > 1$ and $T_1 < 1$ for positive γ. The sign of γ is determined by the sign of n_2 and the phase shift ϕ. Interestingly, these expressions are formally identical to those of the photorefractive coupling. The major difference is that the γ for Kerr media is proportional to the total power density of the waves, according to (125).

Fig. 10 illustrates the intensity variation with respect to z for the case when $g = 10$ cm/MW, $\alpha = 0.1$ cm^{-1}, $I_1(0) = 100$ kW/cm^2, and $I_2(0) = 1$ kW/cm^2. Note that even with the presence of absorption, the intensity of beam 2 increases as a function of z until $z = l_c$, where the gain equals the loss. Beyond $z = l_c$, the intensities of both beams are decreasing functions of z.

Similar results were obtained earlier by other workers in a study of stimulated scattering of light from free carriers in semiconductors [50].

According to (114), (115), and (120), the gain coefficient g is a function of the frequency detuning and can be

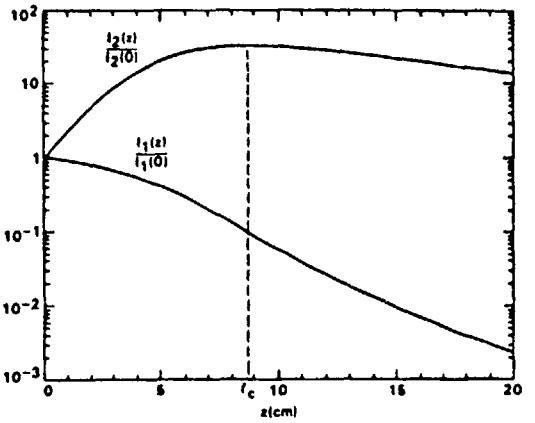

Fig. 10. Intensity variation with respect to z in the Kerr medium.

written

$$g = \frac{2\pi n_{20}}{\lambda \cos(\theta/2)} \cdot \frac{-\Omega\tau}{1 + (\Omega\tau)^2} \tag{129}$$

where we recall that $\Omega = \omega_2 - \omega_1$ is the frequency detuning and τ is the grating decay time constant. We notice that the gain coefficient is positive for the beam with lower frequency provided that n_{20} is positive. Such a gain coefficient is maximized at $\Omega\tau = \pm 1$. Such a dependence on frequency detuning can be used to measure the time constant τ. Some experimental works will be discussed in Section IV-E.

2) Contradirectional Two-Wave Mixing: We now consider the case of contradirectional two-wave mixing in which beam 1 enters the medium at $z = 0$, and beam 2 enters the medium at $z = L$. The coupled-mode equations for the beam intensities can be obtained in a similar manner and are written

$$\frac{d}{dz} I_1 = -g I_1 I_2 - \alpha I_1$$

$$\frac{d}{dz} I_2 = -g I_1 I_2 + \alpha I_2 \tag{130}$$

where the intensity gain coefficient g is given by

$$g = \frac{2\pi}{\lambda \sin(\theta/2)} n_2 \sin\phi, \quad \pi/2 < \theta \leq \pi. \tag{131}$$

We notice a slight difference between the two cases as compared with (120) for the codirectional coupling. Here, we recall that θ is the angle between the positive direction of the two wave vectors. Thus, for codirectional coupling, the angle θ is always less than 90°, whereas $\pi/2 < \theta < \pi$ for the contradirectional coupling. This is a result of the boundary condition in which we assume that the waves and the medium are all of infinite extent in a plane perpendicular to the z axis.

Solutions of (130) for the case of lossless medium are given by

$$\text{Trans} \Rightarrow \frac{I_1(z)}{I_1(0)} = \frac{1-\rho}{1-\rho e^{-g\sigma z}}$$

$$\text{Refl} \Rightarrow \frac{I_2(z)}{I_2(0)} = \frac{1-\rho}{e^{g\sigma z}-\rho} \tag{132}$$

where σ and ρ are constants and are related to the intensities at $z = 0$,

$$\rho = \frac{I_2(0)}{I_1(0)}$$

$$\sigma = I_1(0) - I_2(0). \tag{133}$$

The constant σ may be regarded as the net power flux through the medium.

The solutions of (132) are expressed in terms of $I_1(o)$ and $I_2(0)$, which are not input intensities. In the contradirectional coupling, we note that the incident intensities are $I_1(0)$ and $I_2(L)$.

For interaction L, such that $g\sigma L \gg 1$, the intensity growth for beam 2 is exponential and is given by, according to (124),

$$I_2(0) = \frac{I_2(L)}{(1-\rho)} e^{g\sigma L}. \tag{134}$$

In SBS, $I_2(L)$ is virtually zero and represents intensity of noises or scattered light. The parameter $\rho = I_2(0)/I_1(0)$ is the phase-conjugate reflectivity of the SBS process. It is always less than unity for two reasons. First, in SBS there is no beam 2 incident at $z = L$; therefore, $\rho \leq 1$ is required by the conservation of energy. Second, the exponential gain per unit length $g\sigma$ is proportional to the power throughput. A reflectivity of $\rho = 100$ indicates a zero power flux and consequently zero gain.

B. Electrostrictive Kerr Effects

The Kerr effect arises from several physical phenomena. These include molecular orientation, molecular redistribution, third-order nonlinear polarizability [3], electrostriction, and thermal changes. In liquids such as CS_2, contribution to the Kerr effect is dominated by the electrostriction.

The coupling of two electromagnetic waves via electrostriction has been known for some time and is responsible for SBS. Although this subject has been studied extensively [51], little attention has been paid to the "photorefractive" nature of such a process, which, we believe, can provide a great deal of insight into generalizing the SBS process. For example, there exists a similar spatial phase shift of 90° between the induced index grating and the light interference pattern in conventional SBS [52]. Such a spatial phase shift of 90° is responsible for the energy exchange between the incident wave and the phase-conjugated wave in SBS. In addition, self-pumped phase conjugation in $BaTiO_3$ crystals [53], [54] is very similar to the phase conjugation in SBS [55], [56]. The spatial phase shift of 90° can be utilized in other SBS configurations (e.g., injected SBS at $\theta \neq 180°$). In this section, we investigate the photoinduced index grating in nondegenerate two-wave mixing and focus our attention on the complex Kerr coefficient and the spatial phase shift.

Basic equations for the electrostrictive coupling between photons and phonons have been formulated and several theoretical papers on SBS have been published [51]. Most of the earlier work was concentrated on backward-wave coupling. Very little attention was paid to codirectional nondegenerate two-wave mixing. The mathematical formulation of such a coupling in Kerr media including material absorption has been recently solved and is described in Section IV-A. In this section, we focus our attention on the derivation of the photoinduced index grating as well as the relation between the photoelastic coefficient and the electrostrictive constant.

The electrostrictive pressure in liquids is given by

$$p = -\tfrac{1}{2}\gamma \langle E^2 \rangle \tag{135}$$

where $\langle E^2 \rangle$ is the time average of the varying electric field and is given by (109), and γ is the electrostrictive coefficient which is defined as

$$\gamma = \rho\left(\frac{\partial \epsilon}{\partial \rho}\right) \tag{136}$$

where ρ is the density and ϵ is the dielectric constant.

As a result of the electrostrictive pressure according to (135) and (109), a density wave in the medium is generated. By solving the isothermal Navier-Stokes equation [51] we obtain the complex amplitude of the induced density wave as

$$\Delta\rho = -\frac{1}{2}\frac{K^2\gamma}{\Omega^2 - \Omega_s^2 - i\Omega\Gamma_s} A_1^* A_2 e^{i(\Omega t - \vec{K}\cdot\vec{r})} \tag{137}$$

where Ω_s may be regarded as the resonance phonon frequency and is given by

$$\Omega_s = vK \tag{138}$$

with v as the velocity of the acoustic wave, and Γ_s is the inverse of the phonon lifetime and is given by

$$\Gamma_s = \eta K^2/\rho \tag{139}$$

with η as the viscosity coefficient.

Using $\Delta\epsilon = 2n\epsilon_0\Delta n$ and the definition of the electrostrictive coefficient equation (135), we obtain the linear relation between the index grating and the density wave

$$\Delta n = \frac{\gamma}{2n\rho\epsilon_0}\Delta\rho. \tag{140}$$

Using the complex number representation, the induced index change can be written, according to (112),

$$\Delta n = n_2 e^{i\phi} A_1^* A_2 e^{i(\Omega t - \vec{K}\cdot\vec{r})}. \tag{141}$$

Substituting (141) for Δn and (137) for $\Delta\rho$ in (140), we obtain the following expression for the complex Kerr coefficient:

$$n_2 e^{i\phi} = \frac{-K^2\gamma^2}{4n\rho\epsilon_0(\Omega^2 - \Omega_s^2 - i\Omega\Gamma_s)}. \tag{142}$$

Note that this complex Kerr coefficient is a function of the frequency difference between the two waves. At resonance $\Omega = \pm\Omega_B$, the Kerr coefficient is purely imaginary, indicating a 90° phase shift between the index grating and the intensity pattern.

The complex Kerr coefficient derived above is different from the traditional one used in self-focusing and self-phase modulation as described in [61]. The Kerr coefficient measured in those experiments may be regarded as the dc Kerr coefficient and is related to that of (142) by putting $\Omega = 0$. Such a dc Kerr coefficient is written

$$n_2(\Omega = 0) = \frac{\gamma^2}{4n\rho v^2\epsilon_0} \quad \phi = 0 \tag{143}$$

where we recall that v is the acoustic velocity and ρ is the density. At resonance ($\Omega = \pm\Omega_B$), the Kerr coefficient becomes, according to (142),

$$n_{2\text{Res}} = \frac{\gamma^2}{4n\rho v^2\epsilon_0}\left(\frac{\Omega_B}{\Gamma_B}\right) \quad \phi = \pm\pi/2 \tag{144}$$

where the sign $\pm$ depends on the sign of $\Omega = \omega_2 - \omega_1$. According to (120) and (144), we note that gain coefficient g is positive when $\omega_2 < \omega_1$. In other words, the beam with lower frequency always gains.

Notice that the magnitude of the Kerr coefficient at resonance is increased by a factor of

$$Q = \frac{\Omega_B}{\Gamma_B} \tag{145}$$

which may be regarded as the Q parameter of the acoustic oscillation.

This parameter Q depends on the phonon frequency and thus depends on the angle between the two beams at acoustic resonance. According to (138) and (139), we obtain

$$Q = \frac{\rho v}{\eta K}. \tag{146}$$

The angular dependence is now obtained by using

$$K = 2k \sin\tfrac{1}{2}\theta \tag{147}$$

where $k = 2\pi n/\lambda$ and θ is the angle subtended by the wave vectors of the beams. This leads to

$$Q = \frac{\rho v}{2\eta k} \cdot \frac{1}{\sin\frac{1}{2}\theta} \tag{148}$$

which can also be written

$$Q = Q_{\text{SBS}} \frac{1}{\sin\frac{1}{2}\theta} \tag{149}$$

where Q_{SBS} is the Q parameter for backward SBS with $\theta = \pi$. For liquids such as CS_2, Q_{SBS} is of the order of 100. This parameter increases as θ becomes small and can reach as high as 10 000

According to (144) and (149), the gain coefficients at resonance also depend on the angle θ between the beams. For contradirectional coupling, the angular dependence is, according to (149), (144), and (131),

$$g = g_{\text{SBS}} \frac{1}{(\sin\frac{1}{2}\theta)^2} \tag{150}$$

where we recall that $\pi/2 < \theta < \pi$, and g_{SBS} is the gain coefficient at $\theta = \pi$, and is given by (for $\Omega = \omega_2 - \omega_1 = -\Omega_B$)

$$g_{\text{SBS}} = \frac{2\pi}{\lambda} \frac{\gamma^2}{4n\rho V^2\epsilon_0}\left(\frac{\Omega_B}{\Gamma_B}\right). \tag{151}$$

For codirectional coupling, the angular dependence is given by [according to (149), (144) and (120)]

$$g = g_{\text{SBS}} \frac{2}{\sin\theta} \tag{152}$$

where g_{SBS} is given by (151) and θ is less than $\pi/2$ but greater than 0.

We note that the gain coefficient g increases significantly for the codirectional case as θ decreases. This high gain may be difficult to observe because the phonons generated by two-wave mixing tend to walk out of the interaction region and thus reduce the resonance enhancement.

The electrostrictive Kerr effect and the photoelastic effect are very similar in nature. Both are related to the change of index of refraction as a result of the squeezing of the medium. Consequently, these two coefficients are related. Such a relationship has been derived [62] and is given by

$$n_2 = \frac{n^7\epsilon_0 p^2}{4B} \tag{153}$$

where B is the bulk modulus, p is the photoelastic coefficient [1], and n is the index of refraction. Using the following relation:

$$B = \rho v^2 \tag{154}$$

where ρ is the mass density and v is the acoustic velocity, the Kerr coefficient can also be written

$$n_2 = \tfrac{1}{4}n_0\epsilon_0 v^2 M_2 \tag{155}$$

or

$$n_2 = \tfrac{1}{4}\epsilon_0 M_3 \tag{156}$$

where M_2 and M_3 are the acoustooptic figures-of-merit [1],

$$M_2 = \frac{n^6 p^2}{\rho v^3} \quad M_3 = \frac{n^7 p^2}{\rho v^3}. \tag{157}$$

C. *Nonlinear Optical Bragg Scattering*

Acoustooptic Bragg scattering is a well-known phenomenon and has been widely used for beam steering, beam modulation, frequency shifting, and other applications. It is a physical process in which an incident laser beam is scattered from an acoustic field. The scattered

beam is shifted in frequency by an amount which is exactly the frequency of the acoustic field. In addition, the scattered beam propagates along a new direction which is determined by the Bragg condition [1].

If the Bragg cell is made of a nonlinear optical medium, the traveling interference pattern formed by the incident beam and the scattered beam may induce a volume index grating. Such a volume index grating will then affect the propagation of these two beams. If the optical nonlinearity of the medium is due to the electrostrictive Kerr effect, then an additional sound wave can be generated due to the two-beam coupling. This additional sound wave is added to the applied acoustic field, and thus enhances the diffraction efficiency under appropriate conditions.

From the quantum mechanical point of view, for each photon scattered, there is one phonon generated or annihilated depending on whether the frequency is downshifted or upshifted. In the case of frequency downshift, there is one phonon generated for each photon scattered. Thus the number of generated phonons is proportional to the scattered intensity. For low intensity light, these additional phonons are much smaller in number relative to the phonons of the applied acoustic field. However, for high-intensity laser beams, the number of generated phonons can be much larger than those of the applied acoustic field. The presence of these additional phonons effectively enhances the acoustic field and thus increases the diffraction efficiency.

Both acoustooptic Bragg scattering and nondegenerate two-wave mixing in Kerr media have been individually treated by previous scientists [1], [40]. In addition, the amplification of sound waves through the interaction of two laser beams with different frequencies has been observed experimentally [63]. The coupling between the Bragg scattered beam and the incident beam due to Kerr effect has recently been studied [64]. Such coupling leads to nonlinear optical Bragg scattering. In a Bragg cell with a low acoustic field, the diffraction efficiency may be low at low optical intensity. When the optical intensity is above some threshold, the phonon regenerative process leads to an avalanche in which all the photons are diffracted. Here, we describe a coupled-mode theory of the nonlinear optical Bragg scattering in Kerr media. An exact solution is obtained for the nonlinear diffraction efficiency.

Consider the nondegenerate two-wave mixing in the Bragg cell (see Fig. 11). If an acoustic field is applied such that the wave A_2 is generated by scattering of the incident wave A_1 from the sound wave, then the condition $\Omega = \pm vK$ is automatically satisfied provided that the wave A_1 is incident along a direction which satisfies the Bragg condition. Under these circumstances, the coupled-mode equations that govern the propagation of these two waves in the medium can be written

$$\frac{d}{dz}A_1 = -\tfrac{1}{2}g|A_2|^2A_1 - i\kappa A_2 \tag{158}$$

$$\frac{d}{dz}A_2 = \tfrac{1}{2}g|A_1|^2A_2 - i\kappa^*A_1 \tag{159}$$

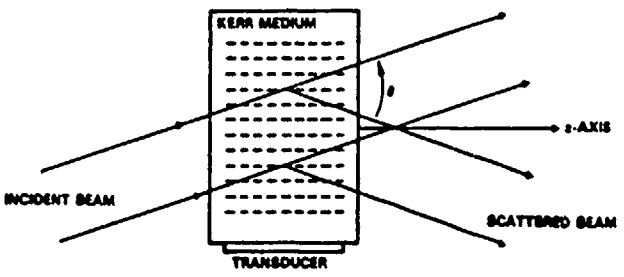

Fig. 11. Schematic drawing of nonlinear Bragg scattering in Kerr media.

where κ is the Bragg coupling constant [1] and g is the Kerr intensity coupling constant given by (120).

Note that the angle θ is twice the Bragg angle θ_B ($2k \sin \theta_B = K$). The phase ϕ is either $+90$ or $-90°$ depending on the sign of $\Omega = \omega_2 - \omega_1$. For the case when beam 2 is scattered with a frequency downshift (as shown in Fig. 11), the phase ϕ is $+90°$, indicating a gain for beam 2.

We again write

$$A_1 = \sqrt{I_1}e^{-i\psi_1} \quad A_2 = \sqrt{I_2}e^{-i\psi_2} \tag{160}$$

where ψ_1 and ψ_2 are the phases of the amplitudes A_1 and A_2, respectively. Using (160), the coupled equations can be written

$$I_1' - 2I_1i\psi_1' = -gI_1I_2 - 2i\kappa\sqrt{I_1I_2}e^{-i(\psi_2-\psi_1)}$$

$$I_2' - 2I_2i\psi_2' = gI_1I_2 - 2i\kappa^*\sqrt{I_1I_2}e^{-i(\psi_1-\psi_2)}, \tag{161}$$

respectively, where the prime indicates a differentiation with respect to z.

By rewriting κ as $\kappa \exp(-i\sigma)$ so that κ is now a positive number and splitting the real and imaginary parts, we obtain

$$I_1' = -gI_1I_2 - 2\kappa\sqrt{I_1I_2}\sin\Delta\psi \tag{162}$$

$$I_2' = gI_1I_2 - 2\kappa\sqrt{I_1I_2}\sin\Delta\psi \tag{163}$$

and

$$\psi_1' = \kappa(I_2/I_1)^{1/2}\cos\Delta\psi \tag{164}$$

$$\psi_2' = \kappa(I_1/I_2)^{1/2}\cos\Delta\psi \tag{165}$$

where

$$\Delta\psi = \psi_2 - \psi_1 + \sigma. \tag{166}$$

These equations are very similar to those that describe mode coupling in ring laser gyros [65], [66]. In fact, the relative phase between the waves can be written, according to (165), (166)

$$\Delta\psi' = \kappa\left[(I_1/I_2)^{1/2} - (I_2/I_1)^{1/2}\right]\cos\Delta\psi \tag{167}$$

which is similar to the well-known phase-coupling equations in ring laser gyros. In our case, since the wave A_2 is generated by Bragg scattering of the wave A_1 from the acoustic field, it is legitimate to assume that the phase of A_2 is connected to that of the incident wave A_1. Thus

$$\Delta\psi = \pi/2, \quad 3\pi/2 \tag{168}$$

are good solutions of (167).

For $g = 0$, exact solution of the coupled equations (158) and (159), subject to the boundary condition of $A_2(0) = 0$, yields a relative shift of $\Delta\psi = \pi/2$. We will take this as the proper solution to (167). Substitution of $\Delta\psi = \pi/2$ into (162) and (163) leads to

$$I_1' = -gI_1I_2 - 2\kappa\sqrt{I_1I_2}$$
$$I_2' = gI_1I_2 - 2\kappa\sqrt{I_1I_2}. \tag{169}$$

The coupled equation (169) can be integrated exactly, and the solution is

$$I_1(z) = I\cos^2 u$$
$$I_2(z) = I\sin^2 u \tag{170}$$

where I is the incident intensity at $z = 0$ (i.e., $I_1(z) = I$ and $I_2(z) = 0$ at $z = 0$), and u is given by [64]

$$\tan u = \frac{\tan(\kappa z\sqrt{1-b^2})}{\sqrt{1-b^2} - b\tan(\kappa z\sqrt{1-b^2})} \tag{171}$$

with

$$b = \frac{gI}{4\kappa} = \frac{\gamma L'}{4\kappa L} \tag{172}$$

where $\gamma = gI$ and L is the length of interaction. We note that b is a dimensionless parameter which is the ratio of Kerr coupling to Bragg coupling. Equation (171) is valid for all values of b. When the magnitude of b becomes greater than 1 (i.e., $|b| > 1$), $\sqrt{1-b^2}$ becomes $i\sqrt{b^2-1}$ and $\tan\kappa z\sqrt{1-b^2}$ becomes $i\tanh\kappa z\sqrt{b^2-1}$. We also note that κ is a positive number as defined earlier. The Kerr coupling constant g can be either positive or negative depending on whether the frequency of beam 2 is downshifted or upshifted.

We now examine the intensity variation with respect to z for various values of b. For $b > 1$, $I_2(z)$ reaches its maximum value I (100 percent energy transfer) at distance z such that $\tanh(\kappa z\sqrt{b^2-1}) = \sqrt{b^2-1}/b$. Beyond this point, the intensity $I_2(z)$ decreases and reaches its asymptotic value of $I/[2b(b-\sqrt{b^2-1})]$ which becomes I when b approaches infinity.

For $b = 1$, $I_2(z)$ reaches its maximum value I at $z = 1/\kappa$. Beyond this point, the intensity $I_2(z)$ decreases and reaches its asymptotic value of $I/2$ at $z = \infty$.

For $0 \le b < 1$, $I_2(z)$ is a periodic function of z with maximum value I at points when $\tan(\kappa z\sqrt{1-b^2}) = \sqrt{1-b^2}/b$. The minimum value of $I_2(z)$ is zero, which occurs when $\tan(\kappa z\sqrt{1-b^2}) = 0$. Note that maximum or minimum occurs when $I_1I_2 = 0$.

For $-1 < b < 0$, $I_2(z)$ is also a periodic function of z with maximum value I at points when $\tan(\kappa z\sqrt{1-b^2}) = \sqrt{1-b^2}/b$. Compared with the case $0 \le b < 1$, we note that it takes a longer interaction length for I_2 to reach its maximum value because of the negative Kerr coupling. Minimum value of $I_2(z)$ is zero which also occurs when $\tan(\kappa z\sqrt{1-b^2}) = 0$.

For $b = -1$, $I_2(z)$ is a monotonically increasing function of z with an asymptotic value of $I_2(z) = I/2$ at $z = \infty$. For $b < -1$, $I_2(z)$ is also a monotonically-increasing function of z with an asymptotic value of $I_2(z) = I/(2b^2 - 2b\sqrt{b^2-1})$ at $z = \infty$. Fig. 12 plots the intensity of $I_2(z)$ as a function z at various values of b.

We now examine the diffraction efficiency which is defined as

$$\eta = \frac{I_2(L)}{I} = \sin^2 u \tag{173}$$

as a function of intensity I (or b) for a given Bragg coupling constant κ and a length of interaction L. Fig. 13 plots the diffraction efficiency η as a function of the parameter b for various values of κL. We note that for $b > 0$ (or $g > 0$) the diffraction efficiency η is an increasing function of intensity and can reach nearly 100 percent at high optical intensities. The enhancement in the diffraction efficiency due to strong Kerr coupling can be employed for the steering of high-power lasers.

When $b >> 1$ and $b\kappa L >> 1$, the asymptotic expression for the diffraction efficiency is, according to (171) and (173)

$$\eta = 1 - 4b^2\exp(-4\kappa Lb). \tag{174}$$

We note that the diffraction efficiency approaches 100 percent exponentially at large b (high intensity). When b approaches $-\infty$, the asymptotic form of the diffraction efficiency is, according to (171) and (173)

$$\eta = \frac{1}{4b^2}\left[1 - 2\exp(-2\kappa L|b|)\right]. \tag{175}$$

According to (172) and (174), for small κL, high diffraction efficiency occurs when $\gamma L >> 1$ (or $gIL >> 1$), which corresponds to the Kerr regime. However, the diffraction efficiency is zero when $\kappa L = 0$, according to (171) and (173).

At $b = 0$, (173) reduces to $\eta = \sin^2\kappa L$, which is the familiar expression of the Bragg cell diffraction efficiency.

For such nonlinear Bragg scattering to be seen, the Kerr coupling constant must be comparable with the Bragg coupling constant. Thus the parameter b must be of the order of 1. If $b = 1$ is used as an example, the Kerr intensity-coupling constant must be

$$gI = 4\kappa.$$

We now take a Bragg coupling constant of $\kappa = 1\ \text{cm}^{-1}$ as an example and use a nonlinear medium such as CS_2. From the data available in [51], the Kerr coupling constant g for a Bragg angle of 5° ($\theta = 10°$) is $g = 1.5$ cm/MW, and the radio frequency required is 640 MHz. Thus, the optical intensity needed for observation of a significant nonlinearity in Bragg scattering, according to the above condition, is approximately 2.7 MW/cm^2.

The results show that diffraction efficiency is a nonlinear function of the optical intensity and can be greatly enhanced by increasing the intensity of the optical wave.

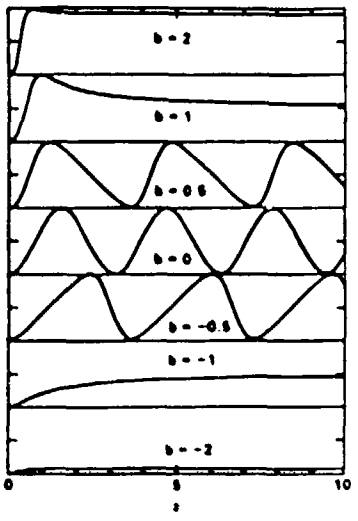

Fig. 12. Intensity variation of the scattered beam $I_2(z)$ as a function of z for various values of b.

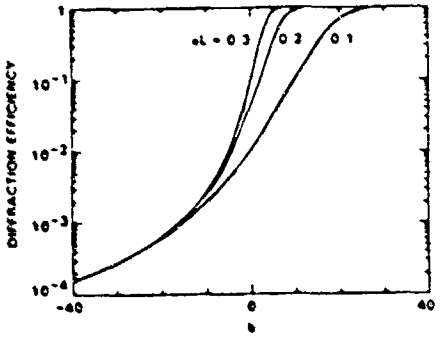

Fig. 13. Diffraction efficiency η as a function of the parameter b for various values of aL.

It can be used as a nonlinear device in which high-efficiency diffraction only occurs when the optical intensity is above a threshold.

D. SBS, SRS, and Photorefractive Two-Wave Mixing

Thus far we have discussed two-wave mixing in photorefractive crystals and Kerr media. In photorefractive two-wave mixing the frequency difference between the two beams is zero or small (a few Hertz). For two-wave mixing in Kerr media or stimulated Brillouin scattering (SBS), the frequency difference can be as large as a few gigahertz. Energy exchange between two beams also occurs in stimulated Raman scattering (SRS) [2]. The frequency difference between the beams in Raman scattering is in the range of terahertz.

There are several common features among the three types of two-wave mixing. All three types of wave mixing show nonreciprocal energy exchange without phase cross-talk. In fact, if we examine their coupled-mode equations (15) and (116), we note that the mathematical formulations are very similar. A fundamental difference exists between these types of two-wave mixing. In SBS and SRS, the gain coefficient (125) is proportional to the total intensity, whereas the photorefractive gain coefficient is independent of the intensity. Thus, for high-power applications, SBS and SRS can be efficient means for beam coupling. In addition, the frequencies of the idler wave are very different. In SRS, the idler wave is optical phonon. In SBS, the idler wave is acoustic phonon. Also, in photorefractive two-wave mixing, the idler wave is a holographic grating. As a result of the finite frequency of the idler wave, the coupled waves in these three processes are different in frequencies. For SBS and nondegenerate two-wave mixing in photorefractive media, the frequency difference is small so that the two waves propagate at virtually the same speed. In SRS, the large Stokes shift may lead to a significant difference in the phase velocity of the two waves due to dispersion. This may result in a phase mismatch in the wave coupling.

The coupled equations for stimulated Raman scattering are identical to those of the stimulated Brillouin scattering, except for the possibility of dispersion. In fact, it is known that, like SBS, SRS also exhibits phase conjugation [67]. The energy coupling in both SBS and SRS is due to the imaginary part of the third-order dielectric susceptibility [2]. If we examine (10) and (13), we notice that the energy coupling in photorefractive crystal is due to the out-of-phase term of the index grating. This spatial phase shift is 90° in crystals such as $BaTiO_3$, which operates by diffusion only. If we interpret the idler wave in SBS and SRS as a traveling index grating, then the spatial phase shift is also exactly 90° in resonant scattering [see (142)].

In view of the above discussion, we may generalize the meaning of photorefractive effect to include other phenomena such as the Kerr effect. In other words, the generalized photorefractive effect is a phenomenon in which a change of the index of refraction is induced by the presence of optical beams. Thus, we may view SBS and SRS as nondegenerate photorefractive two-wave mixing in nonlinear media.

E. Experimental Work

It was shown earlier that energy transfer in two-wave mixing requires a finite spatial phase shift between the intensity pattern and the induced index grating. In Kerr media where the response is local, such a spatial phase shift can be induced by the use of moving gratings in the medium. Thus, energy transfer is possible in nondegenerate two-wave mixing in Kerr media.

Although the concept of using moving gratings in local media for the energy coupling between two beams had been suggested in the 1970's [41]-[49], no experimental results were reported until recently. In 1986, a steady transfer of energy was observed in a two-wave mixing experiment in atomic sodium vapor [65]. In that experiment, a flash-pumped dye laser was used to pump a cell of sodium vapor that was inserted into a ring resonator. The laser frequency was detuned slightly from the sodium D line. The parametric gain due to the two-wave mixing leads to a unidirectional oscillation in a ring resonator.

The frequency of the oscillating beam in the ring resonator was measured and was found to be lower than that of the pump beam. In a later experiment using a CW dye laser, a frequency shift of several MHz's was measured [69]. The frequency shift agrees with our theoretical result [see (120) and (115)], which indicates that the low-frequency beam gets amplified when the Kerr coefficient is positive. By tuning the frequency of the dye laser to the other side of the D line, an opposite sign of the frequency shift was observed. This indicates the reverse of sign of the Kerr coefficient at this new frequency. In addition, the frequency of oscillation and the intensity of oscillation are functions of the cavity length. Oscillation ceases at cavity lengths when the frequency shifts are less than 8 or more than 50 MHz. Similar observations on the dependence on cavity length were found in photorefractive unidirectional ring resonators [70], [71].

In a two-wave mixing experiment, a fluorescent-doped boric acid glass is used as the nonlinear material [72]. In this experiment, a frequency shift of 0.1 Hz was induced by reflecting one of the beams off a mirror that was translated at a constant velocity by a piezoelectric transducer (PZT). By varying the frequency difference between the beams and monitoring the change in intensity of the probe beam, a time constant of 100 ms was measured. In a similar experiment, a ruby crystal is used as the nonlinear medium [73]. Energy coupling at a frequency shift of up to 500 Hz was observed. A time constant of 3.4 ms was determined by measuring the probe intensity at various frequency shifts. In addition, a net gain (exceeding the absorption and reflection loss) of more than 50 percent was observed.

Recently, energy transfer between two coherent beams in liquid crystals has been observed by several workers [74]. The energy exchange is due to the thin holograms in the medium. In these configurations, the scattering of light by the induced grating is in the Raman-Nath regime due to the small interaction length. The presence of higher order scattering terms results in a multiwave mixing that leads to the energy transfer from the strong beam to the weak beam. If the interaction length is increased, the energy transfer will decrease because the interaction will be in the Bragg regime.

V. Applications

The photorefractive coupling of two waves in electrooptic crystals has a wide range of applications. These include real-time holography, self-pumped phase conjugation [53], ring resonators [54], [70], [71], [75], laser gyros [72], nonreciprocal transmission [76], image amplification [20], vibrational analysis [77], and image processing [78], [79], etc. Some of these applications will be discussed in this section.

A. Photorefractive Resonators

The coherent signal beam amplification in two-wave mixing can be used to provide parametric gain for unidirectional oscillation in ring resonators. Such oscillation has been observed by using a $BaTiO_3$ crystal pumped with an argon ion or a HeNe laser [54]. Unlike the conventional gain medium (e.g., He-Ne), the gain bandwidth of photorefractive two-wave mixing is very narrow (a few hertz's for $BaTiO_3$; see also Fig. 4). Despite this fact, the ring resonator can still oscillate over a large range of cavity detuning. This phenomenon was not well understood until a theory of photorefractive phase shift was developed [70]. The theory shows that oscillation can occur at almost any cavity length despite the narrow-band nature of two-wave mixing gain, provided the coupling is strong enough. Such a theory is later verified experimentally by studying the frequency of unidirectional ring oscillation at various cavity detunings [71].

Referring to Fig. 14, we now investigate the oscillation of a ring resonator in which a photorefractive crystal is inserted. Let us focus our attention on the region occupied by the photorefractive crystal and examine the gain due to two-wave mixing. The results of nondegenerate two-wave mixing derived in Section II-C can be used to explain the ring oscillation.

In a conventional ring resonator, the oscillation occurs at those frequencies

$$f = f_o + N\frac{c}{S} \tag{176}$$

which lie within the gain curve of the laser medium (e.g., He-Ne). Here, S is the effective length of a complete loop, f_o is a constant, and N is an integer. For $S \leq 30$ cm, these frequencies (176) are separated by the mode spacing $c/S \geq 1$ GHz. Since the width of the gain curve for the conventional gain medium is typically several GHz due principally to Doppler broadening, oscillation can occur at almost any cavity length S. On the contrary, if the bandwidth of the gain curve is narrower than the mode spacing c/S, then oscillation can sustain, provided the cavity loop is kept at the appropriate length.

Unlike the conventional gain medium, the bandwidth of photorefractive two-wave mixing is very narrow. Using photorefractive crystals that operate by diffusion only, e.g., $BaTiO_3$, the coupling constant can be written, according to (45)

$$\gamma = \frac{\gamma_o}{1 + (\Omega\tau)^2} \tag{177}$$

where γ_o is the coupling constant for the case of degenerate two wave mixing (i.e., $\Omega = \omega_2 - \omega_1 = 0$) and is given by

$$\gamma_o = \frac{4\pi\Delta n}{\lambda\cos(\theta/2)} \tag{178}$$

The parametric two wave mixing gain is given by, according to (50)

$$g = \frac{I_1(L)}{I_1(0)} = \frac{1+m}{1+me^{-\gamma L}}e^{-\alpha L} \tag{179}$$

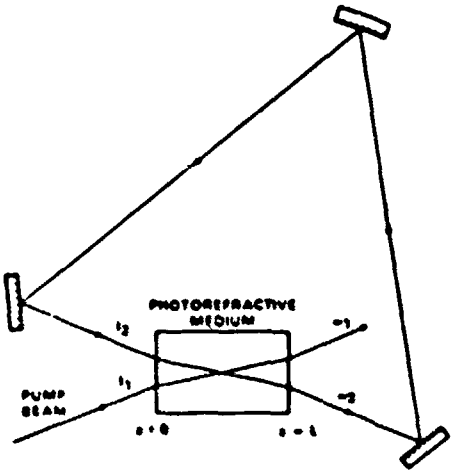

Fig. 14 Schematic drawing of a unidirectional photorefractive ring resonator.

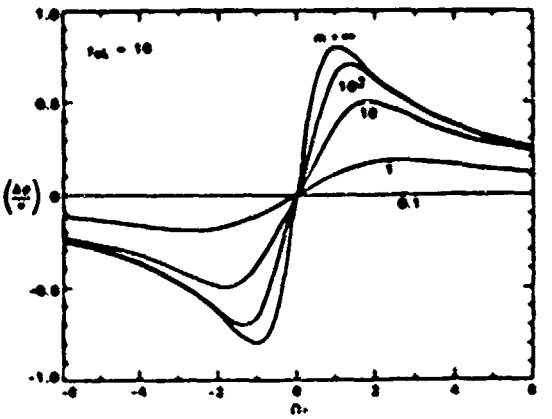

Fig. 15. Photorefractive phase shift $\Delta\psi$ as a function of $\Omega\tau$ for various values of m.

where we recall that m is the input beam ratio $m = I_1(0)/I_2(0)$ and L is the length of interaction. Note that amplification ($g > 1$) is possible only when $\gamma > \alpha$ and $m > (1 - e^{-\alpha L})/(e^{-\alpha L} - e^{-\gamma L})$. Also note that g is an increasing function of m (i.e., $\partial g/\partial m > 0$) and g is an increasing function of L, provided $\gamma > \alpha$ and

$$L \leq \frac{1}{\gamma} \ln\left[\frac{m(\gamma - \alpha)}{\alpha}\right]. \tag{180}$$

The gain as a function of frequency ω_2 (or equivalently as a function of $\Omega = \omega_2 - \omega_1$), has been plotted in Fig. 4 for various values of m. Note that gain is significant only when $|\omega_2 - \omega_1|\tau < 1$. For materials such as $BaTiO_3$ and SBN, τ is between 1 and 0.1 s. Thus, the gain bandwidth is only a few hertz. In spite of such an extremely narrow bandwidth, unidirectional oscillation can still be observed easily at "any" cavity length in ring resonators using $BaTiO_3$ crystals as the photorefractive medium. Such a phenomenon can be explained in terms of the additional phase shift [(24) and (25)] introduced by the photorefractive coupling. This phase shift is a function of the oscillation frequency and is plotted in Fig. 15 as a function of $\Omega\tau$. For $BaTiO_3$ crystals with $\gamma L > 4\pi$, this phase shift can vary from $-\pi$ to $+\pi$ for a frequency drift of $\Delta\Omega\tau = \pm 1$. Such a phase shift is responsible for the oscillation of the ring resonator which requires a round-trip phase shift of an integer times 2π.

1) Oscillation Conditions: We now examine the boundary conditions appropriate to a unidirectional ring oscillator. At steady-state oscillation, the electric field must reproduce itself, both in phase and intensity, after each round-trip. In other words, the oscillation conditions can be written

$$\Delta\psi + \int k\, ds = 2N'\pi \tag{181}$$

and

$$gR = 1 \tag{182}$$

where $\Delta\psi$ is the additional phase shift due to photorefractive coupling, the integration is over a round-trip beam path, the parameter R is the product of the mirror reflectivities, and g is the parametric gain of (179).

If we define a cavity detuning parameter $\Delta\Gamma$ as

$$\Delta\Gamma = 2N'\pi - \int k\, ds \tag{183}$$

where N' is an integer chosen in such a way that $\Delta\Gamma$ lies between $-\pi$ and $+\pi$, then the oscillation condition (181) can be written

$$\Delta\psi = \Delta\Gamma + 2M\pi \tag{184}$$

where M is an integer. In other words, oscillation can be achieved only when the cavity detuning can be compensated by the photorefractive phase shift.

Equations (181) and (182) may be used to solve for the two unknown quantities $m = I_1(0)/I_2(0)$ and $\Omega = \omega_2 - \omega_1$. If we fix the pump intensity $I_1(0)$ and the pump frequency ω_1, then (181) and (182) can be solved for the oscillation frequency ω_2 and the oscillation intensity $I_2(0)$. Substituting (179) for g in (182) and using (25), we obtain

$$\Delta\psi = -\frac{\beta}{\gamma} \ln\left(Re^{-\alpha L}\right). \tag{185}$$

This equation can now be used to solve for the oscillation frequency $\Omega\tau$. For the case of pure diffusion, using (46) for $\phi_s = \pi/2$ and (19) and (20), we obtain from (185)

$$\Omega\tau = \frac{2\Delta\psi}{\alpha L - \ln R} = \frac{2(\Delta\Gamma + 2M\pi)}{\alpha L - \ln R} \tag{186}$$

where $\Delta\Gamma$ is the cavity detuning and is given by (183). Substituting (179) for g in (182), we can solve for m and obtain

$$m = \frac{I_1(0)}{I_2(0)} = \frac{1 - Re^{-\alpha L}}{Re^{-\alpha L} - e^{-\gamma L}}. \tag{187}$$

Since m must be positive, we obtain from (187) the threshold condition for oscillation

$$\gamma L > \gamma_t L = \alpha L - \ln R \qquad (188)$$

where γ_t is the threshold parametric gain constant. Since γ is a function of frequency Ω, (188) dictates that the parametric gain is above threshold only in a finite spectral regime. Using (177) for γ, (188) becomes

$$|\Omega\tau| < \left[\frac{\gamma_o L}{\alpha L - \ln R} - 1\right]^{1/2} \qquad (189)$$

where we recall that γ_o is the parametric gain at $\Omega = \omega_2 - \omega_1 = 0$. Equation (189) defines the spectral regime where the parametric gain γ is above threshold (i.e., $\gamma > \gamma_t$).

We have thus far obtained expressions for the oscillation frequency [(186)] and the spectral regime where the gain is above threshold. The ring resonator will oscillate only when the oscillation frequency falls within this spectral region. The oscillation frequency $\omega_2 = \omega_1 + \Omega$ is determined by (186), with $\Delta\Gamma$ being the cavity detuning (183).

The same oscillation frequency must also satisfy (189). Thus, we obtain the following oscillation condition:

$$\frac{2|\Delta\psi|}{\alpha L - \ln R} < \left[\frac{\gamma_o L}{\alpha L - \ln R} - 1\right]^{1/2}. \qquad (190)$$

which can also be written

$$\gamma_o L > \gamma_t L + \frac{1}{\gamma_t L}(2\Delta\psi)^2 = G_t L \qquad (191)$$

where γ_t is the threshold parametric gain of (188) for the case when $\Delta\psi = 0$, and G_t may be considered as the threshold gain for the case when $\Delta\psi \neq 0$. According to (191), the threshold gain increases as a function of the cavity detuning $\Delta\Gamma$. The cavity detuning $\Delta\Gamma$ not only determines the oscillation frequency [(186)], but also the threshold gain G_t.

The $\Delta\Gamma$ in (183) is the cavity detuning and is defined between $-\pi$ and π. However, the photorefractive phase shift (25) can be greater than π. When this happens, the unidirectional ring resonator may oscillate at more than one frequency. These frequencies are given by (186), with $M = 0, \pm 1, \pm 2, \cdots$, etc., and with their corresponding threshold gain given by

$$G_t L = \gamma_t L + \frac{1}{\gamma_t L}\left[2(\Delta\psi + 2M\pi)\right]^2. \qquad (192)$$

In other words, for each cavity detuning $\Delta\Gamma$, the ring resonator can support multimode oscillation, provided the coupling constant γ_o is large enough. Fig. 16 shows the oscillation intensity, as well as the oscillation frequency as functions of cavity detuning $\Delta\Gamma$. Note that for larger $\gamma_o L$, the resonator can oscillate at almost any cavity detuning $\Delta\Gamma$, whereas for small $\gamma_o L$, oscillation occurs only when the cavity detuning is limited to some small region around $\Delta\Gamma = 0$.

In summary, ring oscillation occurs when the two-wave mixing gain dominates cavity losses and the round-trip optical phase reproduces itself (to within an integer multiple of 2π). The condition on phase is unique because of a significant contribution to the optical phase shift due to nondegenerate photorefractive two-wave mixing. This condition is satisfied at any cavity length if the oscillation frequency is slightly detuned from the pump frequency, since the photorefractive phase shift [(185)] depends on the detuning. The frequency difference Ω ($= \omega_2 - \omega_1$) between the pumping and oscillating beams can be written

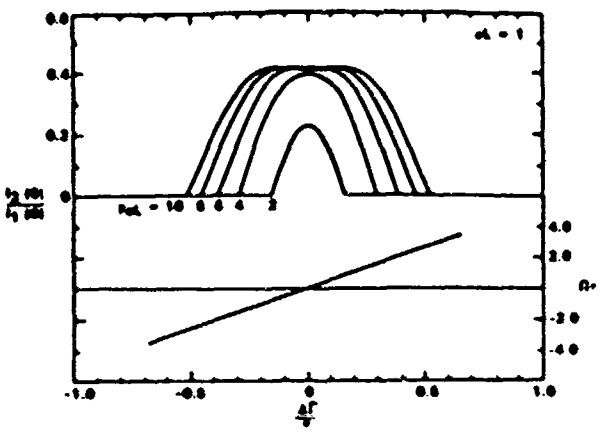

Fig. 16. Oscillation intensity as a function of cavity detuning $\Omega\tau$ for various values of $\gamma_o L$.

$$\Omega = \left[2(\Delta\Gamma + 2M\pi)/\tau A\right] \qquad (193)$$

where $\Delta\Gamma$ is the cavity-length detuning with respect to an integer multiple of optical pump waves in the cavity, M is an integer, τ is the photorefractive time response, and A represents the total cavity loss. There are threshold conditions for oscillation involving cavity loss and gain (taking M to be zero):

$$|\Omega| \leq (1/\tau)(\gamma L/A - 1)^{1/2} \qquad (194)$$

$$|\Delta\Gamma| \leq (A/2)(\gamma L/A - 1)^{1/2} \qquad (195)$$

where γ is the degenerate two-wave mixing coupling coefficient, L is the interaction length, and $A = -\ln(RT_iT_p)$ (with R being the product of the reflectivities of the cavity mirrors and output coupler; T_i is the transmission through the photorefractive crystal accounting for the absorption, Fresnel reflections, and scattering (or beam fanning); and T_p is the effective transmission through the pinhole aperture).

This theory predicts that the unidirectional ring resonator will oscillate at a frequency different from the pump frequency by an amount directly proportional to the cavity-length detuning. Furthermore, in a photorefractive material with moderately low τ, the theory postulates a threshold where oscillation will cease if the cavity detuning (frequency difference) becomes too large. Such a theory has been validated experimentally in a $BaTiO_3$ photorefractive ring resonator [71].

The experiments performed to examine the above theory will now be discussed in detail. Fig. 17 shows the experimental setup. A single-mode argon-ion laser (514.5

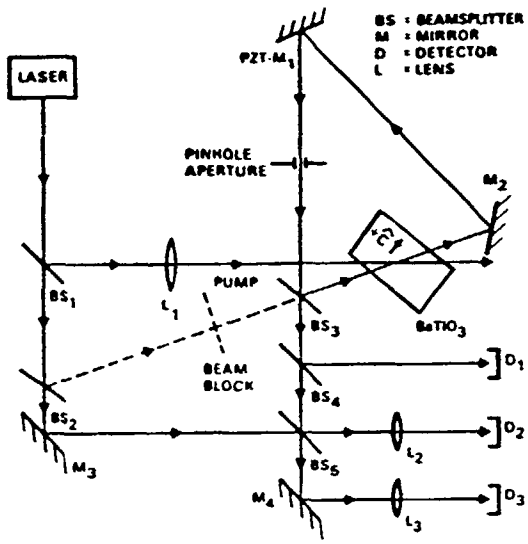

Fig. 17. Optical setup for the photorefractive unidirectional ring resonator with variable cavity length. The beat frequency between the self-oscillation and pump beams is derived from the motion of the interferograms at D_2 or D_3 [71].

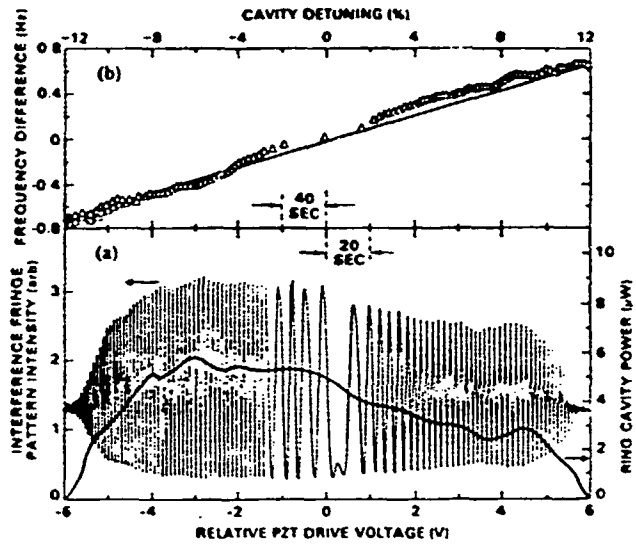

Fig. 18. Characteristics of the unidirectional self-oscillation as a function of ring-cavity length (i.e., PZT voltage or cavity detuning, where 100 percent implies a detuning of one full optical wave): (a) ring-cavity intensity (right) and beat-frequency signature (left); (b) frequency difference between the self-oscillation and the pumping beam [71].

nm) is used to pump a $BaTiO_3$ crystal which is inserted into a ring resonator. Two-wave mixing in $BaTiO_3$ provides the parametric gain needed for the oscillation in the unidirectional ring cavity, formed by two planar mirrors (M_1 and M_2) and a planar beam splitter (BS_3). The oscillation beam in the ring-cavity is sampled through the output coupler BS_3, its intensity being detected at D_1 while the beat frequency between it and the pumping beam is determined using complementary fringe patterns formed at detectors D_2 and D_3. Without a ring-cavity pinhole aperture, unidirectional oscillation can be observed at any cavity length. However, dynamically unstable multiple spatial modes are evident [80], [81] in the fringe patterns at D_2 and D_3. To obtain a single mode (and clean fringe patterns), a 200 μm pinhole is placed in the ring cavity. The basic premises of the theory [70] are verified by slowly ramping the PZT voltage and observing the beat frequency, along with the ring-cavity oscillation intensity. Typical results are shown in Fig. 18(a) for an 80 mW pump beam incident at 40° from the c axis of $BaTiO_3$ and at 20° from the oscillating beam (both angles are external in air).

The intensity of the unidirectional oscillation versus cavity length [Fig. 18(a)] indicates threshold gain conditions [(194) and (195)]. The beat frequency between oscillating and pumping beams, as observed in the time variation of the fringe-pattern intensity [Fig. 18(a)], clearly corresponds to the position of the PZT $- M_1$. When M_1 is exactly at the correct position (chosen as the origin), the fringe pattern is stationary, i.e., there is no frequency shift. As M_1 moves away from this origin, the fringe motion becomes faster and the frequency difference increases. Fig. 18(b) shows the linear dependence of the frequency difference on cavity detuning with the ramping period equal to 20 000 s for improved resolution.

The frequency difference changes sign as M_1 slowly moves through the origin. The observed sign is consistent with the sign of the phase shift between the light intensity pattern and index modulation that determines the direction of energy exchange in two-wave mixing. The beat-frequency signature [Fig. 18(a)] is also a periodic function of PZT mirror position. The observed beat-frequency signature reproduces itself with a M_1 displacement of every $-\lambda/2$, as expected (i.e., a cavity length detuning periodicity of λ). Experimentally, the frequency threshold for oscillation is approximately a linear function of the pumping-beam intensity, as shown in Fig. 19(a). According to Fig. 18(a), this frequency threshold is inversely proportional to τ, but τ can be approximately proportional to the inverse of the pump intensity (assuming that the cavity intensity is negligible by comparison) when the photoconductivities dominate [82]. Therefore, the observed dependence [Fig. 19(a)] agrees with theory.

The oscillation conditions for the unidirectional ring resonator are dependent on the two-wave mixing gain (γL) in the photorefractive medium. γL is varied by rotating the $BaTiO_3$ crystal with respect to the pumping and oscillating beams [83]. When the gain is too small, no unidirectional oscillation is observed, regardless of ring-cavity length. For γL just above threshold, two pronounced differences are evident, contrasting with γL large. First, the amount of cavity detuning that is accommodated before oscillation ceases is greatly reduced. Second, the maximum frequency difference between the pumping and oscillating beams is much less. The quantitative trends of these two effects are given in Fig. 19(b) for a pump power of 80 mW.

The threshold oscillation conditions given in expressions (194) and (195) agree with the data [Fig. 19(b)].

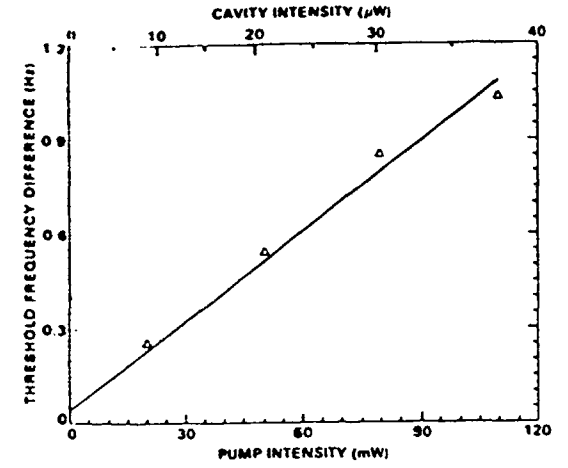

(a)

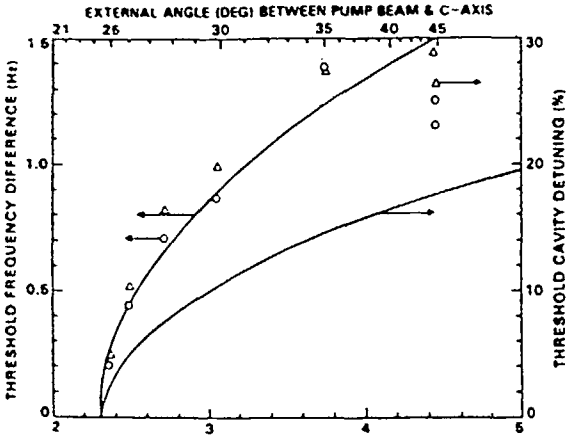

(b)

Fig. 19. Oscillation threshold behavior for the unidirectional ring resonator: (a) maximum beat frequency as a function of pumping-beam or ring-cavity power along with a linear fit (solid-line); (b) maximum beat frequency (left) and cavity detuning (right) as a function of two-wave mixing gain γL, where γL is related to the external angle that the pumping beam makes the crystal's c axis as shown (top scale). Note: the two solid curves in (b) correspond to the evaluation of (194) and (195) as described in text [71].

The solid curve associated with the left-hand scale of Fig. 19(b) is generated from (194) for $A = 5.1$ and $\tau = 0.53$ s. This cavity-loss factor A is estimated independently from $R \times 0.99 \times 0.91 \times 0.81$ (for M_1, M_2, and BS_3, respectively), $T_s = 0.52$, and $T_p = 0.016$ (for a cavity length of 50 cm). Accumulating these contributions gives $A = 5.2$, in excellent agreement with the observed 5.1. The right-hand scale of Fig. 19(b) shows the dependence of threshold cavity detuning (i.e., the maximum detuning that will still support self-oscillation) on γL, along with the prediction from (195), where $\Delta\Gamma$ is normalized by 2π. Remarkable agreement is obtained using $A = 5.1$ from Fig. 19(a) and no adjustable parameters.

The interdependence of the optical cavity length and the beat frequency between the oscillating and pumping beams is a general property of photorefractive resonators. These results are not unique to the optical setup shown in Fig. 17. Similar behavior is observed with other configurations. First, the orientation of the $BaTiO_3$ crystal in Fig. 17 can be altered so that the pumping and oscillating beams enter the a face but in such a way that no self-pumping occurs [53]. Second, the $BaTiO_3$ can be replaced by crystals of strontium barium niobate [84], [85] (nominally undoped and cerium doped). Third, a linear resonator (Fig. 20) can act as a self-pumped phase conjugator [54]. The observed frequency shift of the phase-conjugate beam is exactly twice that of the self-oscillation, which is necessary to satisfy energy conservation for slightly-nondegenerate four-wave mixing [86]. In all three variations, the measured frequency differences correlate with cavity length detuning; results equivalent to those shown in Fig. 18 are obtained.

In summary, the experimental results indicate that the frequency difference between the oscillating and pumping beams in the unidirectional ring resonator depends on the optical cavity length. This dependence supports the theory [70] that uses a photorefractive phase shift associated with slightly-nondegenerate two-wave mixing to satisfy the round-trip phase-oscillation condition for the resonating beam. Similarly, the observed frequency shifts in other photorefractive resonators, including self-pumped phase conjugators, may also be explained by the same mechanism. This is the subject of the next section.

B. Resonator Model of Self-Pumped Phase Conjugators

The theory of unidirectional photorefractive ring resonators described in the previous section can be extended to explain the phenomenon of self-pumped phase conjugation using $BaTiO_3$ crystals (sometimes referred to as the cat mirror [53]). It is known that optical four-wave mixing can be used to generate phase conjugated waves. In self-pumped phase conjugation, no counterpropagating beams are supplied externally to provide the pumps needed in the four-wave mixing process. In addition, self-pumped phase conjugators using photorefractive crystals such as $BaTiO_3$ have received considerable attention because of the relatively high reflectivities (e.g., 30–50 percent) that can be easily achieved even with low-power lasers [53], [54], [87]. There have been several models developed for the self-pumped phase conjugation inside $BaTiO_3$ crystals. These include backscattering via 2-k gratings [55], [56], two coupled interaction regions [57], enhanced coupling via frequency-shifted waves [58], time-dependent four-wave mixing [59], and photovoltaic contributions [60]. In what follows, we present a resonator model of self-pumped phase conjugation. Such a model explains the origin of phase conjugation inside a $BaTiO_3$ crystal and also explains the frequency shift of the order of ± 1 Hz [56], [80], [89].

Referring to Fig. 21, we consider the incidence of a laser beam into a cube of photorefractive cyrstal. The crystal cube can be viewed as a dielectric optical cavity which supports a multitude of modes. These modes are trapped inside the crystal due to total internal reflection at the surfaces. When a laser beam is incident into the crys-

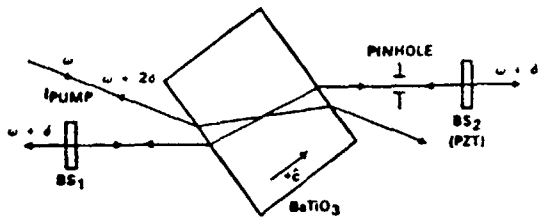

Fig. 20. Self-pumped phase conjugator using external reflectors to generate the self-oscillation with frequency shift δ and the phase-conjugate reflection with a frequency shift 2δ, where δ is proportional to the linear cavity length [71].

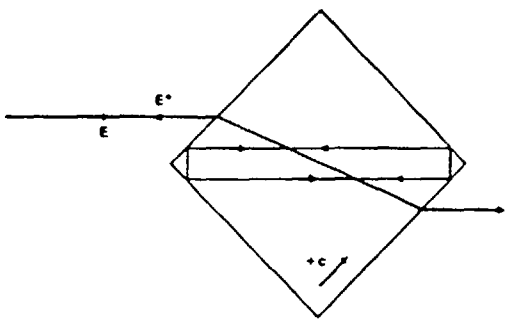

Fig. 21. Resonator model of self-pumped phase conjugators.

tal, some of the modes may be excited, as a result of the strong parametric gain due to two-wave mixing. In particular, ring oscillations such as those shown in Fig. 21 can be generated according to the theory developed earlier. When the configuration of the resonance cavity relative to the incident laser beam support bidirectional oscillation, a phase-conjugate beam is generated via the four-wave mixing process.

According to this theory, the frequency of oscillation inside the crystal can be slightly detuned from that of the pump beam. Let ω be the frequency of the incident laser beam; the frequency of the internal oscillation can be written

$$\omega' = \omega + \delta \tag{196}$$

where δ is the frequency detuning and is on the order of ± 1 Hz for $BaTiO_3$. Note that this frequency detuning depends on the path length of the ring oscillation inside the crystal. The bidirectional oscillation provides the counter propagating beams needed for the pump. As a result of the conservation of energy, the phase conjugated beam has a frequency of $\omega + 2\delta$.

The resonator model presents a simple explanation of the frequency shift observed in $BaTiO_3$ self-pumped phase conjugators [56], [88], [89]. In addition, experimental evidence indicates that internal oscillations inside the crystal play a key role in the generation of phase conjugated waves [90].

C. Optical Nonreciprocity

We mentioned earlier that the energy transfer in two-wave mixing may have application in optical nonreciprocity. We now discuss in some detail the nonreciprocal intensity transmission and nonreciprocal phase shifts due to two-wave mixing in photorefractive media. It is known in linear optics that the transmittance as well as the phase shift experienced by a light beam transmitting through a dielectric layered medium is independent of the side of incidence. This is known as the left- and right-incidence theorem and is a result of the principle of reversibility [91]. This theorem is no longer true when the photorefractive coupling is present. Such nonreciprocal transmittance was first predicted by considering the coupling between the incident beam and the reflected beam inside a slab of photorefractive medium [92]. The reflected beam is due to the dielectric discontinuity at the slab boundaries. As a result of the photorefractive contradirectional two-wave mixing, energy exchange occurs between the incident and reflected beams. Such an energy exchange leads to an asymmetry in the transmittance. Fig. 22 shows the two transmittances as a function of the coupling constant. Notice that a significant nonreciprocal transmittance is present due to the photorefractive coupling. In the extreme case of strong coupling ($\gamma L \gg 1$), the slab almost acts as a "one-way" window. Such nonreciprocal transmission has been observed in $BaTiO_3$ and $KNbO_3$:Mn crystals in the visible spectral regimes [93], [94].

In addition to the nonreciprocal intensity transmission, there exists a nonreciprocal phase shift in contradirectional two-wave mixing according to (37), provided $\beta \neq 0$. Such nonreciprocal phase shifts may be useful in some applications, including the biasing of ring laser gyros [66], [75] [94]. In what follows, we consider the photorefractive coupling of the counterpropagating beams inside a ring resonator.

Referring to Fig. 23, we consider the insertion of a thin slab of photorefractive crystal into a ring resonator. The photorefractive crystal is oriented such that nonreciprocal transmission occurs. In the absence of the photorefractive medium, the two oppositely-directed ring oscillators are degenerate in frequency in an inertial frame. As a result of the nonreciprocal transmission, the symmetry is broken and the degeneracy is removed. Since this may lead to a split in the frequency of oscillations, it provides a bias for the ring laser gyro operation.

Using the result derived in Sections II-B and II-C, we obtain the following expression for the transmittance of the two waves:

$$T_1 \equiv \frac{I_1(L)}{I_1(0)} = \frac{1 + m^{-1}}{1 + m^{-1}\exp(\gamma L)}$$

$$T_2 \equiv \frac{I_2(0)}{I_2(L)} = \frac{1 + m}{1 + m\exp(-\gamma L)} \tag{197}$$

where m is the incident intensity ratio $m \equiv I_1(0)/I_2(L)$. Note that $T_1 < 1$ and $T_2 > 1$ for positive γ. The sign of γ depends on the direction of the c axis.

With $I_1(z)$ and $I_2(z)$ given by (33), the phases ψ_1 and ψ_2 can be integrated directly from (31). The phase shifts

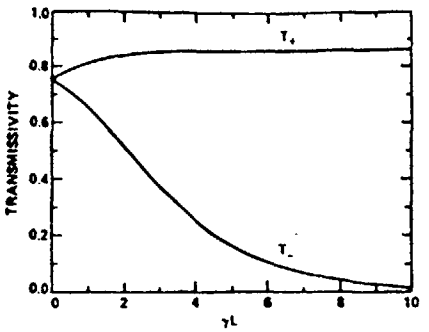

Fig. 22. Transmissivities from the right-hand side and the left-hand side as functions of photorefractive coupling γL.

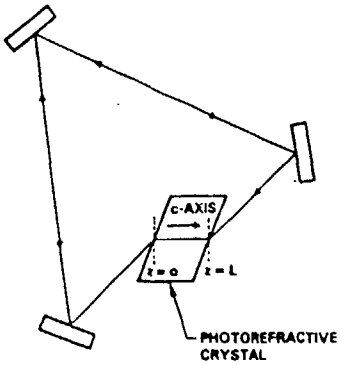

Fig. 23. Schematic drawing of a ring laser resonator filled with a photorefractive crystal plate.

in traversing through the medium are $kL + \psi_1(L) - \psi_1(0)$ and $kL + \psi_2(0) - \psi_2(L)$ for waves E_1 and E_2, respectively. These two phase shifts are different by an amount $\Delta = \psi_2(0) - \psi_2(L) - [\psi_1(L) - \psi_1(0)]$, which, according to (31) is given by

$$\Delta = -\int_0^L d(\psi_1 + \psi_2) = -\int_0^L \beta \frac{I_2 - I_1}{I_2 + I_1} dz. \quad (198)$$

Note that this difference in phase shifts is zero when $I_2(z) = I_1(z)$ between $z = 0$ and $z = L$, which corresponds to $C = 0$ in (33) (recall that $I_1(z) - I_1(z) = 2C$]. Using (33) and carrying out the integration in (198), we obtain the following expression for this phase shift difference:

$$\Delta = \frac{2\beta}{\gamma} \ln T_2 - \beta L \quad (199)$$

where T_2 is the beam intensity transmittance given by (197). Note that Δ can also be written as $\Delta = (2\beta/\gamma) \log T_1 + \beta L$. For small couplings, i.e., $\gamma L << 1$, this difference in phase shifts can be written approximately as

$$\Delta = \beta L \frac{m - 1}{m + 1} + \beta \gamma L^2 \frac{m^2}{(1 + m)^3} \quad (200)$$

where we recall that $m = I_1(0)/I_2(L)$.

In a conventional ring laser gyro, the oscillation frequency as well as the intensity are the same for two beams in an inertial frame. The oscillation occurs at thos frequencies

$$f = N\frac{c}{S} \qquad N = \text{integer} \quad (201)$$

which lie within the gain curve of the laser medium (e.g., He–Ne). Here S is the effective length of a complete loop and N is a larger integer. For $S \leq 30$ cm, these frequencies (201) are separated by the mode spacing $c/S \geq 1$ GHz. Since the width of the gain curve is typically 1.5 GHz due to principally Doppler broadening, the gyro usually oscillates at a single longitudinal mode.

The oscillation intensity inside the laser cavity is determined by the gain as well as the loss and is given by [88]

$$I_o = \kappa(g_o - g_t) \quad (202)$$

where κ is the constant which depends on the laser medium, g_o is the unsaturated gain factor per pass, and g_t is the threshold gain factor. Note that both g_o and g_t are dimensionless. In a conventional ring resonator, the threshold gain for both traveling waves is given by

$$g_t = \alpha L - \ln R \quad (203)$$

where α is the loss constant (including bulk absorption and scattering) and R is the product of the three-mirror reflectivities.

In the presence of the photorefractive coupling, the unequal transmissivities make the threshold gain different for the two waves which now become

$$g_{t1} = \alpha L - \ln T_1 R \qquad g_{t2} = \alpha L - \ln T_2 R \quad (204)$$

where T_1 and T_2 are the beam transmittances given by (197). The difference in the threshold gain leads to a split in the oscillation intensity. The fractional difference in the oscillation intensity is given approximately by

$$\frac{I_2 - I_1}{I_2 + I_1} = \frac{\ln_2 - \ln T_1}{(g_o - g_t)} = \frac{\gamma L}{2(g_o - g_t)}. \quad (205)$$

If we now assume that the beam intensities are nearly uniform in the photorefractive material (i.e., $\gamma L << 1$), the difference in phase shift Δ can be written, according to (198) and (205)

$$\Delta = -\frac{\beta \gamma L^2}{2(g_o - g_t)}. \quad (206)$$

This expression agrees with (200) provided $(g_o - g_t) << 2$, which is legitimate because $(g_o - g_t)$ is typically on the order of 10^{-2}.

The unequal phase shift for the oppositely-directed traveling waves corresponds to different effective optical path lengths for the waves. This results in a difference Ω between the angular frequencies of the laser oscillation of the two beams. The difference is $\Omega \equiv \omega_2 - \omega_1 = -c\Delta/S$, which can be written, according to (206), (19), and (20)

$$\Omega = \frac{c}{S} \cdot \frac{-L^2}{2(g_o - g_t)} \cdot \frac{2\pi^2}{\lambda^2} n_1^2 \sin\phi \cos\phi \quad (207)$$

where we recall that ϕ is the relative phase shift between the index grating and the interference pattern. We note that Ω is not zero provided $\sin\phi\cos\phi \neq 0$.

We now examine the angular frequency split Ω for various cases. For the pure diffusion case (i.e., no external electric field) in photorefractive material, the phase shift ϕ is given by $\phi = \pi/2 - \tan^{-1}\Omega\tau$, according to (46). Thus (207) becomes

$$\Omega = \frac{4\pi^2(\Delta n_s)^2 L^2 c\Omega\tau}{\lambda^2 S(g_o - g_t)(1+\Omega^2\tau^2)^2} \tag{208}$$

which has three solutions. The trivial one is $\Omega = 0$, which corresponds to an unsplit oscillation. The other roots are given by

$$\Omega_o = \pm\frac{1}{\tau}\frac{2\pi\Delta n_s}{\lambda}L\left[\frac{c\tau}{S(g_o - g_t)} - 1\right]^{1/2}. \tag{209}$$

Taking $\tau = 100$ ms, $S = 30$ cm, $g_o - g_t = 0.01$, $L = 1$ mm, $\Delta n_s = 10^{-5}$, $\lambda = 0.6328$ μm, (209) yields $\Omega_o = 10^3$ s^{-1}, which corresponds to a frequency split of 160 Hz. Whether the ring gyro will oscillate at the same frequency ($\Omega = 0$) or with a split Ω_o, or both, is a subject of mode stability.

It is shown that there are three modes of oscillations. The stability of these modes will determine the actual mode of oscillation at steady state. To investigate this issue, we need to examine the effect of small perturbation on the oscillation frequencies. Using (207) and $\phi = \pi/2 - \tan^{-1}\Omega\tau$, we consider that the frequency difference Ω is slightly deviated from the solution by $\delta\Omega$. This $\delta\Omega$ will change the holographic grating phase shift by $\delta\phi$. Equation (207) will then yield the resulting frequency difference $\Omega + d\Omega$ after substituting $\phi + \delta\phi$ for ϕ on the right-hand side. The criterion for stable oscillation is

$$\left(\frac{d\Omega}{\delta\Omega}\right) < 0. \tag{210}$$

Using (46) and (207), we can plot the right-hand side of (207) as a function of $\Omega\tau$. The solution of (207) can then be obtained by drawing a straight line through the origin with a slope of $1/\tau$. The intersections of the straight line with the curve give the solutions of (207). The ratio $(d\Omega/\delta\Omega)$ is proportional to the slope at the intersections. We note that the solution at $\Omega = 0$ has a positive slope which indicates that this mode of oscillation is unstable according to the criterion equation (210). The other two solutions of (209) are stable because they have a negative slope. Negative slope indicates that any deviation $\phi\Omega$ caused by perturbation will eventually damp out.

In summary, we found that if the crystal is acentric, the nonlocal response of the crystal leads to unequal transmittance and phase shifts of the two waves. These, in turn, lead to a split in the oscillation intensity as well as oscillation frequency. The frequency split may be utilized to bias a laser gyro away from its lock-in region. In the above derivation, the bulk absorption in the photorefractive material is neglected. This is legitimate provided $\alpha << \gamma$, which is generally true in most photorefractive crystals. The attenuation in the crystal may affect the difference in phase shift according to (198) because $I_2 - I_1$ is no longer a constant. Numerical analysis is required to include the attenuation and obtain a more accurate result.

D. Real-Time Holography and Beam Processing

We mentioned the holographic implications of two-wave mixing in photorefractive media earlier. Let us now elaborate on this idea in some detail. The formation of an index grating due to the presence of two coherent laser beams inside a photorefractive crystal is formally analogous to the recording process in conventional holography. Consider the procedure shown in Fig. 24(a), in which two laser beams intersect and form an induced index grating. The index grating, as given by (10), contains the product of the amplitudes A_1 and A_2. This index grating is a hologram formed by a "reference" beam A_1, and an "object" beam A_2. The transmission function of such a hologram can be written

$$t \sim \Delta n \sim A_1^* A_2 \exp(-i\vec{K}\cdot\vec{r}) + A_1 A_2^* \exp(i\vec{K}\cdot\vec{r}) \tag{211}$$

where A_1 and A_2 denote the complex amplitudes of the reference and object fields, respectively.

In the reconstruction step [see Fig. 24(b)], the hologram is illuminated by the reference beam $A_1 \exp(-i\vec{k}_1\cdot\vec{r})$. The diffracted beam can be written

$$\eta A_1 A_1^* A_2 \exp(-i\vec{k}_2\cdot\vec{r}) \tag{212}$$

where η is the diffraction efficiency. We notice that the phase of A_1 cancels out and the diffracted beam is a reconstruction of the object beam $A_2 \exp(-i\vec{k}_2\cdot\vec{r})$. Similarly the "reference" beam A_1 can be reconstructed by illuminating the hologram with "object" beam A_2 [see Fig. 24(c)], provided beam A_2 is a phase object (i.e., A_2 has phase variation with $|A_2|$ = constant).

In addition to the holographic analog, two-wave mixing exhibits amplification which is a unique feature not available in conventional holography. Using these two properties, two-wave mixing can be used for beam processing. As a result of the real-time holographic nature, photorefractive two-wave mixing exhibits nonreciprocal energy transfer without any phase crosstalk [96]. This characteristic can be seen directly by examining the coupled equations (17) and (18).

The lack of phase crosstalk can be understood also in terms of the diffraction from the self-induced index grating in the photorefractive crystal. Normally, if a beam that contains phase information $\psi(r, t)$ is diffracted from a fixed grating, the same phase information also appears in the diffracted beam. In self-induced index grating, the phase information $\psi(r, t)$ is impressed onto the grating in such a way that diffraction from such a grating will be accompanied by a phase shift $-\psi(r, t)$. Such a dynamic hologram makes self-cancellation of phase information

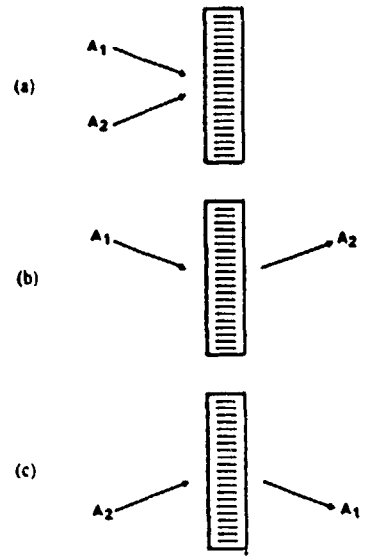

Fig. 24. Real-time holography.

possible when the incident beam is diffracted from the grating produced by the incident and the reference beams. Such a self-cancellation of phase information is actually equivalent to the reconstruction of the reference beam when the hologram is read out by the object beam.

Energy transfer without phase crosstalk can be employed to compress both the spatial and the temporal spectra of a light beam [97]. In other words, the energy transfer without phase crosstalk can be utilized to clean up both the spatial-wavefront and temporal wavefront aberrations. In what follows, we will describe separately the cleanup of these two types of aberration.

In the cleanup of spatial aberration, a spatial mode filter (e.g., a pinhole mirror) is used to select a clean part of the aberrated beam. The rest of the beam consists of several spatial-frequency components. After the separation, these two portions of the beam are brought together at a photorefractive crystal. Because of the energy transfer without phase crosstalk, the signal beam can be amplified without bearing any phase information from the aberrated part of the beam.

The experimental configuration is shown schematically in Fig. 25. An argon-ion laser beam with output power of a few hundred milliwatts at 514.5 nm is used as the coherent light source. The polarization of the laser output is rotated 90° into the plane of incidence so that the largest effective electrooptic coefficient of the SBN crystal, essentially r_{33}, can be used. The beam splitter BS is used to split the incoming beam into the pump and the signal beams, which are mutually coherent. The beams are then loosely focused onto the sample S by the focusing lenses FL_1 and FL_2, respectively. The average spot size of each beam inside the sample is approximately 3 mm in diameter. The sample used for the experiment was a crystal of single ferroelectric domain of SBN with a 5 × 6 mm cross section and a thickness of 6 mm. The external angle θ subtended by the two beams was approximately 10°.

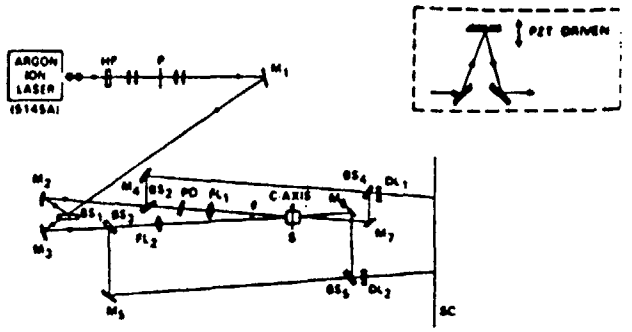

Fig. 25. Schematic diagram of the experimental setup for spatial wavefront correction. For temporal wavefront correction, the phase distorter (PD) is replaced by the set of mirrors shown in the inset. BS, beam splitter; DL, diverging lens; FL, focusing lens; HP, half-wave plate (5145 nm); M, plane mirror; P, polarizer; PD, phase distorter; S, sample; SC, screen [96].

The beam splitters BS_2 and BS_4 together with the mirrors M_4 and M_7 constitute a Mach–Zehnder interferometer whose output fringe pattern represents the spatial phase of the pump output. Similarly, the beam splitters BS_3 and BS_5 and the mirrors M_5 and M_6 constitute another interferometer for displaying the spatial phase of the signal output. The diverging lenses DL_1 and DL_2 are used to magnify the fringe pattern projected onto the screen SC.

Without the spatial phase distorter PD in the paths of the beams, the fringes of each are concentric circles, representing the spherical wavefront introduced by the converging lenses FL_1 and FL_2. Pictures of such fringes are shown in Fig. 26(a). With the phase distorter PD (a microscope slide etched with hydrofluoric acid) in the path of the pump beam (see Fig. 25), the spatial wavefront of the pump becomes strongly aberrated, as shown on the left-hand side of Fig. 26(b). The wavefront of the amplified beam, however, remains essentially undistorted [the right-hand side of Fig. 26(b)].

With the pump intensity on the order of 400 mW/cm^2 (total power of the order of 30 mW) and a signal-beam intensity on the order of 8 mW/cm^2, a signal gain (defined as the ratio of signal output power with and without the pump beam) of about 10 has been achieved with our SBN sample, for the experimental configuration described above, with no special care or optimization. For the case corresponding to the pictures shown in Fig. 26, the signal gain decreases from 10 to 7 as the phase aberrator is introduced. Our experimental results clearly demonstrate that energy transfer without phase crosstalk can be realized by two-wave mixing in photorefractive media.

The cleanup of temporal aberration can be understood in terms of nondegenerate two-wave mixing in photorefractive media. Let the frequencies of the two beams be f_1 and f_2, respectively. In the photorefractive medium, these two beams generate a traveling interference pattern. This interference pattern induces an index grating. The index grating has a frequency of $(f_2 - f_1)$. As a result of the nonlocal response of the crystal, energy transfer occurs that allows one beam to accept and the other beam to donate energy. Note that when beam 2 is diffracted from

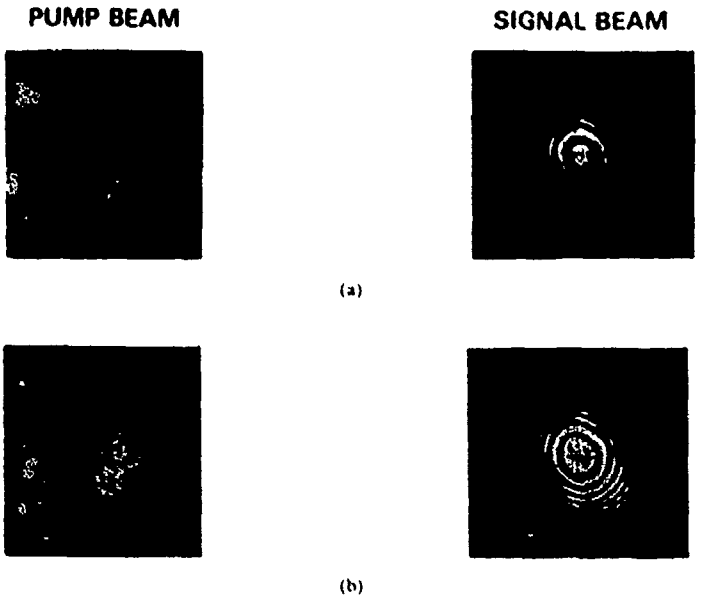

Fig. 26. Interference fringes representing the spatial phase of the pump output and the amplified signal output. (a) With no phase distorter in both arms. (b) With phase distorter in the pump beam prior to entering the photorefractive material [96].

the holographic grating, its frequency is shifted to f_1 because the index grating is traveling with a frequency of $(f_2 - f_1)$. Thus photons of frequency f_2 can be converted to photons of frequency f_1. A temporally-aberrated beam may be considered as a superposition of several frequency components. Thus, by using a frequency filter to select a single-frequency component and then to recombine it with the rest of the beam at a photorefractive crystal, it is possible to clean up the temporal aberration of light beams. In our experimental work, we use a piezoelectrically driven mirror to introduce the temporal wavefront aberration. The experimental setup is almost identical to that used in the previous experiment except that the spatial distorter PD (see Fig. 25) is now replaced by a temporal phase modulator. As the mirror moves at a constant velocity v, the frequency f of the pump beam is Doppler shifted by an amount Δf given by

$$\Delta f = 2fv/c$$

where f is the original pump frequency, v is the linear velocity of the moving mirror, and c is the velocity of light in air. This frequency shift, or, equivalently, the temporal phase modulation, is picked up by a detector at the output port of the Mach–Zehnder interferometer. The temporal phase variation of the pump outside with a frequency modulation of 2 Hz is shown in the lower trace of the oscillogram (Fig. 27). The corresponding temporal phase variation of the amplified signal, as picked up by a similar detector, is represented by the upper trace of the oscillogram. Notice that the temporal phase of the amplified signal is essentially unperturbed. The signal gain, however, drops rapidly as the pump modulation frequency is increased. Experimental results for the signal gain versus pump modulation frequency at various pump and signal power levels are given in Fig. 28.

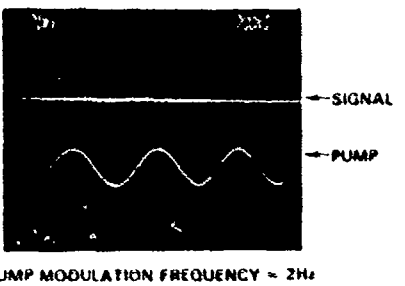

Fig. 27. Temporal phase variation of the pump output and amplified signal output [96].

The experiment described above can be viewed as a nearly degenerate two wave mixing experiment with a very small frequency offset (Δf) of a few hertz. The solid lines in Fig. 28 represent the theoretical fits based on (48) and (50) using the time constant τ as the adjustable parameter. The dependence of the material time constant on the input beam intensity ratio and the total input intensity can thus be deduced. A typical result is illustrated in Fig. 29. Note that the time constant is relatively insensitive to input beam intensity ratio.

In conclusion, we have demonstrated nonreciprocal energy transfer without phase crosstalk and have succeeded in beam cleanup by using photorefractive two wave mixing in SBN crystals. Both spatial and temporal phase aberration of laser beams can be cleaned up, provided that the phase aberration does not change significantly over a period that is the time constant of the material. The hologram recording time τ of SBN crystals is also obtained

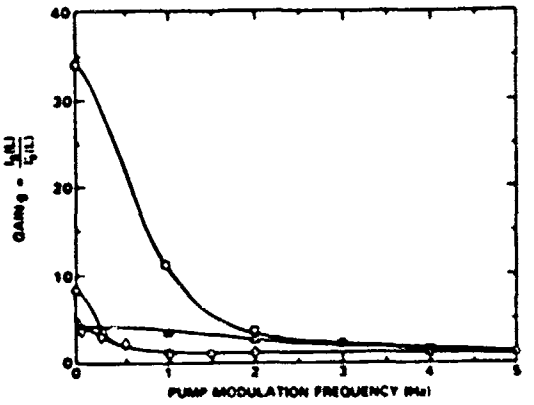

Fig. 28 Signal gain versus pump modulation frequency at various pump and signal power levels. $I_s(0)$, signal input power; $I_p(0)$, pump input power, $I_s(L)$, signal output power with pump beam on; $I_s'(L)$, signal output power with pump beam off. ○: $I_p(0) = 10$ mW, $I_s(0) = 0.26$ mW; ◇: $I_p(0) = 10$ mW, $I_s(0) = 2.5$ mW; □: $I_p(0) = 200$ mW, $I_s(0) = 0.4$ mW, △: $I_p(0) = 200$ mW, $I_s(0) = 48$ mW. The solid lines are the theoretical fits with the time constant τ as the adjustable parameter [96].

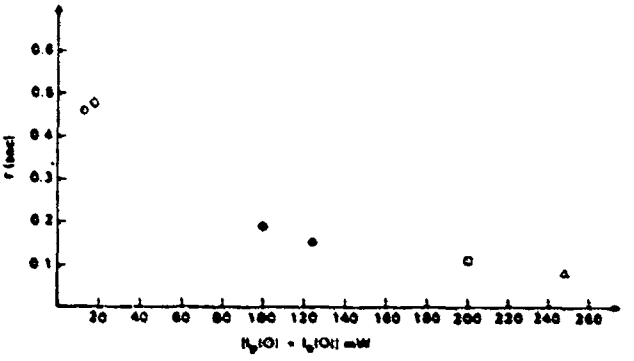

Fig. 29 Dependence of the time constant (hologram recording time) of the SBN sample on total input power and the beam power ratio. $I_s(0)$, signal input power, $I_p(0)$, pump input power, $m = I_p(0)/I_s(0)$. ○ $I_p(0) = 10$ mW, $I_s(0) = 0.26$ mW, $m = 40$. ◇: $I_p(0) = 10$ mW, $I_s(0) = 2.5$ mW, $m = 4$. ◆: $I_p(0) = 100$ mW, $I_s(0) = 0.2$ mW, $m = 500$. ●: $I_p(0) = 100$ mW, $I_s(0) = 24$ mW, $m = 4$; □: $I_p(0) = 200$ mW, $I_s(0) = 0.4$ mW, $m = 500$. △: $I_p(0) = 200$ mW, $I_s(0) = 48$ mW, $m = 4$ [96].

experimentally. Although the physical mechanism is different from the Raman coupling, the phenomenon of energy exchange without phase crosstalk is similar to the Raman beam cleanup [98]-[100].

The laser beam cleanup technique can also be used in conjunction with a phase conjugation to correct for the distortion due to crystal imperfection. Such a scheme has been used to clean up laser beams using a SBN crystal for two-wave mixing and a $BaTiO_3$ crystal as the conjugator [101].

Two-wave mixing in nonlinear media can be used for applications in optical information processing. The formation of holograms (volume index grating) can be used for the storage of three-dimensional information [12]. The nonreciprocal energy transfer can be used for the amplification of spatial images [77]. In the area of optical computing, digital logic operation using two-beam coupling in photorefractive materials has been proposed and demonstrated [102]. Such logic operations use the nonlinear phenomena of signal beam saturation and pump beam depletion in two-wave mixing. In addition, the erasure of hologram by a third beam can be used to control the efficiency of two-beam coupling. Recently, the transient response of the photorefractive effect was used for the time differentiation of coherent optical images.

VI. Conclusions and Discussions

In conclusions, we have considered the coupling of two electromagnetic waves in various nonlinear media, including photorefractive crystals, Kerr media, and cubic semiconductors. The energy transfer as well as the phase shift due to coupling were derived and discussed. The results were then used to understand the oscillation of photorefractive ring resonators as well as the physical origin of self-pumped conjugators. We also presented a coupled-mode analysis of the coupling of two polarized beams in cubic photorefractive crystals. Cross-polarization two-beam coupling was discussed in some detail. In the last part of the paper, we discussed several applications using two-beam coupling in photorefractive crystals. These include ring laser gyros, real-time holography, beam processing, and information processing.

Appendix A
Kerr Coefficients

A. Conversion Between Units and Definitions

The Kerr effect is traditionally described by a dependence of the index of refraction on the electric field by

$$n = n_0 + n_2\langle E^2\rangle \qquad \text{(A1)}$$

where n_0 is the index of refraction at $E = 0$, n_2 is the Kerr coefficient, and the brackets $\langle\ \rangle$ stand for time-average. Some workers adopted the following definition:

$$n = n_0 + n_2 I \qquad \text{(A2)}$$

where I is the intensity of electromagnetic radiation measured in units of W/m^2 in the MKS system of units. The conversion from both definitions and between MKS and ESU units is given in Table III. We note that

$$I = c\epsilon_0\langle E^2\rangle \qquad \text{(A3)}$$

and

$$\text{for } E \quad 1 \text{ ESU} = 3 \times 10^4 \text{ V/m}$$

$$\text{for } I \quad 1 \text{ ESU} = 10^{-3} \text{ W/m}^2$$

B. Relationship Between n_2 and $\chi^{(3)}$

The Kerr coefficient n_2 is also related to the third-order dielectric susceptibility $\chi^{(3)}$. Here we derive the relationship between them for isotropic media such as liquids or gases. In addition to the CGS and MKS units, there are several conventions used in the definition of $\chi^{(3)}$ [1], [2]. In this paper, we adopt the following definition of $\chi^{(3)}$:

$$P = \epsilon_0\chi^{(1)}E + \chi^{(3)}E^3 \qquad \text{(A4)}$$

TABLE III
CONVERSION TABLE FOR KERR COEFFICIENTS

$n = n_0 + n_2 \langle E^2 \rangle$		$n = n_0 + n_2 I$	
ESU	MKS $(v/V)^2$	ESU	MKS (m^2/W)
1	$1/9 \times 10^{-8}$	4.2×10^{-10}	4.2×10^{-7}
10^{-11}	$1/9 \times 10^{-19}$	4.2×10^{-21}	4.2×10^{-18} (for CS_2)

where P is the polarization and E is the electric field. Using the complex number representation [1] for sinusoidal varying field such as the one given in (6), the complex amplitude of the polarization at frequency ω is

$$P(\omega) = \epsilon_0 \chi^{(1)} E + 3/4\, \chi^{(3)} E^* E E. \quad \text{(A5)}$$

If we rewrite (A5) as

$$P(\omega) = [\epsilon_0 \chi^{(1)} + 3/4\, \chi^{(3)} E^* E] E \quad \text{(A6)}$$

then the index of refraction can be written

$$\epsilon_0 (n^2 - 1) = \epsilon_0 \chi^{(1)} + 3/4\, \chi^{(3)} E^* E] E. \quad \text{(A7)}$$

We now compare (A7) with

$$\Delta n = n_2 \langle E^2 \rangle = 1/2\, n_2 E^* E \quad \text{(A8)}$$

and we obtain

$$n_2 = \frac{3}{4 \epsilon_0 n} \chi^{(3)}. \quad \text{(A9)}$$

APPENDIX B

The solution of the nonlinear coupled differential equations (118) and (119) is derived in this appendix.

By adding the two equations in (118) and carrying out the integration, we obtain

$$I_1 + I_2 = C \exp(-\alpha z) \quad \text{(B1)}$$

where C is a constant equal to $I_1(o) + I_2(o)$. Using (B1) and (118), we can eliminate I_2 and obtain

$$\frac{d}{dz} I_1 + (\alpha + gCe^{-\alpha z}) I_1 = g I_1^2 \quad \text{(B2)}$$

which is a Bernoulli equation and can be integrated directly. The solution is

$$I_1(z)^{-1} = e^{|P(z)|} \left\{ -g \int e^{-|P(z)|} + C' \right\} \quad \text{(B3)}$$

where C' is a constant of integration and $P(z)$ is given by

$$P(z) = \alpha + gCe^{-\alpha z} \quad \text{(B4)}$$

To simplify (B3), we need to use the following integral formula

$$\int e^{-ae^{-bx} - cx} dx = \frac{1}{ab} e^{be^{-bx} - cx} \quad \text{(B5)}$$

Using (B4) and (B5), (B3) can be written

$$I_1(z) = \frac{Ce^{-\alpha z}}{1 + CC' \exp\left[-\frac{1}{\alpha} gC \exp(-\alpha z)\right]} \quad \text{(B6)}$$

Putting $z = o$ in (B6) and solving for C', we obtain

$$C' = \frac{1}{C} \frac{I_2(0)}{I_1(0)} \exp\left[\frac{1}{\alpha} gC\right] \quad \text{(B7)}$$

where we recall that $C = I_1(0) + I_2(0)$. Using the definitions for m and γ from (124) and (125), respectively, and (B7), $I_1(z)$ can be rewritten in the form of (122). The solution for $I_2(z)$ can be obtained from (122) and (B1). This completes the solution for $I_1(z)$ and $I_2(z)$.

Solutions for the phases ψ_1 and ψ_2 can be obtained by substituting (122) and (123) for $I_1(z)$ and $I_2(z)$, respectively, into (119) and carrying out the integration. The process requires the following integral formula:

$$\int \frac{e^{-\alpha x}}{1 + B \exp\left[\frac{1}{\alpha} A \exp(-\alpha x)\right]} dx = \frac{1}{A} \log\left\{1 + \frac{1}{B} \exp\left[-\frac{1}{\alpha} A \exp(-\alpha x)\right]\right\}. \quad \text{(B8)}$$

Using the expressions for $I_1(z)$ and $I_2(z)$ and the above formula, we arrive at (126) and (127). This completes the derivation of $I_1(z)$ and $I_2(z)$.

ACKNOWLEDGMENT

The author wishes to acknowledge helpful discussions and collaborations with his colleagues M. Khoshnevisan, M. D. Ewbank, A. E. T. Chiou, I. McMichael, and T. Chang. The author also acknowledges the referees for their careful and critical review of the manuscript and their comments.

REFERENCES

[1] See, for example, A. Yariv and P. Yeh, *Optical Waves in Crystals*. New York: Wiley, 1984.
[2] E. N. Leith and J. Upatnieks, "Wavefront reconstruction with different illumination and three-dimensional objects," *J. Opt. Soc. Amer.*, vol. 54, p. 1295, 1964.
[3] See, for example, Y. R. Shen, *Principles of Nonlinear Optics*. New York: Wiley, 1985.
[4] See, for example, *Laser Handbook*, vol. 4, M. L. Stitch and M. Bass, Eds. New York: Elsevier, 1985, pp. 333–485.
[5] See, for example, D. Pepper, "Applications of optical phase conjugation," *Sci. Amer.*, vol. 254, p. 74, 1986.
[6] A. Yariv, "Phase conjugate optics and real-time holography," *IEEE J. Quantum Electron.*, vol. QE-14, pp. 650–660, 1978.
[7] A. Ashkin, G. D. Boyd, J. M. Dziedzic, R. G. Smith, A. A. Ballman, J. J. Levinstein, and K. Nassau, "Optically induced refractive index inhomogeneities in $LiNbO_3$ and $LiTaO_3$," *Appl. Phys. Lett.*, vol. 9, pp. 72–74, 1966.
[8] V. L. Vinetskii, N. V. Kukhtarev, S. G. Odulov, and M. S. Soskin, "Dynamic self-diffraction of coherent light beams," *Sov. Phys.—Usp.*, vol. 22, pp. 742–756, 1979.
[9] N. V. Kukhtarev, V. B. Markov, S. G. Odulov, M. S. Soskin, and V. L. Vinetskii, "Holographic storage in electrooptic crystals: Beam coupling and light amplification," *Ferroelectrics*, vol. 22, pp. 961–964, 1979.
[10] J. Feinberg, D. Heiman, A. R. Tanguay, Jr., and R. Hellwarth, "Photorefractive effects and light-induced charge migration in barium titanate," *J. Appl. Phys.*, vol. 51, p. 1297, 1980.—*J. Appl. Phys.*, vol. 52, p. 537, 1981. S. Ducharme and J. Feinberg, "Speed of the photorefractive effect in a $Bi_{12}TiO_{20}$ crystal," *J. Appl. Phys.*, vol. 56, p. 839, 1984.
[11] R. A. Mullen and R. W. Hellwarth, "Optical measurements of the photorefractive parameters of BSO," *J. Appl. Phys.*, vol. 58, 1985.

[12] D. L. Staebler and J. J. Amodei, "Coupled wave analysis of holographic storage in $LiNbO_3$," *J. Appl Phys.*, vol 43, p 1042, 1972
[13] V. Markov, S. Odulov, and M. Soskin, "Dynamic holography and optical image processing," *Opt. Laser Technol.*, vol 11, p 95, 1979.
[14] A. Marrakchi, J. P. Huignard, and P. Gunter, "Diffraction efficiency and energy transfer in two-wave mixing experiments with $Bi_{12}SiO_{20}$ crystals," *Appl. Phys.*, vol. 24, p. 131, 1981
[15] J. Feinberg and R. W. Hellwarth, "Phase conjugating mirror with continuous wave gain," *Opt. Lett.*, vol. 5, pp. 519-521, 1980
[16] D. W. Vahey, "A nonlinear coupled-wave theory of holographic storage in ferroelectric materials," *J. Appl. Phys.*, vol 46, p 3510, 1975
[17] J. Feinberg, "Asymmetric self-defocusing of an optical beam from the photorefractive effect," *J. Opt. Soc. Amer.*, vol 72, p 46, 1982
[18] P. Yeh, "Contradirectional two-wave mixing in photorefractive media," *Opt. Commun.*, vol. 45, pp. 323-326, 1983.
[19] Y. H. Ja, "Energy transfer between two beams in writing a reflection volume hologram in a dynamic medium," *Opt. Quantum. Electron.*, vol 14, p. 547, 1982
[20] J. P. Huignard and A. Marrakchi, "Coherent signal beam amplification in two-wave mixing experiments with photorefractive BSO crystals," *Opt. Commun.*, vol. 38, p. 249, 1981.
[21] L. K. Lam, T. Y. Chang, J. Feinberg, and Hellwarth, "Photorefractive-index gratings formed by nanosecond optical pulses in $BaTiO_3$," *Opt. Lett.*, vol. 10, p. 475, 1981.
[22] P. Yeh, "Fundamental limit of the speed of photorefractive effect and its impact on device applications and material research," *Appl. Opt.*, vol. 26, p. 602, 1987, *Appl. Opt.*, vol. 26, p. 3190, 1987.
[23] E. Voit, M. Z. Zha, P. Amrhein, and P. Gunter, "Reduced $KNbO_3$ crystals for fast photorefractive nonlinear optics," in *Tech. Dig. Top. Meet. Photorefractive Materials, Effects, Devices*, Los Angeles, CA, Aug. 12-14, 1987 vol. 17, paper WA1-2, p. 2
[24] A. M. Glass, M. B. Klein, and G. C. Valley, "Fundamental limit of the speed of photorefractive effect and impact on device applications and materials research: Comment," *Appl. Opt.*, vol. 26, p. 3189, 1987
[25] M. B. Klein, "Beam coupling in undoped GaAs at 1.06 μm using the photorefractive effect," *Opt. Lett.*, vol. 9, p. 350, 1984
[26] G. Albanese, J. Kumar, and W. H. Steier, "Investigation of the photorefractive behavior of chrome-doped GaAs using two-beam coupling," *Opt. Lett.*, vol. 10, p. 650, 1986. ——, *Opt. Lett.*, vol. 12, p. 120, 1986
[27] D. Rak, I. Ledoux, and J. P. Huignard, "Two-wave mixing and energy transfer in $BaTiO_3$, application to laser beam steering," *Opt. Commun.*, vol. 49, p. 302, 1984
[28] Ph. Refregier, L. Solymar, H. Rajbenbach, and J. P. Huignard, "Two-beam coupling in photorefractive $Bi_{12}SiO_{20}$ crystals with moving gratings: Theory and experiments," *J. Appl. Phys.*, vol. 58, p. 45, 1985
[29] M. D. Ewbank, private communication
[30] P. Yeh, "Photorefractive two-beam coupling in cubic crystals," *J. Opt. Soc. Amer. B*, vol. 4, p. 1382, 1987
[31] T. Y. Chang, A. E. T. Chiou, and P. Yeh, "Photorefractive two beam coupling with polarization flip in gallium arsenide," in *Tech. Dig. Top. Meet. Photorefractive Materials, Effects, Devices*, vol 17, Washington, DC: Opt. Soc. Amer., 1987, pp. 55-58
[32] P. Yeh and L. J. Cheng, "Cross polarization two beam coupling in photorefractive GaAs crystals," in *Tech. Dig. Top. Meet. Photorefractive Materials Effects, Devices*, vol 17, Washington, DC: Opt. Soc. Amer., 1987, pp. 59-61
[33] L. J. Cheng and P. Yeh, "Cross polarization two beam coupling in photorefractive GaAs crystals," *Opt. Lett.*, vol. 13, p. 50, 1988
[34] B. Fischer, J. O. White, M. Cronin-Golomb, and A. Yariv, "Nonlinear vectorial two beam coupling and linear four wave mixing in photorefractive materials," *Opt. Lett.*, vol. 11, p. 239, 1986
[35] M. Cronin-Golomb, J. O. White, B. Fischer, and A. Yariv, "Exact solution of a nonlinear model of four wave mixing and phase conjugation," *Opt. Lett.*, vol. 7, pp. 313-315, 1982
[36] J. M. Machado and P. Yeh, "Phase shifts of photorefractive gratings and phase conjugate waves," *Opt. Lett.*, vol. 12, p. 48, 1987
[37] P. Yeh, "Contradirectional two wave mixing in photorefractive media," *Opt. Commun.*, vol. 45, pp. 323-326, 1983
[38] L. J. Cheng and G. Liaw, "Photorefractive GaAs as an optical processing medium," presented at CLEO 88, Anaheim, CA, Apr. 25-29, 1988, paper THQ1
[39] B. Imbert, H. Rajbenbach, S. Mallick, J. P. Herriau, and J. P. Huignard, "High photorefractive gain in two-beam coupling with moving fringes in GaAs:Cr crystals," *Opt. Lett.*, vol. 13, pp. 327-329, 1988
[40] P. Yeh, "Exact solution of a nonlinear model of two-wave mixing in Kerr media," *J. Opt. Soc. Amer. B*, vol. 3, pp. 747-757, 1986
[41] Y. Anan'ev, "Possibility of dynamic correction of wave fronts," *Sov. J. Quantum Electron.*, vol. 4, pp. 929-931, 1975
[42] D. I. Stasel'ko and V. G. Sidorovich, "Efficiency of light-beam conversion by dynamic three-dimensional phase holograms," *Sov. Phys.—Tech. Phys.*, vol. 19, pp. 361-365, 1974
[43] V. G. Sidorovich and D. I. Stasel'ko, "Transformation of light beams by dynamic corrections using three-dimensional displacement phase holograms," *Sov. Phys.—Tech. Phys.*, vol. 19, pp. 1593-1597, 1975
[44] D. I. Stasel'ko and V. G. Sidorovich, "Efficiency of light-beam transformation by dynamic phase holograms. I," *Sov. Phys—Tech. Phys.*, vol. 21, pp. 205-208, 1976
[45] V. Vinetskii, N. Kukhtarev, S. Odulov, and M. Soskin, "Dynamic conversion of light beams by phase-shifted free-carrier holograms," *Sov. Phys.—Tech. Phys.*, vol. 22, pp. 729-732, 1977
[46] V. L. Vinetskii, N. V. Kukhtarev, and M. S. Soskin, "Transformation of intensities and phases of light beams by a transient 'unshifted' holographic grating," *Sov. J. Quantum Electron.*, vol. 7, pp. 230-233, 1977.
[47] V. L. Vinetskii, N. V. Kukhtarev, S. G. Odulov, and M. S. Soskin, "Dynamic self-diffraction of coherent light beams," *Sov. Phys.—Usp.*, vol. 22, pp. 742-756, 1969
[48] V. L. Vinetskii, N. V. Kukhtarev, and T. I. Semenets, "Kinetics of dynamic self-diffraction of light beams in bulk media with local response," *Sov. J. Quantum Electron.*, vol. 11, pp. 130-132, 1981
[49] N. V. Kukhtarev, P. D. Pavlik, and T. I. Semenets, "Optical hysteresis in wavefront reversal by traveling holographic gratings," *Sov. J. Quantum Electron.*, vol. 14, pp. 282-284, 1984
[50] P. A. Apanasevich and A. A. Afanas'ev, "Stimulated scattering of light from free carriers created in a semiconductor by absorption of light," *Sov. Phys.—Solid State*, vol. 20, no. 1, pp. 53-56, 1978
[51] See, for example, W. Kaiser and M. Maier, "Stimulated Rayleigh, Brillouin and Raman spectroscopy," in *Laser Handbook*, F. T. Arecchi and E. O. Schulz-Dubois, Eds. Amsterdam, The Netherlands: North-Holland, 1972, ch. E2
[52] D. Poul and W. Kaiser, "Time-resolved investigation of SBS in transparent and absorbing media: Determination of phonon lifetimes," *Phys. Rev. B*, vol. 1, pp. 31-43, 1970
[53] J. Feinberg, "Self-pumped continuous-wave phase conjugator using internal reflection," *Opt. Lett.*, vol. 7, pp. 486-490, 1982. ——, "Continuous-wave self-pumped phase conjugator with a wide field of view," *Opt. Lett.*, vol. 8, pp. 480, 1983
[54] J. O. White, M. Cronin-Golomb, B. Fischer, and A. Yariv, "Coherent oscillation by self-induced gratings in photorefractive crystals," *Appl. Phys. Lett.*, vol. 40, pp. 450-452, 1982
[55] T. Y. Chang and R. W. Hellwarth, "Optical phase conjugation by backscattering in the photorefractive crystal barium titanate," *Opt. Lett.*, vol. 10, pp. 408-410, 1985
[56] J. P. Lam, "Origins of phase conjugate waves in self-pumped photorefractive mirrors," *Appl. Phys. Lett.*, vol. 46, pp. 909-911, 1985
[57] K. R. MacDonald and J. Feinberg, "Theory of a self-pumped phase conjugator with two coupled interaction regions," *J. Opt. Soc. Amer.*, vol. 73, pp. 548-553, 1983
[58] K. R. MacDonald and J. Feinberg, "Enhanced four-wave mixing by use of frequency-shifted optical waves in photorefractive $BaTiO_3$," *Phys. Rev. Lett.*, vol. 53, pp. 821-822, 1984
[59] D. J. Gauthier, P. Narum, and R. W. Boyd, "Observation of deterministic chaos in a phase conjugate mirror," *Phys. Rev. Lett.*, vol. 58, pp. 1640-1643, 1987
[60] M. C. Gower, "Photoinduced voltages and frequency shifts in a self-pumped phase conjugating $BaTiO_3$ crystal," *Opt. Lett.*, vol. 11, pp. 458-460, 1986
[61] See, for example, T. Y. Chang, "Fast self-induced refractive index changes in optical media: A survey," *Opt. Eng.*, vol. 20, pp. 220-232, 1981
[62] M. Khoshnevisan and P. Yeh, "Relationship between nonlinear electrooptic and Kerr effects and acousto-optics," *Proc. SPIE*, vol. 739, pp. 82-86, 1987
[63] A. Rosen, R. Adler, and B. Alpiner, "Direct observation of optically induced generation and amplification of sound," *Appl. Phys. Lett.*, vol. 5, pp. 86-87, 1964

[64] P. Yeh and M. Khoshnevisan, "Nonlinear optical Bragg scattering in Kerr media," *J. Opt. Soc. Amer. B*, vol. 4, pp. 1954-1960, 1988.
[65] P. Yeh, "Photorefractive coupling in ring resonators," *Appl. Opt.*, vol. 23, pp. 2974-2978, 1984.
[66] P. Yeh and M. Khoshnevisan, "Phase conjugate ring gyros and photorefractive-biased ring gyros," *SPIE*, vol. 487, pp. 102-109, 1984.
[67] B. Ya. Zel'dovich and V. V. Shkunov, "Wavefront reproduction in stimulated Raman scattering," *Sov. J. Quantum Electron.*, vol. 7, pp. 610-615, 1977.
[68] G. Grynberg, E. LeBihan, and M. Pinard, "Two-wave mixing in sodium vapour," *J. Physique*, vol. 47, pp. 1321-1325, 1986.
[69] D. Grandclement, G. Grynberg, and M. Pinard, "Observation of cw self-oscillation due to pressure-induced two-wave mixing in sodium," *Phys. Rev. Lett.*, vol. 59, pp. 40-43, 1987.
[70] P. Yeh, "Theory of unidirectional photorefractive resonators," *J. Opt. Soc. Amer. B*, vol. 2, pp. 1924-1928, 1985.
[71] M. D. Ewbank and P. Yeh, "Frequency shifted cavity length in photorefractive resonators," *Opt. Lett.*, vol. 10, pp. 496-498, 1985.
[72] M. Kramer, W. Tompkin, and R. Boyd, "Nonlinear-optical interactions in fluorescein-doped boric acid glass," *Phys. Rev. A*, vol. 34, pp. 2026-2031, 1986.
[73] I. McMichael and P. Yeh, "Nondegenerate two-wave mixing in ruby," in *Dig. Int. Conf. Quantum Electron.* Washington, DC: Opt. Soc. Amer., 1987, paper MDD3, pp. 10-13.
[74] See, for example, I. C. Khoo and T. H. Liu, "Probe beam amplification via two- and four-wave mixing in a nematic liquid crystal film," *IEEE J. Quantum Electron.*, vol. QE-23, pp. 171-173, 1987, and references therein.
[75] P. Yeh, "Photorefractive coupling in ring resonators," *Appl. Opt.*, vol. 23, pp. 2974-2978, 1984.
[76] ——, Electromagnetic propagation in photorefractive layered media," *J. Opt. Soc. Amer.*, vol. 73, pp. 1268-1275, 1983.
[77] J. P. Huignard and A. Marrackchi, "Two-wave mixing and energy transfer in $Bi_{12}SiO_{20}$ crystals: Application to image amplification and vibration analysis," *Opt. Lett.*, vol. 6, pp. 622-624, 1981.
[78] V. Markov, S. Odulov, and M. Soskin, "Real-time contrast reversal using two-wave mixing in $LiNbO_3$," *Opt. Laser Tech.*, vol. 11, pp. 95-99, 1979.
[79] P. Yeh and A. E. T. Chiou, "Real-time contrast reversal via four-wave mixing in nonlinear media," *Opt. Commun.*, vol. 64, pp. 160-166, 1987.
[80] J. Feinberg and G. D. Bacher, "Self-scanning of a continuous-wave dye laser having a phase-conjugate resonator cavity," *Opt. Lett.*, vol. 9, pp. 420-422, 1984.
[81] G. Valley and G. Dunning, "Observation of optical chaos in a phase conjugate resonator," *Opt. Lett.*, vol. 9, pp. 513-515, 1984.
[82] P. Gunter, "Holography, coherent light amplification and optical phase conjugation with photorefractive materials," *Phys. Rep.*, vol. 93, pp. 201-299, 1982.
[83] As the orientation of the two-wave mixing fringe pattern with respect to the crystal axes changes, the effective electrooptic coefficient (and coupling efficiency of the index grating) is modified. γL is independently measured by removing ring-cavity mirror M_2 and using an attenuated probe beam from BS_1 with an external angle of 20° between probe and pump beams.
[84] Provided by R. Neurgaonkar, Rockwell International, Thousand Oaks, CA.
[85] B. Fischer, M. Cronin-Goulomb, J. O. White, A. Yariv, and R. Neurgaonkar, *Appl. Phys. Lett.*, vol. 40, p. 863, 1982.
[86] P. Yeh, M. D. Ewbank, M. Khoshnevisan, and J. M. Tracy, "Doppler-free phase-conjugate reflection," *Opt. Lett.*, vol. 9, pp. 41-43, 1984.
[87] R. A. McFarlane and D. G. Steel, "Laser oscillator using resonator with self-pumped phase-conjugate mirror," *Opt. Lett.*, vol. 8, pp. 208-210, 1983.
[88] W. B. Whitten and J. M. Ramsey, "Self-scanning of a dye laser due to feedback from a $BaTiO_3$ phase-conjugate reflector," *Opt. Lett.*, vol. 9, pp. 44-46, 1984.
[89] K. R. MacDonald and J. Feinberg, "Anomalous frequency and phase shifts in self-pumped phase conjugators," *J. Opt. Soc. Amer. A*, vol. 1, p. 1213, 1984.
[90] M. D. Ewbank and P. Yeh, "Frequency shifts of self-pumped phase conjugators," *Proc. SPIE*, vol. 613, pp. 59-69, 1986.
[91] See, for example, Z. Knittl, *Optics of Thin Films*. New York: Wiley, 1976, p. 240.
[92] P. Yeh, "Electromagnetic propagation in a photorefractive layered media," *J. Opt. Soc. Amer.*, vol. 73, pp. 1268-1271, 1983.
[93] M. Z. Zha and P. Gunter, "Nonreciprocal optical transmission through photorefractive $KNbO_3$:Mn," *Opt. Lett.*, vol. 10, pp. 184-186, 1985.
[94] K. R. MacDonald, J. Feinberg, M. Z. Zha, and P. Gunter, "Asymmetric transmission through a photorefractive crystal of $BaTiO_3$," *Opt. Commun.*, vol. 50, pp. 146-150, 1984.
[95] See, for example, A. Yariv, *Quantum Electronics*. New York: Wiley, 1975, p. 187, eqs. (9.3)-(15).
[96] A. E. T. Chiou and P. Yeh, "Beam cleanup using photorefractive two-wave mixing," *Opt. Lett.*, vol. 10, pp. 621-623, 1985.
[97] P. Yeh, "Spectral compression using holographic two-wave mixing," in *Dig. Conf. Lasers, Electro-Optics*. Washington, DC: Opt. Soc. Amer., 1985, p. 274.
[98] V. I. Bespalov, A. A. Betin, and G. A. Pasmanik, "Reproduction of the pump wa[illegible] in stimulated scattering radiation," *Izv. Vyssh. Uchreb. Zaved. Radiofiz.*, vol. 21, p. 961, 1978.
[99] J. Goldhar and J. R. Murray, "Intensity averaging and four-wave mixing in Raman amplifiers," *IEEE J. Quantum Electron.*, vol. QE-18, p. 399, 1982.
[100] R. S. F. Chang and N. Djeu, "Amplification of a diffraction-limited Stokes beam by a severely distorted pump," *Opt. Lett.*, vol. 8, pp. 139-141, 1983.
[101] A. E. T. Chiou and P. Yeh, "Laser beam cleanup using photorefractive two-wave mixing and optical phase conjugation," *Opt. Lett.*, vol. 11, pp. 461-463, 1986.
[102] Y. Fainman, C. C. Guest, and S. H. Lee, "Optical digital logic operations by two-beam coupling in photorefractive material," *Appl. Opt.*, vol. 25, pp. 1598-1603, 1986.

Pochi Yeh (M'78-SM'87), photograph and biography not available at the time of publication.

Photorefractive Optics at Near-Infrared Wavelengths

Reprinted from SPIE Vol 1060—Nonlinear Optical Beam Manipulation and High Energy Beam Propagation Through the Atmosphere

Photorefractive optics at near-infrared wavelengths

P. H. Beckwith, W. R. Christian, I. C. McMichael and P. A. Yeh
Rockwell International Science Center
Thousand Oaks, California 91360

ABSTRACT

Measurements of two-wave mixing gain and phase-conjugate response in barium titanate using GaAlAs diode laser sources emitting at 830 nm are discussed. Gain coefficients as large as 18 cm^{-1} have been obtained with optimized mixing geometries. With an optically isolated barium titanate ring passive phase-conjugate mirror we have obtained phase-conjugate reflectivities as large as 56% (uncorrected for Fresnel reflection losses) and response times on the order of tens of seconds. These results represent significant improvements over corresponding values previously reported in the literature.

1. INTRODUCTION

To date, nonlinear optical effects such as two-wave mixing (TWM) and phase conjugation in photorefractive materials like barium titanate ($BaTiO_3$) and strontium barium niobate ($Sr_xBa_{1-x}Nb_2O_6$:Ce) have been examined primarily at visible wavelengths near 515 nm. Recent interest in near-infrared wavelengths has been brought about by the availability of low-cost, highly efficient, compact semiconductor diode lasers that operate at these wavelengths. While some two-wave mixing and phase conjugation experiments have been performed using diode lasers,[1-4] a careful investigation of the nonlinear properties of photorefractive materials at these wavelengths has not been reported previously. In this paper we describe measurements of TWM gain and response time using $BaTiO_3$ at 830 nm, as well as measurements of phase-conjugate response time and reflectivity for $BaTiO_3$ in a ring conjugator configuration at this wavelength.

2. TWO-WAVE MIXING

Two-wave mixing in photorefractive materials is dependent upon many different factors. When performing a two-wave mixing experiment, the two most critical parameters are typically the two-wave mixing gain coefficient, Γ and the time response of the photorefractive process in the material. The two-wave mixing gain coefficient, Γ of a photorefractive crystal such as $BaTiO_3$ can be written as[5]

$$\Gamma = \frac{A \sin\theta}{1 + \frac{\sin^2\theta}{B^2}} \left[\frac{\cos 2\theta_i}{\cos\theta_i} \right] \qquad (1)$$

where 2θ is the external crossing angle between the two beams, $2\theta_i$ is the internal crossing angle, and the parameters A and B relate to the photorefractive properties of the material as follows:

$$A = \frac{8\pi^3 n^3 k_B T}{\varepsilon \lambda^2} \qquad (2)$$

$$B = \frac{\varepsilon \lambda}{4\pi} \sqrt{\frac{N_{eff}}{\varepsilon \varepsilon_0 k_B T}} \qquad (3)$$

where r_{eff} is the effective electro-optic coefficient, k is the magnitude of the grating wavevector, $\zeta(k)$ accounts for electron-hole competition, n is the refractive index, $k_B T/e$ is the thermal energy per charge, and λ is the free space wavelength. N_{eff} is the effective density of photorefractive charge, and $\varepsilon\varepsilon_o$ is the dc dielectric constant along the direction of the grating wavevector. The steady-state two-beam coupling gain G, is defined as

$$G = \frac{I_s}{I_p} \tag{4}$$

where I_s is the transmitted probe beam through the crystal with the pump beam on, and I_p is the transmitted probe beam with the pump off. For large pump/probe ratios, the gain can be related to Γ by

$$G = \exp(\Gamma L) \tag{5}$$

where L is the interaction length in the crystal for the pump and probe beams.

The time response of the photorefractive process in a material is given by[6,7]

$$\tau = \tau_{di} \frac{\left(1 + \frac{1}{\delta}\frac{E_D}{E_q}\right)}{\left(1 + \frac{E_D}{E_q}\right)} \tag{6}$$

where the dielectric relaxation time is

$$\tau_{di} = \frac{\varepsilon\varepsilon_o \gamma_R R}{e\mu s I_o (1 - R)} \tag{7}$$

and the factors E_D, E_q, and δ are defined as

$$E_D = \frac{k_B T k}{e} \tag{8}$$

$$E_q = \frac{eN_A}{\varepsilon\varepsilon_o k}(1 - R) \tag{9}$$

$$\delta = \frac{\gamma_R \varepsilon \varepsilon_o}{e\mu (1 - R)} \tag{10}$$

The recombination rate is γ_R, $R = N_A/N_D$ where N_A (N_D) is the number density of photorefractive acceptors (donors), μ is the mobility, s is the photoionization cross section, and I_o is the light intensity.

Equations 1-10 illustrate the many factors that must be considered when attempting to maximize both the gain and the speed of the photorefractive process in a given material. Figure 1 shows the experimental setup we used for optimizing TWM in $BaTiO_3$. The single mode diode laser was operated at 828.8 nm and was temperature stabilized to better than 0.1°C. The output of the laser was then collimated by Lens L_1 (focal length f=8 mm), with the horizontal polarization component

passing through polarizing beamsplitter PBS. Beam asymmetry was corrected with an anamorphic prism pair. This beam was split by the 50% beamsplitter BS into a pump and a probe beam. Neutral density (ND) filters attenuated the probe beam allowing for a variable pump/probe ratio. Shutters SH were used for blocking either beam, while lenses L_2 and L_3 (f=40 cm, located ~30 cm from the sample) lightly focussed the beams into a $BaTiO_3$ crystal (5 mm per side cube) immersed in a temperature controlled oil bath (index-matched to the glass cuvette). Spot size in the crystal was 1.5 mm. The transmitted probe beam was monitored by detector D. The probe and pump beams had incident angles of α and β with respect to the face normal of the glass cuvette, with pathlengths matched to within a few centimeters. The crystal was also tilted with respect to the cuvette window by an angle γ. After taking into account Fresnel reflections and scattering losses, a linear absorption coefficient of 0.08 cm^{-1} was measured for the crystal at 830 nm. Between successive two-wave mixing measurements, all gratings in the crystal were erased by a uniform intensity beam from either an argon ion laser (514.5 nm) or a HeNe laser (632.8 nm).

Table 1 lists measured TWM gain, G (see Eq. 4) for various intensities and geometries (for negative α, the pump and probe beams were incident from opposite sides of the cuvette face normal; see Fig. 1). A geometry consisting of angles α=25°, β=50°, and γ=30° (cases F and G in Table 1) proved best as it allowed access to the large r_{42} electro-optic coefficient in $BaTiO_3$ while still maintaining good overlap of the pump and probe beams in the crystal. For this orientation the grating wavevector/c-axis angle was calculated to be 31°. Figure 2 plots the measured TWM gain coefficient versus crystal temperature for this configuration. In this case, a pump beam intensity of 680 mW/cm^2 was used. A large pump/probe ratio (>10^5) was also used to ensure minimal pump depletion (unsaturated gain). At room temperature, the net intensity gain was 5200, which for a 5 mm interaction length corresponds to a gain coefficient of 17 cm^{-1}. The gain increased to 8000 (18 cm^{-1}) when the crystal was cooled to 11 °C, which is on the edge of a tetragonal-to-orthorhombic phase transition (reported to be in the range from 5-10°C[5,8] for $BaTiO_3$). Note that these gain coefficients are comparable to those measured in the visible,[9] suggesting that N_A is not significantly reduced in the infrared. While the known temperature dependencies of r_{eff} and ϵ in Eqs. 1-3 predict a strong enhancement of the photorefractive gain upon cooling, the observed improvement was actually quite small. Further study is needed to explain this discrepancy.

Figure 3 plots the measured TWM time response (time required for the TWM gain to reach $(1-e^{-1})^2$ of its maximum value when the pump beam is unblocked) versus crystal temperature. As shown, the temperature dependence of the time response was relatively slight, increasing from ~50 seconds at room temperature to ~100 seconds at 11°C. The most notable feature of these results is that they are two to three orders of magnitude larger than response times previously measured at visible argon-ion wavelengths.[10,11] This increase is believed to be attributable to a reduction of the photoionization cross-section at longer wavelengths.

3. SELF-PUMPED PHASE CONJUGATION

The advent of efficient and compact semiconductor diode lasers has increased interest in using phase conjugation in photorefractive materials to provide distortion correction for these devices.[12-14] In the first reports of photorefractive response at 830 nm with light from a GaAlAs diode laser, a ring passive phase-conjugate mirror was formed using $BaTiO_3$ as the real-time holographic medium.[1,2] A phase-conjugate reflectivity of 16% was obtained with an incident power of 3.6 mW (126 mW/cm^2, uncorrected for Fresnel reflections). The time needed to reach 90% of its steady state value was 40 sec (time-response intensity product ~5 $W\text{-}sec/cm^2$). This reflectivity was also obtained when the GaAlAs laser was replaced by an argon-ion laser emitting 35 mW (1.4 W/cm^2) at 1090 nm, although the time response intensity product at this longer wavelength increased to 500 $W\text{-}sec/cm^2$.[2] In another study, a phase-conjugate reflectivity of 30% was obtained using a 3 mW (150 mW/cm^2) beam.[3] About 120 seconds were needed to establish a

phase-conjugate beam. When the crystal was rotated ± 90°, comparable phase-conjugate reflectivities were obtained with longer start-up times. Similar reflectivities were obtained using a 35 mW (1 W/cm^2) Nd:YAG laser operating at 1.06 nm. Start-up times, however, were on the order of 10 minutes.[3]

In our experiments, we have obtained phase-conjugate reflectivities as large as 56% (not corrected for Fresnel reflections) with response times on the order of tens of seconds. This represents a significant improvement over previously reported work.

Figure 4 is a schematic diagram of the experimental setup we used for self-pumped phase conjugation at 830 nm. A temperature-stabilized single-mode diode laser operating at 828.8 nm was collimated by lens L_1 (focal length f=8 mm). The horizontal polarization component of this beam was then transmitted through a polarizing beamsplitter PBS. Asymmetry in the beam was corrected by a prism pair before it was focussed by lens L_2 through a Faraday isolator FR (35 dB isolation). The transmitted beam was then collimated by lens L_3 to a spot size of approximately 2 mm. The polarization of the beam (at 45° with respect to the plane of the paper due to the Faraday rotator) was rotated back to horizontal by a half-wave ($\lambda/2$) plate. This beam was then incident on a passive ring conjugator (a $BaTiO_3$ crystal immersed in a temperature controlled oil bath and two external mirrors M_3 and M_4, with angles θ_1 and θ_2 both roughly 30°). A pellicle beamsplitter placed in front of the crystal was used to sample the incident beam and the phase-conjugate reflection (using detectors D1 and D2, respectively) to determine phase-conjugate reflectivity.

Figure 5 illustrates the measured temporal response of the self-pumped phase conjugator for incident power levels of 2.6, 5.5, and 13 mW. Between measurements all gratings in the crystal were erased with an argon-ion laser beam. The turn-on time of the conjugator decreased from 16 seconds at 2.6 mW (80 mW/cm^2) to 8 seconds at 13 mW (410 mW/cm^2) incident power. Once the device turned on, the phase-conjugate signal increased to saturation in about 10 seconds. In all cases, the saturation value corresponded to a phase-conjugate reflectivity of 56%, not including correction for Fresnel losses at the air-cuvette-oil-crystal interfaces. At all power levels, the phase-conjugate reflectivity was relatively independent of crystal temperature, which was varied from room temperature to 10°C during the experiment. In previous studies examining two-interaction region conjugator reflectivities, the reflectivity was found to be enhanced by cooling.[4,15] This discrepancy may be due to the gain being sufficiently large over the entire temperature range we examined that the reflectivity of the conjugator was always saturated. In contrast to the reflectivity, the time-response of the conjugator was temperature dependent. It increased with cooling, as expected from the results of our two-wave mixing measurements reported in the previous section.

The above results on the passive self-pumped ring conjugator represent the highest phase-conjugate reflectivity and the fastest time response reported to date for photorefractive $BaTiO_3$ in the near infrared wavelength region. As we have already mentioned, in previous experiments considerably lower phase-conjugate reflectivities and longer response times were measured.[2-4] In these experiments the diode laser was not optically isolated from phase-conjugate reflections. When we removed the Faraday isolator from our experimental setup, the previously reported results were duplicated. Figure 6 plots phase-conjugate reflectivity versus time when the isolator is removed ($\lambda/2$ plate is also removed). Notice that the time response is much slower with the isolator removed, even though we increased the incident power to 15 mW (475 mW/cm^2). The maximum reflectivity we could obtain without isolation was 28%, with significant fluctuations. Most likely, these fluctuations were due to phase instabilities caused by the conjugate signal reentering the laser.

With no optical isolation, we examined the effect of various levels of phase-conjugate feedback on the frequency spectrum of the laser using a 2 GHz free spectral range spectrum analyzer. The feedback level was controlled by placing neutral density filters in front of the ring conjugator. Figure 7 illustrates the mode spectrum observed for various levels of phase-conjugate feedback. With no feedback (photo A), the laser operated single mode. Note that the photo covers two free

spectral ranges. As pictured in photo B, with 0.04% of the output reinjected (measured outside the laser facet with a pellicle beamsplitter), the spectrum was multimode (bandwidth 1 GHz). With >0.06% reinjected (photos C and D), the spectrum from the analyzer appeared flat indicating a bandwidth much greater that 2 GHz. Separate measurements with a 1/4 m monochromator indicated that the spectral bandwidth for these injection levels was >5 nm.

4. CONCLUSIONS

In summary, we have described TWM measurements in photorefractive $BaTiO_3$ using 830 nm radiation from a GaAlAs diode laser. A TWM gain of 5200 (17 cm^{-1}) was measured at room temperature, increasing to 8000 (18 cm^{-1}) at 11°C. These values are comparable to those previously measured in the visible. TWM response times were measured and found to be on the order of 50 seconds at room temperature. Cooling the crystal increased the response time by a factor of two.

Using a $BaTiO_3$ self-pumped phase conjugator operating at 830 nm, we have shown that good optical isolation from phase-conjugate reflections is required to obtain optimal conjugator performance. Phase-conjugate reflectivities as large as 56% (not correcting for Fresnel losses) with response times on the order of tens of seconds have been observed. These values represent significant improvements over those previously reported in the literature.

5. ACKNOWLEDGEMENTS

This work was supported by the U. S. Air Force.

REFERENCES

1. M. Cronin-Golomb, in Digest of Conference on Lasers and Electro-optics (Optical Society of America, Washington, D. C., 1985), paper THT3.
2. M. Cronin-Golomb, K. Y. Lau, and A. Yariv, Appl. Phys. Lett. **47**, 567 (1985).
3. B. T. Anderson, P. R. Forman, and F. C. Jahoda, Opt. Lett. **10**, 627 (1985).
4. M. Cronin-Golomb and A. Yariv, Opt. Lett. **11**, 455 (1986).
5. M. D. Ewbank, R. R. Neurgaonkar, W. K. Cory, and J. Feinberg, J. Appl. Phys. **62**, 374 (1987).
6. G. C. Valley, M. B. Klein, Opt. Eng. **22**, 704 (1983).
7. F. Vachss, "Non-linear holographic response in photorefractive materials," Ph.D. dissertation (Stanford University, Palo Alto, Calif., 1988).
8. S. H. Wemple, M. Didomenico, Jr., and I. Camlibel, J. Phys. Chem. Solids, **29**, 1797 (1968).
9. Y. Fainman, E. Klancnik, and S. H. Lee, Opt. Eng. **25**, 228 (1986).
10. R. L. Townsend and J. T. LaMacchia, J. Appl. Phys. **41**, 5188 (1970).
11. S. Ducharme and J. Feinberg, J. Appl. Phys. **56**, 839 (1984).
12. A. E. Chiou and P. Yeh, Opt. Lett. **11**, 461 (1986).
13. I. McMichael, P. Yeh, M. Khoshnevisan, P. Beckwith, and W. Christian, in Proc. IEEE Lasers and Electro-optics Society (LEOS) Annual Meeting (OPTCON'88, Santa Clara, CA, 1988), paper FE.3.
14. W. R. Christian and I. C. McMichael, "Laser beam cleanup at 830 nm," this proceeding.
15. M. Cronin-Golomb, G. A. Rakuljic, and A. Yariv, Proc. Soc. Photo-Opt. Instrumen. **613**, 106 (1986).

Table 1. Measured two-wave mixing gain for $BaTiO_3$

	I_{probe}(mW)[a]	I_{pump}(mW)[a]	γ(deg)[b]	α(deg)[b]	β(deg)[b]	T(°C)[c]	G[d]
A	1.2	2.6	0	-15	15	22.2	1.4
B	1.2	2.6	15	-15	15	22.2	1.8
C	6.1	12.7	15	-15	15	22.2	2.3
D	0.098	12.7	15	-15	15	22.2	9.2
E	0.098	12.7	15	-15	15	10.7	9.7
F	7.3×10^{-5}	12	30	25	50	22.2	5200
G	7.3×10^{-5}	12	30	25	50	11.0	8000

[a]Measured before crystal
[b]See Fig. 1 for geometry
[c]Crystal temperature
[d]Two-wave mixing gain, see Eq. 5

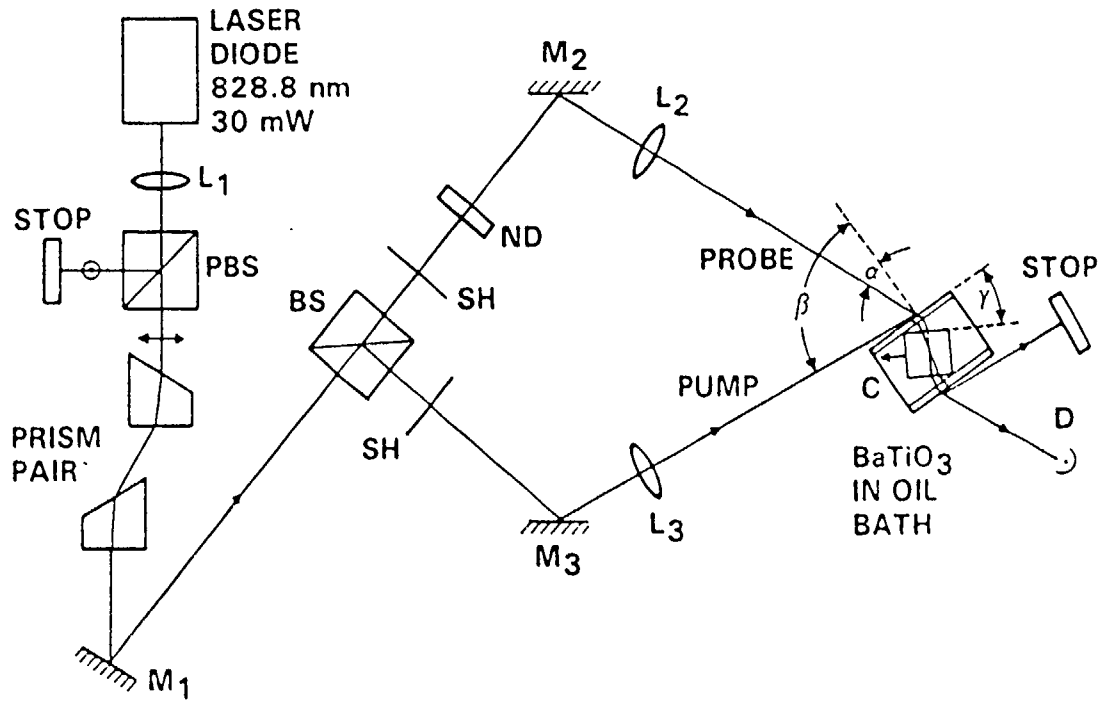

Figure 1. Experimental setup for two-wave mixing in $BaTiO_3$ at 830 nm

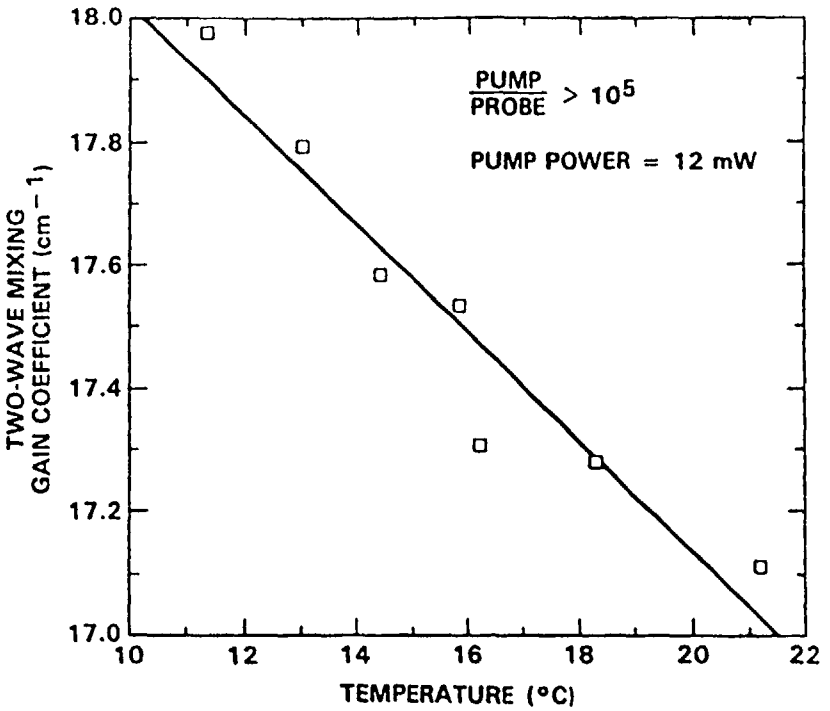

Figure 2. Two-wave mixing gain coefficient versus temperature. TWM geometry consists of angles α =25°, β =50°, and γ =30°.

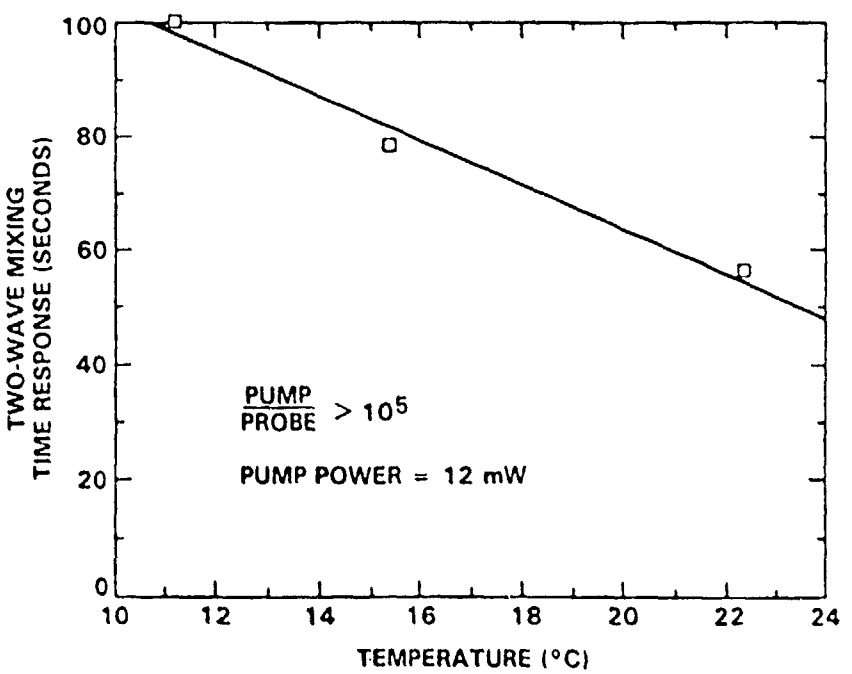

Figure 3. Two-wave mixing time response versus temperature. TWM geometry consists of angles α =25°, β =50°, and γ =30°.

SC5538.FR

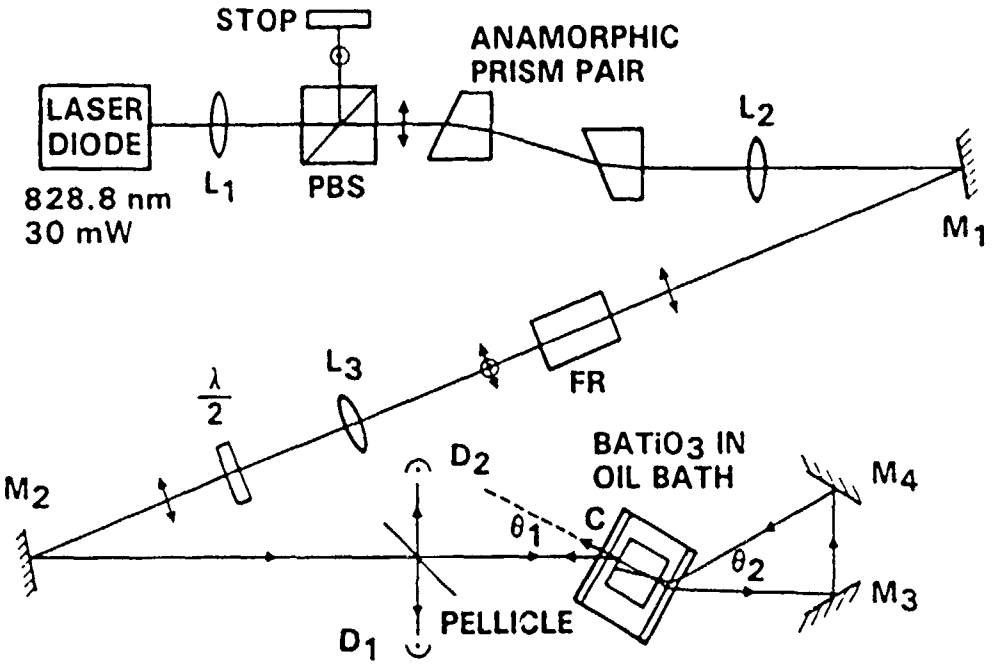

Figure 4. Schematic diagram of setup for self-pumped phase conjugation in $BaTiO_3$

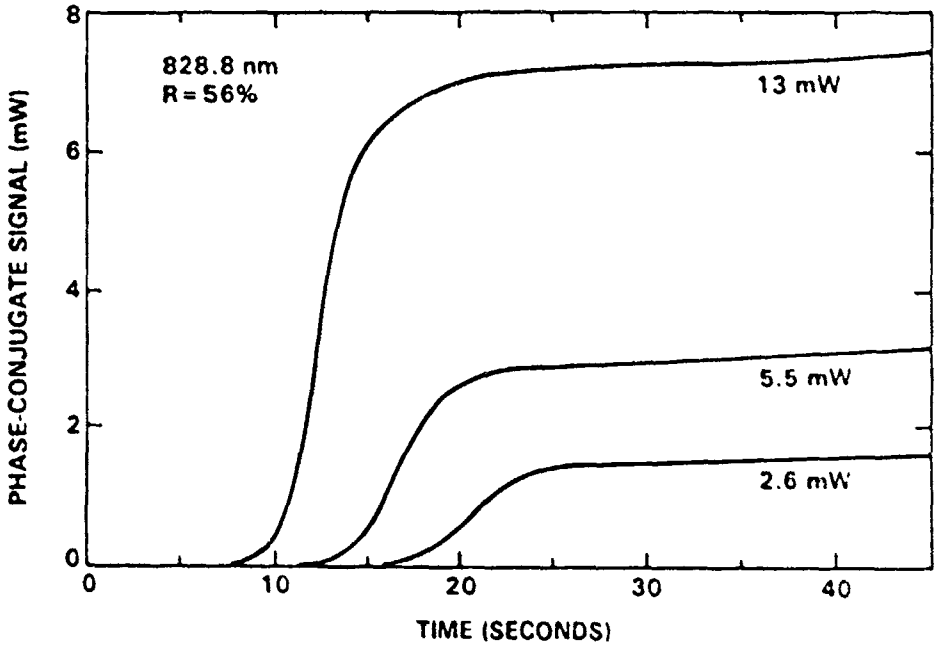

Figure 5. Time response of the self-pumped phase conjugator with isolation

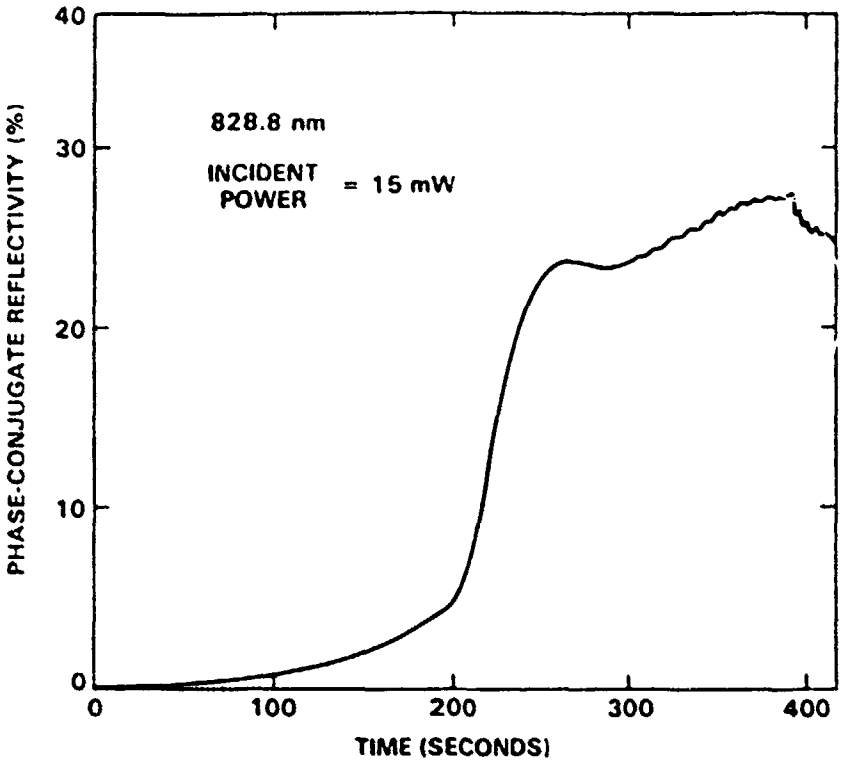

Figure 6. Time response of the self-pumped phase conjugator without isolation

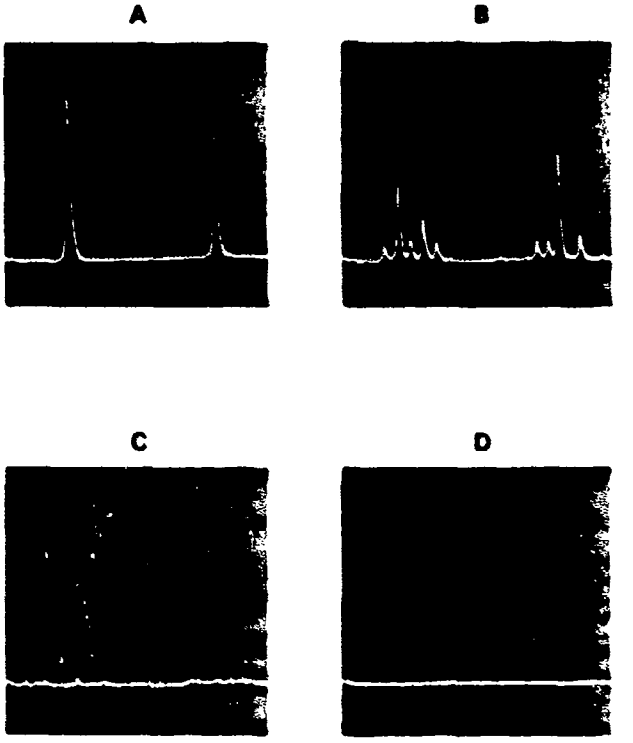

Figure 7. Mode spectrum of diode laser for various phase-conjugate feedback levels. (A) 0.0% (B) 0.04% (C) 0.065% (D) 0.12%

Phase Conjugate Oscillators

TUESDAY 17th

1:45 PM
TUX2 Phase conjugate oscillators

WUN-SHUNG LEE, SIEN CHI, National Chiao Tung U., Hsinchu, Taiwan, China, POCHI YEH, RAGINI SAXENA, Rockwell International Science Center, 1049 Camino Dos Rios, Thousand Oaks, CA 91360.

Optical resonators containing a phase conjugate mirror (PCM) have been a subject of great interest, where the PCM is employed as an end mirror of the resonator cavity for intracavity aberration correction.[1] Recent theoretical analysis indicates that the insertion of a PCM inside a ring laser cavity results in a reduction of the lock-in threshold and reduces the imbalance between the amplitudes of the oppositely directed traveling waves.[2] In the extreme case of phase conjugate oscillation without conventional gain, lock-in can be completely eliminated.[3] We have developed a general theory for nondegenerate oscillations in a phase conjugate oscillator (PCO) i.e., an optical resonator with a PCM as an intracavity element. The PCM consists of a nonlinear transparent medium pumped by a pair of counterpropagating laser beams so that phase conjugation of an input beam with possible gain is achieved by nondegenerate four-wave mixing (NFWM). The linear absorption/gain in the medium is also taken into account. In the absence of any conventional mirrors so that the PCO behaves like an ordinary PCM, we recover the results of phase conjugation by NFWM.[4] Our study shows that the nonlinear gain required for oscillation is considerably increased/decreased due to the linear absorption/gain in the medium, while the bandwidth and the sidelobe structure of the bandpass filter are also affected. In the case when there is only one conventional mirror, the PCO reduces to a phase conjugate resonator (a resonator bounded by a conventional mirror and a PCM). Our theory shows that nondegenerate oscillation is possible in such a resonator. The theory can also be used to study the effects of linear absorption/gain on the filter operation.

1. A. E. Siegman, P. A. Belanger, and A. Hardy, Optical Phase Conjugation, R. A. Fisher, Ed. (Academic, New York, 1983), Chap. 13 and the references therein.
2. J. C. Diels and I. C. McMichael, Opt. Lett. 6, 219 (1981).
3. P. Yeh, J. Feinberg, and M. Khoshnevisan, Proc. Soc. Photo-Opt. Instrum. Eng. 412, 240 (1983); P. Yeh and M. Khoshnevisan, Proc. Soc. Photo-Opt. Instrum. Eng. 457, 102 (1984).
4. D. M. Pepper and R. L. Abrams, Opt. Lett. 3, 213 (1978).

2:00 PM
TUX3 Perturbation analysis of photorefractive phase conjugation

GUIFANG LI, BAHAA E. A. SALEH, U. Wisconsin-Madison, Dept. Electrical & Computer Engineering, Madison, WI 53706-1691.

Using perturbation theory, we examine the fidelity of the photorefractive degenerate four-wave mixing (DFWM) phase conjugator when the probe wave is spatially and temporally varying. Previous theories are based on linearized undepleted pump approximation and Laplace transform technique. Fully nonlinear solutions assume a single monochromatic plane wave probe. We have considered instead the more general case in which the probe is spatially varying (a beam) and/or temporally varying (a pulse), and the pumps are allowed to deplete. The probe wave is expanded as a sum of monochromatic plane waves of frequencies $\omega_i = \omega_p + \Omega_i$, wavevectors $\mathbf{k}_i$, and complex amplitudes $A_i(\Omega_i, \mathbf{k}_i)$, where ω_p is the frequency of the pumps. Using a perturbation approach up to the third order, we found that the components of the probe interact in pairs, so that the component of the conjugate wave at $-\Omega_i, -\mathbf{k}_i$ is

$$A_c(-\Omega_i, -\mathbf{k}_i) = [M(\Omega_i, \mathbf{k}_i) + \sum_j \rho(\Omega_i, \mathbf{k}_i; \Omega_j, \mathbf{k}_j)]A_i^*(\Omega_i, \mathbf{k}_i) \quad (1)$$

$M(\Omega_i, \mathbf{k}_i)$ is the linearized response, $\rho(\Omega_i, \mathbf{k}_i; \Omega_j, \mathbf{k}_j)$ represents crosstalk when $j \neq i$, and self-nonlinear effect otherwise. Both functions exhibit resonance behavior. We use Eq. (1) to determine the response of the conjugate to pulsed beams.

2:15 PM
TUX4 Studies on the transient buildup of a photorefractive double phase conjugate mirror

QI-CHI HE, CHI C. SUNG, J. GRAEME DUTHIE, U. Alabama in Huntsville, Physics Dept., Huntsville, AL 35899.

In the application of a photorefractive double phase conjugate mirror, the transient buildup and the dynamic behavior are both interesting and important. The temporal instabilities of the driven DPCM were studied recently.[1] In this work we present a numerical study of the transient buildup as a function of various parameters: total intensity, beam ratio, steady state photorefractive coupling gain, and seeding levels. We take the standard four-wave mixing model[2] including the Debye relaxation equation for the space-charge electron field, using the typical boundary condition for the DPCM and no initial space-charge field. We find that (1) the buildup time of the DPCM, which is defined as the time the phase conjugate reflectivity reaches 90% of its steady state reflectivity, is also inverse proportional to the total intensity, (2) the buildup time decreases and tends to saturate as the steady state coupling gain increases, (3) the buildup time increases approximately quadratically as incident beam ratio deviates unity.

These results, including the seeding level effect, the external electric field effect, as well as some experimental results, are also presented.

1. W. Krolikowski *et al.*, in *Technical Digest of Conference on Quantum Electronics and Laser Science* (Optical Society of America, Washington, DC, 1989), paper WDD11.
2. M. Cronin-Golomb *et al.*, IEEE J. Quantum Electron. QE-20, 12 (1984).

2:30 PM
TUX5 Two-wave mixing of optical signals in the plasma medium

J. A. TATARONIS, G. C. PAPEN, U. Wisconsin-Madison, Dept. Electrical & Computer Engineering, Madison, WI 53706-1691.

Amplification resulting from two-wave mixing of optical signals occurs in nearly degenerate or, equivalently, transient conditions, subject to the restriction that the response of the nonlinear material to the incident wave is not instantaneous. Recent work has focused on Kerrlike materials.[1] In the present study, we explore the time dynamics of two-wave mixing in a Kerrlike ($\Delta n \propto I$), but nonlocal, plasma where the required delay process is induced either by a simple collision mechanism or by Landau damping. Maxwell's equations are coupled to the appropriate governing equations of the plasma, followed by linearization based on a strong undepleted pump wave and simplification by the slowly varying envelope approximation. Two plasma models are explored: (i) a warm collisional plasma and (ii) a Vlasov plasma to simulate the effects of Landau damping. In each case, the resulting equations are solved via Laplace transform techniques. In the presence of a delay mechanism, the two-wave mixing geometry produces spatial amplification of an applied probe wave in transient (or nearly degenerate) conditions. An enhancement of the plasma response occurs when a moving intensity grating propagating at a velocity of a natural mode of the plasma is generated. This enhancement of two-wave mixing can be considered a form of stimulated Brillouin scattering.

1. P. Yeh, IEEE J. Quantum Electron. QE-21, 454 (1985).

Tuesday MORNING
25 April 1989 TUI
CONVENTION CENTER ROOM 317

10:30 AM Photorefractive Nonlinear Optics: 1

Marvin B. Klein, Hughes Research Laboratories, Presider

TUI1 Recent advances in photorefractive nonlinear optics

PO04 YEH, Rockwell International Science Center, Thousand Oaks, CA 91360.

Photorefractive crystals such as $BaTiO_3$, SBN, BSO, and BGO are by far the most efficient materials for the generation of phase conjugate waves and the recording of holograms. In addition, self-pumped phase conjugation occurs in many of these crystals at relatively low laser power.[1,2] These conjugators are by far the most convenient phase conjugate mirrors available. Recently, there have been several significant developments in mutually pumped phase conjugators (MPPCs). In these conjugators, two incident incoherent laser beams can pump each other to produce a pair of phase conjugate beams inside a photorefractive crystal. The spatial wavefronts of the beams are conjugated, and the temporal information is exchanged. The phase conjugation requires the simultaneous presence of both beams. Such conjugators were demonstrated experimentally using two incoherent laser beams in $BaTiO_3$.[3-5] Mutually pumped phase conjugation has also been demonstrated in a ring resonator which is filled with two photorefractive $BaTiO_3$ crystals.[6] Although the bidirectional oscillation in the resonator[6] can be viewed as a possible mechanism for the phase conjugation, MPPC in single crystal can also be explained in terms of hologram sharing[3,5] and self-oscillation.[5]

A new type of phase conjugate interferometer was conceived[7] and demonstrated[8] using an MPPC. In the new interferometer, one of the mirrors of a conventional Sagnac ring interferometer is replaced with an MPPC. This interferometer has the dual nature of Michelson and Sagnac interferometry. Such an interferometer was constructed using a $BaTiO_3$ and was used to perform parallel image subtraction over a large aperture. When optical fiber loops are inserted in the optical path, fiber optic gyros can be constructed for rotation sensing.

Cross-polarization two-wave mixing in cubic crystals was predicted[9] and demonstrated.[10,11] Cubic crystals such as GaAs, InP exhibit significantly faster photorefractive response than many of the oxide materials. In addition, the optical isotropy and the tensor nature of electrooptic coefficients allow the possibility of cross-polarization two-wave mixing in which the s component of one beam is coupled to the p component of the other beam and vice versa. Such two-wave mixing provides an extremely strong SNR in many of the applications which employ photorefractive TWM.

A new method of reconfigurable optical interconnection was conceived and demonstrated.[12] Such a new method utilizes the nonreciprocal energy coupling in photorefractive holograms and provides a reconfigurable interconnection between an array of laser sources and an array of detectors. Conventional reconfigurable multiple-beam systems all have at least energy loss which leads to an energy efficiency of $1/N$, where N is the number of detectors. Using a combination of a photorefractive crystal, an SLM and a beam splitter, a volume hologram is constructed which provides the interconnection without the fanout energy loss. The result is a reconfigurable interconnection with high energy efficiency. The interconnection can be reconfigured using a different SLM pattern. The reconfiguration time is limited by the formation of holograms inside the crystal. Once the hologram is formed, the interconnection via Bragg diffraction is at the speed of light.

In summary: We address some of the most important and interesting photorefractive phenomena and their uses including mutually pumped phase conjugation, cross-polarization two-wave mixing in cubic semiconductors phase conjugate interferometers, and photorefractive interconnection. (Invited paper, 25 min)

1. J. O. White *et al.*, Appl. Phys. Lett. 40, 450 (1982).
2. J. Feinberg, Opt. Lett. 7, 486 (1982); 8, 480 (1983).
3. M. D. Ewbank, Opt. Lett. 13, 47 (1988).
4. S. Weiss, S. Sternklar, and B. Fischer, Opt. Lett. 12, 114 (1987).
5. R. W. Eason and A. M. C. Smout, Opt. Lett. 12, 51 (1987); 12, 498 (1987).
6. P. Yeh, T. Y. Chang, and M. D. Ewbank, J. Opt. Soc. Am. B 1, 1743 (1988).
7. P. Yeh, submitted to Opt. Lett. (1988).
8. M. Cronin-Golomb *et al.*, IEEE J. Quantum Electron. QE-20, 12 (1984).
9. I. McMichael, M. D. Ewbank, and P. Yeh, in *Technical Digest, Conference on Lasers and Electro-Optics* (Optical Society of America, Washington, DC, 1988), paper TUQ2.
10. P. Yeh, J. Opt. Soc. Am. B 4, 1382 (1987).
11. T. Y. Chang, A. E. T. Chiou, and P. Yeh, in *Technical Digest, Topical Meeting on Photorefractive Materials, Effects, and Devices* (Optical Society of America, Washington, DC, 1987), paper WC4.
12. P. Yeh and T. J. Chang, in *Technical Digest, Topical Meeting on Photorefractive Materials, Effects and Devices* (Optical Society of America, Washington, DC, 1987), paper WC5.
13. T. Y. Chang, A. E. T. Chiou, and P. Yeh, J. Opt. Soc. Am. B 5, 1724 (1988).
14. T. J. Chang and P. Yeh, Opt. Lett. 13, 50 (1988).
15. P. Yeh, A. E. Chiou, and J. Hong, Appl. Opt. 27, 2093 (1988).

Double Phase-conjugate Oscillators

POSTERS

was sufficient to resolve an isolated Doppler-broadened component, many of the hyperfine structures are only partially resolved due to overlapping of the components. A least-squares technique was used to fit the observed line contours to a six-parameter model of the platinum hyperfine structure. These parameters include the Doppler width, isotope shift, and upper and lower level hyperfine splitting coefficients. Accurate isotope shifts and hyperfine splitting coefficients for many of the known levels of neutral platinum were determined from the analysis of over 100 transitions.

(Poster paper)

MR24 Spectral properties of light scattered by a moving one-dimensional diffuser

EMIL WOLF, U. Rochester, Physics & Astronomy Department, Rochester, NY 14627

There exists a vast literature relating to the statistical properties of light obtained by scattering laser light by a moving diffuser. Some publications are restricted to an analysis of the effects produced by a uniformly moving diffuser with a slit aperture along its direction of motion.[1,2] We show that this case is rather exceptional, because it generates a field that is spatially completely coherent at each frequency.[3] The physical reasons for this result are discussed. We also derive an expression for the spectrum of the far field produced by scattering of a polychromatic plane wave incident normally on the diffuser. We find that it differs from the spectrum of the incident field in two respects. It suffers a Doppler shift due to the motion of the diffuser, and it is modified in a manner that depends on the correlation properties of the diffuser. Numerical examples are given which show that, although these effects are relatively small, they are within the range of experiment.

(Poster paper)

1. J. W. Goodman, *Statistical Optics* (Wiley, New York, 1985), Sec. 5.3.3.
2. H. Stark and Y. Famman, J. Opt. Soc. Am. A 2, 437 (1985).
3. L. Mandel and E. Wolf, Opt. Commun. 36, 247 (1981).

MR25 Approximate solution to nonlinear pulse propagation in optical fibers

PIERRE-ANDRE BELANGER, F. MORIN, P. MATHIEU, U. Laval, Physics Department-LROL, Sainte-Foy, P.Q. G1K 7P4, Canada

Soliton pulse propagation in optical fibers is now currently exploited. Since the original proposal by Hasegawa and Tappert[1] of using solitons in optical communication, many other applications have been proposed including the control of a laser by a soliton formed in an optical fiber.[2] Generally in applications, the initial pulse parameters are not exactly equal to those required to generate pure soliton solutions. In such a case the nonlinear Schrödinger equation must be solved numerically. However, to extract the salient features of the solution, it is of interest to search for a simple approximate solution. Such a solution is presented here. It consists in a hyperbolic secant with a variable width and linearly chirped phase. In a first-order approximation, the nonlinear Schrödinger equation is reduced to a nonlinear differential equation for the width, which can be integrated easily. This also yields simple relations for the linear chirp coefficient and peak amplitude. These results are then compared with the numerical solutions obtained by the beam propagation method. A good agreement is observed for the amplitude and phase terms up to energies of the order of the energy of an $N = 2$ soliton solution. The results obtained here by the approximate solution are also similar to those obtained by Anderson[3] using a variational approach based on Gaussian trial functions. Our simple model could be useful for some application (for example, modeling the soliton laser), and it provides a better understanding of the interplay between dispersion and nonlinear effects.

(Poster paper)

1. A. Hasegawa and F. Tappert, Appl. Phys. Lett. 23, 142 (1973).
2. L. F. Mollenauer and R. H. Stolen, Opt. Lett. 9, 13 (1984).
3. D. Anderson, Phys. Rev. A 27, 3135 (1983).

MR26 Angle-tuned multiline stimulated Raman scattering

BRADLEY BOBBS, J. A. GOLDSTONE, MICHAEL M. JOHNSON, Rockwell International Corp., Rocketdyne Division, Canoga Park, CA 91303

The stimulated Raman scattering gain of a multiline pump laser spanning a sufficiently wide spectral range is significantly reduced from that of a narrowband laser. This is due to destructive interference between the narrowband Raman effect and the Raman-resonant four-wave mixing effect which couples the lines together. However, this interference can be constrained to be always constructive by angle tuning of the pump and Stokes seed input beams to satisfy a phase matching condition for the four-wave mixing. The narrowband Raman gain will then be obtained. Calculations for a two-line XeF laser in a Raman conversion cell show that submilliradian beam angles can shorten the required cell length by factors of ~2, while loosening the pump intensity variation tolerance by an order of magnitude. Calculations for lasers with wider spectra indicate the potential for much larger gain increases and cell length reductions.

(Poster paper)

MR27 Weak dispersive effects in Raman amplification

CHARLES WARNER, BRADLEY BOBBS, Rockwell International Corp., Rocketdyne Division, Canoga Park, CA 91303

Linear medium dispersion can reduce the stimulated Raman scattering gain for a broadband laser. This increases the Raman cell length required for Stokes frequency conversion and also limits the ultimate conversion efficiency achievable in a long cell. Modeling of these effects, particularly the latter one, must account for depletion of the pump laser intensity as it is converted. Inclusion of depletion effects into previous undepleted pump modeling efforts may be accomplished using a perturbation technique for weak dispersion. Numerical results for a 351-nm laser in 3.5 atm of hydrogen with a 1-cm bandwidth show that a fourth-order perturbation calculation is adequate to predict a conversion efficiency 9% below the quantum limit. The efficiency is found to decrease approximately quadratically with increasing bandwidth for bandwidths up to ~2.3 cm^{-1}. An equivalent dispersion formulation may be used to extend these results to include the effects of a small angular misalignment between the pump and Stokes seed beams.

(Poster paper)

MR28 Empirical thermal design of Fabry-Perot interferometer mechanical supports

JOSEPH M. GORD, JR., NASA Langley Research Center, Hampton, VA 23665-5225; RAYMOND C. ROMANOFSKY, PRC System Services, 303 Butler Farm Rd., Hampton, VA 23666; CHARLES B. FOX, G.E. 3rd Systems Corp., 28 Research Dr., Hampton, VA 23666

Fabry-Perot interferometers have been used in many applications for wavelength and spectral measurements. Our objective is to develop and construct a wavemeter to provide laser wavelength centroid measurements of tunable solid-state lasers. Because of the high resolution and prior use in many applications, the classical Fabry-Perot-based wavemeter was chosen. With interferometers, one of the most difficult problems is to maintain thermal stability over ambient temperature excursions. For the wavemeter, a two-stage thermal control has been evaluated. The interferometer is mounted in a thermal-vacuum chamber with fine temperature control. This interferometer system is then enclosed with a second housing with course thermal control. In both cases, the temperature control is above ambient to provide simpler regulation. With the thermal control provided, the other variable is how to mount the Fabry-Perot interferometer to minimize thermally induced mechanical mounting stresses. Several support fixtures were evaluated using a Zeeman stabilized single frequency He-Ne laser as the source and a photodiode array as the detector. The laser is considered a perfect source with any end-to-end interferometer output variations caused by thermal-mechanical mounting stresses. A wide range of end-to-end measurements on a three-finger flexture support provides data to within the stabilization specification of the He-Ne laser.

(Poster paper)

MR29 Double phase-conjugate oscillators

IAN McMICHAEL, PAUL BECKWITH, POCHI YEH, Rockwell International Science Center, Thousand Oaks, CA 91360

When two phase-conjugate mirrors with gain are placed near each other, an oscillation will build up between them. This is called a double phase-conjugate oscillator (DPCO). DPCOs have many interesting physical properties that can be used to make sensors. For example, the frequencies of the counterpropagating oscillations in a linear DPCO are independent of the reciprocal optical path length of the resonator and dependent on the nonreciprocal optical path length. This is the exact opposite of linear oscillators using conventional mirrors (i.e., lasers). Since inertial effects produce nonreciprocal phase shifts, the DPCOs can be used to sense motion. In fact, the DPCO is the only oscillator that is known to be capable of measuring translation. Although conventional optics can be used to make rotation sensing oscillators (i.e., ring laser gyros), these devices cannot use solid-state gain media due to gain competition and they suffer from the problem of frequency locking. These problems do not exist in phase-conjugate oscillators.

The double phase-conjugate resonator can also be used for communications where each phase conjugate acts as a transceiver. Information can be exchanged between the phase-conjugate mirrors by modulating the phase amplitude or polarization of one of the mirrors. The phase-conjugate communication link has the desirable properties of high directionality, self-aligning, and aberration correction. To study the properties of DPCOs, we constructed a double phase-conjugate ring oscillator using a single crystal of barium titanate. The predicted properties of this oscillator were verified by introducing reciprocal and nonreciprocal elements into the ring and by observing the resulting effect on the frequencies of the two counterpropagating oscillations.

(Poster paper)

Recent Advances in Photorefractive Nonlinear Optics

SC5538.FR

RECENT ADVANCES IN PHOTOREFRACTIVE NONLINEAR OPTICS

(Invited Paper)

Pochi Yeh
Rockwell International Science Center
Thousand Oaks, California 91360

ABSTRACT

There have been several significant new developments in the area of photorefractive nonlinear optics during the past few years. This paper briefly describes some of the important and interesting phenomena and applications.

1.0 INTRODUCTION

The photorefractive effect is a phenomenon in which the local index of refraction is changed by the spatial variation of light intensity. This spatial index variation leads to a distortion of the wavefront and is referred to as "Optical Damage."[1] The photorefractive effect has since been observed in many electro-optic crystals, including $LiNbO_3$, $BaTiO_3$, SBN, BSO, BGO, GaAs, InP, and CdTe. This effect arises from optically generated charge carriers which migrate when the crystal is exposed to a spatially varying pattern of illumination with photons of sufficient energy.[2,3] Migration of charge carriers produces a space-charge separation, which then gives rise to a strong space-charge field. Such a field induces a change in index of refraction via the Pockels effect.[4] Photorefractive materials are, by far, the most efficient media for optical phase conjugation[5,6] and real-time holography using relatively low intensity levels (e.g., 1 W/cm^2).

2.0 TWO-WAVE MIXING

When two beams of coherent radiation intersect inside a photorefractive medium, an index grating is formed. This index grating is spatially shifted by $\pi/2$ relative to the intensity pattern. Such a phase shift leads to nonreciprocal energy transfer when these two beams propagate through the index grating. The hologram formed by the two-beam interference inside the photorefractive media can be erased by illuminating the hologram with light. Thus dynamic holography is possible using photorefractive materials.[7,8] Some of the most important and interesting applications are discussed as follows.

Laser Beam Cleanup

Two-wave mixing in photorefractive media exhibits energy transfer without any phase crosstalk.[9,10] This can be understood in terms of the diffraction from the self-induced index grating in the photorefractive crystal. Normally, if a beam that contains phase information $\phi(r,t)$ is diffracted from a fixed grating, the same phase information appears in the diffracted beam. In self-induced index gratings, the phase information $\phi(r,t)$ is impressed onto the grating in such a way that diffraction from this grating will be accompanied by a phase shift $-\phi(r,t)$. Such a self-cancellation of phase information is equivalent to the reconstruction of the reference beam when the hologram is read out by the object beam. Energy transfer without phase crosstalk can be employed to compress both

the spatial and the temporal spectra of a light beam.[10] This has been demonstrated experimentally using $BaTiO_3$ and SBN crystals.[9-11]

Photorefractive Resonators

The beam amplification in two-wave mixing can be used to provide parametric gain for unidirectional oscillation in ring resonators. The oscillation has been observed using $BaTiO_3$ crystals.[12] Unlike the conventional gain medium (e.g., He-Ne), the gain bandwidth of photorefractive two-wave mixing is very narrow (a few hertz's for $BaTiO_3$). Despite this fact, the ring resonator can still oscillate over a large range of cavity detuning. This phenomenon was not well understood until a theory of photorefractive phase shift was developed.[13] This theory also predicts that the unidirectional ring resonator will oscillate at a frequency different from the pump frequency by an amount directly proportional to the cavity-length detuning. Furthermore, in a photorefractive material with moderately slow response time τ, the theory postulates a threshold where oscillation will cease if the cavity detuning becomes too large. The theory has been validated experimentally in a $BaTiO_3$ photorefractive ring resonator.[14]

Optical Nonreciprocity

It is known in linear optics that the transmittance as well as the phase shift experienced by a light beam transmitting through a dielectric layered medium is independent of the side of incidence.[15] This is no longer true when photorefractive coupling is present. Such nonreciprocal transmittance was first predicted by considering the coupling between the incident beam and the reflected beam inside a slab of photorefractive medium.[16] The energy exchange due to the coupling leads to an asymmetry in the transmittance. In the extreme case of strong coupling ($\gamma L \gg 1$), the slab acts as a "one-way" window. Nonreciprocal (optical) transmission has been observed in $BaTiO_3$ and $KNbO_3$:Mn crystals.[17,18] In addition, there exists a nonreciprocal phase shift in contra-directional two-wave mixing. Such nonreciprocity may be useful in applications such as the biasing of ring laser gyros.[18,19]

Conical Scattering

When a laser beam is incident on a photorefractive crystal, a cone of light (sometimes several cones) emerges from the crystal. This has been referred to as Photorefractive Conical Scattering. It is known that fanning of light occurs when a laser beam is incident on a photorefractive crystal.[20] Because of the strong two-beam coupling, any scattered light may get amplified and thus lead to fanning. In conical scattering, the noisy hologram formed by the incident light and the fanned light further scatters off the incident beam. The fanning hologram consists of a continuum of grating vectors, but only a selected portion of grating vectors satisfies the Bragg condition for scattering. This leads to a cone of scattered light. Photorefractive conical scattering has been observed in several different kinds of crystals.[21-23]

Cross-Polarization Two-Wave Mixing

Cubic crystals such as GaAs and InP exhibit significantly faster photorefractive response than many of the oxide crystals. In addition, the isotropy and the tensor nature of the electro-optic coefficients allow the possibility of cross-polarization two-wave mixing in which the s component of one beam is coupled to the p component of the other beam and vice versa. A coupled mode theory of

photorefractive two-wave mixing in cubic crystals was developed.[24] The theory predicts the existence of cross-polarization two-wave mixing in crystals possessing a point group symmetry of $\bar{4}3m$. Such a prediction was validated experimentally using photorefractive GaAs crystals.[25-27] Cross-polarization two-wave mixing provides extremely high signal-to-noise ratios in many of the applications which employ photorefractive two-wave mixing.

Photorefractive Optical Interconnection

A new method of reconfigurable optical interconnection using photorefractive dynamic holograms was conceived and demonstrated.[28] Reconfigurable optical interconnection using matrix-vector multiplication suffers a significant energy loss due to fanout and absorption at the spatial light modulators. In the new method, the nonreciprocal energy transfer in photorefractive media is employed to avoid the energy loss due to fanout. The result is a reconfigurable optical interconnection with a very high energy efficiency. The interconnection can be reconfigured by using a different SLM pattern. The reconfiguration time is limited by the formation of holograms inside the crystal. Once the hologram which contains the interconnection pattern is formed, such a scheme can provide optical interconnection between an array of lasers and an array of detectors for high data rate transmission.

3.0 OPTICAL PHASE CONJUGATION

Optical phase conjugation has been a subject of great interest because of its potential application in many areas of advanced optics.[4-6] For nonlinear materials with third-order susceptibilities, the operating intensity needed in four-wave mixing is often too high for many applications, especially for information processing. Photorefractive materials are known to be very efficient at low operating intensities. In fact, high phase conjugate reflectivities have been observed in $BaTiO_3$ crystals with very low operating power. In what follows, we will briefly describe some of the most important and interesting recent developments.

Self-Pumped Phase Conjugation

A class of phase conjugators which has received considerable attention recently are the self-pumped phase conjugators.[12,29] In these conjugators, there are no externally supplied counterpropagating pump beams. Thus, no alignment is needed. The reflectivity is relatively high at low laser power. These conjugators are, by far, the most convenient phase conjugate mirrors available. Although several models have been developed for self-pumped phase conjugation,[30-34] the phenomena can be easily understood by using the resonator model.[13,14,35] In this model, the crystal is viewed as an optical cavity which supports a multitude of modes. When a laser beam is incident into the crystal, some of the modes may be excited as a result of the parametric gain due to two-wave mixing. If the incident configuration supports bi-directional ring oscillation inside the crystal, then a phase conjugate beam is generated via the four-wave mixing. The model also explains the frequency shift of these conjugators.[35]

Mutually Pumped Phase Conjugators

Another class of phase conjugators consists of the mutually pumped phase conjugators (MPPC) in which two incident incoherent beams can pump each

other to produce a pair of phase conjugate beams inside a photorefractive crystal. The spatial wavefronts of the beams are conjugated and the temporal information is exchanged. The phase conjugation requires the simultaneous presence of both beams. Recently, conjugators were demonstrated experimentally using two incoherent laser beams in $BaTiO_3$.[36,38,39] These phenomena can be explained in terms of either hologram sharing[39,40] or self-oscillations[37] in a four-wave mixing process or resonator model.[41]

Phase Conjugate Michelson Interferometers

We will now consider a Michelson interferometer which is equipped with phase conjugate mirrors. Such an optical setup is known as a phase conjugate Michelson interferometer and has been studied by several workers.[42-44] By virtue of its names, this interferometer exhibits optical time reversal. Consequently, no interference is observed at the output port. The output port is, in fact, totally dark.[44] Such an interferometer is ideal for parallel subtraction of optical images because the two beams arriving at the output port are always out of phase by π. This has been demonstrated experimentally using a $BaTiO_3$ crystal as the phase conjugate mirrors.[45] Using a fiber loop as one of the arms, such an interferometer can be used to sense nonreciprocal phase shifts.[46] A phase conjugate fiber optic gyro has been built and demonstrated for rotation sensing using $BaTiO_3$ crystals.[47,48]

Phase Conjugate Sagnac Interferometers

Using the mutually pumped phase conjugators mentioned earlier, a new type of phase conjugate interferometer was conceived and demonstrated.[49] In the new interferometer, one of the mirrors of a conventional Sagnac ring interferometer is replaced with a MPPC. Such a new interferometer has a dual nature of Michelson and Sagnac interferometry. As far as wavefront information is concerned, the MPPC acts like a retro-reflector and the setup exhibits phase conjugate Michelson interferometry and optical time reversal.[44] As for the temporal information, the MPPC acts like a normal mirror and Sagnac interferometry is obtained. Such a new phase conjugate interferometer can be used to perform parallel image subtraction over a large aperture. With optical fiber loops inserted in the optical path, we have constructed fiber-optic gyros and demonstrated the rotation sensing.

Other Developments Related to Photorefractive Nonlinear Optics

In addition to those described above, there are other significant developments. These include polarization-preserving conjugators,[50] phase shifts of conjugators,[51] optical matrix algebra,[52] fundamental limit of photorefractive speed,[53] nondegenerate two-wave mixing in ruby crystal,[54] and nonlinear Bragg scattering in Kerr media.[55]

REFERENCES

1. Ashkin, A., et al, Appl. Phys. Lett. 9, 72 (1966).
2. Vinetskii, V.L., et al, Sov. Phys. Usp. 22, 742 (1979).
3. Kukhtarev, N.V., et al, Ferroelectrics 22, 961 (1979).
4. Yariv, A., and Yeh, P., "Optical Waves in Crystals," (Wiley, 1984).
5. See, for example, Pepper, D., Sci. Am. 254, 74 (1986).
6. Yariv, A., IEEE J. Quantum Electronics, QE-14, 650 (1978).

7. Staebler, D.L., and Amodei, J.J., J. Appl. Phys. 34, 1042 (1972).
8. Vahey, D.W., J. Appl. Phys. 46, 3510 (1975).
9. Chiou, A.E.T., and Yeh, P., Opt. Lett. 10, 621 (1985).
10. Yeh, P., CLEO Technical Digest (1985) p. 274.
11. Chiou, A.E.T., and Yeh, P., Opt. Lett. 11, 461 (1986).
12. White, J.O., et al, Appl. Phys. Lett. 40, 450 (1982).
13. Yeh, P., J. Opt. Soc. Am. B2, 1924 (1985).
14. Ewbank, M.D. and Yeh, P., Opt. Lett. 10, 496 (1985).
15. Knittl, Z., Optics of Thin Films (Wiley, New York, 1976), p. 240.
16. Yeh, P., J. Opt. Soc. Am. 73, 1268-1271 (1983).
17. Zha, M.Z., and Gunter, P., Opt. Lett. 10, 184-186 (1985).
18. Yeh, P., and Khoshnevisan, M., SPIE 487, 102-109 (1984).
19. Yeh, P., Appl. Opt. 23, 2974-2978 (1984).
20. Feinberg, J., J. Opt. Soc. Am. 72, 46 (1982).
21. Odoulov, S., Belabaev, K., and Kiseleva, I., Optics. Lett. 10, 31 (1985).
22. Temple, D.A., and Warde, C., J. Opt. Soc. Am. B3, 337 (1986).
23. Ewbank, M.D., Yeh, P., and Feinberg, J., Opt. Comm. 59, 423 (1986).
24. Yeh, P., J. Opt., Soc. Am. B4, 1382 (1987).
25. Cheng, L.-J. and Yeh, P., Opt. Lett. 13, 50 (1988).
26. Chang, T.Y., Chiou, A.E.T. and Yeh, P., OSA Tech. Digest 17, 55 (1987).
27. Chang, T.Y., Chiou, A.E.T. and Yeh, P., J. Opt. Soc. Am. B5, 1724 (1988).
28. Yeh, P., Chiou, A.E., and Hong, J., Appl. Opt. 27, 2093 (1988).
29. Feinberg, J., Opt. Lett. 7, 486 (1982); Opt. Lett. 8, 480 (1983).
30. Chang, T.Y. and Hellwarth, R.W., Opt. Lett. 10, 408 (1985).
31. Lam, J.F., Appl. Phys. Lett. 46, 909 (1985).
32. MacDonald, K.R., and Feinberg, J., J. Opt. Soc. Am. 73, 548 (1983).
33. Ganthica, D.J., et al, Phys. Rev. Lett. 58, 1644 (1987).
34. Gower, M.C., Opt. Lett. 11, 458 (1986).
35. Ewbank, M.D., and Yeh, P., Proc. SPIE Vol. 613, 59 (1986).
36. Ewbank, M.D., Opt. Lett. 13, 47 (1988).
37. Cronin-Golomb, M., et al, IEEE J. Quantum Electron. QE-20, 12 (1984).
38. Weiss, S., Sternklar, S. and Fischer, B. Opt. Lett. 12, 114 (1987).
39. Eason, R.W., Smout, A.M.C., Opt. Lett. 12, 51 (1987); 12, 498 (1987).
40. Yeh, P., submitted to Opt. Lett. (1988).
41. Yeh, P., Chang, T.Y., and Ewbank, M.D., J. Opt. Soc. Am. B5, 1743 (1988).
42. Ewbank, M., Yeh, P., and Khoshnevisan, M., SPIE Proc. Vol. 464, 2 (1984).
43. Chen W.H., et al, SPIE Proc. Vol. 739, 105 (1987).
44. Ewbank, M.D., et al, J., Opt. Lett. 10, 282 (1985).
45. See, for example, Chiou, A.E.T., and Yeh, P., Opt. Lett. 11, 306 (1986).
46. Yeh, P., McMichael, I., and Khoshnevisan, M., Appl. Opt. 25, 1029 (1986).
47. McMichael, I., and Yeh, P., Opt. Lett. 11, 686 (1986).
48. McMichael, I., Beckwith, P., and Yeh, P., 12, 1023 (1987).
49. McMichael, I., et al, CLEO Tech. Digest Vol. 7, 134 (1988).
50. McMichael, I., Yeh, P., and Khoshnevisan, M., Opt. Lett. 11, 525 (1986).
51. McMichael, I., and Yeh, P., Opt. Lett. 12, 48 (1987).
52. Yeh, P., and Chiou, A.E.T., Opt. Lett. 12, 138 (1987).
53. Yeh, P., Appl. Opt. 26, 602 (1987).
54. McMichael, I., Yeh, P., and Beckwith, P., Opt. Lett. 13, 500 (1988).
55. Yeh, P., and Koshnevisan, M., J. Opt. Soc. Am. B4, 1954 (1987).

Double Phase-Conjugate Oscillators

Annual Meeting of the Optical Society of America, Santa Clara, CA (1988)

Double Phase-Conjugate Oscillators

Ian McMichael, Paul Beckwith, and Pochi Yeh

Rockwell International Science Center

ABSTRACT

We describe the physics and applications of double phase-conjugate oscillators, and we investigate the properties of such oscillators using photorefractive phase-conjugate mirrors.

SUMMARY

When two phase-conjugate mirrors with gain are placed near each other, an oscillation will build up between them.[1] This is called a double phase-conjugate oscillator (DPCO). DPCO's have many interesting physical properties that can be used to make sensors. For example, the frequencies of the counterpropagating oscillations in a linear DPCO are independent of the reciprocal optical path length of the resonator, and dependent on the non-reciprocal optical path length. This is the exact opposite of linear oscillators using conventional mirrors (i.e. lasers). Since inertial effects produce nonreciprocal phase-shifts, the DPCO's can be used to sense motion. In fact, the DPCO is the only oscillator that is known to be capable of measuring translation.[2] Although conventional optics can be used to make rotation sensing oscillators (i.e., ring laser gyros), these devices can not use solid state gain media due to gain competition, and they suffer

from the problem of frequency locking. These problems do not exist in phase-conjugate oscillators. The double phase-conjugate resonator can also be used for communications, where each phase-conjugator acts as a transceiver. Information can be exchanged between the phase-conjugate mirrors by modulating the phase, amplitude, or polarization at one of the mirrors. The phase-conjugate communication link has the desireable properties of high directionality, self tracking, and aberration correction. To study the properties of DPCO's, we constructed a double phase-conjugate ring oscillator using a single crystal of barium titanate. The predicted properties of this oscillator were verified by introducing reciprocal and nonreciprocal elements into the ring, and by observing the resulting effect on the frequencies of the bidirectional oscillations.

This research is supported by the U.S. Air Force Office of Scientific Research under contract F49620-88-C-0023.

1. J. Lam and W. Erown, Opt. Lett. 5, 61 (1980); M. Cronin-Golomb, B. Fischer, S. Kwong, J. White, and A. Yariv, Opt. Lett. 7, 353 (1985).

2. P. Yeh, M. Khoshnevisan, M. Ewbank, and J. Tracey, Opt. Commun. 57, 387 (1986).

INTRODUCTION

When two phase-conjugate mirrors with gain are placed near each other, an oscillation will build up between them.[1] This is called a double phase-conjugate oscillator (DPCO). DPCO's have many interesting physical properties that can be used to make sensors. For example, the frequencies of the counterpropagating oscillations in a linear DPCO are independent of the reciprocal optical path length of the resonator, and dependent on the non-reciprocal optical path length. This is the exact opposite of linear oscillators using conventional mirrors (i.e. linear lasers). Since inertial effects produce nonreciprocal phase-shifts, the DPCO's can be used to sense motion. In fact, the DPCO is the only optical oscillator in which the frequencies of oscillation are linearly proportional to the velocity.[2] Although conventional optics can be used to make rotation sensing oscillators (i.e., ring laser gyros), these devices can not use solid state gain media due to gain competition, and they suffer from the problem of frequency locking. These problems do not exist in DPCO's. The DPCO can also be used for communications, where each phase-conjugator acts as a transceiver. Information can be exchanged between the phase-conjugate mirrors by modulating the phase, amplitude, or polarization at one of the mirrors. The phase-conjugate communication link has the desirable properties of high directionality, self tracking, and aberration correction.

1. J. Lam and W. Brown, Opt. Lett. 5, 61 (1980); M. Ewbank, P. Yeh, and M. Khoshnevisan, Opt. Lett. 10, 282 (1985); M. Cronin-Golomb, B. Fischer, S. Kwong, J. White, and A. Yariv, Opt. Lett. 7, 353 (1985).

2. P. Yeh, M. Khoshnevisan, M. Ewbank, and J. Tracy, Opt. Commun. 57, 387 (1986).

FREQUENCY SPLITTING OF THE COUNTERPROPAGATING MODES

Consider the linear oscillator formed by two phase-conjugate mirrors PCM a and PCM b as shown to the right. The roundtrip phase condition is given by,

$$\phi_a - \phi_b + \Delta\omega\, L/c + \phi_{nr} = 2\pi n \qquad (1)$$

where ϕ_a and ϕ_b are the phase shifts for reflection from the phase conjugate mirrors a and b respectively, $\Delta\omega = \omega_1 - \omega_2$ is the frequency splitting between the counterpropagating oscillations (note, if $\omega_1 = \omega_0 + \Delta\omega/2$, where ω_0 is the pump wave frequency for the phase-conjugate mirrors, then $\omega_2 = \omega_0 - \Delta\omega/2$), L is the length of the resonator, and ϕ_{nr} is the roundtrip nonreciprocal phase shift in the resonator. To gain some insight into how the phase condition determines the frequencies of oscillation, we make three simplifying assumptions. First we assume the case of weak coupling for which the phase of the phase conjugate reflection is given by [3],

$$\phi_3 = \phi_1 + \phi_2 - \phi_4 + \pi/2 + \phi_{\Delta n} + \phi_g \qquad (2)$$

where ϕ_1 and ϕ_2 are the phases of the pumping waves, ϕ_4 is the phase of the incident wave, $\phi_{\Delta n}$ is the phase of the complex change in index, and ϕ_g is the phase shift of the grating with respect to the intensity pattern. Second, we assume that the frequency shift is small so that $\phi_g \approx \phi_{g0} + \Delta\omega\,\tau/2$, where ϕ_{g0} is the phase shift of the grating in the absence of any frequency shift, and τ is the response time of the phase-conjugate mirror. Third, we assume the phase-conjugate mirrors are identical, or the same, so that $\phi_a - \phi_b = \phi_{ga} - \phi_{gb} = \Delta\omega\,\tau$. Substituting into Eq. 1 we obtain the frequency splitting of the zeroth order counterpropagating modes.

$$\Delta\omega = \phi_{nr} / (\tau + L/c) \qquad (3)$$

3. S. Kwong, A. Yariv, M. Cronin-Golomb, and B. Fischer, J. Opt. Soc. Am. A 3, 157 (1986); I. McMichael and P. Yeh, Opt. Lett 12, 48 (1987).

LINEAR POSITION SENSOR

The effect of motion is to produce a nonreciprocal phase shift for light traveling in the resonator. Consider the case when the resonator is moving with velocity v in the direction from PCM a to PCM b. For light traveling in the direction of motion, the apparent cavity length is increased by an amount vL/c, so that the phase of the light is increased by an amount $2\pi vL/c\lambda$. The phase of the light traveling against the direction of motion is decreased by the same amount, so that the net effect of motion is to introduce a nonreciprocal phase shift $\phi_{nr} = 2\pi vL/c\lambda$. Substituting into Eq. 3 we obtain,

$$\Delta\omega = 2\pi (v/\lambda) / [1 + \tau (c/L)] \qquad (4)$$

This frequency splitting can be measured by beating the two outputs from the resonator. If the response time of the phase conjugate mirrors is much faster than the time it takes for light to travel across the resonator, then the beat frequency f is simply given by,

$$f = v/\lambda \qquad (5)$$

For a wavelength of 1 μm, a beat frequency of 1 Hz is obtained with a velocity of approximately 0.1 μm/s.

The theory of the linear position sensor assumes that motion has no other effect than to add a nonreciprocal phase shift for light traveling in the resonator. This requires that the phase-conjugate mirrors be pumped by separate frequency stabilized sources. To understand this, consider what would happen if both phase-conjugate mirrors are pumped by a source located at PCM a. In this case the light traveling from the source at a that provides pumping at b will also experience the same phase shift due to motion as the light in the resonator. The net effect will be that the phase-conjugate reflection will have a term $\phi_{nr}/2$ instead of $-\phi_{nr}/2$, so that the roundtrip phase change due to motion will be 0 instead of ϕ_{nr}.

PHASE-CONJUGATE OSCILLATOR GYROS

Consider the phase-conjugate ring resonator shown at the right. If the resonator is rotating clockwise with an angular velocity Ω, then light traveling in the resonator experiences a non-reciprocal phase shift due to the Sagnac effect of $\phi_{nr} = 4\pi A\Omega/c\lambda$ radians, where A is the area enclosed by the resonator. Since this oscillator uses a single four-wave mixing medium for both phase-conjugate mirrors, the conditions for Eq. 3 are met automatically. Substituting into Eq. 3 we obtain,

$$\Delta\omega = (4\pi A\Omega/P\lambda) / [1 + \tau (c/P)] \qquad (6)$$

where P is the perimeter of the resonator. By combining the two outputs from the ring resonator one can measure a beat frequency $f = \Delta\omega/2\pi$, that is proportional to the angular velocity Ω. If the response time of the phase conjugate mirrors is much faster than the time it takes for light to travel around the resonator, then the beat frequency is simply given by,

$$f = 4A\Omega/P\lambda \qquad (7)$$

This is the beat frequency obtained in ring laser gyros. However, since there is no gain competition between counterpropagating waves in the phase-conjugate resonator (the counterpropagating waves in fact support each other in the phase-conjugate resonator) the phase conjugate gyros can use homogeneously broadened solid state media. In addition, improved lock-in characteristics have been predicted[4].

4. J. Diels and I. McMichael, Opt. Lett. 6, 219 (1981); M. Tehrani, Proc. SPIE 412, 186 (1983); P. Yeh, J. Tracy, and M. Khoshnevisan, Proc. SPIE 412, 240 (1983).

DEMONSTRATION OF A DOUBLE PHASE-CONJUGATE RING OSCILLATOR AND THE SENSING OF NONRECIPROCAL PHASE SHIFTS

The experimental setup of our double phase-conjugate ring oscillator is shown at the right. Light from an argon laser is incident on a $BaTiO_3$ crystal to form a self-pumped "cat" conjugator. The ring resonator is then formed by mirrors M1-M3 and the crystal. Greater than unity phase-conjugate reflectivity via four-wave mixing in the crystal (the incident light from the laser and its conjugate reflection provide the counterpropagating pump waves) is the gain source for the bidirectional oscillations. The outputs from M1 were combined and beat on detector D. As predicted by Eq. 3, in the absence of any nonreciprocal phase shift, the frequencies of the bidirectional oscillations are very nearly degenerate, and we measured a beat frequency ~ 10^{-3} Hz. When a Faraday cell was placed in the oscillator to produce a nonreciprocal phase shift, the bidirectional oscillations became nondegenerate, and we measured a beat frequency ~ 0.2 Hz. The qualitative dependence of the fringe motion at detector D on the magnitude and direction of the magnetic field applied to the Faraday cell agrees with the theory. Quantitative measurements are in progress.

SUMMARY

Unlike the case in conventional lasers, the frequencies of the counterpropagating oscillations in double phase conjugate oscillators are nondegenerate, and their frequency splitting is linearly proportional to the nonreciprocal phase shift in the resonator. Since motion produces nonreciprocal phase shifts, these oscillators can be used for inertial sensing of linear and rotational motion. Finally, we constructed a double phase-conjugate ring oscillator and have demonstrated its ability to the sense nonreciprocal phase shifts.

This research was partially supported by the U.S. Air Force Office of Scientific Research under contract F49620-88-C-0023.

Fig 1. Double phase-conjugate linear oscillator formed by phase-conjugate mirrors PCM a and PCM b.

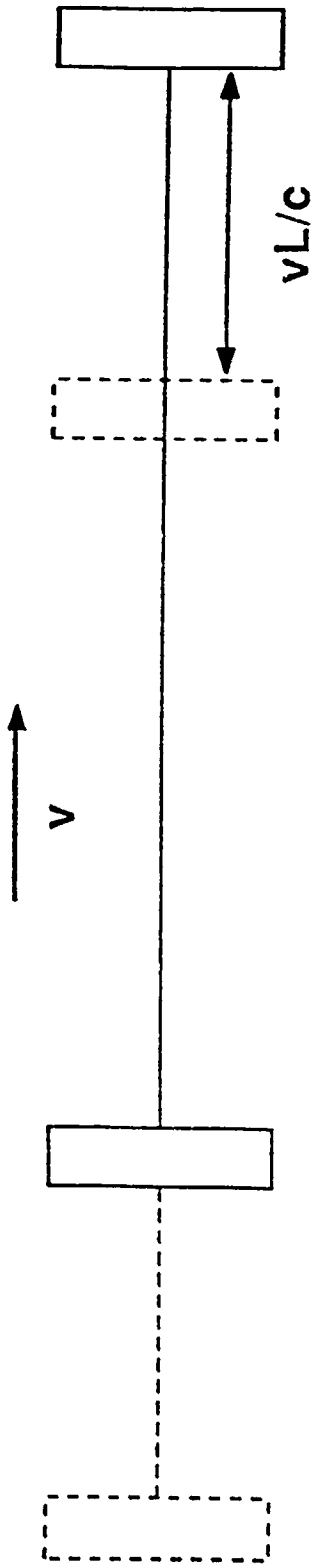

Fig 2. Velocity sensing in the double phase-conjugate linear oscillator.

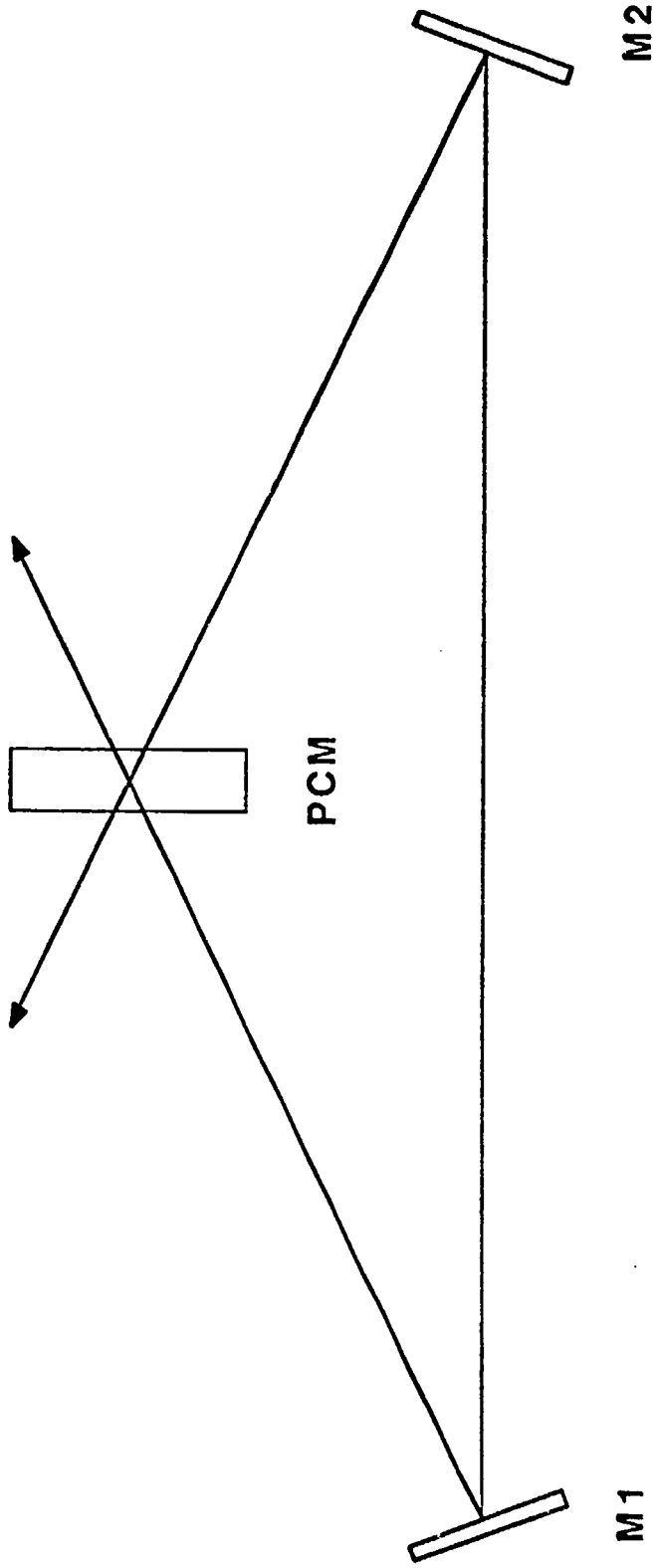

Fig 3. Double phase-conjugate ring oscillator formed by phase-conjugate mirror PCM and conventional mirrors M1 and M2.

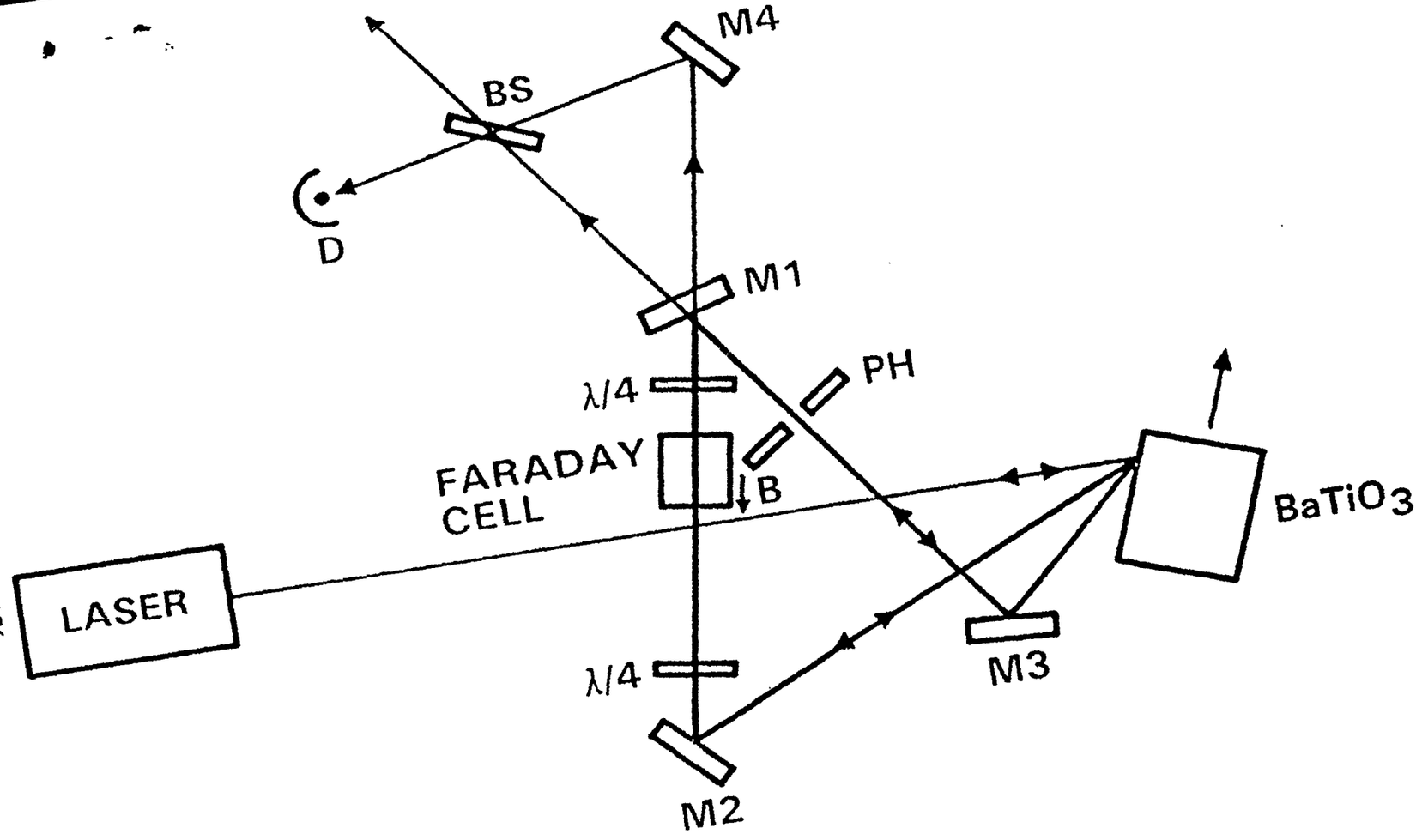

Fig 4. Experimental setup of the double phase-conjugate ring oscillator.